UNIVERSITY OF CALIFORNIA, SAN DIEGO

SAN DIEGO STATE UNIVERSITY

Evaluation of Seismic Overstrength Factors for Anchorage into Concrete of Nonstructural Components

A dissertation submitted in partial satisfaction of the requirements for the degree

Doctor of Philosophy

in

Engineering Sciences (Structural Engineering)

by

Timothy Paul Johnson

Committee in charge:

University of California, San Diego

Professor Tara Hutchinson, Co-Chair
Professor Jose Restrepo
Professor Peter Shearer

San Diego State University

Professor Robert Dowell, Co-Chair
Professor Julio Valdes

2017

The Dissertation of Timothy Paul Johnson is approved, and it is acceptable in quality and form for publication on microfilm and electronically:

Co-Chair

Co-Chair

University of California, San Diego

San Diego State University

2017

DEDICATION

To Kira with all my love.

TABLE OF CONTENTS

LIST OF FIGURES

LIST OF TABLES

ACKNOWLEDGEMENTS

Hilti Corporation provided funding and support for this project under the Hilti Structural Engineering Research Project (SERP) titled “Simulation and Testing to Support Seismic Design of Anchorage.” Initially this research program was joint with the University of California San Diego (UCSD), San Diego State University (SDSU), and the University of Stuttgart (IWB) when testing began in 2011, but it was separated into individual programs in 2012. Dr. Philipp Grosser was the program administrator from 2011 to 2014 and Dr. Roberto Piccinin was the program administrator from 2014 to 2017. Project oversight and support was provided by Dr. Ulrich Bourgund and Mr. John Silva. The financial and technical support provided by Hilti was instrumental in the development of this dissertation and the recommendations presented herein and is greatly appreciated. All opinions, recommendations, and conclusions presented in this dissertation are solely those of the author, and do not necessarily represent the views of Hilti or any of its employees.

I would like to thank my doctoral committee members for providing me with a challenging and vigorous environment with which to grow over the course of my degree. Professor Tara Hutchinson provided the UCSD oversight of my degree, and her constant challenging of conclusions and observations made within my research program was enormously helpful in producing a comprehensive and rigorous scientific thesis. My courses and discussions with Professor José Restrepo were fundamental in developing my programming and analysis skills for tackling nonlinear problems – something I did not realize I would need at the time of taking the courses, but quickly became an integral part of my work. From the time I first set foot in one of his undergraduate courses in 2009, Professor Julio Valdes has always had an open door

to discuss technical challenges, and we have shared many vivid discussions over the years. As part of my out-of-department studies, I had the privilege and delight of taking a seismology course with Professor Peter Shearer, whose presentation of seismological theory provided excellent foundational knowledge for both my research and teaching obligations.

Additionally, I would like to thank my advisor, Professor Robert Dowell, for his exceptional mentoring and dedication to my success as a young engineer and researcher. We met in 2009 when I was an undergraduate student taking Structural Analysis I, where he challenged me to pursue the rigor of structural engineering over my interest in transportation engineering at the time. He jokingly stated that structural engineering would provide more intellectual reward versus “merely counting cars,” and I haven’t looked back since. Over the years we have become close friends in addition to advisor and student, and the countless hours we have spent discussing complicated problems – both directly related to my work and not – have been seminal in my growth as an engineer. Without his patience, guidance, and dedication to my success, this degree would not have been possible.

As the first joint doctoral student in the newly-formed SDSU Civil Engineering and UCSD Structural Engineering program, there were an exhausting number of administrative details that arose on an almost monthly basis. Mr. Donovan Geiger at SDSU always had an open door, and provided an exorbitant amount of support to me for any and all non-academic details during all phases of my degree. Mrs. Yvonne Wollman at UCSD provided exceptional support for me along the way, as even though she started halfway through my program, she was highly supportive and helpful in dealing with many issues faced that were beyond her direct control.

As my research involved a significant amount of full-scale structural testing, I could not have completed my laboratory work without a great deal of support. During my first exposure with the Hilti Seismic Project, prior to starting my doctoral work, Dr. Matthew Hoehler and Mr. Justin Scheidel opened the necessary doors for me to continue working with Hilti into my graduate studies. Mr. Greg Morris and Mr. Michael Lester, the structural engineering laboratory technicians at SDSU, provided an enormous amount of assistance on my project from component fabrication to construction advice. Additionally, I had the support of a legion of skilled and dedicated graduate students – Mr. Emrah Saritac, Mr. Reza Banan, Mr. Akash Patel, Mr. Bestun Rashid, Mr. Joshua Reece, Ms. Crystal Garcia, Mr. Ward Schrimsher, and Mr. Rory Klinger – as well as undergraduate students – Mr. Mike Ellis, Mr. Ben Toth, Mr. Lucas Cardenas, and Ms. Gemsin Morrone – who all contributed greatly to the structural testing program.

Finally, I am deeply thankful for my family and close friends who provided me with unwavering support through every step of the long, arduous process of a joint doctoral degree. I had no knowledge of the C# programming language prior to this work, and the detailed application written for this dissertation would not have been possible without my brother, David, spending countless hours offering advice and mentoring on its development. My father has been endlessly supportive from the day I started, and was always available to help sort through emergencies and give advice whenever needed. Last, but certainly not least, my mother was the pillar whom I could rely on to vent frustrations, provide encouragement, and keep me steady from start to finish; without her support, I never would have made it past the first year. Thanks, mom – you're the best!

The following publications are reproduced in part in this dissertation, with minor modification, with permission from Elsevier and ASCE as applicable:

Chapter 1:

Johnson, T.P.; Dowell, R.K.; and Silva, J.F. (2016). "A Review of Code Seismic Demands for Anchorage of Nonstructural Components." *Journal of Building Engineering*, Vol 5. pp. 249-253. [Elsevier]

Chapters 2 and 4:

Johnson, T.P. and Dowell, R.K. (2017 - Acceptance Pending). "Evaluation of Nonstructural Component Anchorage into Concrete via Dynamic Shaking Table Tests." *Journal of Building Engineering*. [Elsevier]

Chapter 7:

Johnson, T.P, Dowell, R.K., and Silva, J.F. (2017 - Acceptance Pending). "Recommendations for Ω_0 for Anchorage into Concrete for Upright Nonstructural Components." *J. Struc. Eng.* [ASCE]

VITA

Education

2008 A.A., Liberal Arts and Sciences. Palomar College. San Marcos, CA.

2011 B.S., Civil Engineering. San Diego State University. San Diego, CA.

Minor in Mathematics, Magna Cum Laude

2017 Ph.D., Engineering Sciences (Structural Engineering). University of California San Diego, San Diego State University. San Diego, CA.

Experience

2010-2011 **San Diego State University**

Grader (CIVE 321 Structural Analysis I / CIVE 421 Reinforced Concrete)

2011-2017 **San Diego State University**

Graduate Student Researcher & Lecturer

[Served as full instructor and did curriculum development for each course.]

CIVE 301 – Solid Mechanics (1 Section)

CIVE 302 – Solid Mechanics Laboratory (11 Sections)

CIVE 321 – Structural Analysis I (1 Section)

CIVE 608 – Earthquake Engineering (1 Section)

2015-2015 **Kleinfelder**

Assistant Bridge Engineer / Intern

Publications

Dowell, R.K. and **Johnson, T.P**. (2011). "Shear and Bending Flexibility in Closed-form Moment Solutions for Continuous Beams and Bridge Structures." *Engineering Structures*. Vol 33, December 2011, pp. 3238-3245

Dowell, R.K. and **Johnson, T.P**. (2012). "Closed-form Shear Flow Solution for Box–Girder Bridges under Torsion." *Engineering Structures*. Vol 34, January 2012, pp. 3238-3245

Johnson, T.P.; Dowell, R.K.; and Silva, J.F. (2016). "A Review of Code Seismic Demands for Anchorage of Nonstructural Components." *Journal of Building Engineering*. Vol 5, pp. 249-253.

Johnson, T.P. and Dowell, R.K. (2017 - Acceptance Pending Revisions). "Evaluation of the Overstrength Factor for Nonstructural Component Anchorage into Concrete via Dynamic Shaking Table Tests." *Journal of Building Engineering*.

Johnson, T.P.; Dowell, R.K.; and Silva, J.F. (2017 – Acceptance Pending Revisions). "Recommendations for Ω0 for Anchorage into Concrete for Upright Nonstructural Components." *J. Struct. Eng*.

Johnson, T.P. and Dowell, R.K. (2017 – Acceptance Pending). "Single Node Stiffness Formulation for Rocking Cantilever Structures with Inelastic Anchorage." *Computers & Structures*.

Awards

2009	Invitee, California Transportation Federation Symposium
2011	Structural Engineers Association of San Diego Student Scholarship
2011	SDSU Stone Award for Outstanding Civil Engineering Student

Professional Licensure

Engineer-in-Training, California #137533

ABSTRACT OF THE DISSERTATION

Evaluation of Seismic Overstrength Factors for Anchorage

into Concrete of Nonstructural Components

by

Timothy Paul Johnson

Doctor of Philosophy in Engineering Sciences (Structural Engineering)

University of California, San Diego, 2017
San Diego State University, 2017

Professor Robert Dowell, Co-Chair
Professor Tara Hutchinson, Co-Chair

During earthquakes, nonstructural components and other objects of sizeable mass attached to building structures may be subjected to significant levels of seismic excitation. These systems require engineered anchorage systems to resist imposed demands, with the earliest attempts to produce qualitative and quantitative metrics for this process taking place in the early 1990s. Over the next two and a half decades, the provisions the design engineer must follow for determining a suitable anchorage system have rapidly expanded, and while some topics have been thoroughly researched and documented, others have not. One such term, the overstrength factor Ω_0 used to modify code demands for ductile versus non-ductile anchorage

into concrete for tension-dominated systems, has suffered from particularly sparse academic and scientific background. The first portion of this dissertation establishes a scientific framework for evaluating existing code values of Ω_0 by means of two full-scale testing programs on anchorage systems using a shaking table. Both real earthquake and broadband earthquake motions are used in the testing sequences, and four different major anchorage force-displacement responses are considered: brittle linear-elastic behavior with large initial stiffness, highly plastic ductile behavior with comparable initial stiffness to the brittle anchor, soft elastic behavior with large displacement capacity, and a pull-through anchor with non-material-based plastic response characteristics. Results from these different anchor types are compared and benchmarked against expected code performance standards.

The second portion of this dissertation presents a highly efficient, customized numerical analysis tool that was developed for simulating the seismic response of seismically-driven oscillators with translational and rotational mass degrees of freedom. This program is validated against the structural testing results and existing finite element programs, and offers run times three orders of magnitude faster than standard analysis methods. Detailed parameter studies are then performed looking at both upright and hanging components, targeting specifically the appropriate values of Ω_0 which result in intended system performance.

The structural testing and analytical results are then compiled into recommendations for existing code guidelines related to Ω_0. Discussion is provided regarding existing ductility provisions for anchorage into concrete, specifically with respect to the expected benefits versus the real and measured benefits of ductile anchor response.

CHAPTER 1: INTRODUCTION

1.1 – Motivation for Research

The primary goal of this research was to investigate current design code provisions for tension-dominated anchorage that attaches non-structural components and systems (NCSs) to concrete. NCSs may experience significant inertial loading during seismic events, and anchorage systems must be engineered to ensure intended performance features of the component can be met both during and following earthquakes. Precedent for modern anchor performance standards is described by Drake and Bachman (1996), in which they detail the philosophy behind the newly-introduced NCS lateral design force equation presented in the 1994 National Earthquake Hazard Reduction Program (NEHRP) provisions. This equation has remained essentially untouched over the past two decades, and while anchorage does not explicitly appear in any of its terms, Drake and Bachman state that "component anchorage ductility and energy absorption" was one of seven key performance criteria that the design equation was intended to fulfill.

In the aftermath of the 1989 Loma Prieta and 1994 Northridge earthquakes in California, significant research efforts took place on the west coast of the United States to develop new performance standards to strengthen structural members against imposed seismic demands. A wealth of empirical evidence from these programs pushed for widespread adoption of ductility- and displacement-based designs, which have since become standard practice in the seismic design of building structures. Connection detailing at the interface between structural members became a particularly important topic, such as beam-to-column joints in steel frame structures (Gilton and Uang, 2002; Bruneau et al., 2011) and plastic hinge regions in reinforced concrete

structures (Priestley et al., 1996). Given the many similarities between NCS and building structure performance from the perspective of structural dynamics theory, philosophical treatment of the design process of NCSs has largely followed in the footsteps of building structures; namely, it is presumed that ductile response provides significant benefit to seismic performance, and non-ductile response of seismically-critical elements should be discouraged and limited as much as possible.

Design provisions for anchorage into concrete are provided by the American Concrete Institute (ACI) in the code document *ACI-318: Building Code Requirements for Structural Concrete*. Provisions specific to anchorage into concrete are handled by ACI 318-14 Chapter 17, which was formerly ACI 318-11 Appendix D when this research program began. Primary focus of this dissertation was placed on requirements in ACI 318-11 Appendix D Section 3.3.4, which prescribes different options the engineer has in designing tension-dominated anchor systems via the application of ductile and non-ductile anchorage. Foremost among code requirements is the application of a penalty factor, Ω_0, on non-ductile anchorage, which mandates that non-ductile anchors be designed for 2.5 times the lateral earthquake force as ductile anchors to ensure strictly elastic response at load levels well below yield. This factor has been the subject of a great deal of contention within the structural engineering community, as it stems from empirical observation and internal code committee discussions rather than experimental study (this is discussed in detail in Section 1.4).

The primary goal of the body of work presented within this document was thus to develop a scientifically-based assessment of Ω_0 and evaluate the extent to which philosophical assumptions about the benefits of ductility in NCSs with tension-dominated anchorage systems are correct.

1.2 – Performance of Tension-Dominated NCS Anchorage

NCSs have a broad range of categorization that typically falls under one of three branches: architectural components, mechanical components, or building contents. Specific subcategories beneath the wings of these broad branches – such as electrical cabinets, heavy HVAC equipment, and telecom racks – require high performance anchorage systems to resist imposed seismic demands. Quantification and qualification of the economic and social impacts of NCS damage began to be documented in earnest around the time of the 1971 El Centro earthquake, where structures such as the iconic Olive View Hospital in Los Angeles showed a wide range of structural and nonstructural deficiencies (EERIC, 1971). Specific mention was made to the performance of slender NCSs, such as boilers, which had failed anchorage and relative horizontal movement upwards of four feet. This particular hospital was also subjected to the 1994 Northridge earthquake where, despite improved structural performance (Celebi, 1997), severe NCS damage such as ruptured roof-mounted water tanks was observed (Tokas, 2011).

More recent major seismic events have shown that shortcomings still exist with regards to these types of NCSs. A strong example can be taken from the 2011 Christchurch earthquake in New Zealand, where anchor failure caused the uplift and lateral movement of 25,000 lb industrial equipment with resultant lateral displacements of around three feet (Gould and Marshall, 2012). Recent studies have shown the construction process often leaves the seismic design of nonstructural components diffused between architects, engineers, contractors, and owners, resulting in poor detailing and inadequate anchorage of critical NCS systems (Perry et al., 2009). Still other studies from Christchurch show significant damage to large vertical facades and partition walls, with the latter experiencing widespread anchor failures (Baird et al., 2012).

Parallels to this performance can be seen in the 2010 Haitian earthquake, where evaluation of large electrical switchboxes showed significant damage for poorly anchored cabinets but minimal damage for well-anchored cabinets (Goodno et al., 2011). Similar documentation can be found for the 2010 Chilean earthquake, which showed well-anchored systems performed admirably while unanchored or poorly anchored systems showed considerable damage (Soules et al., 2016). This could be seen in suspended systems as well as floor-mounted systems, and poor communication between engineers, contractors, and owners was linked to several observed NCS failures (Miranda et al., 2012).

Despite the philosophical intent of ductile anchor behavior to provide beneficial seismic response, performance of anchors relative to this design criterion is not well understood. The logistical thought process behind anchor design is summarized by Silva and Hoehler (2008), where it is noted the design philosophy for anchorage adopted in the 2006 IBC, ASCE 7-05, and ACI 318-05 design codes – which saw the first major expansions of seismic criteria in the design process – comes largely from empirical observation. Specifically, non-ductile anchorage systems typically showed catastrophic failure mechanisms, while many ductile anchorage systems had significant, observable plastic elongation. Arguments in favor of the benefits of ductile anchorage can be seen in many sources, such as Wey et al. (2010), who cite the principles of response modification as a major incentive for the use of ductile anchors. These types of recommendations imply an expected reduction of lateral force acting on the NCS, and assume that equivalent elastic displacements and plastic displacements can be related via the equal displacement principle. Unfortunately for design engineers, the actual code language and documentation for implementing this design philosophy was dispersed across multiple documents released at asynchronous intervals until ACI 318-11, and attempts to harmonize the

language into a single document required several cycles of multiple independent code documents to achieve (Silva, 2010).

As knowledge of subpar performance has grown, the design of NCSs has expanded to incorporate a great deal of development of prequalification procedures for evaluating NCS behavior under seismic loads. These prequalification procedures are governed by the AC 156 loading protocol, which subjects components to a "broadband" earthquake motion intended to represent upper-bound seismic demands for a given design level. This protocol is typically implemented on a tri-axial shaking table, such as UB-NCS at the University of Buffalo or the Richmond Field Station at the University of California, Berkeley (Mosqueda, 2009). Prequalification testing is typically performed by the NCS manufacturer, and mounting to the table is intended to represent a system designed with minimally-designed anchorage. No further detail is required for anchorage, other than it is expected to simulate realistic field installation conditions. Prequalification of post-installed anchors is performed independent of this process, as recommended by ACI 355.2-07 for mechanical anchors or ACI 355.4-11 for adhesive anchors.

To the author's knowledge, no research has been undertaken studying component-anchorage performance as a coupled system to specifically target ductile versus non-ductile anchorage behavior. Some attempts have been made to perform analytical modeling (Rustogi and Gupta, 2004) of the component-anchor system benchmarked against structural tests, which have noted that conventional finite element modeling assumptions of anchors providing fixity to the NCS is inaccurate, but these testing programs do not specifically target design code guidelines and simply act as case studies. This body of work thus provides the first comparative metrics to evaluate the benefit of ductile anchor versus non-ductile anchorage performance with respect to existing design code provisions.

1.3 – Current Anchor Design Philosophy

Design for anchorage into concrete is currently handled by a combination of two code documents: ASCE/SEI 7 and ACI 318. ASCE 7 governs the magnitudes of the demands to which the anchorage system and component are to be subjected, while ACI 318 defines anchor performance criteria and determination of anchor capacities. When work on this dissertation started, ACI 318-11 was a newly released code document, and provisions for anchorage were handled in Appendix D. ACI 318-14 recognized the increasing level of complexity in the anchorage design process, however, and Appendix D was consolidated into the newly-formed Chapter 17. This was largely a structural change in the format of the code document, and the topics relevant to this dissertation were unchanged between versions.

Anchor design philosophy borrows largely from the capacity design process for building structures, and can be visualized in a similar manner. Figure 1-1 displays the equal displacement principle as it is applied to building structures, which posits that the fully nonlinear response of a structure can be related to an equivalent elastic response assuming that displacements between the two are equal. Theoretically, this principle is valid for systems with natural frequencies of vibration < 2 Hz, but its applicability varies as systems begin to respond in the higher frequency range (Newmark and Hall, 1982). Building structures typically respond at frequencies at or much lower than 2 Hz due to their geometrical and spatial distribution of structural members, and thus the validity of the equal displacement principle is rarely questioned.

The equivalent elastic response in a structure is given by the force level $V_e = S_{DS} \cdot W$, where S_{DS} is the short-period design spectral acceleration and W is the total structural weight. This idealized behavior is represented by the $K_{elastic}$ line in Figure 1-1; the real structural response, however, is denoted by the red line. It can be observed that the system will never

reach V_e, as it will yield at some lower shear force, V_s. The real structure's elastic response is thus scaled down by the response modification factor, R, which is the ratio of these two shear forces. To compensate for hardening effects post yield, which can result in system forces being higher than a simple assumption of the real structure behaving elasto-plastically immediately after yield, the first yield force V_s can be scaled back up to the ultimate force associated with this elasto-plastic idealization, V_y. The ratio of this overstrength is denoted by the overstrength factor, Ω_0, which is simply the ratio of V_y / V_s. These values are typically derived via empirical means, and assume a great deal of structural redundancy. Proper application of this theory allows a designer to reasonably capture nonlinear structural behavior using elastic analysis, which greatly reduces the time, complexity, and cost of the design process.

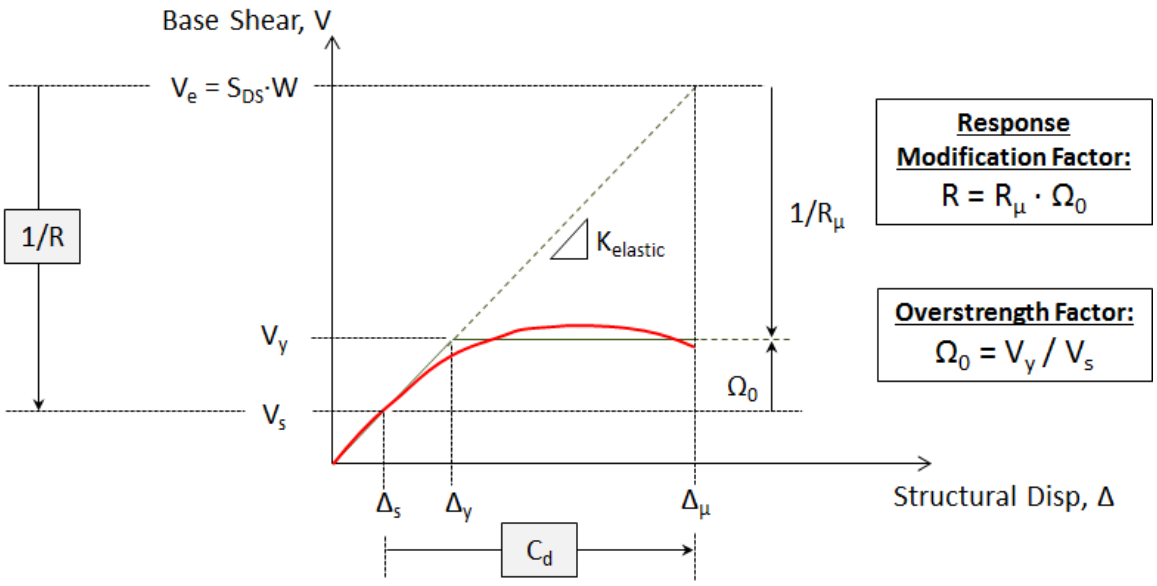

Figure 1-1: Diagram of Code Design Process for Displacement-Based Design Principles

The above process is adapted into equation form for NCSs using Equation 13.3-1 in ASCE 7-10, which is shown below in Eq. 1-1. Nonstructural components are distinguished from building structures by subscripting relevant values with "p". The NCS design force is conceptualized as the equivalent linear response, V_e, reduced based on the nonlinearity of the system to a force level of V_s. This reduced force is represented by $V_s = F_p$.

$$F_P = \frac{0.4a_p S_{DS} W_p}{\frac{R_p}{I_p}} \left[1+2\left(\frac{z}{h}\right)\right] \qquad \textbf{(1-1)}$$

Each part of Eq. 1-1 can be related to the concepts presented in Figure 1-1 and the spectral acceleration design curve from ASCE 7-10 shown in Figure 1-2. The equivalent elastic design force of the component is designated by the term $V_e = S_{DS} \cdot W_p$, where W_p is the component's seismic weight. This force is then reduced by the response modification factor, R_p, with the system importance factor, I_p, allowing for less reduction in design forces (and thus higher anchor demand forces) for critical NCSs. Two other adjustments unique to NCSs are then added to the equation, namely $0.4a_p$, where a_p is the component amplification factor, and $1 + 2(z/h)$, which is a floor location factor of the component within the building. Sufficiently stiff components, defined in ASCE 7-10 to be those with first mode natural periods $T_n \leq 0.06$s, are designed at a force level equivalent to that of the peak ground acceleration, $0.4S_{DS}$. Conversely, $1 + 2(z/h)$ is a rough approximation of a first-mode response of the building structure, with the assumption that accelerations increase linearly up the building height to a maximum of three

times the ground acceleration at the roof level. There is currently some debate about the appropriateness of several current parameters, which is discussed in more detail in Section 1.5.

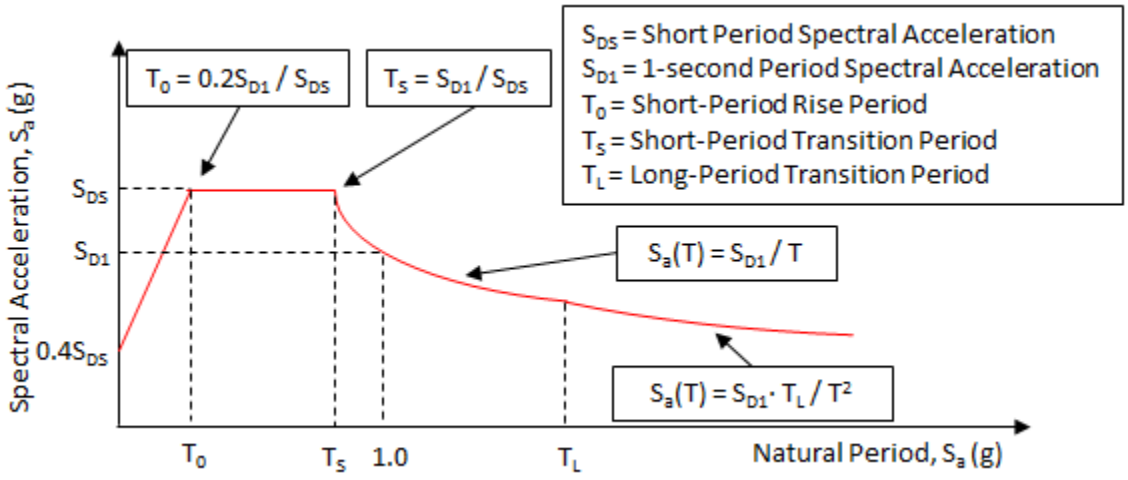

Figure 1-2: ASCE 7-10 Spectral Acceleration Design Curve

Once the designer has determined this lateral demand force acting on the component, the component can be designed using the standard LRFD load factor equations in ASCE 7-10 12.4.3.2 where the redundancy factor, ρ, is set equal to 1. These are given by the formulations in Eq. 1-2.

$$(1.2+0.2S_{DS})D+\rho F_p+L+0.2S$$
$$(0.9-0.2S_{DS})D+\rho F_p+1.6H \quad \textbf{(1-2)}$$

A conceptual complication arises when the designer is asked to design the anchorage for this system, however. ASCE 7 defers the designer to ACI 318 for design of anchorage into concrete, and within ACI 318 the designer is required to perform an evaluation of the ductility

characteristics of the anchors being chosen for the design. If the designer can meet all required criteria, the seismic demand force is simply taken to be F_p; if not, the designer is referred back to the load factor equations with an amplified lateral design force, $\Omega_0 F_p$.

$$(1.2+0.2S_{DS})D+\Omega_0 F_p+L+0.2S$$
$$(0.9-0.2S_{DS})D+\Omega_0 F_p+1.6H \quad \textbf{(1-3)}$$

The load factor equations in Eq. 1-3 are identical between building structure and NCS design, but Ω_0 represents different physical phenomena for each of these cases. For building structures, Ω_0 represents expected overstrength caused by redundancy of numerous nonlinear mechanisms in the building which represent gradual softening as elements yield in succession. For anchors, however, Ω_0 represents a protection factor for non-ductile anchors, as it is assumed that non-ductile anchors perform more poorly than ductile anchors under seismic loading conditions.

This implementation of Ω_0 has some benefits and some drawbacks. The primary advantage of sharing load factor equations is that the application of Ω_0 is familiar to the structural engineer, and no new notations or load factor equations need to be introduced into code documentation. A major disadvantage to this presentation, however, is that Ω_0 for anchorage design is used in a way that is conceptually different from Ω_0 for building structure design, resulting in a great deal of confusion as to where the factor comes from or what the factor represents.

In the original revisions of ASCE 7-10 and ACI 318-11, when Ω_0 was first introduced to anchor design via code language, no values of Ω_0 were given to designers to use. This was amended in Supplement No. 1 of ASCE 7-10, which provided a simple step function based off R_p where $\Omega_0 = 1.5$ for $R_p \leq 2.0$, and $\Omega_0 = 2.5$ for $R_p > 2.0$. The relationship to R_p, the prescribed Ω_0 values, and the location of the step were selected somewhat arbitrarily and have no existing scientific basis outside of the precedent discussed in Section 1.4. These values were recommended simply as placeholders until the work performed in this dissertation could be completed.

1.4 – History of Ω_0 in Code

The earliest form of a factor to address anchors with non-ductile failure modes has its roots in the ACI 349 Appendix B nuclear design code. Industry research performed in the 1980s and 1990s showed that groups of ductile anchors allowed for redistribution of forces during severe loading cases, and thus elastic theory provided for conservative analysis and design of anchor systems. If the designer was not able to achieve ductile performance of anchors, a penalty factor was assessed; while the exact value evolved over time, ACI 349-01 RB.3.6.3 gave this penalty value as 0.6 multiplied by the equivalent ductile anchor force capacity. Several other baselines were provided with this code, such as a minimum anchor elongation of 14% required for ductile anchor classification, that were adopted over time into the ACI 318 Appendix D provisions for ductile anchorage.

Outside of the nuclear arena, multipliers on anchor forces for nonstructural components first surfaced in the 2003 NEHRP Provisions in Section 9.2.2.8.4, which stated "…the attachment

that the anchor is connecting to the structure shall be designed so that the attachment undergoes ductile yielding…or the minimum design strength of the anchors shall be at least 2.5 times the factored forces transmitted by the attachment." The 2.5 factor arose from internal committee discussions and was intended to represent the difference between a fully elastic response spectrum and the design value that incorporates inelastic action, etc. Including the factor as a multiplier on the applied force (as opposed to providing a force reduction factor for ductile anchors) was intended to encourage the use of anchors that could be viewed as ductile for tension-dominated systems.

While this 2.5 factor was beginning to take form in NEHRP, independent developments were occurring in the ASCE 7 Seismic Subcommittee's Task Committee 8 (TC-8) to distinguish between ductile and non-ductile anchor performance. A fundamental goal of TC-8 at this time was to generate specific wording for an anchorage ductility requirement, but the approach was to modify anchor demand forces instead of anchor capacity. The first attempts to do this were in ASCE/SEI 7-05 Section 13.4.2, which took the 1997 NEHRP Provisions and reworded the demand requirements to incorporate certain penalties if ductility specifications could not be met. This section provided demand values to be taken as the lesser of two items: (a) the anchor design force including a 1.3 overstrength multiplier on the component design force or (b) the maximum transferrable force provided by the component or any of its attachments. In addition, a penalty was imposed on the component if the attachment could not be shown to yield at design force levels, or if the anchor could not be shown to be ductile. The penalty took the form of a limit on the value of R_p to be used for the design of the anchorage. The value of 1.5 was selected with reference to the 1994 NEHRP provisions, which characterized components having R_p values of 1.5 as "brittle or buckling failure modes" and those assigned R_p values of 3.0 as "[having] some

minimal level of energy absorption capability." Thus, the anchorage of a component subject to the "R_p penalty" would be designed for a horizontal earthquake force increased by a factor of $R_p/1.5$.

At the time these provisions were developing, R_p values of 2.5 to 3.0 were considered standard for normal nonstructural components, which meant that a limitation of R_p for non-conforming anchors would double the typical anchor demand force found from the component demand force equation. Taking into account the mandatory overstrength factor of 1.3 times the component design force, this generated an increased effective demand multiplier on the anchor of 1.3 x (3/1.5) = 2.6 ≈ 2.5. It should be noted, however, that the 1.3 multiplier is applied to the calculated anchor force including the effects of gravity and the vertical acceleration, whereas the R_p penalty is effectively a multiplier on F_p only. In fact, however, the R_p values for many components were increased in ASCE 7-05 along with an attendant increase in a_p. So while the ratio of a_p/R_p remained roughly equal, the impact of the R_p penalty was unintentionally exaggerated, particularly for piping systems having R_p values of 6 or greater. This situation was exacerbated by a series of errata that were subsequently applied to the paragraph in question. The impact of the errata was to essentially eliminate the R_p penalty for most cases, thus reducing the multiplier to 1.3.

The application of penalty factors directly to anchor capacity was of particular issue for anchorage design while considering the dead load of systems, which – when multiplied by 2.5 – created problems in satisfying other anchorage criteria specified by ACI 318. While the provisions in ASCE/SEI 7-05 did not have this problem, basing penalty factors on R_p was difficult to implement and suffered from significant perception problems. This posed some conceptual difficulties as well, as it implied R_p was effectively a measure of ductility capacity; realistically

speaking, however, R_p is a rational factor derived to approximate nonlinear behavior between yield and ultimate conditions using an equivalent linear-elastic force level. In the development of the equivalent force and displacement methods, Newmark and Hall (1982) caution against the treatment of the response modification factor as a logical substitute for displacement ductility, especially for systems having a natural frequency in excess of 6 Hz. With the vast majority of nonstructural components responding in the high frequency range of the response spectra (Watkins, 2011), this created considerable levels of concern.

The seismic provisions in ASCE/SEI 7-05 were, at this point, quite new, as the transition from the 2002 to 2005 versions expanded ASCE/SEI 7-02's single seismic chapter (Chapter 9) into twelve separate chapters (Chapters 11-22), with the inclusion of a specific chapter for nonstructural component design (Chapter 13). For ASCE 7-10, a decision was made in TC-8 to move away from R_p-controlled parameters for encouraging ductile anchorage. In the interim between ASCE/SEI 7-05 and ASCE/SEI 7-10, a non-ductile penalty was implemented in ACI 318-08. The approach was similar to that present in the 2003 NEHRP provisions, stating that anchorage ductility requirements need not be met if anchor design force capacity was reduced by a factor of 0.4, thus transferring the penalty from the demand side of the equation to the capacity side. Defining "N" as the tensile capacity of an anchor, this resulted in the ASCE 7-05 load factor equations taking the form seen in Eq. 1-4.

$$0.4\emptyset N_{min,anchor} = (1.2+0.2S_{DS})D+F_p+L+0.2S$$
$$0.4\emptyset N_{min,anchor} = (0.9-0.2S_{DS})D+F_p+1.6H \quad \textbf{(1-4)}$$

At the beginning of the 2010-2011 code cycle it was recognized that the application of a multiplier to the anchor force was incorrect, as it simultaneously amplifies all components of the load case. For nonstructural components, this typically means that the weight of the component is increased along with the vertical earthquake force. To address this problem, the overstrength factor, Ω_0, was invoked as a substitute for multipliers on anchor demand and/or strength. While it was recognized that the overstrength concept associated with Ω_0 for buildings cannot strictly be applied to the anchorage problem, the manner in which overstrength is applied in the ASCE 7 provisions provides the correct framework for addressing the design of anchors that are not otherwise protected against premature failure. Thus, it was decided in the relevant subcommittees of ASCE 7 and ACI 318 to adopt the use of Ω_0 for the design of so-called "non-ductile" anchorage in concrete and in masonry, and to remove other provisions relating to multipliers on anchor demand or resistance for cases involving seismic loads. As noted earlier, ASCE/SEI 7-10 retains a maximum R_p of 6 to ensure that anchor demands for high-R_p components (notably ductile pipe) are not reduced to unconservative levels.

Early discussions within TC-8 for the ASCE/SEI 7-16 code cycle considered possible reductions of Ω_0 values for several types of nonstructural components, and a reduction from 2.5 to 2.0 for many components was recently ratified when ASCE/SEI 7-16 was passed as the latest version of the code document.

1.5 – Potential Shortcomings of the F_p Equation

Many recent studies have demonstrated potential inaccuracy in the terms prescribed by the F_p equation given previously in Eq. 1-1. As will be discussed in detail in Chapter 7, error in these values may be – unintentionally – counteracted by the application of Ω_0. This section will briefly discuss each contended term, and provide references to sources which describe the problems in greater detail.

- Component Amplification Factor, a_p:

  Current prescriptions of a_p vary the term discretely between values of 1.0 and 2.5. Research that developed the original a_p values observed amplification greater than 2.5 (Soong et al., 1993), but a maximum of only 2.5 was proposed due to expectations that nonlinearity in the building response will shift the NCS and the building out of phase should amplification in excess of 2.5 be experienced. Fathali and Lizundia (2011) note that these values are considered generally conservative, but are known to be on occasion unconservative for building structures with periods of $0.5s \leq T_n \leq 1.5s$. They prescribe a spectral-shaped variation of a_p in place of the step function, with variations between $a_p = 1.0$ to $a_p = 3.0$. This allows for larger a_p values for shorter period structures (a_p closer to 3) that experience amplification, and reduced a_p values for longer period structures consistent with observations from experimental and measured earthquake data (a_p closer to 1).

  Singh et al. (2006b) propose several changes to the F_p equation, recommending a merger between a_p and the floor acceleration factor $(1 + 2 \cdot z/h)$. From this convolution term, they suggest an equivalent upper bound of $a_p = 6.0$, but propose a more rigorous calculation method of a_p that includes a combined building and NCS response to allow

for smaller values. Also noted in their study is the general adequacy of $a_p = 2.5$, but that it can be unconservative. It is worth noting that nonlinear building behavior was not considered as part of the study.

Smith and Dowell (2010) performed a detailed study using an anchored NCS model mounted on a nonlinear building at varying floor levels. Their results largely mirror the spectral shapes recommended by Fathali and Lizundia (2011), with peak values of a_p noted just below $a_p = 6.0$ and many ordinates in the range of $a_p = 3.0$ to $a_p = 4.0$. Also noted is that a_p values drop below the recommend values in ASCE 7-10 when building periods are larger than $T_n = 1.5s$; this is also in agreement with Fathali and Lizundia (2011).

- Floor Acceleration Factor, $(1 + 2 \cdot z/h)$:

ASCE 7-10 currently prescribes a linear variation of amplification up the height of the structure, valued at 1.0 when z = 0 and 3.0 when z = h, where z is the location of the nonstructural component along the elevation of the building and h is the elevation of the roof level. Miranda and Taghavi (2009) demonstrate a general inadequacy of a maximum value of 3.0 for short-period buildings ($T_n = 0.50s$ in their study), with amplification reaching as high as 4.0. Values were largely dependent on both first and second mode natural periods of, and with the relative flexural and shear rigidity terms of the building. While not addressing a_p directly, they make note of building amplification at the floor levels, and present equivalent a_p values as high as 5.0 in their case study.

In their companion paper to Singh et al. (2006b) – which presents the a_p and $(1+2 \cdot z/h)$ convolution model – Singh et al. (2006a) also present a discussion of floor

accelerations along building height. As with Miranda and Taghavi (2009), they note building characteristics and damping play a substantial role on expected roof amplification. Short period buildings with $T_n \leq 1s$ tend to have amplification at the roof in excess of 3.0, with values around 3.4 for a damping ratio of 5% to upwards of 7 for a damping ratio of 0.5%. Ultimately, they propose a period-dependent floor amplification curve, with a maximum of 4.0 for short period buildings.

Lepage et al. (2011) used a modular shaking table setup with 30 multi-story scaled building models to study floor amplification. Test structures ranged between 6 and 10 stories with a variety of potential plastic hinge locations in both beams and columns and both regular and irregular buildings were considered. Their findings generally replicated the 1997 UBC equation, which posits a linear variation between 1.0 at the ground level to 4.0 at the roof level. In slight modification to this formulation, they add an additional conditional term to allow for reduction of amplification at the roof level depending on the extent of nonlinearity in the building.

- Response Modification Factor, R_p:

While the other terms in the F_p equation can be studied explicitly from building and ground motion characteristics, the response modification factor is a function of the nonlinearity of a specific NCS. As such, determination of R_p is component-dependent, and values are typically taken directly from Tables 13.5.1 and 13.6.1 of ASCE 7-10. Prescribed values for R_p vary significantly, ranging from 1.5 to 12, and to the author's knowledge minimal academic study exists regarding R_p directly. These values are notably higher than early recommendations by Soong et al. (1993), which range from 1.0 to 3.0 with a recommendation that R_p values be generally limited to no more than

2.0. Due to the difficulty of capturing NCS nonlinearity, Sankar. and Medina (2007) studied a floor-level response modification factor termed R_{acc}, which accounts for reductions in floor demand due to building nonlinearity but assumes an elastic NCS. They do not directly address R_p, however, indicating that – much as values of Ω_0 developed behind closed doors – so too have values of R_p.

1.6 – Scope of Dissertation

This dissertation evaluates the existing code prescriptions for ductile versus non-ductile anchorage design and the appropriate Ω_0 "overstrength factor" for various different anchor types. It is arranged into the following chapters:

- Chapter 1 provides discussion of the existing design philosophy in code for anchorage design, as well as a history of the factor being studied due to a lack of pre-existing academic literature on the subject.
- Chapter 2 details the experimental setup of an idealized NCS to be used in shaking table tests, along with detailing the specimens to be tested. It synthesizes a wealth of pre-existing structural testing data developed over several years prior to this research program, and adapts it into the framework of a new testing program to target code performance levels.
- Chapter 3 outlines a structural testing program that aimed study specifically how various anchor systems performed compared with their assumed performance per current code guidelines. The overall testing program and the process governing how pre-designed anchors were mapped against code design guidelines are discussed at length.

- Chapter 4 presents a detailed breakdown of the structural testing program performed, and compares anchor performance at both the anchor and component level.
- Chapter 5 outlines problems encountered attempting to model the structural tests, and lays the groundwork for an alternative numerical solution outside of pre-existing software packages.
- Chapter 6 provides extensive validation of the numerical model presented in Chapter 5 benchmarked against structural testing results and other conventional structural analysis finite element toolsets.
- Chapter 7 presents a bulk of analytical parametric work to study the key influences on anchor performance relative to a wide range of system variables using hundreds of thousands of fully nonlinear time-history analyses.
- Chapter 8 documents the findings of the studies in Chapter 7 as related to recommendations for existing code documents. It also contains recommendations for future work that might be done to expand on that presented in this dissertation, both as they pertain to Ω_0 code implementation and as to further developing the analytical model used for the body of this work

Lastly, the primary goals of the research presented in this dissertation were to address the following three questions:

a. Field observations from recent seismic events have been a primary motivator for the development of ductility standards for nonstructural component anchorage. Do current provisions produce systems that perform as intended under severe seismic events?
b. Ductility standards were adopted for nonstructural components largely due to the breadth of knowledge and the wide array of scientific knowledge surrounding the

performance of building structures. Are analogous seismic performance considerations of nonstructural components appropriate, and does the current definition of ductility provide safe anchor designs versus their non-ductile counterparts? If not, what factors are relevant; if so, is ductility capacity the mechanism providing positive performance or are there more general parameters?

c. What values are appropriate for Ω_0? Are current system metrics for applying Ω_0 sufficient, or is more refinement appropriate? If current implementation is inaccurate or ineffective, how should Ω_0's implementation be changed to result in safe designs?

1.7 – Acknowledgement of Publications

Section 1.4 in this chapter is taken, with minor modification, from the following publication, of which the author of this dissertation assumes primary authorship:

Johnson, T.P.; Dowell, R.K.; and Silva, J.F. (2016). "A Review of Code Seismic Demands for Anchorage of Nonstructural Components." *Journal of Building Engineering*. Vol 5, pp. 249-253.

CHAPTER 2: SUMMARY OF TEST PROGRAM

2.1 – Idealized Nonstructural Component

A significant amount of testing equipment used for dynamic characterization of the nonstructural component anchorage discussed in this chapter was developed by Watkins et al. during a series of structural tests performed at UCSD and SDSU from 2008 – 2010. The work of Watkins and the author of this dissertation were both sponsored by Hilti Corporation, under independent research contracts, designed to evaluate seismic performance of anchorage systems. The structural testing presented in this chapter took place from 2012 – 2014.

Development of the idealized nonstructural component and the anchors discussed in this chapter were done during the 2008 – 2010 research program, and were adapted to the 2012 – 2014 research program presented in this dissertation due to direct applicability to a different set of research goals. Though this chapter discusses most of the significant portions of these previous works as they apply to studying the Ω_0 factor, it is far from comprehensive, and the reader is encouraged to reference these other works for any inquiries about equipment details that have been omitted from this chapter. It should also be noted that Dr. Robert Dowell, the principal investigator for the research presented in this thesis and chair of the author's doctoral committee, was heavily involved with all work presented in this chapter that is not of the author's own creation. Some photographs used are to provide ease of reference and consistency between pre-existing documents, each of which Dr. Dowell is either a primary or co-author, and are used with his permission.

As part of the 2008-2010 research programs at UCSD and SDSU, two idealized nonstructural components were designed to represent statistical benchmarks established by a detailed survey of common equipment installations (Watkins et al., 2009). The first idealized component, called WALLE (Weighted Anchor Laboratory Loading Equipment), was designed for tension-dominated anchor loading that possessed two configurations: "flexible" and "stiff" based on modifiable component weight. A second idealized component, called the Shear Sled, was used for shear-dominated anchor loading; while not used within the scope of this work, tests performed by Scheidel (2010) provide detailed breakdowns of the shear behavior of several anchor types similar to those evaluated in the tensile testing programs. In particular, the N1 stainless steel anchor was identical between both tension and shear test programs, and the monotonic curves for both these responses are presented here for reference.

The provisions of ACI 318-11 Appendix D 3.3.4, which apply to the anchor overstrength factor Ω_0, are limited to the application of tension-dominated anchor systems; thus, WALLE was selected to best simulate appropriate loading conditions. Two options were available: the "rigid" configuration with a natural period of $T_n = 0.10$ seconds, and the "flexible" configuration with a natural period of $T_n = 0.22$ seconds for uncracked concrete. These definitions vary from the prescribed definitions "rigid" and "flexible" in ASCE 7-10 Chapter 11, which define rigid components as having a natural period less than or equal to 0.06 seconds and all other components as flexible, but are used in this chapter to provide continuity with Watkins' work. While both configurations of WALLE would thus be equally valid as flexible under code considerations, WALLE's "flexible" configuration was selected for the following reasons:

a. The overstrength factor for anchorage attempts to simulate the overstrength factor for building structures by emulating capacity protection principles. This application

assumes the equal displacement principle applies equally for nonstructural components as it does for building structures. A component configuration with a natural period closer to that of building structures was thus more desirable.

b. The component and anchor systems are assumed independent in the design process per ASCE 7-10 Chapter 13. WALLE's flexible configuration includes a significant second mode response due to the rotational mass inertia of its simulated mass, which could influence anchor demand forces.

c. The larger weight plate mass for the flexible configuration caused more tension in the anchors for a given ground motion than the stiff configuration. This allowed for all anchors to fail using ground motions within the capacities of SDSU's shaking table.

Watkins provides a thorough and comprehensive description of WALLE in his dissertation (Watkins, 2011), including relevant shop drawings and schematics for its many configurations. Numerical validation of WALLE as a model nonstructural component is also presented, and the reader is encouraged to reference this work for comprehensive documentation on the component's development; Sections 2.4, 5.4, and Appendix A of his work provide the most pertinent information to that discussed in this text. Neither WALLE's rigid configuration nor the Shear Sled were used in this research, so only the flexible configuration will be discussed herein.

Though Watkins states WALLE's first mode natural period in the flexible configuration to be 0.25 seconds as a general rule, it can be noted that the natural period changes slightly between uncracked and cracked concrete which have natural periods of 0.22 and 0.25 seconds, respectively. As this test program dealt strictly with uncracked concrete, a natural period of

0.22s is used in discussion as WALLE's natural first period. The theoretical weights and the measured weights for the systems varied slightly as well, with Figure 2-1 showing the measured values in parenthesis next to the theoretical weight. Typically, a weight of W_p = 2385 lb was used in applications related to the design of WALLE as a nonstructural component (representing what the designer might have as inputs), while the laboratory-measured value of W_p = 2550 lb was used for comparative analysis between analytical models and test behavior. The schematics in pictures (a) and (b) for WALLE are adapted from Hoehler and Dowell (2009), while picture (c) shows WALLE installed on SDSU's shaking table for this test program.

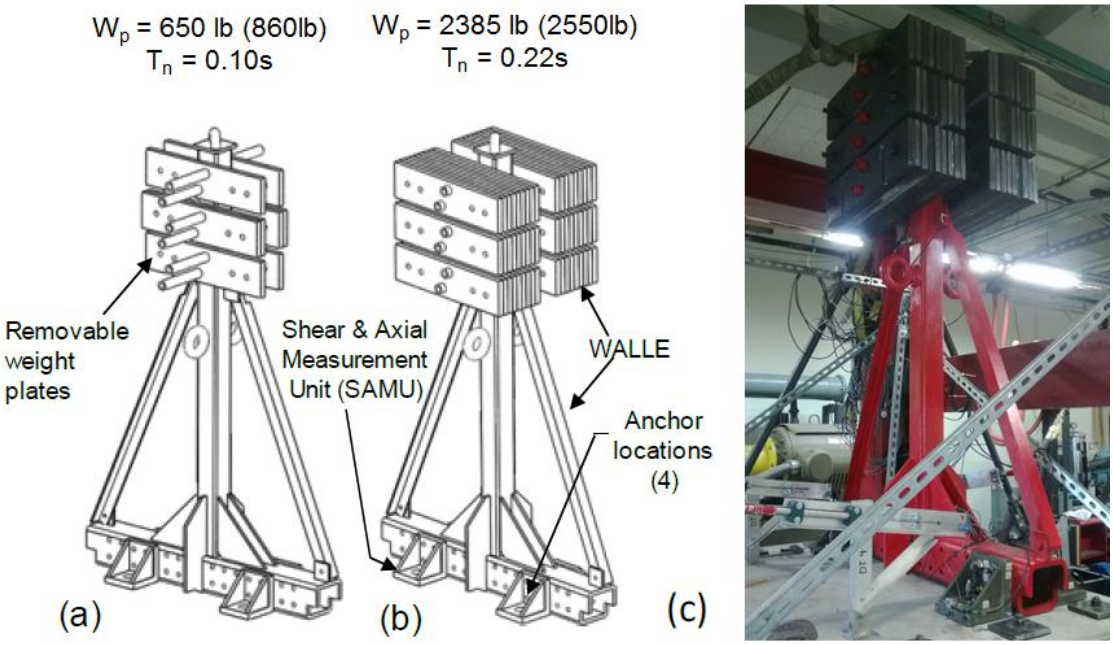

Figure 2-1: WALLE Possible Configurations for Model (a) "Rigid" and (b) "Flexible" Components from Hoehler and Dowell (c) Photo of WALLE Installed for Testing on SDSU Shaking Table

2.2 – SAMU Anchor Loading Devices

Specialized anchor loading and measurement devices were developed by Hoehler et al. (2011) which are capable of loading an anchor in tension and shear while measuring axial forces

/ displacements and shear forces / displacements. Termed Shear and Axial Measurement Units (SAMUs), they are capable of transferring both shear and axial loads to anchors. The SAMU fixture consists of a 6”x6”x1” A36 steel bracket cut into two equal legs of 6 inch length. A 1.5 inch diameter hole is drilled through the center of the bottom face to allow for the anchor to pass through, and a machined collar can be placed over the anchor to fill the hole with a small gap. A set of four pins are used to set the collar in place, which may or may not be instrumented, that also serve as the shear transfer mechanism. Dimensioning for the SAMUs is provided in Figure 2-2.

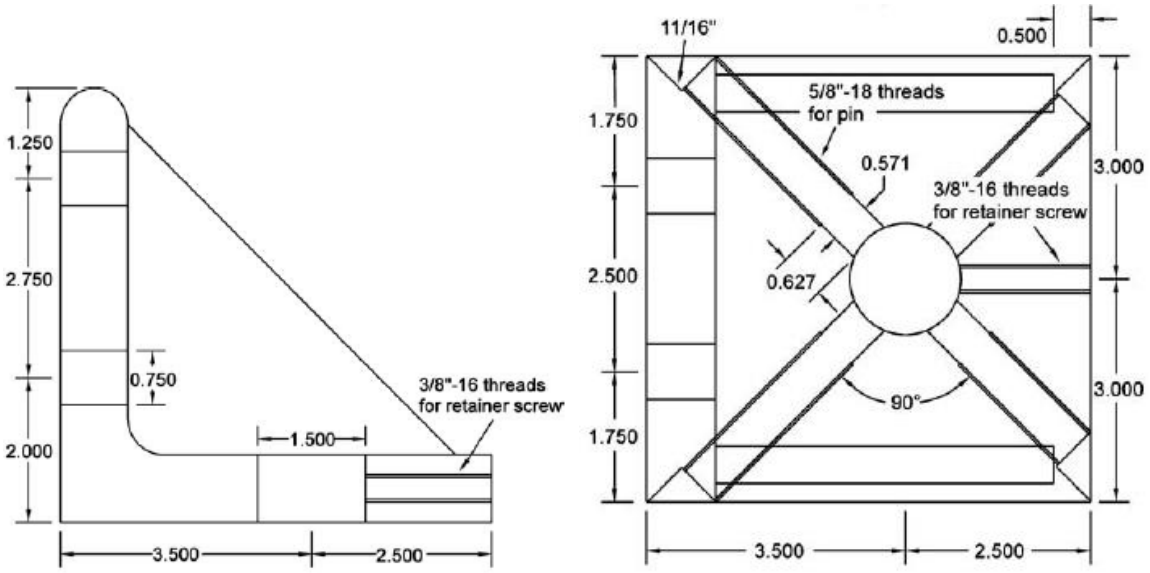

Figure 2-2: SAMU Fixture Detail for Elevation View (left) and Plan View (right) [from Hoehler et al. 2011]

Full instrumentation for the SAMUs allows for the measurement of anchor axial force, axial displacement, shear force, and shear displacement. Axial force is measured by means of a load cell placed over the anchor/collar combination, with spherical washers creating an orthogonal transfer of force to the anchor through the nut. Axial displacements are measured

via a Linear Variable Displacement Transducer (LVDT), which can be attached to the top of the anchor by a magnet. The magnets used were not strong enough to resist impact forces of the SAMU against the anchor, and so a heavy application of hot glue was used to insure fixity. A decision to omit shear measurement was made based on a combination of Watkins' findings that shear forces in the flexible WALLE were negligible, and that the instrumented pins were being used in other research projects for Hilti at the time. The pins require special hardening at the location of bearing on their tips, and fabrication of a second set of pins was determined to be beyond the budget of the project. Thus, in place of the shear pins, "dummy" pins were used to accommodate the appropriate shear transfer mechanism of the SAMU; these provide the same physical function, but are not instrumented to measure any response quantities. Figure 2-3 shows an example SAMU and instrumented anchor in place before a structural test.

Figure 2-3: SAMU in Installation Configuration

2.3 – Tested Anchor Types

Notations for anchors follow those used in the reference tests by Hoehler and Dowell (2009). The anchor type "N4" represented concrete breakout; however, due to the similar force-displacement response with the "N2" brittle steel anchors it was not included in the test program. These reference tests were accompanied by monotonic tests by Hoehler and Dowell (2010), and the combination of these two test programs provides a broad and extensive background for each specimen used in the experimental program presented in this dissertation. Information relevant to the adaptation of the anchors for a dynamic testing program is presented in Section 2.4.

2.3.1 – N1: Stainless Steel Thread Rod Anchor

The first anchor types were stainless steel thread rods, which were selected to represent ductile steel behavior and failure as well as large displacement capacity. Anchors were 3/8-inch (1 cm) thread rod, embedded in Hilti RE500-SD epoxy mortar with a bond length of 4 inches (10.2 cm). Total embedment depth was 6 inches (152 mm), with the 2 inches (51 mm) closest to the surface de-bonded using heat-shrink tubing. An additional two inches of free length were provided above the concrete surface to accommodate the SAMU and loading fixture, resulting in a total free length of 4 inches (102 mm). Total anchor length was approximately 8.75 inches (222 mm). The ductility ratio, measured as the ultimate displacement over the elastic yield displacement, was 130.

Figure 2-4 provides a photograph of this anchor, taken from Hoehler and Dowell (2010) for ease of reference to the characterization tests. Additionally, a to-scale schematic drawing is provided showing the anchor in its installed configuration.

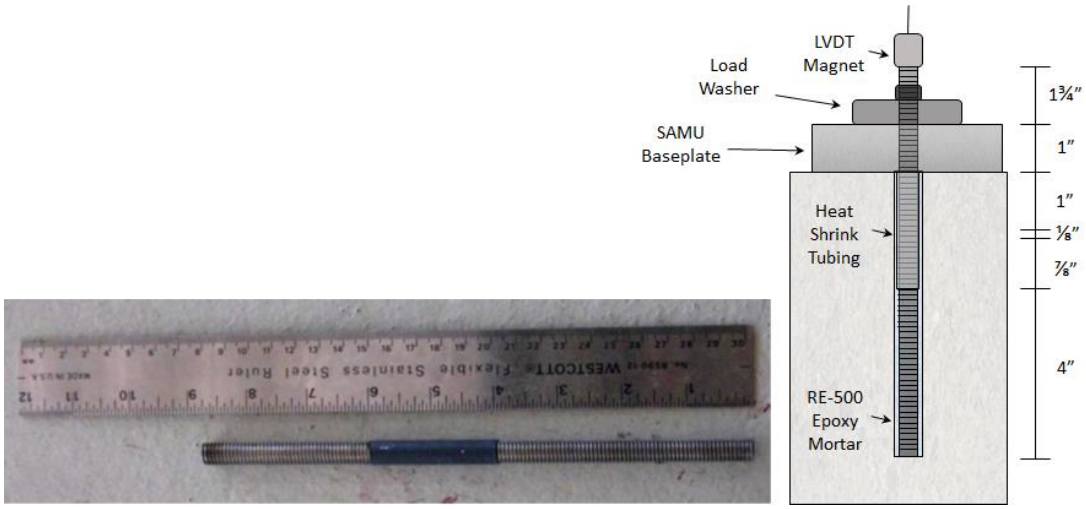

Figure 2-4: "N1" Stainless Steel Pre-installation Picture and Installation Schematic

2.3.2 – N2: B7 Steel Thread Rod Anchor

B7 thread rods (ASTM A193, 2009) were selected to represent non-ductile anchor failure and small displacement capacity. Anchors were 3/8-inch thread rod, embedded in RE500-SD epoxy mortar with a bond length of 4 inches. As B7 steel has a higher tensile strength than stainless steel, the cross-section was reduced over a short distance to allow for parametric comparison between anchors with similar ultimate forces. To provide a force capacity equal to that of the stainless steel anchors, and to ensure non-ductile behavior, the thread rod was notched to a diameter of 0.248 inches (6.3 mm) over a length of 1/8-inch (3.1 mm) using a CNC lathe. The 2 inches of length near the surface of the concrete were de-bonded using heat-shrink tubing. An additional 2 inches of free length were provided above the concrete surface to accommodate the loading fixture. Total anchor length was approximately 8.75 inches (222 mm). The ductility ratio, measured as the ultimate displacement over the elastic yield displacement, was 5.

Figure 2-5 provides a photograph of this anchor, taken from Hoehler and Dowell (2010) for ease of reference to the characterization tests. Additionally, a to-scale schematic drawing is provided showing the anchor in its installed configuration.

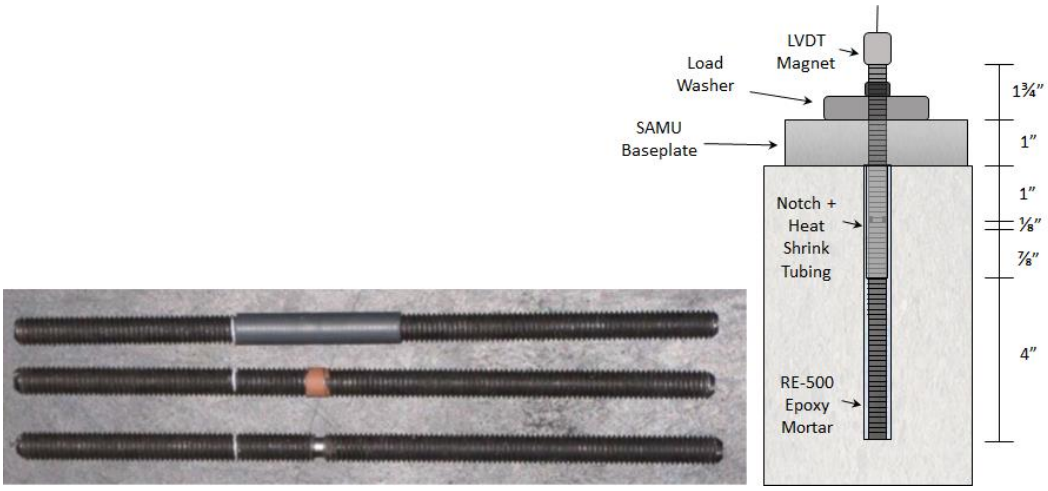

Figure 2-5: "N2" B7 Thread Rod Pre-installation Picture and Installation Schematic

2.3.3 – N3: B7 Steel Spring Anchor

Long B7 thread rods attached to rubber springs were selected to represent large deformation, linear-elastic behavior without ductile or nonlinear response. These were notched in the same manner as the non-ductile B7 thread rod, but no epoxy was used. Instead, the installation hole was drilled clear through the concrete slab, and rubber cylinders (ASTM D2240, 2005) with dimensions of 3-inch diameter by 3.25-inch length (76 mm by 82.5 mm) were attached to the ends of the rod on the underside of the slab. In addition, 4-inch-diameter (102 mm) steel bearing plates were used to mitigate effects of local load concentration on the concrete and spring. A ½-inch diameter hole was cored out of the center of the rubber spring. Force capacity of this anchor was based on the notched B7 strength, while the deformation capacity came primarily from the flexibility of the rubber cylinder positioned beneath the slab.

The ductility ratio, measured as the ultimate displacement over the elastic yield displacement, was 1.

Figure 2-6 provides a photograph of this anchor, taken from Hoehler and Dowell (2010) for ease of reference to the characterization tests. Additionally, a to-scale schematic drawing is provided showing the anchor in its installed configuration.

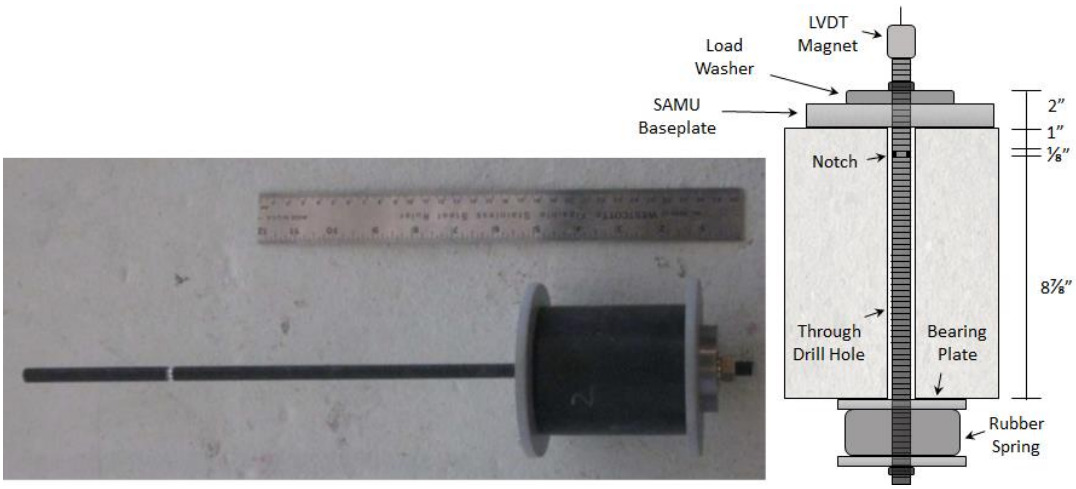

Figure 2-6: "N3" B7 Spring w/Fuse Pre-installation Picture and Installation Schematic

2.3.4 – N5: Expansion Anchor

Expansion anchors were selected to represent a nonlinear force-displacement response with a brittle failure mode. Attachment to the concrete was achieved by hammering the anchor into place, followed by applying an installation torque that caused its headed end to expand and grip the concrete with the aid of an expansion sleeve. The anchors were ½-inch by 7-inch (13 mm x 178 mm) galvanized steel bolts with a washer and hex nut on the free end for torque application. Expansion anchors were installed in 4.5-inch (114 mm) deep holes and hammered to an embedment depth of 3.75 inches (95 mm). An additional two inches of free length was provided above the concrete surface to accommodate the SAMUs and loading fixture. No epoxy

was used for these anchors. The ductility ratio, measured as the ultimate displacement over the elastic yield displacement, was 50.

Figure 2-7 provides a photograph of this anchor, taken from Hoehler and Dowell (2010) for ease of reference to the characterization tests. Additionally, a to-scale schematic drawing is provided showing the anchor in its installed configuration.

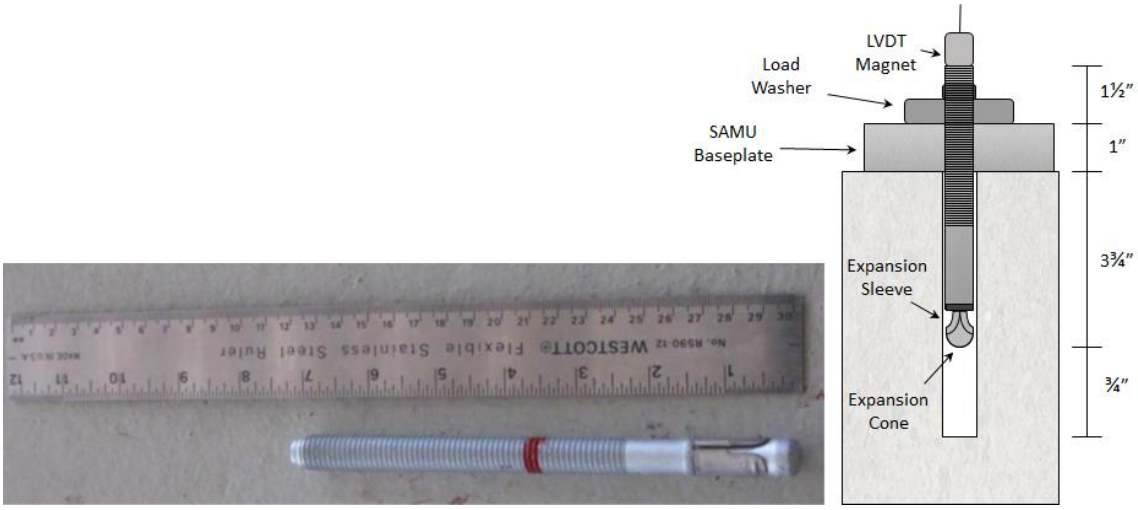

Figure 2-7: "N5" Expansion Anchor Pre-installation Picture and Installation Schematic

2.3.5 – N6: B7 Steel Thread Rod Anchor with Yielding Attachment

A fifth type of anchor system was tested to examine the behavior of a yielding attachment described in ACI 318-11 Appendix D 3.3.4.3 provision (b). This provision allows for non-ductile anchors to be treated as ductile anchors when determining design forces so long that the anchor is protected by a yielding mechanism. Requirements in ACI 318 for this type of attachment are vague, and it was thus desired to evaluate difference in behavior in a non-ductile anchor with a plastic attachment mechanism. To conservatively evaluate this criterion, a

modified SAMU was developed by removing the diagonal stiffeners and reducing the cross-section at the interface between the horizontal and vertical legs. This design had an intended flaw in that the single hinge would create prying action between the anchor and the toe of the SAMU – a common error that a designer might make when conceptualizing a yielding mechanism. The intent of this design was to thus capture any potential benefits or drawbacks from a poorly-realized yielding attachment, referred to henceforth as the "ductile SAMU".

The reduced cross-section of the ductile SAMU was designed for the B7 thread rod anchors (N2) such that a plastic moment would develop in the SAMU and reach ultimate strength at approximately 40% of the anchor's monotonic ultimate strength. This process resulted in a section with a thickness of 0.25 inches, and is detailed in Appendix A. A significant drawback of this design was that it interfered with the holes for the shear pins on the rear portion of the original SAMUs. While shear was not measured in this test sequence, the pins were nevertheless required for shear transfer in the anchor. To accommodate the shear pins, the reduced section was kept to a width of 0.5 inches and the rear pin holes were moved forward and angled at 60 degrees instead of the original orientation of 45 degrees. Figure 2-8 shows a ductile SAMU in isometric view, while other views and associated shop drawings may be found in Appendix B.

It should be noted that the pins required for shear transfer inside the SAMU precluded a more "correct" design of the ductile SAMU to compare against the N6 detail. A proper yielding attachment could be attained by having a second plastic hinge between the anchor and the compression toe, creating a flexural hinge to mitigate prying action on the anchor; however, this type of solution would require reworking the anchor detail and the associated configuration of measuring equipment.

Figure 2-8: Ductile SAMU Isometric View

2.3.6 – Anchor Installation

Anchors were installed using a Hilti TE40-ARV rotary hammer drill with carbide-tipped bits. A drilling stand was used with an adjustable rod that allowed for the precise drilling of the desired hole depth. The stand had adjustable legs that allowed for horizontal leveling on the slab, and subsequently perpendicular drilling to the surface. Prior to drilling, the SAMUs were placed in position, and a special collar set inside the center hole was used to ensure the hole was centered in the fixture. All holes were cleaned with a 3x blow, 3x brush, 3x blow, 3x brush, 3x blow procedure with a steel brush 1/8” larger than the drill hole. All procedures conformed to manufacturer recommended installation specifications.

Epoxied anchors (“N1” and “N2”) were cleaned using acetone and a wire brush prior to installation. Hilti RE-500 SD epoxy mortar was injected into the hole using a Hilti MD-2500 epoxy gun with a piston plug mixer attachment. The holes were overfilled such that, upon anchor

insertion, excess epoxy was forced out. Following this, anchors were squared in the center of the hole and left to cure for 24 hours prior to testing.

2.4 – Reference Test Results

A significant impetus for using WALLE to perform these structural tests was that a wealth of characterization data regarding anchor performance had been done previously on a separate research project. Single anchor reference tests, as well as monotonic pushover tests, developed expected anchor monotonic strengths, as detailed in Hoehler and Dowell (2009/2010). All anchors were designed to have approximately the same ultimate tensile strength of 8.2 kips, and displacement capacities between the ductile N1 anchors and the soft elastic N3 anchors were designed to be roughly the same at 1.3 in. Results from the tensile reference tests are presented in Figure 2-9. While no shear results were performed as part of the test program, anchor shear reference tests are presented in Figure 2-10, primarily to show the shear force versus displacement response for the N1 anchor.

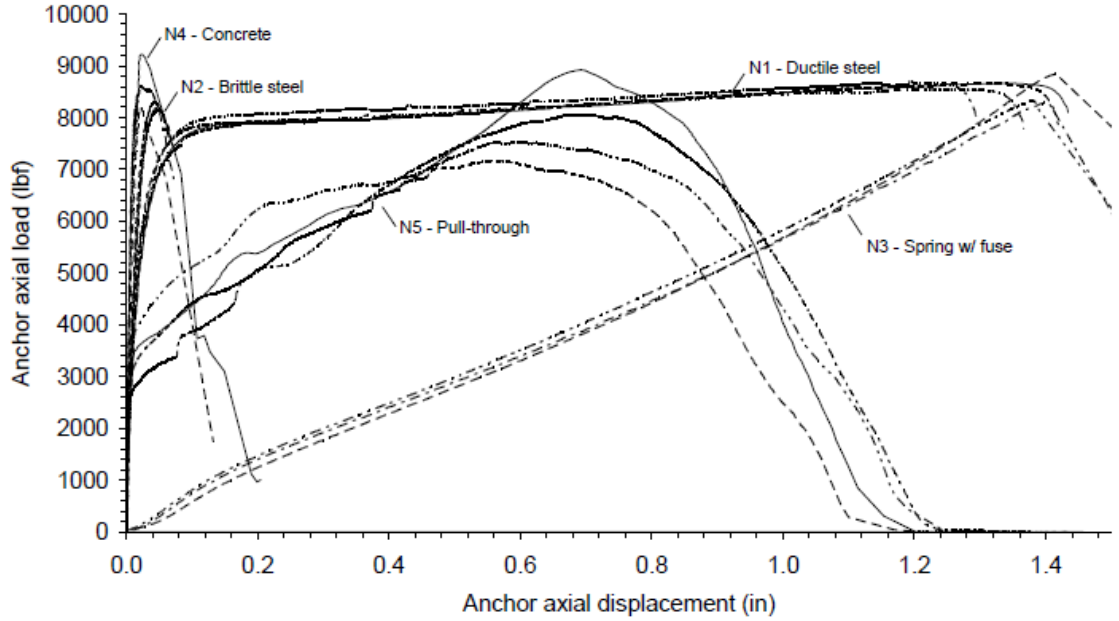

Figure 2-9: Anchor Tensile Force vs. Disp. Results for Pushover Tests [from Hoehler and Dowell, 2011]

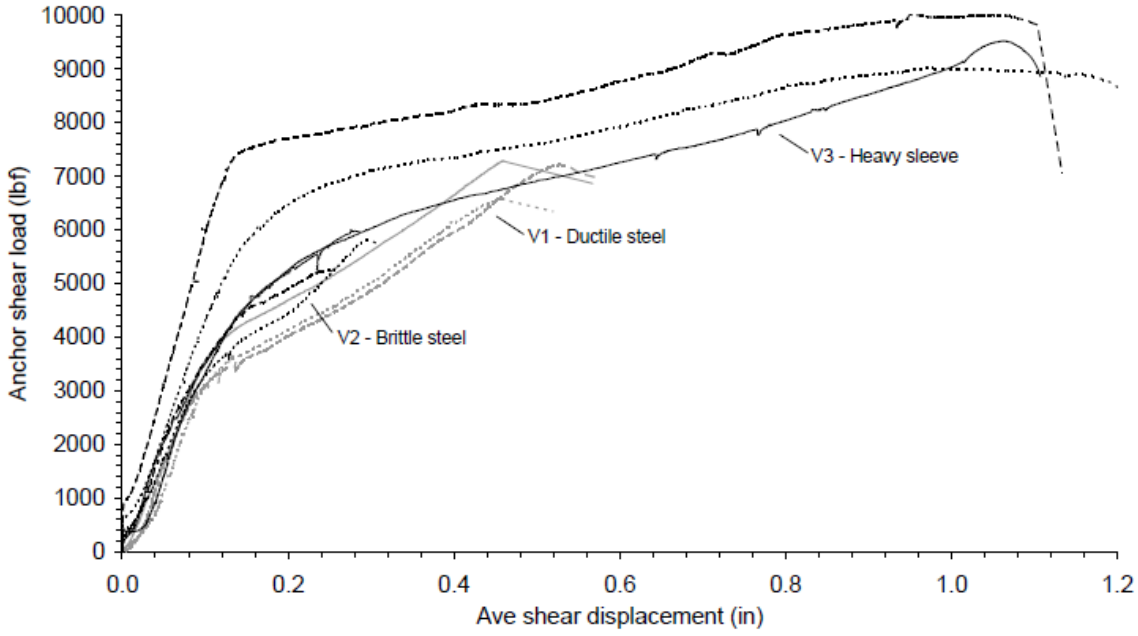

Figure 2-10: Anchor Shear Force vs. Disp. Results for Pushover Tests [from Hoehler and Dowell, 2011]

2.5 – Experimental Setup

2.5.1 – Concrete Slab

Two 5’x5’x10” concrete slabs were poured to fit within the confines of the platen of SDSU’s shaking table. Each slab used 1.5 cubic yards of 202502CD “Green City Mix” concrete provided by Vulcan Materials Company located in San Diego, California. The 28-day design strength of the concrete was f'_c = 2.5 ksi, and uniaxial cylinder tests using standard 6”x”12” test cylinders were performed prior to testing to verify concrete compressive strength met or exceeded this value. Mix design quantities are shown in Figure 2-11.

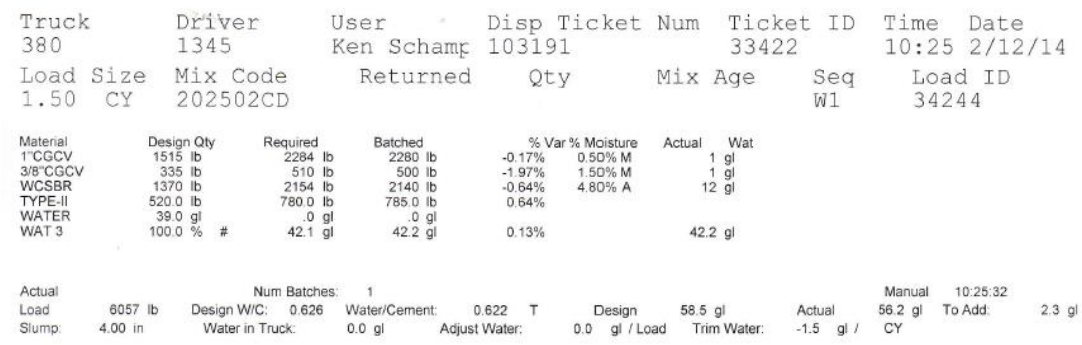

Truck	Driver	User	Disp Ticket Num	Ticket ID	Time	Date
380	1345	Ken Schamp	103191	33422	10:25	2/12/14

Load Size	Mix Code	Returned	Qty	Mix Age	Seq	Load ID
1.50 CY	202502CD				W1	34244

Material	Design Qty	Required	Batched	% Var	% Moisture	Actual	Wat
1"CGCV	1515 lb	2284 lb	2280 lb	-0.17%	0.50% M	1 gl	
3/8"CGCV	335 lb	510 lb	500 lb	-1.97%	1.50% M	1 gl	
WCSBR	1370 lb	2154 lb	2140 lb	-0.64%	4.80% A	12 gl	
TYPE-II	520.0 lb	780.0 lb	785.0 lb	0.64%			
WATER	39.0 gl	.0 gl	.0 gl				
WAT 3	100.0 % #	42.1 gl	42.2 gl	0.13%		42.2 gl	

Actual		Num Batches: 1						Manual	10:25:32
Load	6057 lb	Design W/C: 0.626	Water/Cement: 0.622 T	Design	58.5 gl	Actual	56.2 gl	To Add:	2.3 gl
Slump:	4.00 in	Water in Truck: 0.0 gl	Adjust Water: 0.0 gl / Load	Trim Water:	-1.5 gl /	CY			

Figure 2-11: 202502CD “Green City Mix” Batch Quantities

Reinforcing steel was provided at the top and bottom of each slab to catch potential flexural cracks. Rebar sizing and spacing was intended to limit a wide-open crack from compromising the slab during testing, and was designed to exceed the cracking moment of the concrete with a large factor of safety. A total of ten 1” schedule 40 PVC tubes were included on the edges to allow through-bolting of the slab to the platen. To prevent cage movement during the pour, all bars were tack-welded at intersection points. Additionally, two ¾” lifting inserts

were provided on the south edge of the slab, with four more ¾” inserts provided on the top face.

Figure 2-12 and Figure 2-13 provide pictures of the formwork prior to pour and the measured slump, respectively. A detail drawing for the slab is provided in Appendix B.

Figure 2-12: Reinforcing Steel Layout for Slab Prior to Pour

Figure 2-13: Slump Test Results for Concrete Slabs

2.5.2 – Catcher Systems

A three-tier catcher system was used to limit WALLE's movement post anchor failure, shown below in Figure 2-14. The primary system was composed of two high-strength steel cables, one on the north side of the slab and one on the south side of the slab, which looped through the lifting eyes on WALLE's mast and the edges of the platen. These cables were given enough slack to be loose during the test, but would engage if the anchors failed and the system began to overturn. The required amount of slack for this to occur was determined based on the anchor displacement capacity of each system, a pushover model in SAP2000, and displacements at failure from previous pushover tests.

A secondary system of four high-strength straps was connected through the lifting eye at the top of WALLE and attached to the frame of the shaking table, with required slack lengths computed in the same manner as with the primary system. While the primary catcher system moved relative to the table due to its attachment to the platen, the secondary system was attached to fixed members and had slack lengths adjusted to account for the absolute displacement of the table.

The tertiary catcher system was used to prevent WALLE from "walking" transversely upon anchor failure. These straps were given slack enough to allow WALLE to rock freely, but would become taught if the base exhibited any twisting motion. The primary, secondary, and tertiary systems are highlighted in Figure 2-14 with blue, green, and yellow circles respectively.

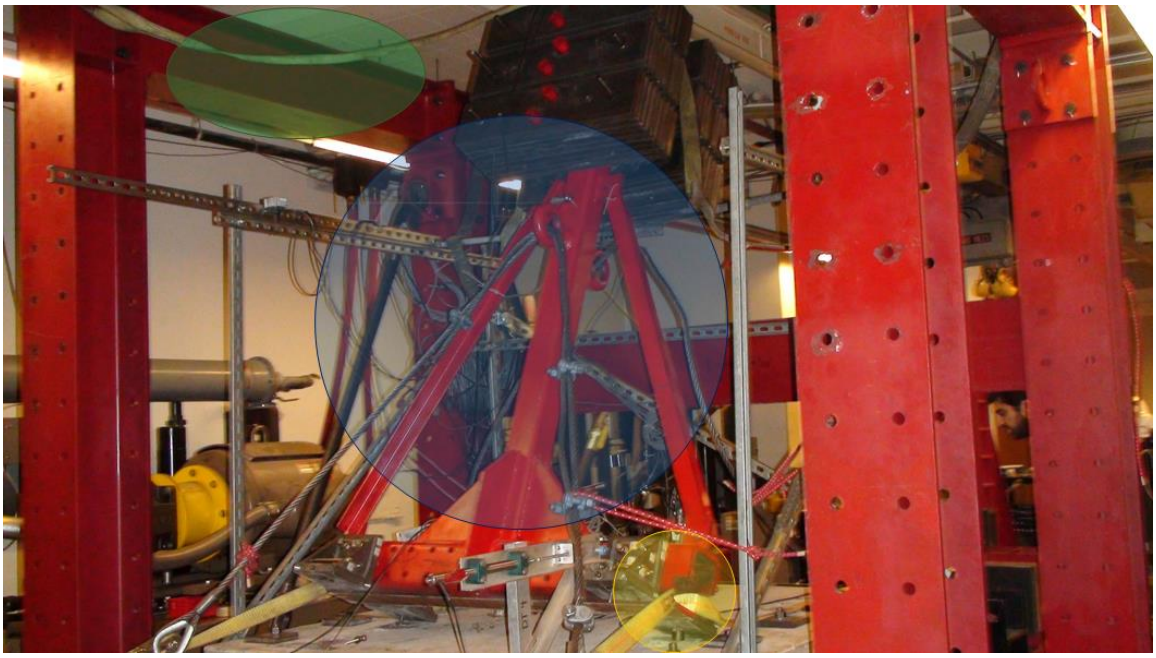

Figure 2-14: WALLE Catcher Systems for (a) Primary (blue), (b) Secondary (green), and (c) Tertiary (yellow)

2.5.3 – Instrumentation

A total of eight accelerometers, five LVDTs, two string pots, and four load cells were used to measure values of interest. Due to the pre-existence of attachment locations on WALLE and the SAMUs, instrumentation locations remained consistent with Hoehler and Dowell (2010). The accelerometers are numbered below in Figure 2-15, and were oriented to allow measurement of the base motion of the slab, various longitudinal accelerations over the height of WALLE, transverse accelerations of WALLE, and selected SAMU vertical accelerations.

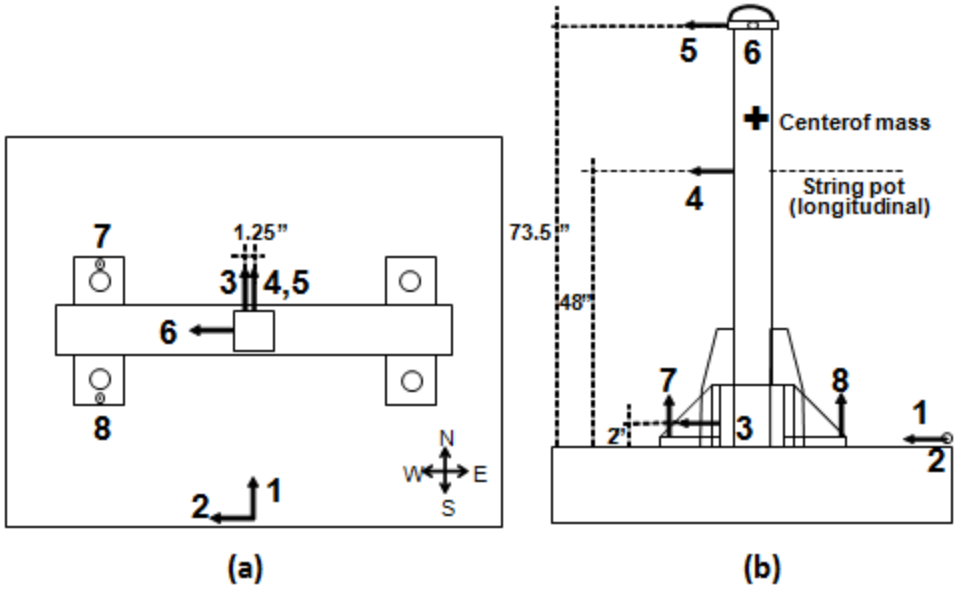

Figure 2-15: Instrumentation Layout and Numbering [From Hoehler et al. 2010]

Measurements were taken using a DaqBook 2000 outfitted with a series of signal conditioning cards: three DBK-43B modules, a DBK-48 module, and a DBK65 module. Data acquisition was performed in DaqView software via a networked PC at a sampling rate of 250 Hz. Anchors were labeled A1-A4, corresponding to the southwest, southeast, northeast, and northwest anchor positions respectively. A schematic of this is shown in Figure 2-16, and individual instrument information is provided in Table 2-1.

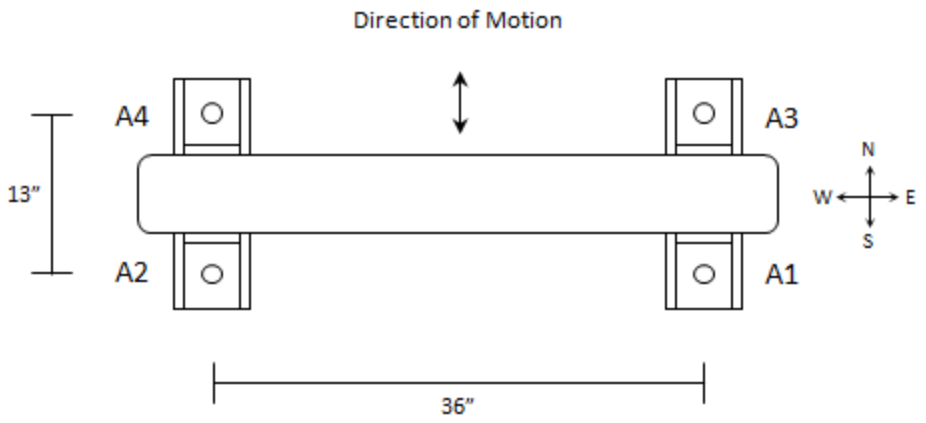

Figure 2-16: Anchor Numbering and Orientation

Table 2-1: Instrumentation List

Instr.#	Instrument Type	Serial #	Manufacturer	Instrument Name
1	50g Accelerometer	960	Dytran 3059A	Accl 1 – Slab Long.
2	50g Accelerometer	1386	Dytran 3059A	Accl 2 – Slab Trans.
3	50g Accelerometer	1733	Dytran 3059A	Accl 3 – WALLE Base Tube Long.
4	50g Accelerometer	1734	Dytran 3059A	Accl 4 – WALLE Mid Mast Long.
5	50g Accelerometer	1735	Dytran 3059A	Accl 5 – WALLE Top Long.
6	50g Accelerometer	1736	Dytran 3059A	Accl 6 – WALLE Top Trans.
7	50g Accelerometer	1737	Dytran 3059A	Accl 7 – SAMU Vertical NW
8	50g Accelerometer	1738	Dytran 3059A	Accl 8 – SAMU Vertical SW
9	25" String Potentiometer		Celesco PT-101	SP1 – Long. String Pot @ 48"
10	55" String Potentiometer		Celesco PT-101	SP2 – Trans. String Pot @ 51.5"
11	48" Linear Potentiometer	0731930	RDP DCTH	DispTab – Table Displacement
12	50 Kip Load Cell	186671A	MTS	Cyl Load – MTS Act. Load Cell
13	4" LVDT	119587	RDP DCTH	Disp A1 – SE Anchor Axial Disp.
14	4" LVDT	119030	RDP DCTH	Disp A2 – SW Anchor Axial Disp.
15	4" LVDT	119032	RDP DCTH	Disp A3 – NE Anchor Axial Disp.
16	4" LVDT	122033	RDP DCTH	Disp A4 – NW Anchor Axial Disp.
17	10 Kip Load Cell	229931	THC-10K-T	LW1 – SE Anchor Axial Force
18	10 Kip Load Cell	239833	THC-10K-T	LW2 – SW Anchor Axial Force
19	10 Kip Load Cell	239834	THC-10K-T	LW3 – NE Anchor Axial Force
20	10 Kip Load Cell	239835	THC-10K-T	LW4 – NW Anchor Axial Force

2.5.4 – Standard Procedure

Each anchor was tested via a series of sequentially-scaling ground motion amplitudes until failure was recorded. The experimental setup for each anchor was as follows:

- Mark anchor positions and move WALLE into place with SAMUs attached.
- Drill anchor holes orthogonal to slab using a drill stand to set appropriate depth. Use aluminum spacer and ½" drilling collar to drill hole in center of SAMU.
- Remove SAMUs.
- Clean holes as required with 3x blow, 3x brush, 3x blow, 3x brush, 3x blow procedure.
- Install anchors, epoxy, and let set (if needed). Square and center in drill hole using an angle, and allow curing time (if needed).
- Place SAMUs over anchors and adjust SAMU collars.
- Bolt SAMUs to WALLE.
- Attach weight plates to WALLE with 250 ft-lb of torque on each bolt.
- Attach accelerometers and string pot. Use levels and angles to ensure string pot is flush.
- Run primary catcher system cables. Adjust slack appropriately, and tie back cables with bungees to prevent excessive movement during test.
- Run secondary catcher system straps. Adjust slack.
- Run straps through WALLE base tube for lateral catcher system.
- Attach load washers. Use spherical washers and Grade 8 hex nuts.
- Place LVDT stands for anchors. Use an angle to adjust the magnets and string to be straight vertical. Hot glue magnets to hex nuts at the top of anchors to help prevent early break-off during tests.
- Hot glue LVDT stands to concrete slab or platen as appropriate.
- Preload anchors to specified levels.
- Turn on hydraulic actuator and warm up oil to 100 degrees Fahrenheit in displacement control using a tapered sine curve with 2 in of displacement at 0.1 Hz.

- Relax anchor preload to desired *in-situ* load levels (N5 only).
- Turn on data acquisition system and run desired level of earthquake motion.
- Turn off data acquisition at end of test. Repeat until all tests in sequence are completed and anchors have failed.

2.5.5 – Installation Parameters

All anchors used standardized installation parameters, which are summarized below in Table 2-2. Expansion anchors were relaxed to half the installation torque prior to start of testing. Tightening of the nuts was only performed at the start of the test program, and not after each motion was run.

Table 2-2: Installation Parameters for Anchors

Parameter	N1 – Stainless	N2 – B7 Rod	N3 – B7 Spring	N5 – Expansion	N6 – D.SAMU
Drill Bit Diameter (in)	1/2	1/2	1/2	1/2	1/2
Drill Hole Depth (in)	6	6	10	4.5	6
Installation Depth (in)	6	6	N/A	3.75	6
Installation Load	50 lb	50 lb	50 lb	40/20 ft-lb	50 lb
Number of Tests	1	1	1	1	1

2.6 – Data Post-Processing

Data channels were post-processed using a combination of Matlab and Excel. Input from the actuator was synchronized to the data acquisition system using the displacement output of the hydraulic actuator and the LVDT attached to the shaking table platen. The actuator was run in displacement control, so a time offset was visually applied such that the measured platen and actuator displacement time-history responses overlapped to the nearest 0.004 second time step (corresponding with the system sampling rates of 250 Hz). Accelerometers and string pots were

zeroed in post processing based on the mean of the first five seconds of response prior to the start of actuator motion, while all other measurement devices were zeroed as appropriate in the data acquisition system at the time of testing. Devices with preloads, such as anchor load cells and LVDTs, were left untouched due to the potential accumulation of plastic displacements and existing preloads.

Accelerometers were filtered using a 4^{th}-order Butterworth filter with frequency cutoffs of 0.2 Hz and 50 Hz. These values were selected based on two factors. First, previous structural tests using WALLE and identical anchor systems considered these bounds to be acceptable. Second, observed responses of the system indicated a lower bound on frequency response of approximately 1 Hz associated with WALLE's free rocking natural period, and an upper bound of roughly 33 Hz associated with WALLE's modal response associated with its rotational mass inertia. Forward and backward filtering was performed using Matlab's "designfilt()" and "filtfilt()" functions to remove filter delay. Filtering of other data channels was not deemed necessary.

Accelerometer filtering was validated by comparing measurements between the MTS actuator and DAQView data acquisition systems, which logged measured values of the tests independently. The filtered values of measured slab acceleration, taken from accelerometer A1, and a corrected center of mass acceleration from accelerometers Accl4 and Accl5 (discussed in Section 2.6.2), were used to determine the inertial forces acting on each element of the shaking table. The total weight of the system was estimated to be 6700 lb: 1025 lb for the steel frame of the platen, 3025 lb for the concrete slab, and 2550 lb for WALLE. The platen acceleration, taken from accelerometer Accl1 in units of g, was multiplied by the sum of the platen and slab weights to obtain the inertial force acting at the slab level. The corrected center of mass acceleration

from Accl4 and Accl5 was multiplied by WALLE's measured weight of 2550 lb to obtain the inertial force of the component. These values were then summed at each time step to determine the total inertial force acting on the system for a given point in time.

The above process determined a simple estimate of the inertial force driving the system from the DAQView data acquisition system, and was compared against the force generated by the MTS hydraulic actuator for the time-history record as measured by the actuator's load cell. An overlay of this process is presented in Figure 2-17 from a sample of the structural tests, which is zoomed in over 6 seconds of strong motion to provide visual resolution for the reader. This nicely confirms independently measured acceleration and force values.

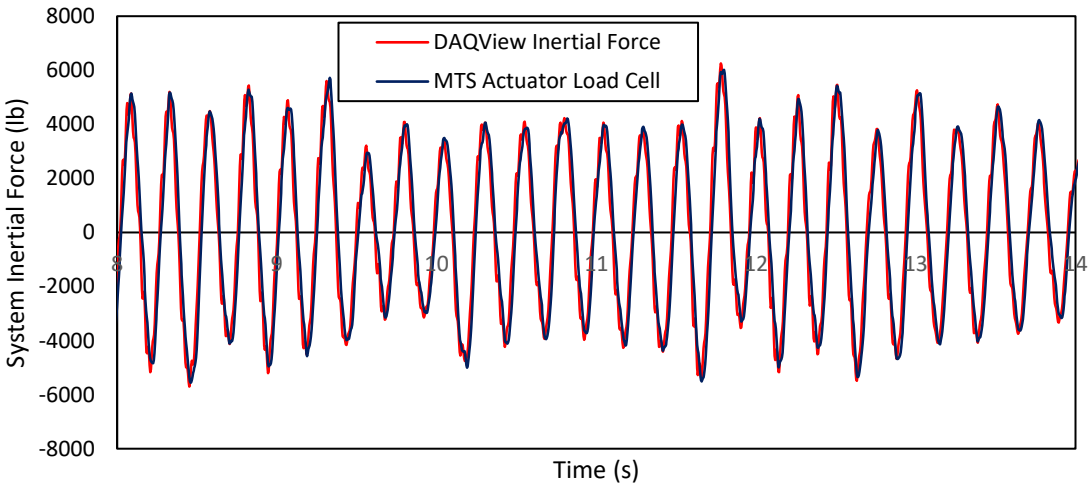

Figure 2-17: Comparison of Inertial Forces of Different Data Acquisition Systems

2.6.1 – Center of Mass Displacement Correction

Displacements were measured at a mast height of 48 inches, compared with a center-of-mass height of 55 inches. Elastic bending and shear deformations of the mast, rigid body

rotation of the mast, and angular adjustment in the string pot were all potential considerations for properly adjusting measured displacements to actual center of mass displacements. Visualizations of each of these deformations are shown in Figure 2-18. Both Hoehler (2010) and Watkins (2011) performed independent assessments of the influences of each individual component, and determined that neglecting elastic deformation differences and string pot uplift were acceptable practices. String pot uplift was beyond the measurable accuracy of the device, and elastic deformation variation was minimal and difficult to capture in post-processing. Using only the rigid body rotational component, Watkins notes errors averaging ≤ 2%, and Hoehler determined a maximum of 8% for the largest measured anchor displacements at their failure points.

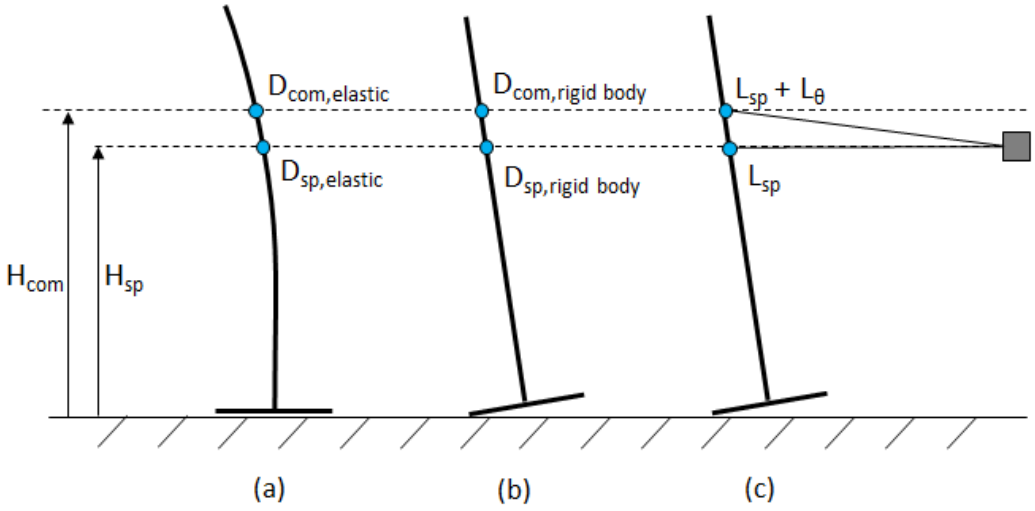

Figure 2-18: Displacement Adjustments for (a) Elastic Deformation, (b) Rigid Body Rotation, (c) String Pot Rotation

As such, the center-of-mass displacement response was simply taken as the ratio given in Eq. 2-1.

$$\Delta_{CoM} = \frac{h_{CoM}}{h_{SP}}\Delta_{SP} = \frac{55\text{ in}}{48\text{ in}}\Delta_{SP} = 1.146\Delta_{SP} \quad \textbf{(2-1)}$$

2.6.2 – Center of Mass Acceleration Correction

Accelerations were corrected to account for the differences in measurement between accelerometers Accl4 and Accl5, which were located at 48” and 73.5” above the concrete surface, respectively. Weighted linear interpolation was used to determine the percentage of which device contributed to the center of mass response at a height of 55 inches above the concrete surface. This is given below in Eq. 2-2.

$$a_{CoM} = a_4\left(\frac{h_5 - h_{CoM}}{h_5 - h_4}\right) + a_5\left(\frac{h_{CoM} - h_4}{h_5 - h_4}\right) = 0.725a_4 + 0.275a_5 \quad \textbf{(2-2)}$$

2.7 – Acknowledgement of Publications

Various parts of several sections in this chapter are taken from the following publication, of which the author of this dissertation assumes primary authorship:

Johnson, T.P. and Dowell, R.K. (2017 - Acceptance Pending Revisions). “Evaluation of the Overstrength Factor for Nonstructural Component Anchorage into Concrete via Dynamic Shaking Table Tests.” *Journal of Building Engineering*.

CHAPTER 3: GROUND MOTION AND ANCHOR DESIGN

3.1 – Ground Motion Selection Criteria

A number of ground motions, taken from the California Strong Motion Instrumentation Program (CSMIP) and the California Earthquake for Engineering Strong Motion Database (CESMD) were selected for use in structural testing. These motions were chosen to provide a suite of earthquakes that would be typically used for time-history analysis in the component design process with a range of peak spectral accelerations between 0 and 0.5 seconds. All motions chosen were "near-field" with residual ground displacements. Complementing these ground motions, for later analytical work, were a suite of 10 floor motions from CESMD. Motions from floors were selected based on ARS characteristics from the building's first and second modes in order to provide peak accelerations within the range of the periods evaluated in the parameter studies discussed in Chapter 7. Given the high variability of floor motion characteristics and their dependence on building response to the ground excitation, these were selected to add diversity to the amplitudes and frequencies of the time-history responses more than as case-studies of individual building type performances.

Lastly, a broadband motion was developed numerically to target the design response curves detailed in this chapter. In addition to ground level response, this broadband motion was used to determine associated floor motions within a five-story special moment frame steel building with full plastic hinging behavior to capture broadband behavior at different floor levels. Information regarding this building is provided in Appendix B. These motions will be referred to as the single earthquake motion (SEM) and broadband motion (BBM) in this text.

3.2 – Suite of Earthquake Motions

In total, 26 motions were used in the body of this work: 10 ground motions from real earthquakes, 10 floor motions from real earthquakes, 1 broadband ground motion, and 5 broadband floor motions staggered on each floor of a five-story building. A summary of all these motions is presented in Table 3-1. The real earthquake ground motions, real earthquake floor motions, and broadband motions are shown below in Figure 3-1, Figure 3-2, and Figure 3-3, respectively. For structural testing purposes, only the ground motions were considered for both broadband and real earthquakes. This was done so that building modeling influences need not be included in the shaking table motion inputs. Conceptual differences between the treatment of floor motions and ground motions, however, were taken into account with the motion scaling and anchor design procedures.

Table 3-1: Details of Earthquake Motions used in Structural Tests / Analytical Work

#	Location	Earthquake	Sensor Location / Channel	CESMD Station #	PGA / PFA (g)	$S_{a,max}$ (g)
1	Ground	Northridge	Santa Monica City Hall N.S Ch1	24538	0.88	3.84
2	Ground	Northridge	Santa Monica City Hall E.W Ch3	24538	0.37	1.77
3	Ground	Northridge	UCLA Grounds N.S Ch1	24688	0.28	1.54
4	Ground	Northridge	UCLA Grounds E.W Ch3	24688	0.47	3.02
5	Ground	Palm Springs	Desert Hot Springs Fire Station N.S Ch1	12149	0.27	1.29
6	Ground	Palm Springs	Desert Hot Springs Fire Station E.W Ch3	12149	0.30	1.91
7	Ground	Northridge	Pacoima Kagel Canyon N.S Ch1	24088	0.23	1.23
8	Ground	Northridge	Pacoima Kagel Canyon E.W Ch3	24088	0.36	1.39
9	Ground	Loma Prieta	Capitola Fire Station N.S Ch1	47125	0.40	1.86
10	Ground	Loma Prieta	Capitola Fire Station E.W Ch3	47125	0.47	3.43
11	Floor	Landers	San Bernadino Library 3rd Floor Ch8	23285	0.18	1.66
12	Floor	Landers	San Bernadino Library Roof Ch4	23285	0.36	4.07
13	Floor	Loma Prieta	Berkeley Hospital 2nd Floor Ch4	58496	0.18	1.02
14	Floor	Loma Prieta	Berkeley Hospital Roof Ch11	58496	0.28	3.35
15	Floor	Loma Prieta	Watson Commercial Bldg 3rd Floor Ch7	47459	0.33	2.08
16	Floor	Loma Prieta	Watson Commercial Bldg Roof Ch6	47459	0.79	3.83
17	Floor	Northridge	Burbank 10 Story Res 4th Floor Ch7	24385	0.39	2.27
18	Floor	Northridge	Burbank 10 Story Res 4th Floor Ch12	24385	0.36	2.12
19	Floor	Northridge	Burbank 10 Story Res Roof Ch2	24385	0.76	5.26
20	Floor	Northridge	Burbank 10 Story Res Roof Ch10	24385	0.52	2.43
21	Ground	Artificial	Broadband Motion [SDS = 1.67g, p = 0.02]	-	0.58	1.977
22	Floor	Artificial	Broadband Steel Bldg 1st Floor	-	0.57	3.18
23	Floor	Artificial	Broadband Steel Bldg 2nd Floor	-	0.65	5.49
24	Floor	Artificial	Broadband Steel Bldg 3rd Floor	-	0.43	5.49
25	Floor	Artificial	Broadband Steel Bldg 4th Floor	-	0.47	3.63
26	Floor	Artificial	Broadband Steel Bldg 5th Floor / Roof	-	0.72	5.25

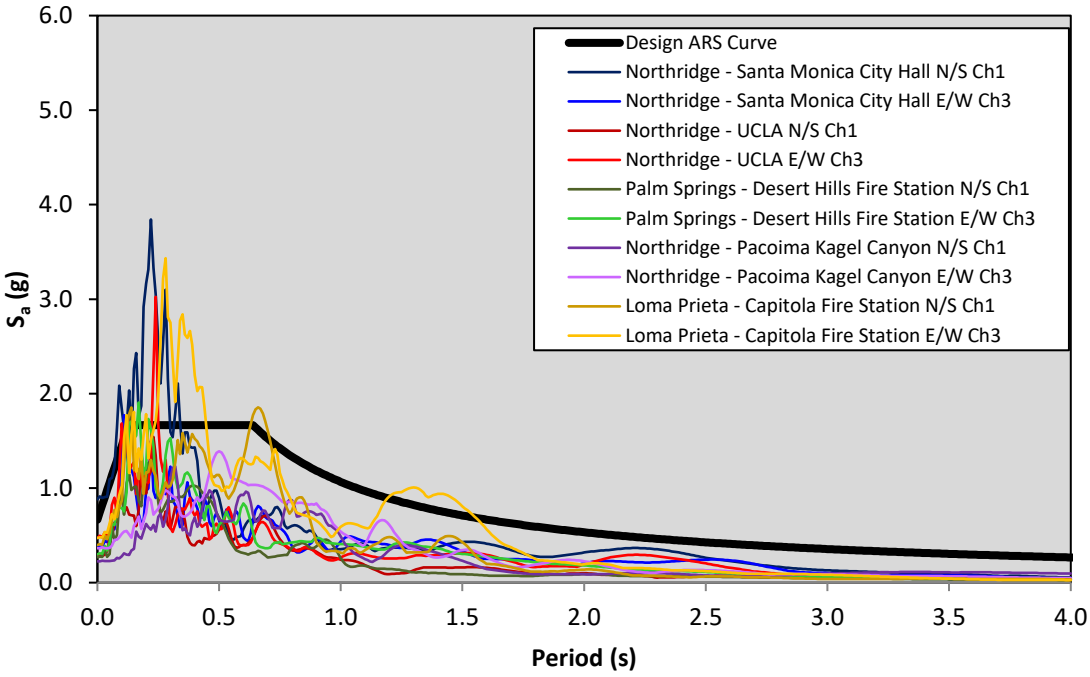

Figure 3-1: Unscaled ARS Curves for 10 Selected Ground Motions

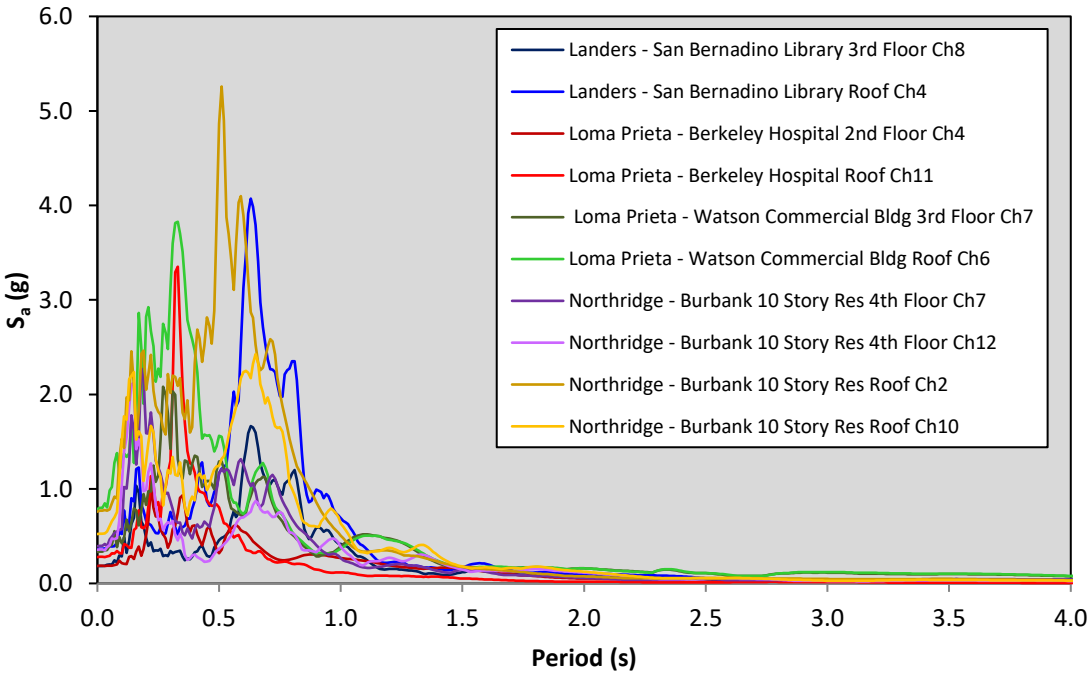

Figure 3-2: Unscaled ARS Curves for 10 Selected Floor Motions

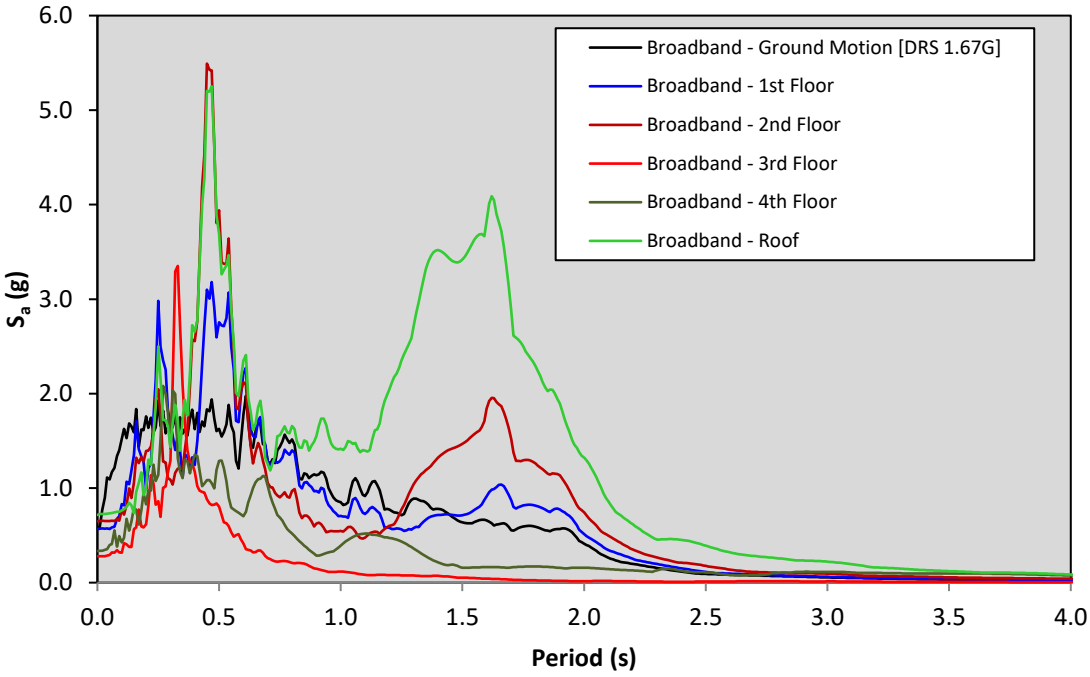

Figure 3-3: Broadband Motion Scaled to 1.67g Spectral Acceleration

3.3 – Scaling Method Options and Selection

As the purpose of the testing program was to target code-specified loading levels in the anchors, it was intended that selected ground motions represent realistic design loads that an anchor would expect to see in the field. For site-specific characterization, ASCE 7-10 Chapter 21.1 specifies the use of five ground motions representative of the predicted site characteristics. Standard process in ASCE 7-10 prescribes geometric mean scaling, which requires that each ground motion be scaled based on a pair of seed motions (typically the directional ordinates measured from a given station for a single recorded motion). This procedure is not specified for nonstructural components, and applies to all seismic design per ASCE 7-10 Chapter 11. As such, a minimum requisite of 10 ground motions is required to perform a standard analysis using

time-history ground motions, though this number is still under contention (Reyes and Kalkan, 2012).

The 10 ground motions chosen previously were selected such that peak amplitudes on the spectral curves for each motion were distributed across the plateau of the intended design response spectrum from ASCE 7-10 (DRS). A first approach was to perform geometric mean scaling per ASCE 7-10 recommendations, which resulted in the scaled ARS curves shown in Figure 3-4. This scaling method combined the square-root-of-the-sum-of-the-squares (SRSS) spectral ordinates of each component of ground motion and minimized them against Euclidian norm to the DRS. The individual ARS curves for each spectral pair were then scaled such that the average ARS ordinate between $0.2T_n$ and $1.5T_n$ fell on the DRS, where T_n was the design first mode period of WALLE taken as $T_n = 0.22s$.

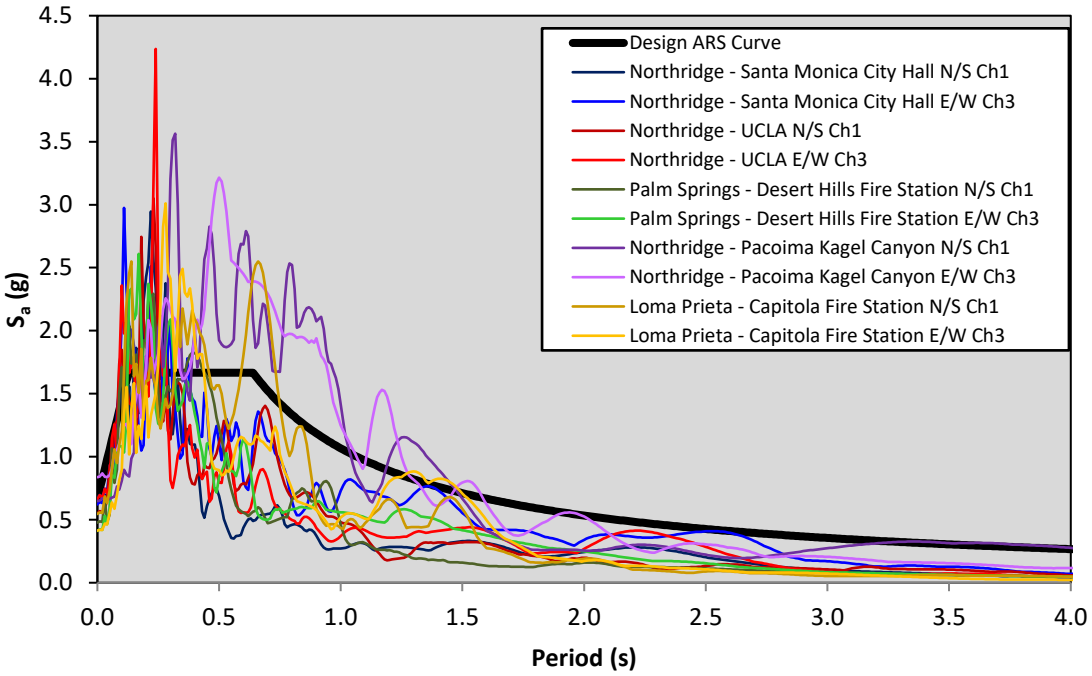

Figure 3-4: Geometric Mean Scaling for 10 Selected Ground Motions

An alternate approach to nonstructural component design comes from provisions in AC156 – Acceptance Criteria for Seismic Certification by Shake-Table Testing of Nonstructural Components. The intent of AC156 is to provide a testing program for evaluation of nonstructural component behavior, and is ideally suited for multi-axial shaking table testing of nonstructural components using state-of-the-art facilities such as the Richmond Field Station at UC Berkeley and UB-NCS at University of Buffalo. Nonstructural components are attached to the platen of the shake table (both the attachment mechanism and the attachment surface are un-prescribed – they must simply represent expected field conditions), and loaded with a "broadband" ground motion designed to simulate maximum possible seismic loading on the component for a given design response curve. Broadband motions are either scaled from an existing ground motion (such as wavelet scaling presented by Mukherjee and Gupta, 2002) or artificially generated to follow a design curve exactly for all potential natural periods with a specified band of frequencies. Wavelet scaling using the program WaveGen is shown in Figure 3-5.

While increasingly popular, wavelet scaling has drawbacks when scaling near-field motions which contain residual ground displacements, and can cause non-trivial amounts of distortion due to its modification of frequency content of the ground motion. When combined with amplitude scaling of individual frequencies, this can create numerical difficulties such as superfluous drift of absolute displacements which was relevant for this suite of motions. Though this problem is generally not important analytically, it has significant limitations when attempting to apply a scaled motion in a shaking table environment. Figure 3-6 shows this drift versus an attempted correction method, which still had excessive ground displacements – 60 inches in this case versus the 20 inches of allowable stroke of the shaking table.

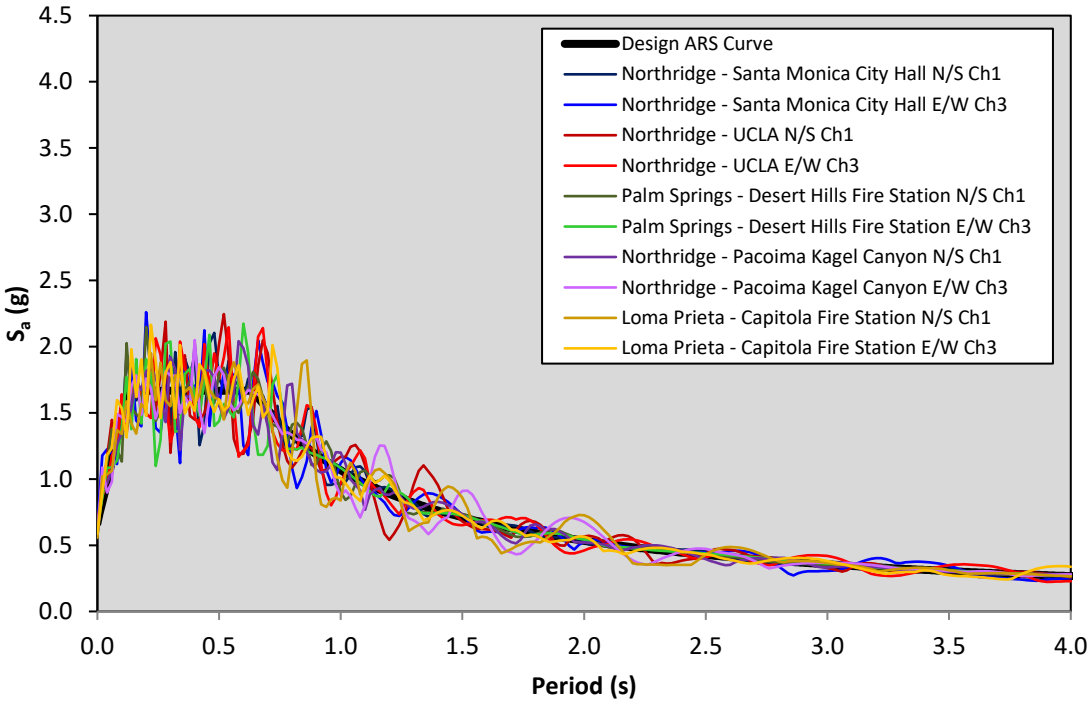

Figure 3-5: Wavelet Scaling for 10 Selected Ground Motions

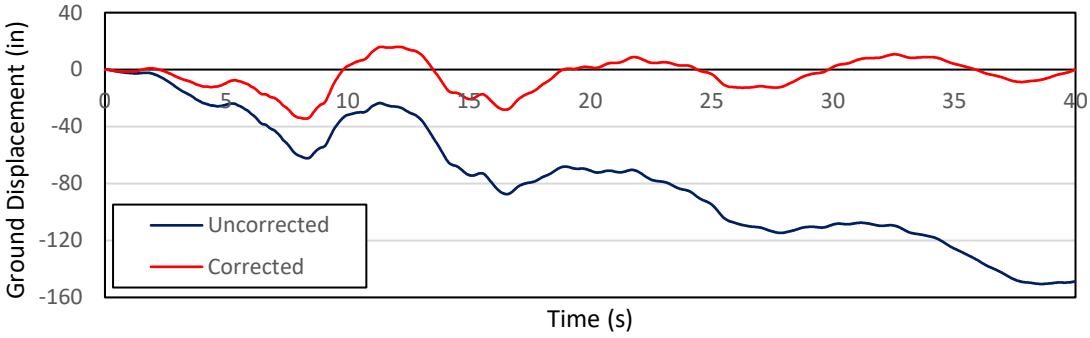

Figure 3-6: Drift of Absolute Displacements from Wavelet Scaling

As an alternative to frequency and amplitude scaling real earthquake motions to meet a required DRS, artificial broadband motions were considered using the program SeismoArtif. This program takes a user DRS and desired time-history intensity function and numerically generates

a ground motion which follows the DRS in the same manner as wavelet-scaled motions. SeismoArtif-generated ground motions were created using a methodology prescribed by Gasparini and Vanmarke (1976), with a user-defined intensity Saragoni and Hart function (1976) over a total duration 40 seconds; peak intensity over 20 seconds with a maximum at 8 seconds; and an ending intensity of 0.2 times the maximum intensity. Many motions were generated, and the final selection of which to use was made based on the estimated displacement demand at failure from the broadband motion versus SDSU's shaking table displacement capacity.

A third approach was taken based on a numerical study performed by Smith and Dowell (2010), which compared the use of these scaling methods with an alternative method called envelope scaling. Envelope scaling amplitude scales ARS curves so that they touch the DRS at only one point. While an individual motion may not represent the intended response of the design curve, including numerous ground motions will cause the DRS to form an envelope over all ground motions. A very practical benefit from envelope scaling is that only the maxima from all performed analyses need to be taken for demand values, where other methodologies like geometric mean scaling use an average due to an individual motion not being representative for the DRS. Envelope scaling is shown in Figure 3-7 for each of the motions.

While envelope scaling and geometric mean scaling are both amplitude scaling methods, a few important distinctions should be discussed. Geometric mean is considered standard acceptable practice, but individual scaled motions are not representative of the design curve outside their average ARS response. As a result, a component's response may be significantly above or below the design curve depending on its individual period, and the addition of more analyzed motions only refines the average of the motions matching the DRS, not the performance of any individual motion. While arguably acceptable for an analytical

approach, shaking table testing has a limited scope of motions that can be used and thus a higher level of refinement for an individual motion was desired.

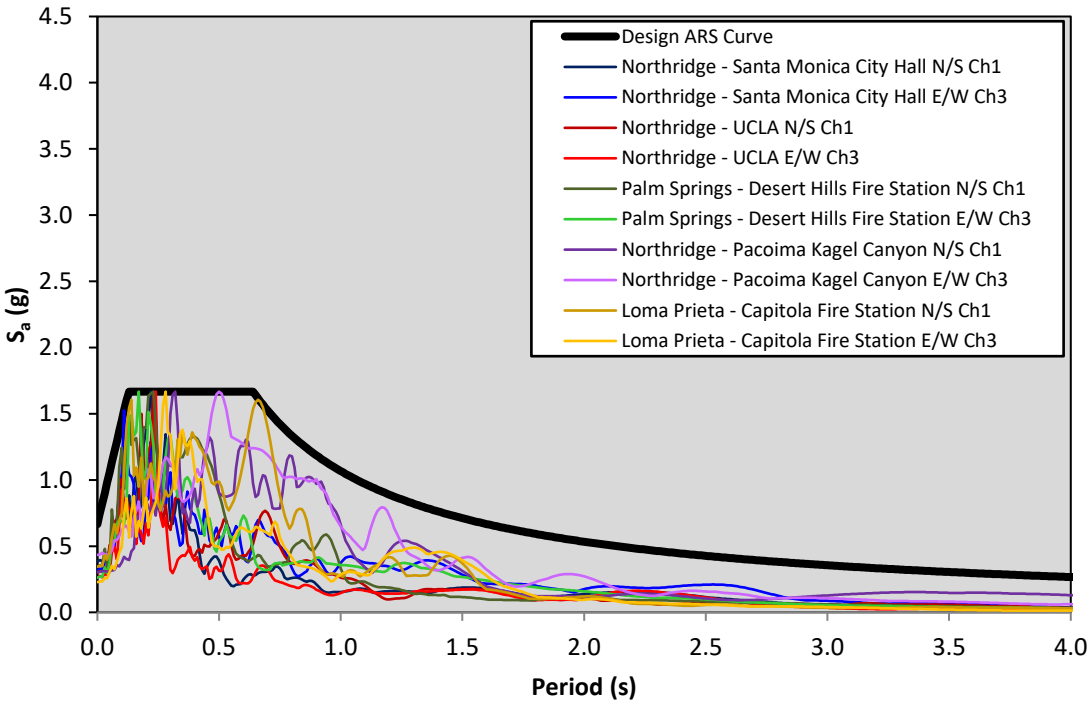

Figure 3-7: Envelope Scaling for 10 Selected Ground Motions

Envelope scaling, while less conservative than geometric mean at face value, allows more control over how well the ground motions represent the design curve. From the motions above, for example, a peak spectral acceleration of 1.67g is generated by envelope scaling, which starkly contrasts with the 3.5g – 4g spectral accelerations of the geometric mean method. When sticking to elastic analysis, an argument can be made to manually select a ground motion which appears to best fit the DRS at the period of interest as a control parameter, but this does not hold true when considering inelastic behavior of the system. Envelope scaling ensures that the DRS remains a maximum. Additionally, as scale factors increase, site factors such as

nonlinear soil behavior may come into play which are not reflected in ground motion, so attempting to keep scale factors as close to the original is considered a best practice even if it is not always feasible.

Additional discussion regarding scaling procedures is provided in a number of sources in the references section. Two are particularly notable, with the first being Heo et al. (2011) who performed a study of 200 nonlinear time-history analyses comparing $S_a(T_1)$ scaling (a procedure similar to envelope scaling where the natural period of the structure is chosen as the scaling ordinate instead of the spectral maximum) with a spectrum-matched response similar to wavelet scaling. Conclusions from their work mirror findings discussed later in 0, which suggest elongations in natural period due to inelastic response may cause amplitude-scaled motions to shift off the DRS. In general, they argue against amplitude-scaled methods, and particularly criticize the $S_a(T_1)$ method due to nonlinearity in system response.

Huang et al. (2011) compare multiple amplitude scaling methods with a wavelet-based procedure using a combination of 50 near-field and 50 far-field motions. Findings from their work suggest that sufficiently large bins of amplitude-scaled motions, properly selected for the structure being analyzed, can produce more realistic and accurate results than the spectrum-matched motions due to the preservation of the natural frequency content of the original earthquakes. While Heo et al. (2011) argue against large dispersion in the chosen ground motion suite, Huang et al. (2011) make note that spectrum-matched methodologies can under-predict median spectral displacements for significantly nonlinear structures. A minimization of dispersion tends to hide these errors. Additionally, they favor $S_a(T_1)$ scaling over geometric mean scaling when looking at amplitude-scaling methods, but prefer a variation of $S_a(T_1)$ – called D-scaling – that allows for the use of multiple ground motions to capture several targeted periods.

In summary, the proper scaling of ground motions is a highly contentious topic. The most important characteristic all methodologies cite, however, is capturing of the intended DRS performance with the selected scaling method.

3.4 – Equivalent Ω_0 Design Levels for Given DRS

A fundamental problem with using pre-defined anchors was that they were not selected for WALLE based on ASCE 7 and ACI 318 guidelines, but instead to provide parametric comparison between different anchor types for characterizing relative anchor performance. Normally, WALLE's parameters would be used in conjunction with the seismic lateral force equation, shown in Eq. 3-1, to determine a minimum amount of required anchor strength to prevent overturning of the system. Anchors would then be selected to meet or exceed this demand. However, because this process was inverted, the actual S_{DS} design level had to be back-solved to determine what seismic design parameters would have been applied to WALLE that would result in the anchorage selected.

$$F_P=\Omega_0 \frac{0.4a_pS_{DS}W_p}{\frac{R_p}{I_p}}\left[1+2\left(\frac{z}{h}\right)\right] \qquad \textbf{(3-1)}$$

Component-relevant values for WALLE were chosen from ASCE 7-10 Table 13.6-1. WALLE was characterized as a general flexible component, which prescribes values of $a_p = 2.5$ and $R_p = 1.5$. Seismic terms were selected from ASCE 7-10 Chapter 11, with $I_p = 1.0$, $W_p = 2.385$ kips, and assumed ground-level mounting such that $z/h = 0$. A design response spectra was chosen with $S_S = 2.5g$, $S_1 = 1.6g$, and $T_L = 12s$ over a site class of B, with S_1 selected to be a large

value to potentially represent site classes of C or D. This precluded the application of site modification factors F_a and F_v while insuring the design curve was representative of worst-case design values from the USGS hazard maps.

Two load factor equations applicable to seismic loading per ASCE 7-10, shown below in Eq. 3-2, are used to calculate the necessary minimum anchor force, N_{min}. For the purposes of the structural tests, the modifiers on the vertical loads on the nonstructural component were ignored, meaning that the 1.2 and 0.9 modifiers on D were set equal to 1. This is due to the difficulty in modifying applied vertical load while preserving appropriate mass; while easily done analytically, it is problematic to model for uniaxial shake table testing. By this same token, the vertical seismic effects were ignored from the $0.2S_{DS}$ term, as SDSU's shaking table is not equipped to simulate these loads. Similarly, the S and H terms were not applicable due to the lack of snow and lateral earth pressures on the component. Lastly, while ACI 318-11 Appendix D prescribes ϕ factors of 0.75 and 0.65 for steel failure of ductile and non-ductile anchors, respectively, a value of ϕ = 0.75 was chosen for all cases to normalize the design process between anchor types.

$$\emptyset N_{min} = (1.2+0.2S_{DS})D+\Omega_0 F_p+L+0.2S$$
$$\emptyset N_{min} = (0.9-0.2S_{DS})D+\Omega_0 F_p+1.6H \quad \textbf{(3-2)}$$

Combining these values and load factor equations, a free body diagram of WALLE can be sketched to resolve appropriate anchor design forces. The allowable tensile strength in the

anchors, ignoring all influences of the concrete such as concrete breakout modes, can be taken as

$$T_{design} = \#_{anchor} \cdot \emptyset \cdot T_{ult} = 2 \cdot 0.75 \cdot 8.2\text{kips} = 12.3\text{kips}$$

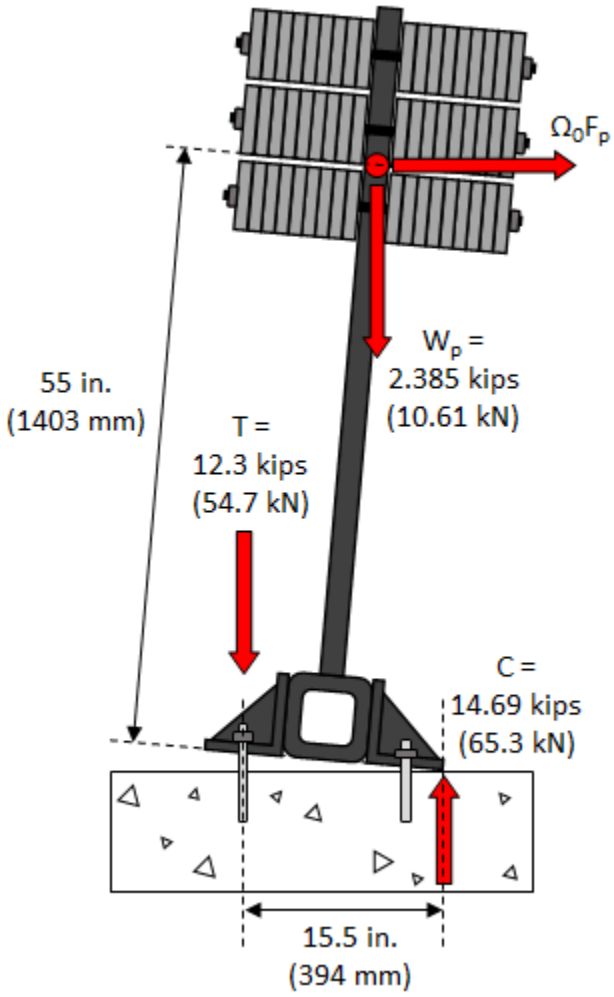

Figure 3-8: WALLE Free Body Diagram for Force Resolution

Applying this value to the free body diagram in Figure 3-8 allows for the resolution for the component lateral design force, $\Omega_0 F_p$. Taking moments about the point of rotation (compression toe) yields

$\Omega_0 F_p \cdot (55in) = 12.3kips \cdot (15.5in) + 2.385kips \cdot (9.0in)$

$\Omega_0 F_p = 3.86$ kips

Setting $\Omega_0 F_p$ equal to the component demand force equation allows the unknown design ground motion spectral acceleration, S_{DS}, to be resolved.

$$\Omega_0 F_p = \frac{0.4 \cdot 2.5 \cdot S_{DS} \cdot 2.385k}{1.5/1.0}\left(1 + 2\frac{0}{h}\right) = 3.86kips$$

Values of $\Omega_0 = 1.0$ and $\Omega_0 = 2.5$ are possible selections based on ductile and non-ductile anchors, respectively. These lead to a value of $S_{DS} = 2.43g$ for ductile anchors, and a value of $S_{DS} = 0.97g$ for non-ductile anchors. To allow for a normalized benchmark for all anchors, these values were scaled against WALLE's anchor-independent design level of $S_{DS} = 1.67g$. A scale factor for ductile anchors can then be calculated as SF = 2.43g / 1.67g = 1.45, and a scale factor for non-ductile anchor anchors can be calculated as 0.97g / 1.67g = 0.58. Summarizing these results visually, a set of design ARS curves can be derived as the baseline for comparison between anchor types as shown in Figure 3-9.

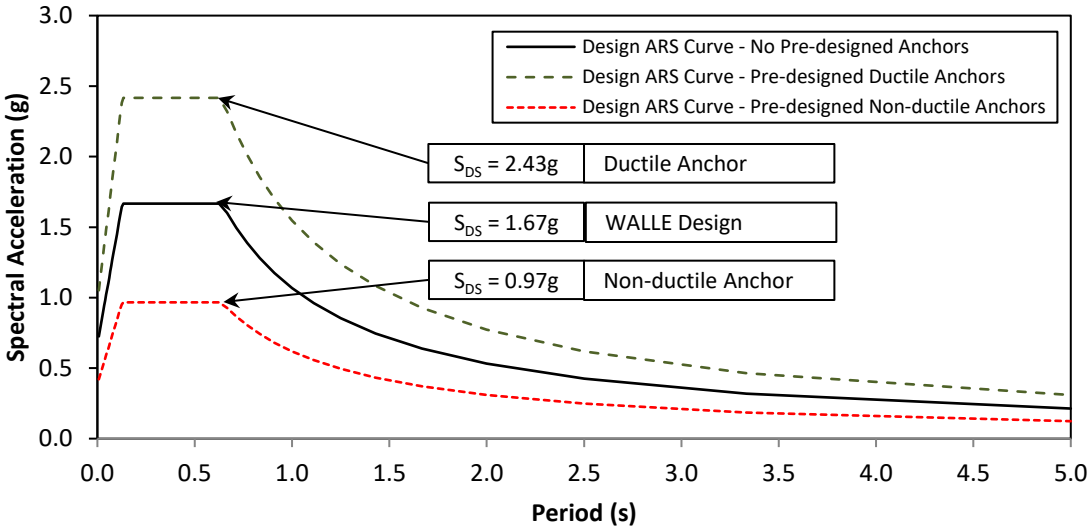

Figure 3-9: Design ARS Levels for WALLE and Anchors

All scale factors discussed were based on the benchmark ARS curve with S_{DS} = 1.67g. Ground motion scale factors for shaking table testing were selected based on the anchor-independent design curve, meaning that the 100% design basis earthquake (DBE) for a non-ductile anchor would have a scale factor of 0.58. The maximum considered earthquake (MCE) would be 1.5x this value, resulting in a scale factor of 0.87. Furthermore, the 100% DBE for a ductile anchor would correspond to the 250% DBE for the non-ductile anchor DBE, which corresponds to a scale factor of 1.45 – thus representing Ω_0 = 1.0. A multiplier of 1.5x the ductile anchor DBE would be associated with the ductile anchor MCE, which would be 375% of the non-ductile anchor DBE with a scale factor of 2.18. Two additional scale factors, 2.90 and 3.22, were selected based on the displacement capacity of SDSU's shaking table using the selected ground motions (500% and 556% of the non-ductile anchor DBE, respectively).

3.5 – Structural Testing Program

From the suite of 10 real earthquake ground motions, a simple rocking SAP2000 model – discussed later in Section 5.1– was used to make prediction analyses for each motion and anchor type. Some motions were incapable of failing all anchors within the shaking table's design limitations, while others were limited by either displacement or acceleration capacity of the actuator. The final motion selected was motion #9 – the north/south channel of the Loma Prieta ground motion taken at the Capitola Fire Station. Prediction models showed all anchors failing within a margin of error below the capacity of the table in the event larger scale factors were required.

Structural testing of each anchor started with a DRS scale factor of 0.58, which corresponded with $\Omega_0 = 2.5$. If the anchors survived this amplitude of motion, the DRS scale factor was then increased incrementally and the test was repeated. This process repeated until anchor failure was obtained, with each DRS scale factor representing a particular spectral acceleration value associated with a code design level.

The number of motions run during this test sequence and their associated scale factors are shown in Table 3-2. A similar process was performed for the broadband testing sequence, and the corresponding values are shown in Table 3-3. The last motion listed for each anchor type in Table 3-2 and Table 3-3 corresponds to the motion in which failure was obtained for that anchor. More detailed analysis of these tables is contained in Chapter 4. The maximum attainable PGA for WALLE's configuration on the SDSU table was 3.0g, the maximum velocity 70 in/s, and the maximum total displacement stroke was 20 in. Demands of the motions selected for testing were within these bounds with acceptable factors of safety, as shown in Table 3-4, with the notation of "BBM (SEM)" when demands from both motions are presented. It should

be noted that due to highly asymmetrical displacement response by the SEM, the platen of the shaking table was offset by 3.86 inches for run numbers 5 and 6 to avoid hitting the piston end caps while still making use of the actuator's full displacement stroke.

Table 3-2: Structural Testing Program for Real Earthquake Motion

Test Number	Anchor Type	Anchor Classification	Equivalent Ω_0	DRS Scale Factor	% Brittle DBE	% Brittle MCE	% Ductile DBE	% Ductile MCE
1	N1	Ductile	2.50	0.58	100	67	**40**	**27**
2	N1	Ductile	1.67	0.87	150	100	**60**	**40**
3	N1	Ductile	1.00	1.45	250	167	**100**	**67**
4	N1	Ductile	0.67	2.18	375	250	**150**	**100**
5	N1	Ductile	0.50	2.90	500	333	**200**	**133**
6	N1	Ductile	0.45	3.22	556	371	**222**	**148**
7	N2	Brittle	2.50	0.58	**100**	**67**	40	27
8	N2	Brittle	1.67	0.87	**150**	**100**	60	40
9	N2	Brittle	1.00	1.45	**250**	**167**	100	67
10	N2	Brittle	0.67	2.18	**375**	**250**	150	100
11	N2	Brittle	0.50	2.90	**500**	**333**	200	133
12	N2	Brittle	0.45	3.22	**556**	**371**	222	148
13	N3	Brittle	2.50	0.58	**100**	**67**	40	27
14	N3	Brittle	1.67	0.87	**150**	**100**	60	40
15	N3	Brittle	1.00	1.45	**250**	**167**	100	67
16	N3	Brittle	0.67	2.18	**375**	**250**	150	100
17	N3	Brittle	0.50	2.90	**500**	**333**	200	133
18	N3	Brittle	0.45	3.22	**556**	**371**	222	148
19	N5	Brittle	2.50	0.58	**100**	**67**	40	27
20	N5	Brittle	1.67	0.87	**150**	**100**	60	40
21	N5	Brittle	1.00	1.45	**250**	**167**	100	67
22	N5	Brittle	0.67	2.18	**375**	**250**	150	100
23	N5	Brittle	0.50	2.90	**500**	**333**	200	133

*Note: Bolded and shaded values represent the percentages associated with the anchor design from ACI 318 classification.

Table 3-3: Structural Testing Program for Broadband Motion

Test Number	Anchor Type	Anchor Classification	Equivalent Ω_0	DRS Scale Factor	% Brittle DBE	% Brittle MCE	% Ductile DBE	% Ductile MCE
1	N1	Ductile	2.50	0.58	100	67	**40**	**27**
2	N1	Ductile	1.67	0.87	150	100	**60**	**40**
3	N1	Ductile	1.00	1.45	250	167	**100**	**67**
4	N2	Brittle	2.50	0.58	**100**	**67**	40	27
5	N2	Brittle	1.67	0.87	**150**	**100**	60	40
6	N3	Brittle	2.50	0.58	**100**	**67**	40	27
7	N3	Brittle	1.67	0.87	**150**	**100**	60	40
8	N3	Brittle	1.00	1.45	**250**	**167**	100	67
9	N3	Brittle	0.67	2.18	**375**	**250**	150	100
10	N5	Brittle	2.50	0.58	**100**	**67**	40	27
11	N5	Brittle	1.67	0.87	**150**	**100**	60	40
12	N5	Brittle	1.00	1.45	**250**	**167**	100	67
13	N6	Ductile	2.50	0.87	150	100	**60**	**40**
14	N6	Ductile	1.67	1.45	250	167	**100**	**67**

*Note: Bolded and shaded values represent the percentages associated with the anchor design from ACI 318 classification.

Table 3-4: Demand Requirements of Table/Actuator for Shaking Table Tests

Run No.	ARS Curve Scale Factor	Total Displacement Stroke (in)	Peak Ground Velocity (in/s)	Peak Ground Acceleration (g)	%DBE – Brittle Anchors	% DBE – Ductile Anchors
1	0.580	3.78 (3.42)	9.42 (6.15)	0.34 (0.20)	100	40
2	0.870	5.67 (5.13)	14.12 (9.22)	0.51 (0.30)	150	60
3	1.450	9.45 (8.56)	23.54 (15.37)	0.85 (0.51)	250	100
4	2.175	14.18 (12.83)	35.31 (23.06)	1.27 (0.76)	375	150
5	2.900	18.90 (17.00)	47.10 (30.75)	1.70 (1.00)	500	200
6	3.220	21.00 (19.00)	52.30 (34.14)	1.89 (1.11)	556	222

*BBM values listed on left, SEM values listed in parenthesis ( ) on right as applicable.

The time history responses for the SEM and the BBM, both representative of the DRS with an S_{DS} spectral acceleration value of 1.67g, are plotted alongside one another in Figure 3-10. It can be observed that the difference in displacement profiles of the two motions are particularly striking, with the BBM containing a total 20 large displacement pulses compared to the SEM's single large pulse. These behavioral differences resulted in different dynamic effects on the anchors which will be discussed in Chapter 4.

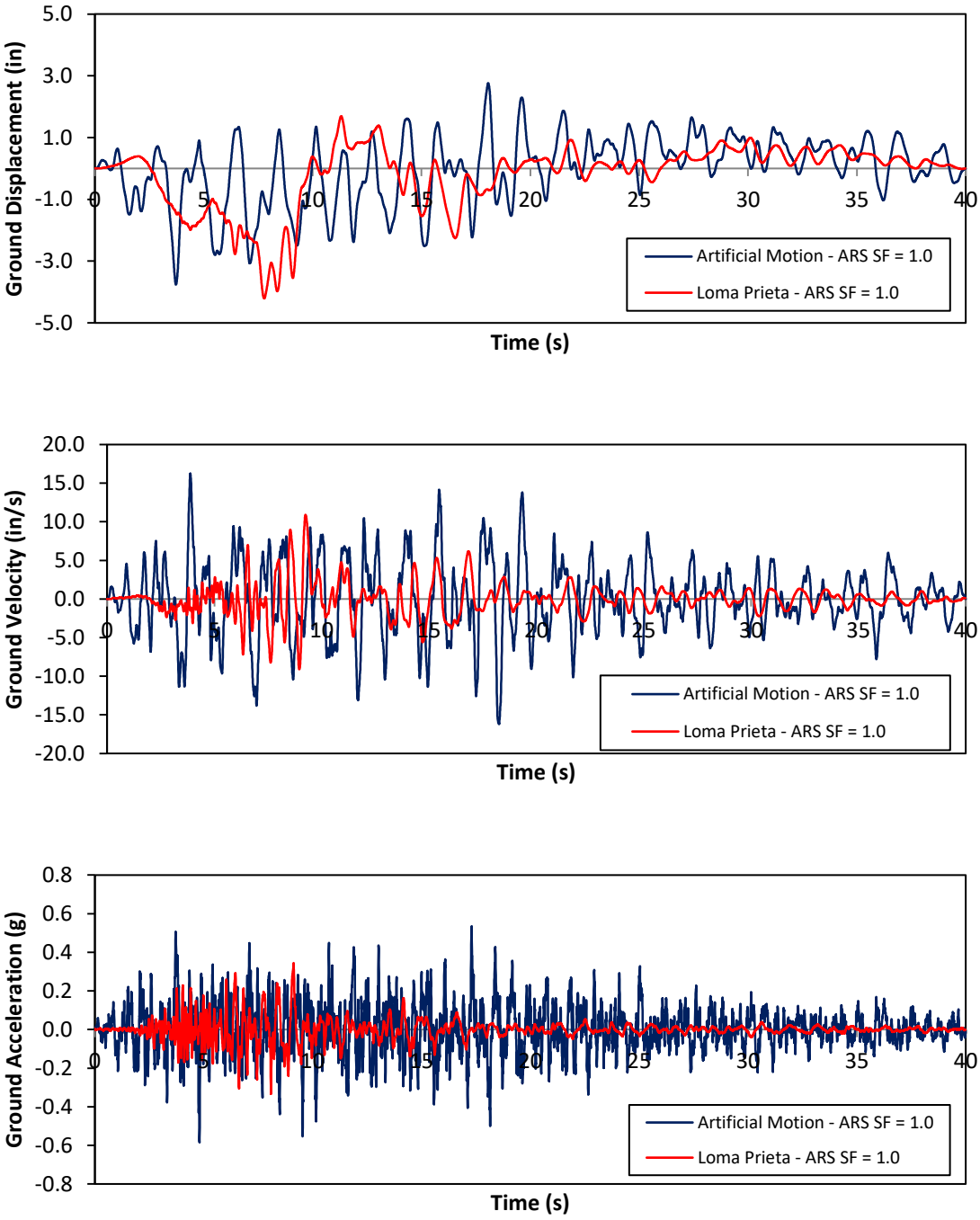

Figure 3-10: Time History Responses for Shaking Table Test Motions

CHAPTER 4: STRUCTURAL TEST RESULTS

4.1 – Single Earthquake vs. Broadband Earthquake

The time-history responses for the motions run in the structural tests and associated base scale factors were presented in Section 3.5. Acceleration response spectra for these motions are presented below in Figure 4-1 alongside WALLE's first mode natural period in uncracked concrete of T_n = 0.22s. It was the intent of the testing sequences that the real earthquake motion simulate a time-history response similar to what WALLE might experience in a field installation, whereas the broadband would represent conditions on par with components subjected to AC 156 qualification procedures for nonstructural components. The Loma Prieta motion was thus intended as a metric to contrast behavioral trends between the anchors, while the broadband motion evaluated conservative bounds on Ω_0. For the purposes of this chapter, the test programs will be discussed as either the single earthquake motion (SEM) or broadband motion (BBM) sequences.

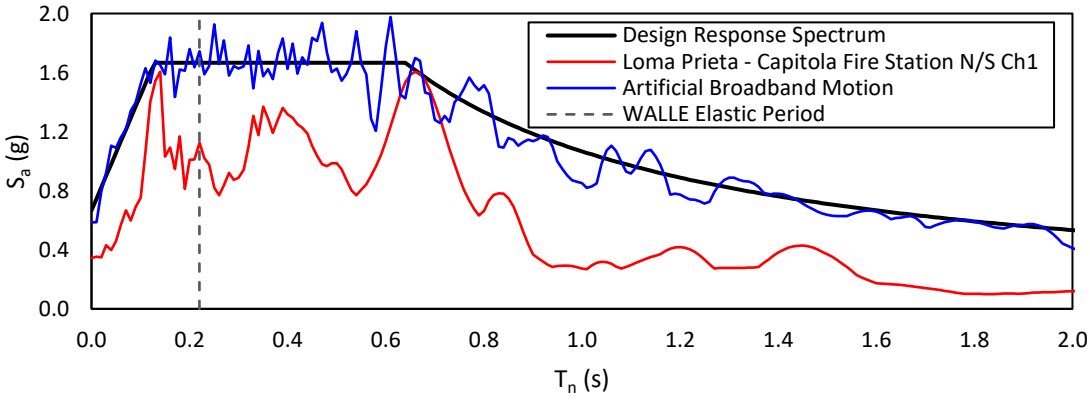

Figure 4-1: Response Spectra for Structural Tests

Table 4-1 and Table 4-2 show the failure levels for each anchor type considering the full input motion and the partial input motion through anchor failure, respectively. With the exception of the B7 thread rod anchor during the BBM, for reasons that will be discussed in Section 4.10, all anchor failures occur at essentially the same load level. This contrasted with expectations from ACI 318, which assume ductile anchors to have higher demand resistance capability than non-ductile anchors due to plastic behavior. Each earthquake motion scale factor was run in sequence with prior scale factors, allowing for accumulation of residual displacements between tests for the plastic N1 and N5 anchors. Notable levels of plastic deformations were accrued during the SEM test sequence at smaller scale factors for both N1 and N5 anchors, but the BBM test sequences consumed most of the anchor's plastic displacement capacity during the failure motion alone.

Table 4-1: Comparison of Failure Levels Using Full Time History Responses

Anchor Type	SEM Ductile DBE %	SEM Non-Ductile DBE %	BBM Ductile DBE %	BBM Non-Ductile DBE %
N1 – Stainless Steel	**222**	556	**100**	250
N2 – B7 Thread Rod	222	**556**	60	**150**
N3 – B7 Spring	222	**556**	150	**375**
N5 – Expansion	200	**500**	100	**250**
N6 – Ductile SAMU	N/A	N/A	**60**	150

Table 4-2: Comparison of Failure Levels Using Partial Time History Responses

Anchor Type	SEM Ductile DBE %	SEM Non-Ductile DBE %	BBM Ductile DBE %	BBM Non-Ductile DBE %
N1 – Stainless Steel	**200**	500	**97**	243
N2 – B7 Thread Rod	209	**522**	59	**147**
N3 – B7 Spring	218	**544**	105	**263**
N5 – Expansion	183	**458**	84	**211**
N6 – Ductile SAMU	N/A	N/A	**59**	147

4.2 – Anchor Results Presentation

Anchor force and displacement responses were essentially the same between anchor pairs on a given side of WALLE (north or south), with the most significant differences peaking at around 10%. Snapshots of all four anchors for two individual motions – the tests prior to failure for the N1 and N5 SEM tests – are provided in Figure 4-2 and Figure 4-3, respectively. It can be observed from both figures that forces and displacements are congruent between anchors in a pair, which was also observed by Hoehler and Dowell (2010) for these same anchors and by Watkins (2011) for moderate to large seismic loading using WALLE. Given that the analytical program discussed in Chapter 7 did not account for variation between anchors, and instead produced an average hysteretic response, forces and displacements for the two anchor pairs were averaged together. In cases where a load washer was damaged for one anchor in a pair or an LVDT detached due to anchor impact, the surviving instrument's readings were taken to be representative of both anchors. To conserve space in the main body of the text, additional hysteretic plots justifying this averaging process are provided in Appendix C. Appendix C also contains full anchor force and displacement time-history responses for both the SEM and BBM test sequences.

Elongation of the component natural period was also of interest to study. Natural periods were measured over the strong motion portion of each earthquake motion, taken to be from 2 seconds through 17 seconds, with each peak-to-peak movement of the component center of mass defined as a single cycle. This is illustrated in Figure 4-4. Plots were then generated that show the natural period of each individual cycle versus its cycle number for each anchor type.

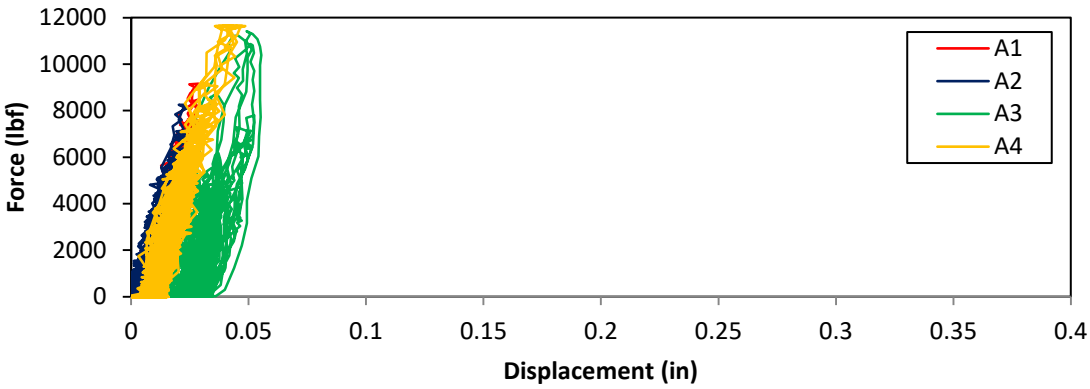

Figure 4-2: Four Anchor Comparison for N2 Anchor 500% Non-Ductile DBE SEM

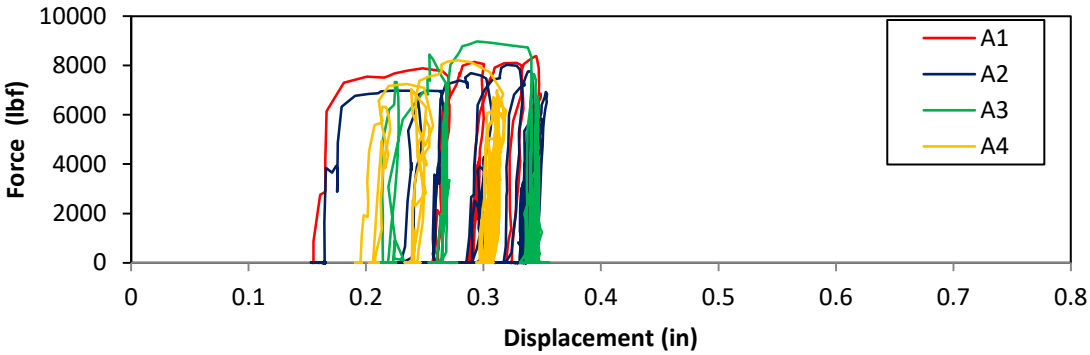

Figure 4-3: Four Anchor Comparison for N5 Anchor 375% Non-Ductile DBE SEM

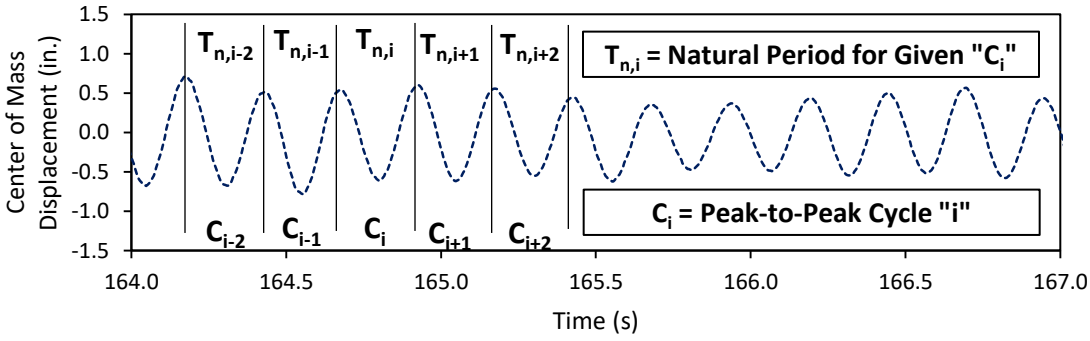

Figure 4-4: Peak-to-Peak Measurement of Natural Period

4.3 – N1: Stainless Steel Anchor Results

Hysteretic responses for the SEM and BBM test sequences, including both south and north anchor pairs, are presented in Figure 4-5. Anchor responses from both tests were well-represented by the monotonic curve for both forces and displacements. These anchors were classified as "ductile" under code ACI 318 provisions, meaning they met the following criteria:

a. No pullout or bond failure – steel fails through yielding.
b. A minimum stretch length of $8d_b$, where d_b is the nominal diameter of the anchor (3/8 in.), was provided. A total of 4 in. of stretch length was provided, where 3 in. was the minimum required.
c. The anchors were restricted to tension-only response, so no buckling restraints were required.
d. The ratio of F_u/F_y, where F_u and F_y are the ultimate and yield tensile strengths, respectively, must be in excess of 1.3. The ultimate tensile strength of the N1 anchor was 8.2 kips with a yield strength of 5.4 kips, resulting in a ratio of F_u/F_y of 1.6.

Failure of the N1 anchors occurred at 222% of the ductile anchor DBE motion for the SEM tests and 100% of the ductile anchor DBE motion for the BBM tests. The adjusted scale factors for the partial motion through failure were 200% and 97%, with Ω_0 values of 0.5 and 1 for the SEM and BBM tests, respectively. Failure photographs are provided in Figure 4-6 for the BBM tests, where residual plastic displacements in the north anchor pair show a height of roughly 3.5 in. above the concrete surface. These anchors had an initial height of 2.65-2.75 in. above the concrete surface with (due to small variability in hole depth from the hammer drilling

process), indicating plastic displacements of 0.75-0.85 in. which are in agreement with Figure 4-5.

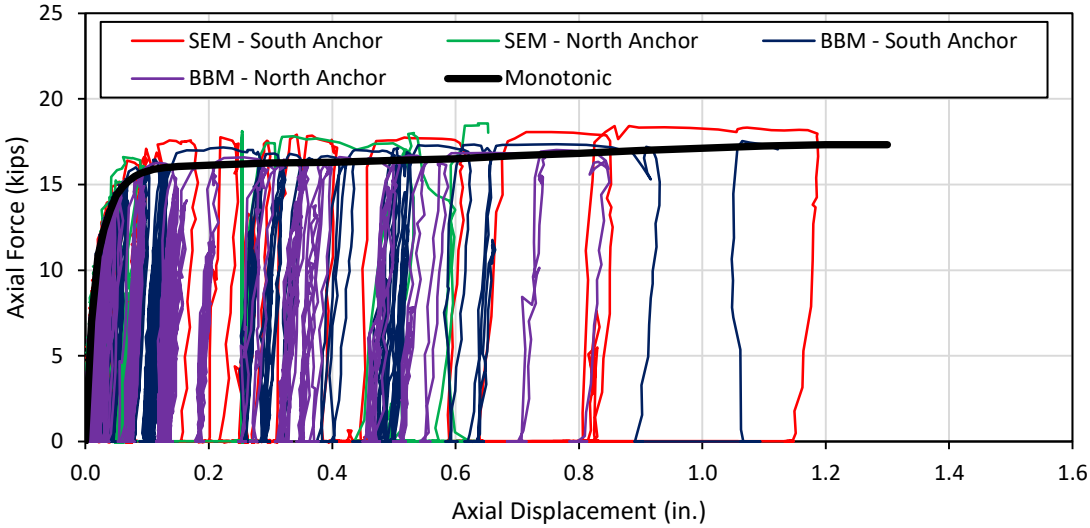

Figure 4-5: N1 Stainless Steel Anchor Hysteretic Behavior for All Tests

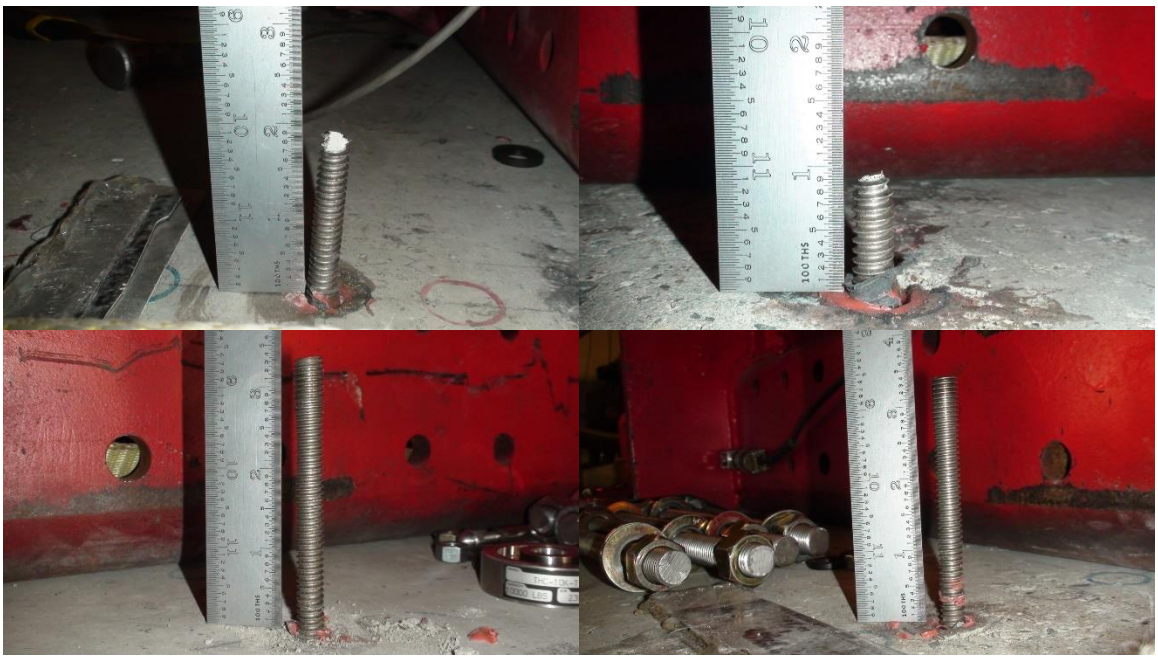

Figure 4-6: N1 Failure Photographs for A1 (top left), A2 (top right), A3 (bottom left), and A4 (bottom right) for BBM Test Sequence

Measurement of period elongations for the N1 anchors including the SEM and BBM tests are provided in Figure 4-7. Three reference lines for observed natural periods – WALLE's rigid natural period in (1) and two elongated periods in (2) and (3) – are provided for reference with the ARS curves from the test motions in Figure 4-8. Of interest to note in Figure 4-8 is that the 150% DBE SEM is largely representative of the $\Omega_0 = 1.0$ design curve for the observed rigid natural period of WALLE along with observed natural periods, and the 200% DBE SEM – which is survived – is lower-bounded by the $\Omega_0 = 1.0$ design curve. Additionally, the 200% DBE SEM shows spectral accelerations consistently above the 100% DBE BBM, which indicates that the N1 anchors were loaded at levels consistent with intended design forces for both test sequences.

Period elongations for the N1 anchors were nontrivial. While some outliers show period increases from 0.22 seconds up to around one second, there are consistent elongations of 0.4 to 0.5 seconds during peak loading. This finding may be particularly important for current code designs which assume "rigid" response of the component by prescribing an amplification factor of $a_p = 1.0$, but are designed with ductile anchorage. System translational stiffness from anchorage and the system translational stiffness from the component itself act in series, which suggests that extremely ductile responses like those from the N1 anchors may result in significant elongation of component natural periods well into the "flexible" range of response.

Overall, these anchors performed well relative to the $\Omega_0 = 1.0$ design level, which agrees with the intended expectations of code design philosophy. It should be mentioned that the ratio of ultimate displacement capacity to elastic yield, presented as the displacement ductility capacity μ_D, was 130 with a maximum elongation of 32%. This is very ductile, as code specifications require a stretch length of only 3 in and an elongation of 14%.

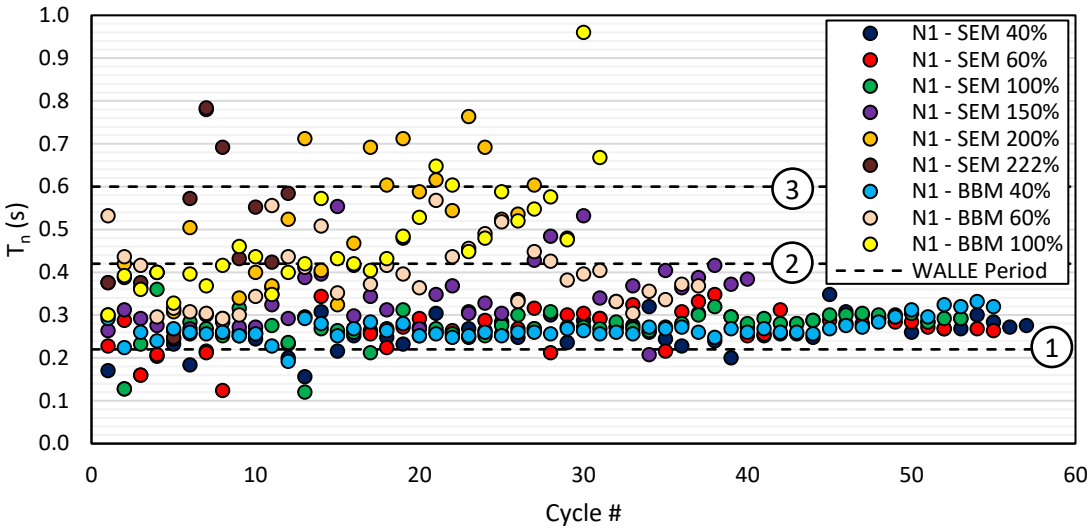

Figure 4-7: Measured Individual-Cycle Natural Periods [Peak-to-Peak] for N1 Anchor

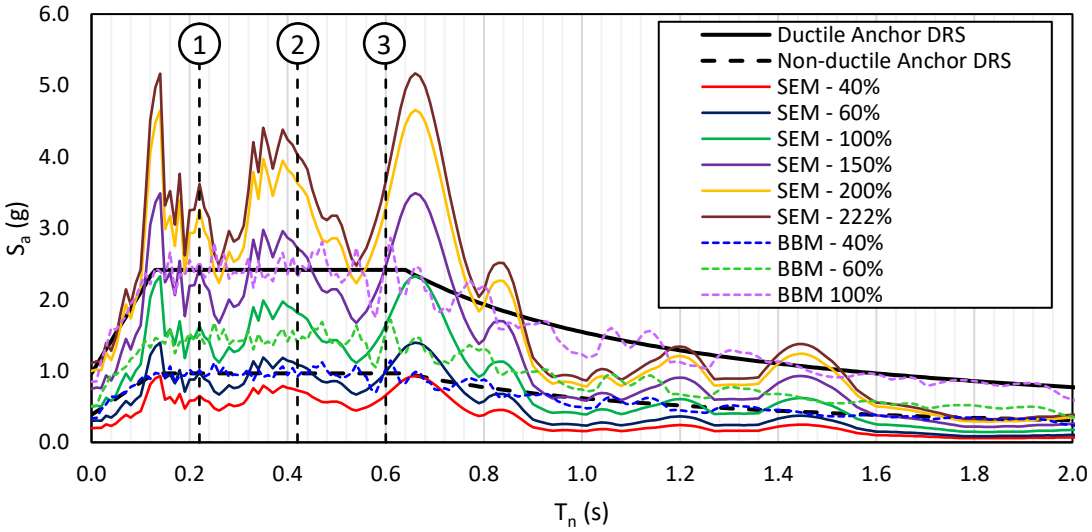

Figure 4-8: Spectral Acceleration Responses for N1 Anchor Test Sequences

4.4 – N2: B7 Steel Anchor Results

Hysteretic responses for the SEM and BBM test sequences, including both south and north anchor pairs, are presented in Figure 4-9. While the N1, N3, and N5 anchors are presented at the same displacement scale for comparison purposes, the displacement axis for the N2 anchor is condensed to allow for greater visual clarity of the hysteretic response. Unlike the N1 anchors which closely followed the monotonic curves, the N2 anchors displayed a consistently stiffer response and had the potential to show forces ≥ 36% higher than those measured monotonically. This is believed to be due to strain rate influences, controlled by low-cycle fatigue conditions as is discussed in detail in Section 4.10. Observed stiffening behavior was consistent within the individual SEM and BBM test sequences. Forces in the SEM test sequence are believed to be real, as they reached the upper bound of the load cell's measurement capabilities – 11.2 kips – repeatedly and consistently, and forces at failure were large enough to cause structural damage to the load cell's steel casing. While the exact magnitude of these forces is unclear, computing peak anchor forces based on center of mass accelerations indicate anchor demands of at least 10.5 kips. Failure photographs of the north anchor pair for the BBM test sequence are provided in Figure 4-10, which show brittle steel fracture of the anchor at the notched region with small-to-minimal concrete damage at the slab surface.

Monotonically, the displacement ductility ratio of these anchors was $\mu_D = 5$, which is $1/26^{th}$ the N1 anchors. This ratio was less dynamically, though very small increments of plastic displacement were accrued each time the anchor cycled above its monotonic force limit. For all N2 anchors, the dynamic displacement capacity was about 0.030 to 0.033 in. – roughly 65% of the monotonic response. This reduction is similar to observed displacement capacity decreases in the soft elastic N3 anchors, which had a reduction in displacement capacity to roughly 68% of

their monotonic values. It is unclear whether or not these reductions are coincidental due to the small sample sizes of anchors tested.

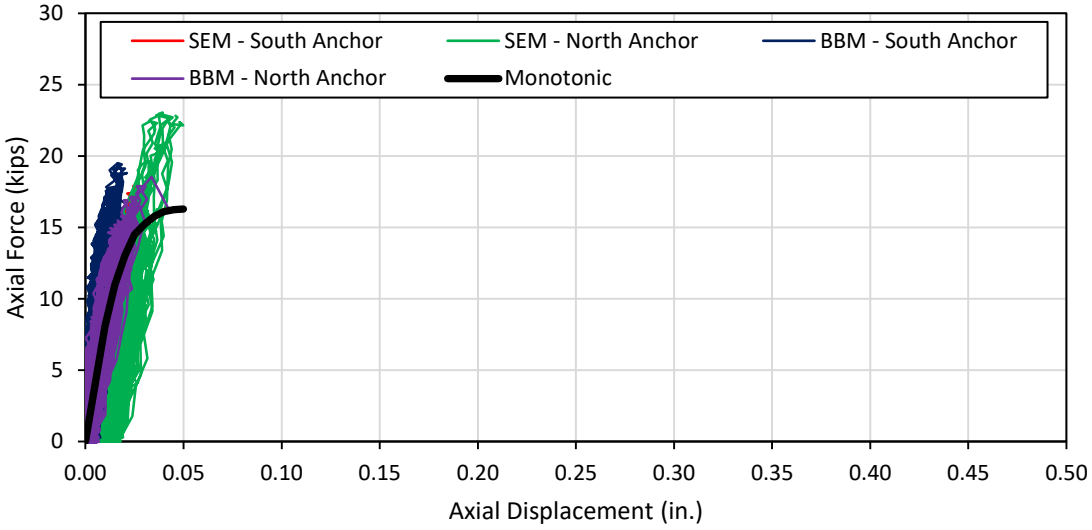

Figure 4-9: N2 B7 Thread Rod Anchor Hysteretic Behavior for All Tests

Figure 4-10: N2 Failure Photographs for A3 Anchor (top left) and Concrete Surface (top right) and A4 Anchor (bottom left) and Concrete Surface (bottom right) for BBM Test Sequence

Of the four anchor types tested, the N2 anchors showed the most resilience to shifts in natural period due to remaining essentially linear-elastic until failure. Figure 4-11 shows WALLE's fixed-base natural period of 0.22s to be moderately representative of system response, with a slight elongation to 0.28s if most cycles are included. Elongations to 0.33s occur during some of the peak portions of the larger ground motions, but WALLE is largely stable in the 0.2s to 0.3s period range. For the SEM ARS curves, this period shifting is significant: periods immediately after 0.22s through 0.30s show decreases in spectral acceleration demands, but as the system period elongates from 0.3s to 0.33s demands sharply increase. This is demonstrated in Figure 4-12.

Also of interest from Figure 4-12 is that the 375% DBE SEM is largely representative of the load levels associated with the $\Omega_0 = 1.0$ design level depending on whether or not the system falls into the "valley" immediately following WALLE's fixed base natural period of 0.22s. The N2 anchors surviving the 500% DBE SEM is equivalent to surviving the 200% ductile anchor DBE, and indicates these anchors resist imposed design-level loads as well as the N1 anchors. For the 500% DBE SEM, spectral accelerations on the component are at or above the $\Omega_0 = 1.0$ design level, with the exception of the 0.26s natural period coordinate which is slightly below the DRS curve. Several measured periods fall close to 0.33s for this motion, represented by (3), which indicates the 500% DBE SEM loads may actually be well in excess of the $\Omega_0 = 1.0$ DRS. These anchors fail at load levels below the $\Omega_0 = 1.0$ DRS for the BBM motion due to low-cycle fatigue, however, which occurred at roughly 10-12 cycles of force levels at or above the monotonic maximum. Each SEM test which exceeded the monotonic force capacity cycled the anchors to this high level of force a total of 3 times, while each BBM test cycled the anchors around 6 times.

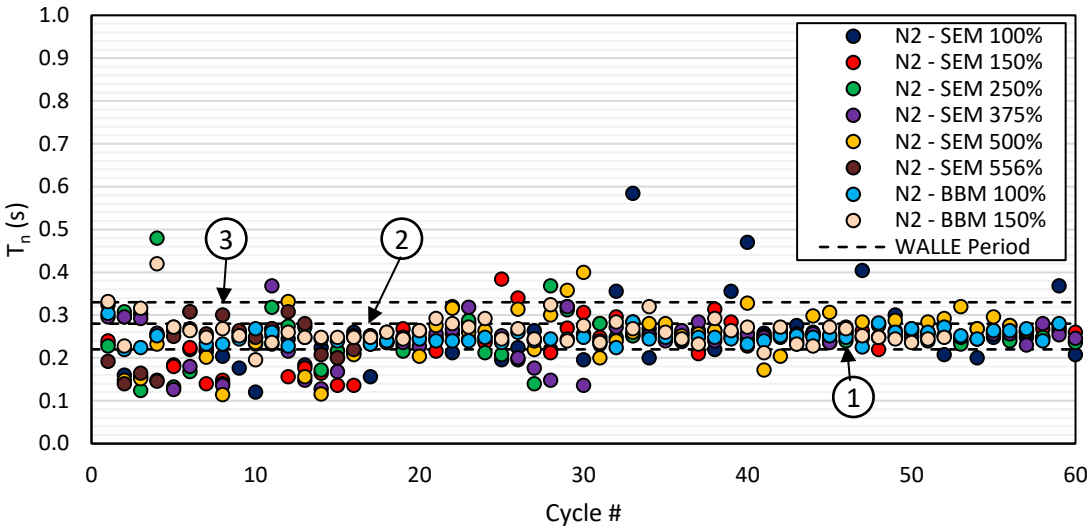

Figure 4-11: Measured Individual-Cycle Natural Periods [Peak-to-Peak] for N2 Anchor

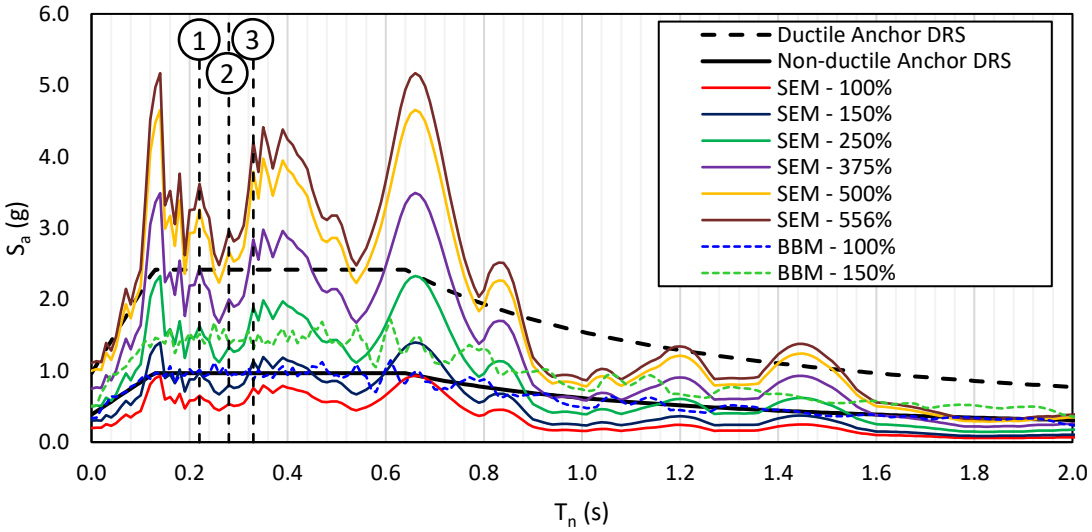

Figure 4-12: Spectral Acceleration Responses for N2 Anchor Test Sequences

4.5 – N3: B7 Spring Anchor Results

Hysteretic responses for the SEM and BBM test sequences, including both south and north anchor pairs, are presented in Figure 4-13. The N3 anchors displayed a dynamic stiffening effect for all tests performed, maintaining the same ultimate force level as from monotonic tests while having reduced displacement capacity. Maintaining the same force level is consistent with the B7 thread rod portion of the anchor acting as a force-controlled fuse element, with the rubber spring controlling displacements. Polyurethane is known to be a highly strain-rate dependent material, and characterizations by Sarva et al. (2007) note stiffening effects between each order of magnitude of strain rate. Loading rates for the monotonic tests of the N3 anchors occurred over approximately 60 seconds, while dynamic loading rates were approximately 0.06 seconds – a difference of three orders of magnitude.

Small amounts of elastic hysteretic damping can be observed in the dynamic tests that were not present in the reference tests (previously discussed in Figure 2-9). Equivalent viscous damping for this region, as discussed later in Section 6.3, is estimated to be about 2.5%. Failure of these anchors, as shown in Figure 4-14, occurred at the interface of the notch with a straight fracture surface. Large increases in force capacity, as seen with the similarly notched N2 anchors, was not observed in the N3 anchors. This suggests overstrength observed in the N2 anchors may be related to strain rate and attachment mechanism (bearing versus bond). Additionally, the majority of anchor cycles occurred at smaller force levels, indicating expected tradeoffs of reduced force demands for increased displacement demands.

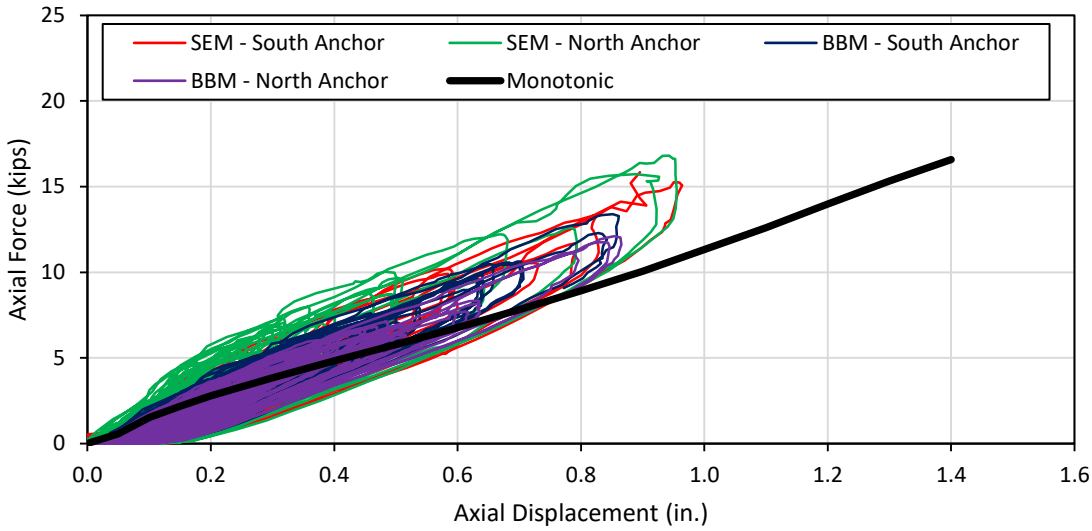

Figure 4-13: N3 B7 Spring Anchor Hysteretic Behavior for All Tests

Figure 4-14: N3 Failure Photographs for A3 Anchor (top left) and Concrete Surface (top right) and A4 Anchor (bottom left) and Concrete Surface (bottom right) for BBM Test Sequence

Significant elongations of natural period were observed for the N3 anchors. Figure 4-15 shows a wide spread of natural periods, with the initial cycles of the input motion agreeing with WALLE's rigid base natural period of 0.22s, but quickly increasing to periods from 0.4s to 0.6s. For the SEM, this particular range shows large peaks of spectral acceleration on either bound, with a "valley" in between of decreased demands. This is displayed in Figure 4-16, where given the spread of periods between 0.4s and 0.6s, the 500% DBE SEM is the first motion in the test sequence to represent the $\Omega_0 = 1.0$ design level. As with the N1 and N2 anchors, the N3 anchors survive this motion, indicating equal performance with the ductile anchor classification.

It can be noted that the elongated period bounds represented by the (2) and (3) lines are very similar to the (2) and (3) lines laid out as bounds for the N1 anchor. Considerably more points fall within these bounds for the N3 anchor, however, which indicates that large period elongations occur far more frequently in a soft elastic anchor with large displacements than a stiff plastic anchor with large displacements. Nevertheless, both the N1 and N3 anchors show consistent period elongations to around 0.6 seconds for the largest amplitudes of both the SEM and BBM test sequences. This, interestingly, shows a certain degree of convergence to a similar level of component softening for an initially stiff, largely plastic anchor response and a strictly soft elastic response.

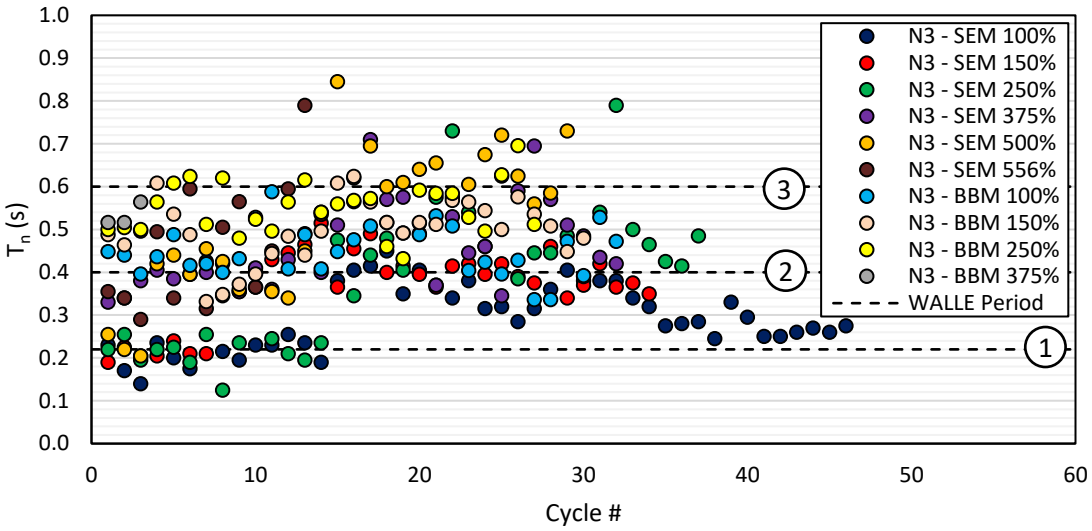

Figure 4-15: Measured Individual-Cycle Natural Periods [Peak-to-Peak] for N3 Anchor

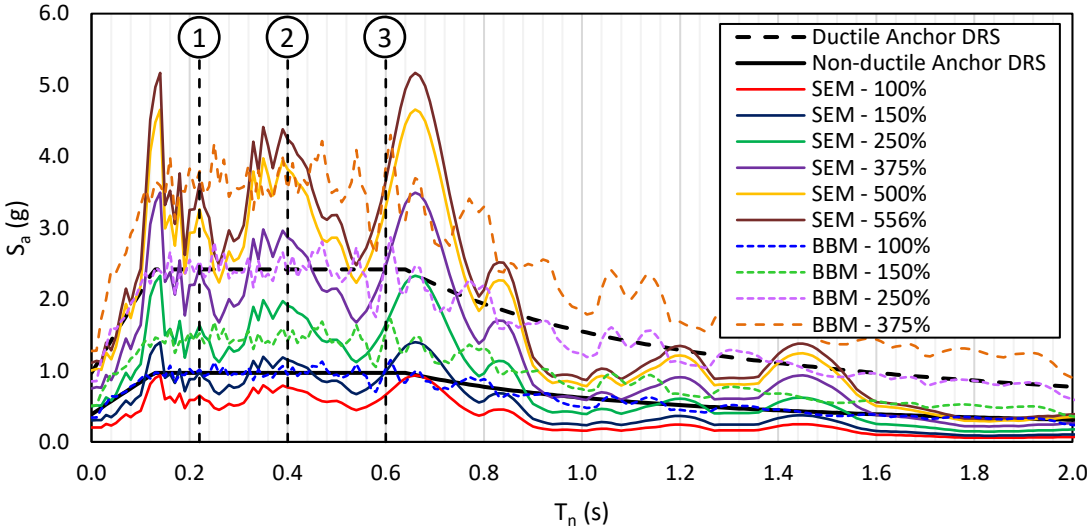

Figure 4-16: Spectral Acceleration Responses for N3 Anchor Test Sequences

4.6 – N5: Expansion Anchor Results

Hysteretic responses for the SEM and BBM test sequences for the N5 anchors, including both south and north anchor pairs, are presented in Figure 4-17. Forces in the N5 anchors were consistently higher dynamically than monotonically by a margin of 20-30%, indicating that the monotonic tests were a conservative predictor of anchor strength. For the BBM tests, these anchors displayed a smooth post-ultimate force negative stiffness branch consistent with the monotonic tests; however, this was not as pronounced for the SEM tests, which displayed abrupt drops in measured force. The expansion sleeves remained in the holes for these anchors upon pullout, and local concrete damage was observed at the concrete surface around the failed anchors for both test sequences. Due to this inconsistency, the force and displacement capacities of the N5 anchors were taken at the point of ultimate force, and the negative-stiffness regions of the anchors were ignored for analytical purposes. It is recommended that anchor displacement capacity be set to this point.

Figure 4-18 shows failure photographs for the N5 anchors for the BBM test sequence. The A1 and A2 anchors – the south anchor pair – pulled out, and local spalling around the hole can be observed. The north anchor pair did not pull out due to engagement of the catcher system. Failure occurred in the north anchor pair for the SEM tests.

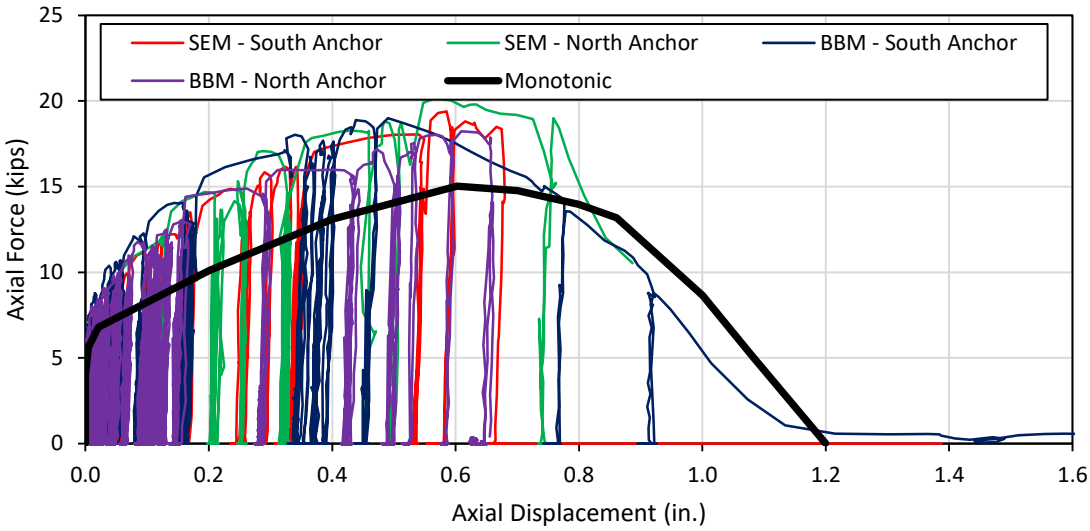

Figure 4-17: N5 Anchor Hysteretic Behavior for All Tests

Figure 4-18: N5 Failure Photographs for A1 Anchor Concrete Surface (top left), A2 Anchor Concrete Surface (top right), A3 Anchor No Pullout (bottom left) and A4 Anchor No Pullout (bottom right) for BBM Test Sequence

Natural period elongations for the N5 anchor share similar trends as the N1 anchor as observed in Figure 4-19. Smaller amplitudes of ground motions cluster around the 0.2s to 0.3s period range, while larger amplitudes that cause plastic displacement show consistent elongation to around 0.4s. As with the N1 anchor, peak period elongations occur at around 0.6s to 0.7s. Despite differing mechanical attachment and resistance mechanisms (bond for the N1 anchor versus friction for the N5 anchor), the N1 and N5 anchors are largely similar in this regard. As these structural tests had a tension-only attachment detail, accrued plastic displacement in the anchor created a gap between the washer and nut, which caused rocking to be an anchor-independent behavior. This resulted in a very soft "free rocking" region of WALLE response in which the axial response of the anchors did not contribute to the rotational stiffness of the component. Indications from these tests suggest that rocking period elongations may be related to a combination of attachment detail and anchor plastic displacement capacity, and would thus be independent of the mechanical behavior of the individual anchor.

Figure 4-20 shows the ARS curves for the N5 anchor for the SEM and BBM test sequences. For the SEM test prior to failure, occurring at the 375% DBE amplitude level, spectral accelerations for all noted periods of response are at or above the ductile anchor DRS. Unlike the other anchor types where the full spectral curve is above the DRS, however, the N5 anchor does not completely satisfy the ductile anchor DRS for the SEM. These differences are small, though, and it should be noted that the provided embedment depth was 3.75 in. for a ½" diameter N5 anchor, which is roughly equivalent to the minimum stretch length required of ductile anchors of $8d_b$. By comparison, the N1 anchors provided a stretch length of

approximately $11d_b$. The extent of plastic displacement capacity thus appears to affect anchor performance, but such influences are relatively small for WALLE.

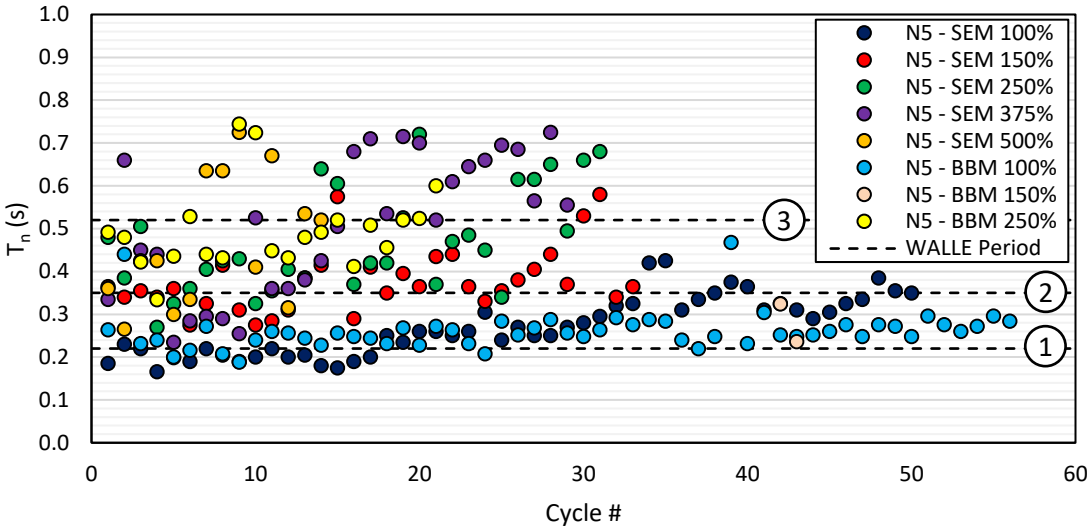

Figure 4-19: Measured Individual-Cycle Natural Periods [Peak-to-Peak] for N5 Anchor

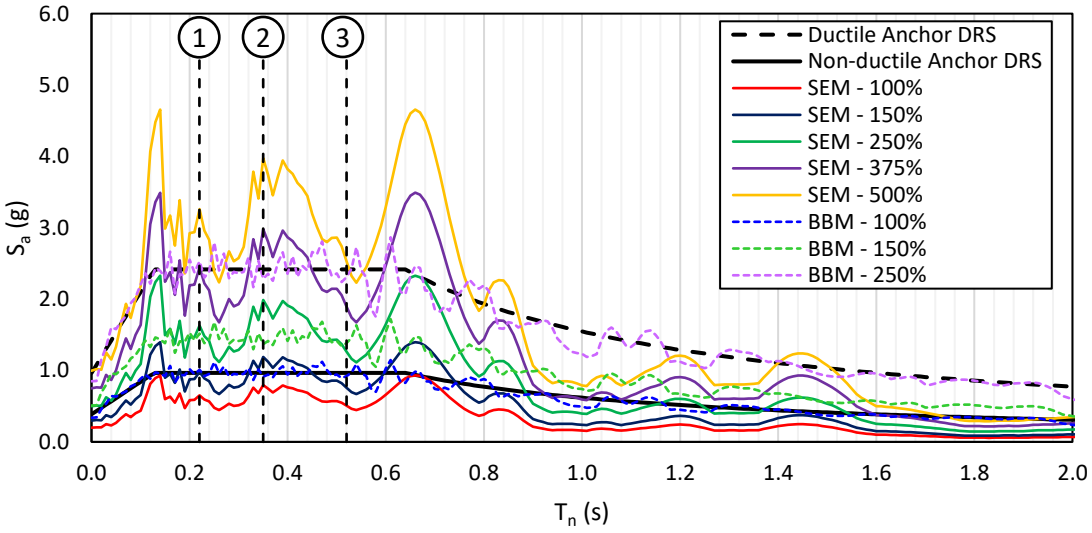

Figure 4-20: Spectral Acceleration Responses for N5 Anchor Test Sequences

4.7 – N6: B7 Steel Thread Rod w/ Ductile SAMU Results

Hysteretic responses for the SEM and BBM test sequences for the N6 anchor, including both south and north anchor pairs, are presented in Figure 4-21. While the N1, N3, and N5 are presented at the same displacement scale for comparison purposes, the displacement axis for the N6 anchors is condensed to allow for greater visual clarity of the hysteretic response. Due to the presence of prying action which did not properly mechanize the ductile SAMU's plastic hinge, the N6 anchor behaved similarly to the N2 anchor. Demonstration of this prying behavior can be seen in Figure 4-22, where clear bearing of the SAMU against the concrete can be observed, but small amounts of flexing in the hinge are also present. The level of increase in force capacity beyond the monotonic curve is significantly smaller than for the N2 anchors, and hysteretic response much more closely follows the monotonic profiles in both measured forces and displacements. This is due to flexing in the hinge reducing impact on the anchors.

On cursory evaluation, the N6 and N2 responses can be considered functionally similar for the ductile SAMU hinge detail used for the BBM test sequence. Failure occurred on the same pulse of the 60% ductile DBE BBM, which is the same as the 150% non-ductile DBE SEM. One key difference, however, is that the N6 anchors have only 3 cycles in which the measured force exceeds the monotonic force capacity, twice at a 5% increase and once at a 10% increase. This starkly contrasts with the 10-12 cycles of the N2 anchor at ≥ 30% increase over the monotonic force capacity, and indicates failure of the N6 was not a fatigue-oriented phenomenon. As such, the strain-rate-dependent behaviors of the N2 anchor do not appear to be present in the N6 anchor. The use of an inelastic hinge detail within the anchor-to-component connection can thus significantly alter the forces and displacements experienced by the anchor, and further

supports observations that the anchor-component system is coupled and each element influences the another. This will be discussed in more detail in Section 4.9.

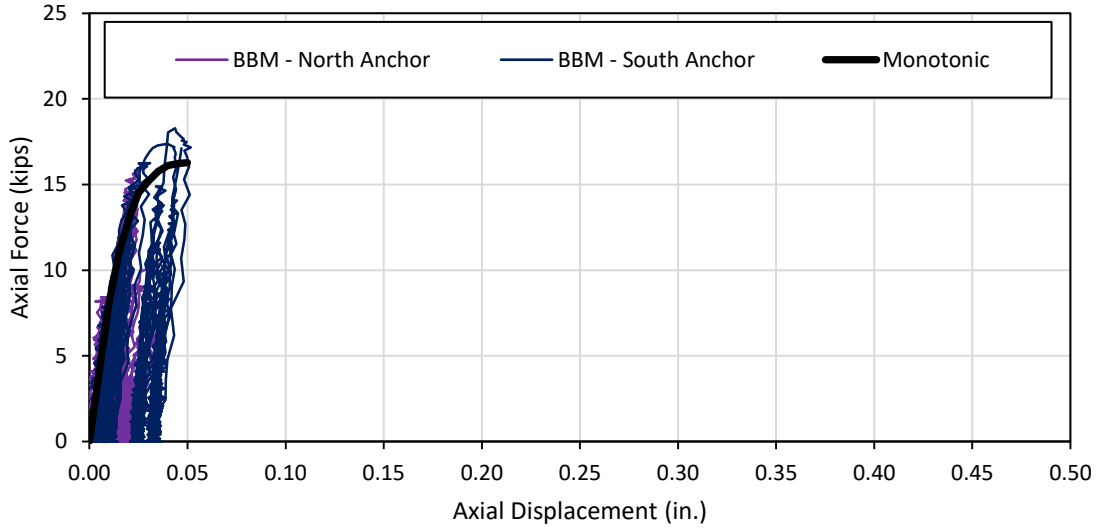

Figure 4-21: N6 Ductile SAMU Anchor Hysteretic Behavior for All Tests

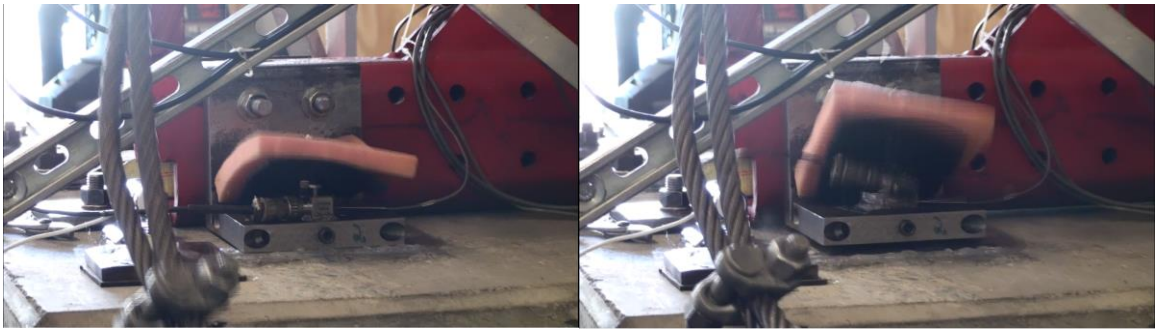

Figure 4-22: Ductile SAMU Prying Action Immediately Before/After Anchor Failure

4.8 – Combined Anchor Comparisons

This section summarizes each anchor presented in the previous sections and combines them into single plots for comparative purposes. Figure 4-23 shows a conglomeration of each

peak-to-peak natural period measured for every input motion used in both test sequences. While most values are close to the rigid WALLE natural period of 0.22 seconds, period elongations were consistent and numerous for all tests. For the three large displacement anchors – N1, N3, and N5 – a large number of cycles occur at periods up through 0.5s. Distribution of measured periods is provided in Figure 4-24, where the majority of response takes place between 0.2s to 0.3s, but a sizeable tail exists for elongated period response. Cumulative percentages show 60% of periods ≤ T_n = 0.3s, 75% of periods ≤ T_n = 0.4s, 88% of periods ≤ T_n = 0.5s, and 95% of periods ≤ T_n = 0.6s.

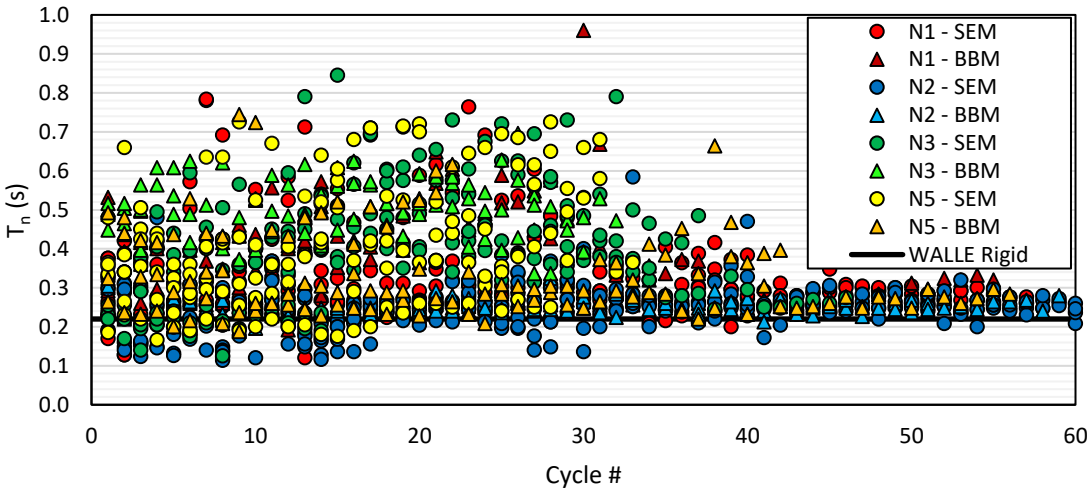

Figure 4-23: Measured Individual-Cycle Natural Periods [Peak-to-Peak] for All Anchors

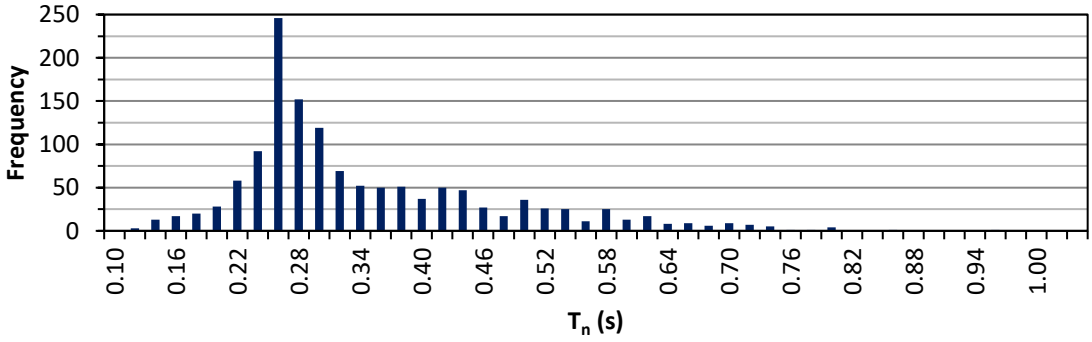

Figure 4-24: Histogram of Measured Component Periods

To validate period elongations for the N1 and N5 anchors, the free rocking natural period of WALLE can be estimated by using the restoring force present when an anchor unloads and resolving the translational acceleration which WALLE is subjected to. The restoring force is equal to the overturning force, given in Eq. 4-1. This can be resolved into acceleration in Eq. 4-2, and then integrated twice into Eq. 4-3. Setting Eq. 4-3 equal to 0, and solving for "t" which would represent a quarter-period yields Eq. 4-4, where d_0 is the displacement of the center of mass at the time of unloading. Using these equations and a plastic anchor displacement of 0.5 in. yields a natural period of T_n = 0.94s.

Results from this equation agree reasonably with structural testing, which show peak periods around 0.7s for the N1 and N5 anchors. In WALLE's real system, a full cycle of free rocking does not occur; WALLE's base touches down on the concrete at a time of approximately T_n / 4. This touchdown stiffens the system for part of the cycle, and contact with anchors as the system finishes a half-cycle provides stiffening as well. WALLE's rigid body rocking period, considering no anchors or influences of ground excitation, is roughly 2.3 seconds.

$$\mathrm{F}_{\text{overturning}} = \frac{W \cdot d_{comp.toe}}{h_{center\ of\ mass}} = \frac{2.55kips \cdot 9in.}{55\ in.} = 0.417\ kips \qquad \textbf{(4-1)}$$

$$a(t) = \frac{\mathrm{F}_{\text{overturning}} \cdot g}{W} \qquad \textbf{(4-2)}$$

$$d(t) = \frac{\mathrm{F}_{\text{overturning}} \cdot g}{2W} t^2 - d_0 \qquad \textbf{(4-3)}$$

$$T_n = 4\sqrt{d_0 \frac{2\mathrm{W}}{F_{overturning} \cdot g}} \qquad \textbf{(4-4)}$$

Combined hysteretic responses for each anchor of the SEM test sequence are presented in Figure 4-25 and Figure 4-26 for the south and north anchors, respectively.

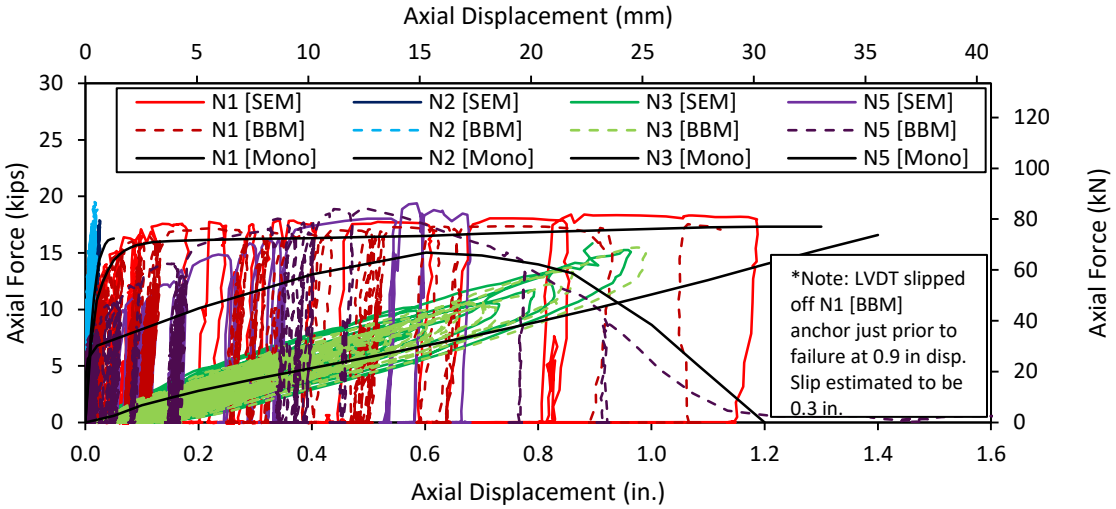

Figure 4-25: Combined Hysteretic Responses for the South Anchor for SEM/BBM Tests

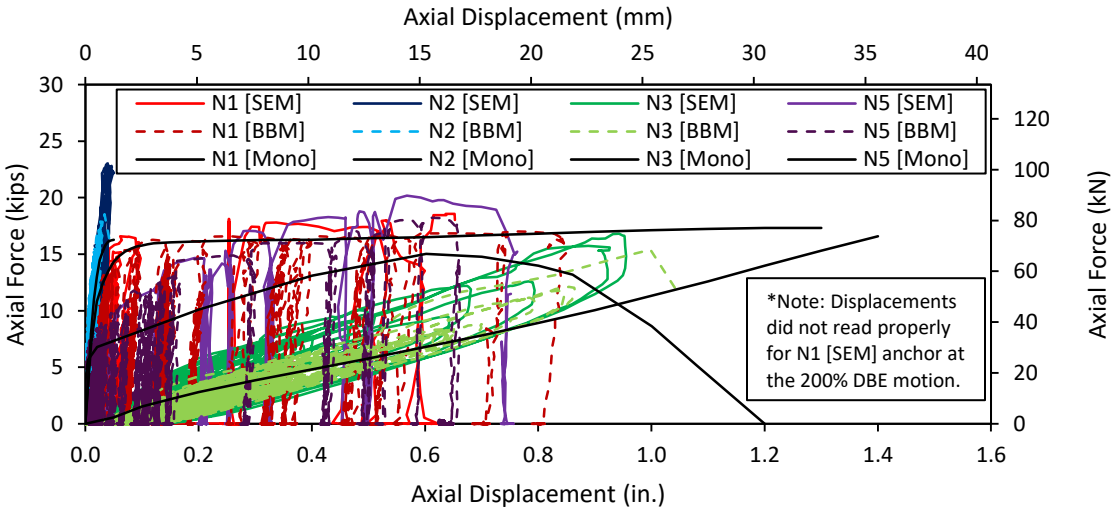

Figure 4-26: Combined Hysteretic Responses for the North Anchor for SEM/BBM Tests

4.9 – Component Center of Mass Results

Component response was evaluated based on a mixture of features both quantitative and qualitative. Table 4-3 and Table 4-4 summarize these metrics, displaying the maxima from each motion run in the single and broadband earthquake sequences, respectively. Appreciable differences exist between both anchor and input motion types, but an important overarching observation is that the component is strongly influenced by its anchorage. Comparing failure and overturn times provides a reasonable insight into component behavior as a whole, with the N3 anchors displaying near-concurrent failure and overturning behavior. This represents visual observations from structural testing video well, where it was noted that WALLE had a particularly violent response when attached to the shaking table with N3 anchors.

Figure 4-27 shows the center of mass acceleration time-history response of WALLE for the 200% ductile anchor DBE SEM test. With the exception of the N5 anchor as failure occurred, maximum acceleration demands are comparable between all anchor types. This was not the case for displacements, shown in Figure 4-28 for this same motion, where the N3 and N5 anchors had larger displacement demands on WALLE compared with the N1 and N2 anchors. Of the N1 and N2 anchors, the N2 anchors had 47% of the N1 anchor displacement demand, and 21% of the N3 and N5 displacement demands. The trends in these plots were consistent for all performed tests, and it can thus be seen that the N2 anchor may offer favorable benefits to component response at the expense of more reliability in anchor response.

Table 4-3: Maxima Comparison for WALLE Behavior for SEM Tests

40% Ductile DBE (Ω_0 = 2.50)	**N1 - Stainless Steel**	**N2 - B7 Thread Rod**	**N3 - B7 Spring**	**N5 - Expansion**
CoM Acceleration (g)	0.30	0.48	0.67	0.60
CoM Disp. (in)	0.19 / 0.37	0.22 / 0.36	0.81 / 1.45	0.59 / 1.10
60% Ductile DBE (Ω_0 = 1.67)	**N1 - Stainless Steel**	**N2 - B7 Thread Rod**	**N3 - B7 Spring**	**N5 - Expansion**
CoM Acceleration (g)	0.34	0.86	0.96	1.47
CoM Disp. (in)	0.33 / 0.61	0.38 / 0.66	1.33 / 2.56	0.95 / 1.75
100% Ductile DBE (Ω_0 = 1.00)	**N1 - Stainless Steel**	**N2 - B7 Thread Rod**	**N3 - B7 Spring**	**N5 - Expansion**
CoM Acceleration (g)	0.80	1.38	1.32	1.65
CoM Disp. (in)	0.58 / 1.10	0.58 / 1.01	1.81 / 3.48	1.41 / 2.51
150% Ductile DBE (Ω_0 = 0.67)	**N1 - Stainless Steel**	**N2 - B7 Thread Rod**	**N3 - B7 Spring**	**N5 - Expansion**
CoM Acceleration (g)	**	2.12	1.56	1.61
CoM Disp. (in)	1.27 / 2.29	0.89 / 1.61	2.80 / 5.28	1.88 / 3.70
200% Ductile DBE (Ω_0 = 0.50)	**N1 - Stainless Steel**	**N2 - B7 Thread Rod**	**N3 - B7 Spring**	**N5 - Expansion**
CoM Acceleration (g)	2.47	2.31	2.18	> 5 (Failure)
CoM Disp. (in)	1.8 / 3.3	0.97 / 1.71	4.56 / 8.84	Overturned
222% Ductile DBE (Ω_0 = 0.45)	**N1 - Stainless Steel**	**N2 - B7 Thread Rod**	**N3 - B7 Spring**	**N5 - Expansion**
CoM Acceleration (g)	> 4 (Failure)	2.4 (Failure)	> 7 (Failure)	N/A
CoM Disp. (in)	Overturned	Overturned	Overturned	N/A
Failure	**N1 - Stainless Steel**	**N2 - B7 Thread Rod**	**N3 - B7 Spring**	**N5 - Expansion**
Failure Time (s)	8.5	6.2	8.8	9.5
Overturn Time (s)	10.0	8.0	9.2	15.1
Failure Behavior	Tension side anchors ruptured, gradual system overturning as catcher system engaged.	All anchors ruptured suddenly, system stabilized briefly and then overturned quickly as catcher system engaged.	Tension side anchors ruptured, system immediately slammed into catcher system in a single, violent motion.	Tension side anchors pulled out, but system stabilized and rocked in place for several seconds with gradual overturning.

* Displacement results presented as “single direction maxima / total maxima both directions”

Table 4-4: Maxima Comparison for WALLE Behavior for BBM EQ Tests

40% Ductile DBE (Ω_0 = 2.50)	**N1 - Stainless Steel**	**N2 - B7 Thread Rod**	**N3 - B7 Spring**	**N5 - Expansion**	**N6 -Ductile SAMU**
CoM Acceleration (g)	0.47	2.00	0.80	**	0.60
CoM Disp. (in)	1.04 / 1.97	0.80 / 1.5	1.71 / 3.45	0.45 / 0.90	**
60% Ductile DBE (Ω_0 = 1.67)	**N1 - Stainless Steel**	**N2 - B7 Thread Rod**	**N3 - B7 Spring**	**N5 - Expansion**	**N6 -Ductile SAMU**
CoM Acceleration (g)	0.70	2.20	1.06	1.87	0.85
CoM Disp. (in)	1.17 / 2.29	Overturned	1.97 / 3.90	1.15 / 2.10	Overturned
100% Ductile DBE (Ω_0 = 1.00)	**N1 - Stainless Steel**	**N2 - B7 Thread Rod**	**N3 - B7 Spring**	**N5 - Expansion**	**N6 -Ductile SAMU**
CoM Acceleration (g)	1.11	N/A	2.07	3.60	N/A
CoM Disp. (in)	Overturned	N/A	3.50 / 6.87	Overturned	N/A
150% Ductile DBE (Ω_0 = 0.67)	**N1 - Stainless Steel**	**N2 - B7 Thread Rod**	**N3 - B7 Spring**	**N5 - Expansion**	**N6 -Ductile SAMU**
CoM Acceleration (g)	N/A	N/A	2.44	N/A	N/A
CoM Disp. (in)	N/A	N/A	Overturned	N/A	N/A
Failure	**N1 - Stainless Steel**	**N2 - B7 Thread Rod**	**N3 - B7 Spring**	**N5 - Expansion**	**N6 -Ductile SAMU**
Failure Time (s)	19.2	18.2	4.1	12.8	17.4
Overturn Time (s)	22.1	N/A	4.1	14.8	N/A
Failure Behavior	Tension side anchors ruptured, and system overturns shortly after. Visual accumulation of plastic displacements in anchors during motion.	Tension side anchors rupture at end of strong portion of motion, other anchors hold on. No overturning.	Failure on first pulse of motion. System overturns immediately in same direction, after anchors fail, to engage catcher system.	Tension side anchors pulled out, but system stabilized and rocked in place for several seconds before overturning on next large pulse.	Tension side anchors rupture at end of strong portion of motion, other anchors hold on. No overturning

* Displacement results presented as “single direction maxima / total maxima both directions”

** Device did not read properly for this test.

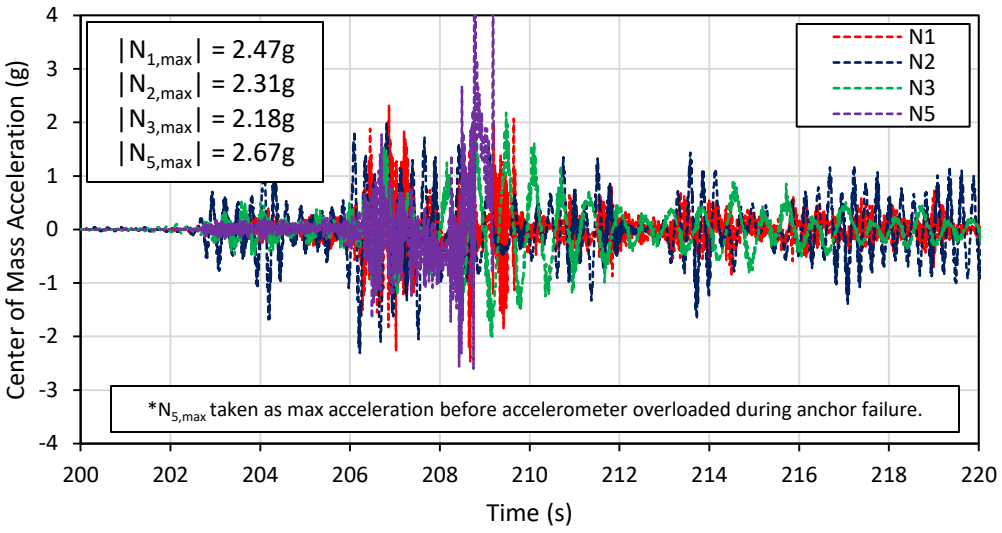

Figure 4-27: Center of Mass Acceleration Time-History Response for 200% Ductile Anchor DBE SEM

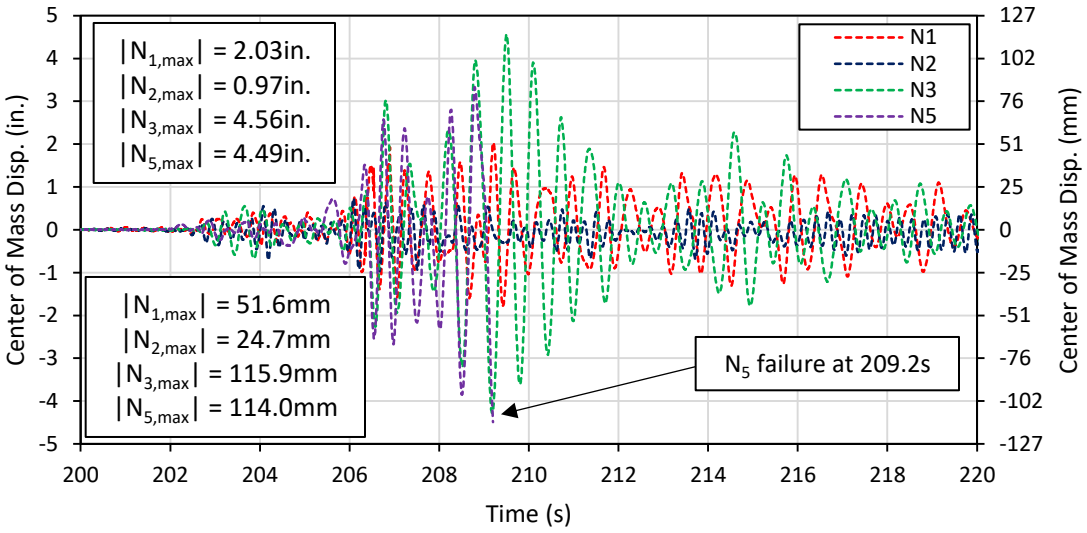

Figure 4-28: Center of Mass Displacement Time-History Response for 200% Ductile Anchor DBE SEM

4.10 – Influences of Strain Rate and Low-Cycle Fatigue

Increases in observed anchor strength between monotonic and dynamic testing were present in all structural tests performed, which is consistent with expectations of steel as a strain-rate dependent material. Seismically relevant loading rates have been shown to produce a stiffening effect in structural steel members, typically resulting in a 5 – 10% increase in force capacity (Bruneau et al., 2011). Knowledge of these influences in anchors is limited, however, as most research regarding strain-rate dependence focuses on concrete failure modes. Hoehler et al. (2011) performed a detailed study on seismically-relevant loading rates for anchors, bounded between rise times from zero to peak load of 0.025 to 0.25 seconds, but included no steel failure modes as a part of their study and note no known work regarding strain-rate influences on steel behavior. Minimum observed rise times in the work presented in this chapter were about 0.06 seconds. With respect to pull-through behavior, research by Klingner et al. (1998) showed a great deal of variation in expansion anchors for cracked and uncracked concrete, but made note of potential increases upwards of 27% of monotonic force capacity. Hoehler (2006) and Hoehler et al. (2011) report similar findings as Klingner et al. (1998) with respect to pull-through failure modes.

The amount of increased force capacity in the anchors above the monotonic capacity of 8.2 kips was variable, but not universally insignificant for testing purposes. As discussed in Section 4.3 and Section 4.5 for the N1 and N3 anchors, respectively, increases for these anchors were between 0-10%, and are largely negligible. The N5 anchors had ultimate force capacities bounded between roughly 7 and 9 kips from the reference tests presented in Section 2.4, and dynamic testing showed forces between 9 and 10.5 kips – averaging around 20%, which is consistent with observations stated above. Measured anchor force increases of over 30% were

noted in the N2 anchors in some tests, however, reaching at least 10.5 kips during several dynamic cycles. This value potentially exceeded the 11.2 kip upper limit of the measurement range of the 10 kip load cells, and was high enough during anchor failure to severely damage the load cell casings. These force levels were reached only in the real earthquake test sequences, and were limited to an increase of roughly 20% for the broadband tests. The mechanisms of this behavior thus appear to be reliant on the characteristics of the ground motion, and are not well understood at this time.

Force increases in the N2 anchors not only exceeded the monotonic capacities by 20%, but were unloaded and re-loaded repeatedly. In the critical anchors, loading cycles with measured forces in excess of the monotonic capacity occurred 10 times for the single earthquake motion and 12 times for the broadband motion. These counts suggest low-cycle fatigue as a cause, as they are complemented by the cyclic loading and unloading of the N2 anchors at large, localized plastic strains. While the base material of the N2 anchors, ASTM A193 B7 steel, is a moderately ductile steel with ultimate strains of approximately 14%, the presence of the notch localizes large plastic strains in a small region of the anchor rather than allowing plasticity to spread over a large region. This causes the notch to act as a strong attractor for fatigue cracks (Manson, 1965).

Silva and Hoehler (2008) note that low-cycle fatigue in anchors is a poorly studied field with minimal research. A proximal study of fatigue tests by Mander et al. (1994) on A615 Grade 60 rebar, a similar high strength carbon steel to A193 B7 steel, demonstrated that the test specimens were capable of sustaining numerous cycles at load levels close to the ultimate force level of the bars. Mander et al. (1994) also note that machining of notches into test specimens generally results in a localized hardening effect that may distort observations in material

behavior within the notched area compared with un-notched regions. Given the differences, however, between Mander's tests and those documented in this chapter, along with a small sample size of N2 anchor tests performed in these tests, further research is required to understand the influences of low-cycle fatigue on steel anchor behavior.

4.11 – Summary of Findings

From the structural tests presented in this chapter, the most prominent finding was that all anchor types performed similarly despite having differing resistance mechanisms. Anchors classified as ductile in ACI 318 did not perform significantly better than those classified as non-ductile, and failure levels were comparable for all anchor types for both a real earthquake motion and a broadband earthquake motion. Plastic displacement capacity in general, and not strictly material ductility, offered two key advantages over stiff-elastic response:

a. Reliability. Anchors with large plastic displacement capacity responded with resistance mechanisms that were represented well by their monotonic force versus displacement response. This benefit appears to be path-independent.
b. System rocking. From physical observation of test video, rocking behavior of the nonstructural component without engaged anchors showed significant elongation of the translational natural period.

While the structural tests showed no distinguishable performance differentials at the anchor level for elastic versus plastic displacement capacity, it should be noted that this may be coincidental in the structural tests due to a low sample size of motions. From the analytical work presented in Chapter 7, the soft elastic anchors showed a wide range of variability based on

system parameters; while they performed well in this test sequence for a particular class of weight and rotational mass, this may not be readily extrapolated to other NCSs.

Also of great importance was the coupled relationship between component and anchor response. Current code provisions treat the two systems as independent entities, where the component is designed and then anchor is designed in accordance with said component's response parameters. Demands on WALLE, however, changed significantly based on anchor type used. As discussed in Chapter 7, the component demand force equation is sensitive to component input parameters when determining conservative design values for anchors, and the influence of anchors on NCSs may alter component behavior significantly.

4.12 – Acknowledgement of Publications

Various parts of several sections in this chapter are taken from the following publication, of which the author of this dissertation assumes primary authorship:

Johnson, T.P. and Dowell, R.K. (2017 - Acceptance Pending Revisions). "Evaluation of the Overstrength Factor for Nonstructural Component Anchorage into Concrete via Dynamic Shaking Table Tests." *Journal of Building Engineering*.

CHAPTER 5: ANALYTICAL MODELING OF STRUCTURAL TESTS

During the structural testing process, an analytical model was developed in the nonlinear finite element program SAP2000 to perform test predictions and select appropriate ground motions to ensure failure on SDSU's shaking table. Upon completion of the testing program, it was also used to perform post-test simulations. This model predicted elastic response of the WALLE with a fair level of accuracy, but had significant shortcomings when modeling large levels of plastic deformation in the anchors. Long run times, convergence issues with large sensitivity to anchor stiffness, and equilibrium problems between the anchor elements and attached hook elements ultimately led to a different analysis option being considered.

The majority of this chapter is devoted to the development of an alternative model to a finite element solution, based on first principles and structural mechanics. This model was developed as an independent program with multiple analysis modules, batch mode processing, post-processing, and several other feature sets. It provided the fundamental backbone for the over 500,000 nonlinear time-history analyses used to develop the Ω_0 recommendations of Chapter 7.

5.1 – Conventional Finite Element Model

Initial modeling for analysis of the shaking table tests was performed using the general purpose finite element program SAP2000. A two-dimensional nonlinear model was built as shown in Figure 5-1, mixing together an array of linear and nonlinear elements. Frame elements were subdivided into two parts: WALLE's mast, which was modeled using a HSS 4"x4"x3/8" steel section, and WALLE's base, which used highly stiff elements to represent a rigid base plate

response. Gap elements were tuned to have zero stiffness when subjected to tensile forces, and an elastic compressive stiffness of 10,000 kips/in. when subjected to compressive forces. Hook elements followed a similar pattern to gap elements, with zero stiffness subjected to compressive forces and 10,000 kips/in. when subjected to tensile forces.

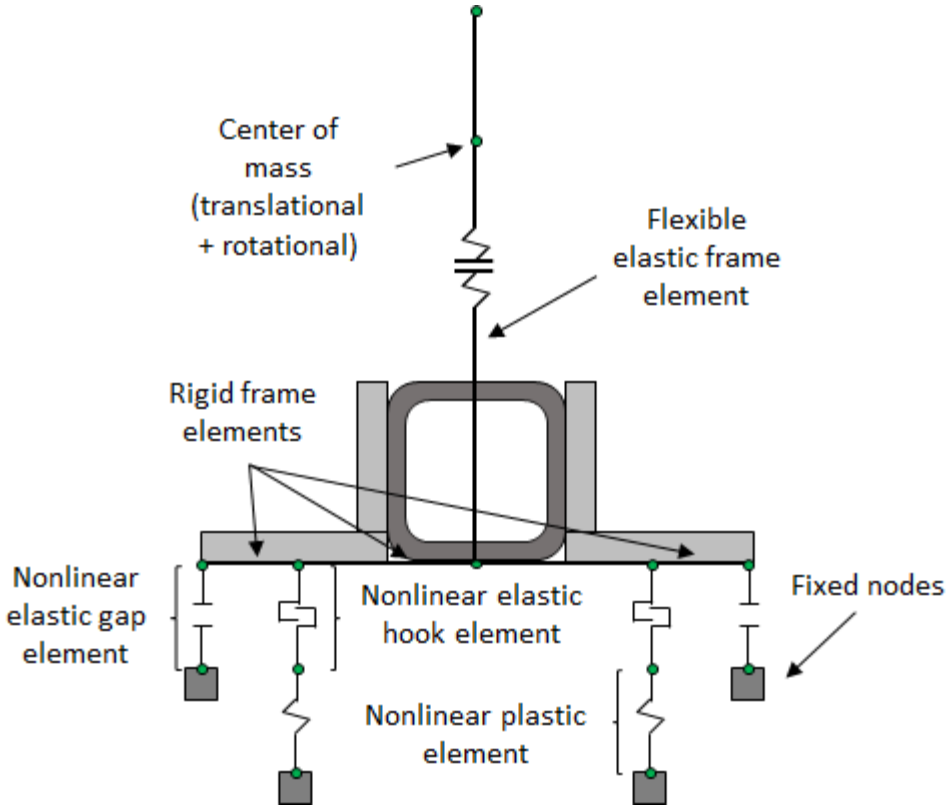

Figure 5-1: Nodal and Frame Element Layout of SAP2000 Model

This model displayed a high level of sensitivity to the relative stiffnesses between the gap/hook elements and anchor elements. Convergence problems tended to occur for the stainless steel [N1] and expansion [N5] anchors, which had stiff initial responses and soft plastic response. Softening the gap/hook elements alleviated some convergence issues, but

consequently caused a loss in accuracy. Run times for the model were fairly long for a single earthquake, ranging between 1 and 3 hours depending on the extent of nonlinear behavior.

Prediction and post-test modeling of the structural tests in 0 were performed using this model, with comparisons between SAP2000 results and structural testing presented in Chapter 6. Analysis used a standard Newmark-Beta direct time-history integration with parameters of $\beta = 0.25$ and $\gamma = 0.50$, which results in the Average Acceleration Method. A mass- and stiffness-proportional Rayleigh damping matrix was constructed using specified natural periods of $T_n = 0.22s$ and $T_n = 0.03s$, which corresponded with WALLE's fundamental first and second mode periods.

Using a uniform equivalent viscous damping ratio of 2%, the SAP2000 model displayed varying levels of accuracy. While it reproduced the structural tests relatively well for the largely elastic B7 thread rod [N2] and B7 spring [N3] anchors, the nonlinear anchors struggled with a great deal of convergence issues. In particular, instantaneous anchor forces from SAP2000's gap elements did not match the forces expected from the associated instantaneous accelerations of the center of mass. Additionally, axial forces inside the nonlinear anchor elements did not always match the nodal forces on either end.

Initially, the parametric work presented in Chapter 7 was intended to be performed using this finite element model verified against structural testing results. A combination of long run times and noted convergence issues, however, limited the number of parameters that could be evaluated and the number of earthquakes that could be run as part of the study. An alternative approach was thus sought that could target the specifics of the rocking problem without the need for general purpose algorithms. In some cases, such as elastic anchorage, this

model worked well, and was thus used largely as a verification tool instead of the primary modeling program for the structural testing sequences.

5.2 – Mechanics-Based Model: NARRAS

A significant part of this research effort was developing an analysis model which could handle the highly nonlinear behavior present in component-anchor seismic response. Even with elastic anchors, the anchored nonstructural component behaves in a nonlinear-elastic manner, and thus nonlinearity is a fundamental part of the rocking problem. Implicit time integration procedures which require stiffness matrix inversion can have convergence problems with large changes in stiffness, and have difficulty capturing the boundary conditions of the rocking component problem. To mediate these problems, the rocking phenomenon was approached from a perspective of first principles, and a series of closed-form solutions were derived in order to capture WALLE's rocking behavior.

The program developed, written in C#, is called NARRAS (Nonlinear Anchor Rocking Response Analysis Solution). Analysis in NARRAS is approximately three to four orders of magnitude faster than an equivalent analysis in SAP depending on the extent of nonlinear behavior; a time-history analysis with one million data points can finish in approximately one second on the author's computer, whereas an equivalent SAP2000 analysis might take two to three hours. Such large numbers of data points are required in order to have a time step small enough to capture response of the second mode.

5.2.1 – General Solution Method

Numerical integration of the equation of motion is performed using an explicit Newmark-Beta method with parameters $\beta = 0.25$ and $\gamma = 0.50$, which results in the widely-used

Average Acceleration Method. Linear interpolation of ground motion time steps is allowed within the program such that the user may define a solution that is numerically convergent without the explicit need to modify the input earthquake motions directly. Two independent solution methods exist: a single-degree-of-freedom solution that employs geometric relationships to map system behavior to anchor behavior, and a two-degree-of-freedom solution which implements modal analysis techniques alongside a unique stiffness matrix and specialized hysteresis rules. For both cases, analysis is treated as a series of sequential elastic analyses segmented by an assortment of nonlinear events in which elastic properties are updated at each time step.

After solution of the equation of motion for a given time step is complete, anchor hysteresis is performed depending on one of three phases for upright components and one of four phases for hanging components. These phases are detailed in Section 5.3, and each time the system transitions between phases or has a stiffness change, a nonlinear event is triggered. Nonlinear event points are tracked for each time step based upon anchor plasticity and system geometry; upon detection, the time step in which an event occurs is discretized and the exact time at which this event occurs is either solved in closed form or iterated depending on the complexity of the solution (SDOF is exact, MDOF must be iterated). All response quantities are adjusted to the nonlinear event time, and the analysis then continues with appropriately updated parameters. The exact number of time steps at the start of the analysis is thus an unknown, and varies widely depending on the extent of nonlinear behavior present in the system.

The program terminates when either the last time step is reached or when an anchor reaches its ultimate displacement as defined by the user's force-displacement curve.

5.2.2 – Single-Degree-of-Freedom Stiffness Solution

For a single-degree-of-freedom system with only translational mass considered, a one-to-one relationship exists between the translational displacement of the center of mass and the associated anchor displacement. This is due to the restoring force being directly related to the moment that develops at the component base. Given this relationship, an envelope of the force-displacement response of the component center of mass can be derived knowing the force-displacement response of the anchors present on either side of the component. With this envelope known, adjustments to the center of mass force displacement response can be performed (such as stiffness reductions from P-delta effects), and an adjusted anchor response can be derived.

To formulate the stiffness solution, the center of mass response is divided into two components: the elastic deformation associated with the restoring force on the component, and the rigid body rotation associated with the elongation of the anchor. For a given level of force acting on the center of mass, there are thus two displacement responses which may be superimposed over a given stiffness value on the force-displacement curve. This process is demonstrated in Figure 5-2 for the monotonically measured response of the N1 stainless steel anchors. The combination of the anchor and component in this way is identical to consolidation of responses using rules to combine stiffness terms in series into an equivalent stiffness.

It can be noted that the anchor flexibility does not contribute until the center of mass force reaches the required threshold to overcome the base moment associated with the component self-weight (the overturning moment). Once the combined response is determined, the curve is discretized in a series of regions with a given stiffness value and displacement/force boundary values. Including P-Delta influences at this point is quite clean; these stiffness values

can be adjusted easily, and the boundary values can be rotated in kind. This formulation is performed prior to any analysis, which means no stiffness computations need be performed during the analysis regardless of the extent of nonlinearity or if the stiffness is positive or negative.

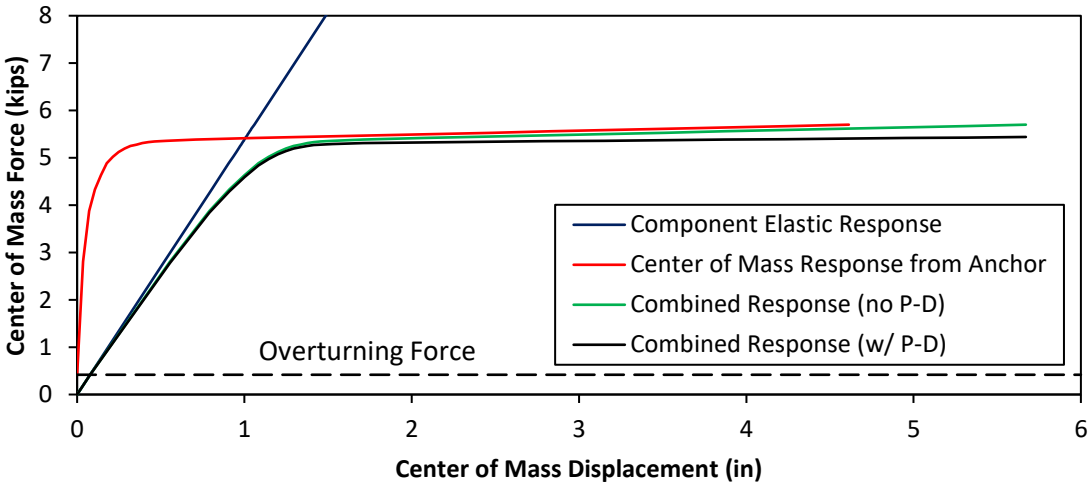

Figure 5-2: Example of SDOF Stiffness Formulation

This envelope need not be symmetrical depending on anchor force-displacement responses and system geometry. From the envelope, hysteretic rules describe the entirety of response during the equation of motion solution. These rules, discussed in Section 5.3, can be determined rationally from a first-principles assessment of how forces must change in the system in order for equilibrium to be maintained. A sample plot of one of the hysteresis verification algorithms is presented in Figure 5-3 to demonstrate how this response is developed. Because a one-to-one relationship exists between the anchor and center of mass responses due to displacement compatibility, anchor behavior can be rationally determined at each time step as the center of mass response is solved.

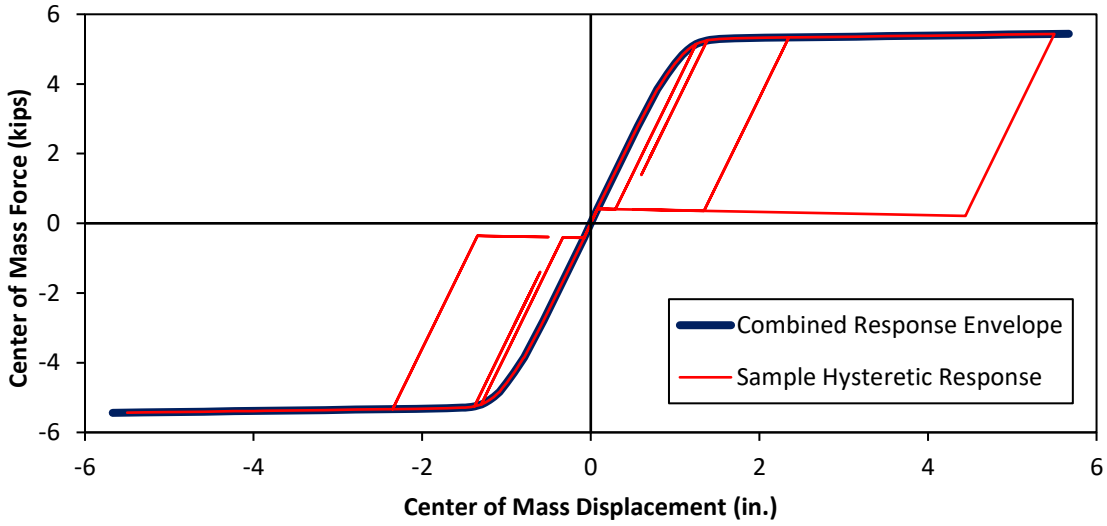

Figure 5-3: Example of SDOF Hysteretic Response w/ P-Delta

One key advantage implicit within this solution method is that the time at which a nonlinear event occurs between two time steps exists as a closed-form solution. The equation of motion can be rearranged as a cubic solution for this exact time step, given below in Eq. 5-1. The general form of this solution at increment "i" where a nonlinear event occurs is taken at a starting time, t_i. Notation for this is as follows: M, C, and K represent the time step mass, damping coefficient, and stiffness values, respectively. Input acceleration, center-of-mass relative velocity, and center-of-mass relative acceleration, are denoted as $\ddot{z}$, $\dot{w}$, and $\ddot{w}$, respectively. Lastly, the center of mass displacement associated with the nonlinear event is given by Δ_{NLE}, and the displacement at the start of the time step is given by Δ_i. Only one unique solution will exist that falls within the bounds of the specified time step.

$$A_t \cdot (t_i + \delta t)^3 + B_t \cdot (t_i + \delta t)^2 + C_t \cdot (t_i + \delta t) + D_t = 0$$

$$A_t = M \cdot (\ddot{z}_{i+1} - \ddot{z}_i)/(t_{i+1} - t_i)$$

$$B_t = 2 \cdot C \cdot \dot{w}_i + 2 \cdot M \cdot \ddot{w}_i - K \cdot (\Delta_{NLE} - \Delta_i) \quad \textbf{(5-1)}$$

$$C_t = 4 \cdot M \cdot \dot{w}_i - 2 \cdot C \cdot (\Delta_{NLE} - \Delta_i)$$

$$D_t = -4 \cdot M \cdot (\Delta_{NLE} - \Delta_i)$$

5.2.3 – Multiple-Degree-of-Freedom Stiffness Solution

For a system including both translational and rotational degrees of freedom, a more complicated solution is required. This is due to the anchor force being influenced both by a restoring force and a restoring moment acting on the center of mass, meaning that a one-to-one relationship between the center-of-mass response and the anchor response is no longer present. To compensate for this, an approach is taken that assesses the influence of the translational and rotational masses as a coupled system via modal analysis and formulation of a matrix solution to the equation of motion. Unlike the relationships demonstrated previously in Figure 5-2, the center of mass force no longer uniquely corresponds to the center of mass displacement, as the driving moment from the rotational mass changes the shear forces acting in the component mast.

This complication creates a large conceptual leap in the solution method, as the rocking behavior of the component base now must be explicitly tracked, whereas in the SDOF solution these results were generated as a byproduct of the process. Traditionally, finite elements would create a solution by providing elements to the base of the component – anchors, compression springs, beam members, etc. – and assigning degrees of freedom to the nodes at the ends of

the anchor elements and rotation points. The resulting system generates a large, multi-term stiffness matrix that now has considerable geometric and spatial influences.

An alternative was sought in this project to condense the entirety of this rocking behavior into the stiffness matrix at the center of mass of the mast – thus removing the two to four additional frame elements needed to capture the base rotational response. A similar principle as the SDOF system was applied to the mast, which supposed that the rocking behavior of the base could be mapped into the component mast as a rotational spring. This spring softens the existing stiffness terms developed for the local stiffness matrix of a standard frame element. Derivation of this process can be found in Appendix A, which results in a modified stiffness matrix for a cantilever beam which takes the form given in Eq. 5-2. The x and y directions represent the horizontal degrees of freedom of the component center of mass, while the z direction represents the vertical degree of freedom.

$$[K] = \begin{matrix} x \\ y \\ z \\ \theta_x \\ \theta_y \\ \theta_z \end{matrix} \begin{bmatrix} \frac{3EI_y}{\ell^3}\left(\frac{1+4\alpha_x}{1+\alpha_x}\right) & 0 & 0 & 0 & \frac{-3EI_y}{\ell^2}\left(\frac{1+2\alpha_x}{1+\alpha_x}\right) & 0 \\ 0 & \frac{3EI_x}{\ell^3}\left(\frac{1+4\alpha_y}{1+\alpha_y}\right) & 0 & \frac{-3EI_x}{\ell^2}\left(\frac{1+2\alpha_y}{1+\alpha_y}\right) & 0 & 0 \\ 0 & 0 & \beta\frac{AE}{L} & 0 & 0 & 0 \\ 0 & \frac{-3EI_x}{\ell^2}\left(\frac{1+2\alpha_y}{1+\alpha_y}\right) & 0 & \frac{3EI_x}{\ell}\left(\frac{1+{}^4\!/_3\,\alpha_y}{1+\alpha_y}\right) & 0 & 0 \\ \frac{-3EI_y}{\ell^2}\left(\frac{1+2\alpha_x}{1+\alpha_x}\right) & 0 & 0 & 0 & \frac{3EI_y}{\ell}\left(\frac{1+{}^4\!/_3\,\alpha_x}{1+\alpha_x}\right) & 0 \\ 0 & 0 & 0 & 0 & 0 & \gamma\frac{JG}{L} \end{bmatrix} \quad \textbf{(5-2)}$$

The α, β, and γ terms in this modified stiffness matrix represent the softening effects the anchors have on the base of the component; α represents rotational softening, β represents axial softening, and γ represents torsional softening. These factors are defined below in Eq. 5-3,

and this matrix reduces to the standard stiffness matrix of a cantilever beam as the anchor contribution in each of these terms approaches infinity. The term k_s represents a rotational spring stiffness that can be derived as discussed below, $K_{A,b}$ represents the axial stiffness of the anchorage system, and $K_{T,b}$ represents the torsional stiffness of the anchorage system. A more thorough presentation of these terms and this method is presented in Johnson and Dowell (2017b).

$$\alpha_x = \frac{k_{s,x}\ell}{4EI_y} \qquad \alpha_y = \frac{k_{s,y}\ell}{4EI_x}$$

$$\beta = \frac{K_{A,b}}{K_{A,b} + {AE}/{L}} \qquad \textbf{(5-3)}$$

$$\gamma = \frac{K_{T,b}}{K_{T,b} + {JG}/{L}}$$

For the modeling of WALLE, only the translational and rotational degrees of freedom were considered. The above stiffness matrix can thus be simplified and reduced into the form in Eq. 5-4. As only one direction of base rotation was considered, the directionality of α need not be considered. The k_s term within α is generically presented, and must be derived for the anchorage system based on first principles or by a numerical process when applying this stiffness formulation to specific problems. For modeling of WALLE, two different k_s values were required for the upright and hanging configurations.

$$[K] = \begin{bmatrix} \frac{3EI}{\ell^3}\left(\frac{1+4\alpha}{1+\alpha}\right) & \frac{-3EI}{\ell^2}\left(\frac{1+2\alpha}{1+\alpha}\right) \\ \frac{-3EI}{\ell^2}\left(\frac{1+2\alpha}{1+\alpha}\right) & \frac{3EI}{\ell}\left(\frac{1+{}^4/_3\,\alpha}{1+\alpha}\right) \end{bmatrix} \qquad \textbf{(5-4)}$$

For components bearing against the concrete on a compression toe with a rigid base plate, k_s can be derived as a function of anchor stiffness, k_a, and the distance of the anchor from the point of rotation, Δ_a, for "n" number of anchors. This is shown below in Eq. 5-5.

$$k_{s,bearing} = \sum_{i=1}^{n} k_{a,i} \cdot \Delta_{a,i}^2 \qquad \textbf{(5-5)}$$

An alternative solution is required for hanging components when the system is not bearing, but hanging freely. A clean general solution for this case cannot be readily derived, but a closed-form solution exists for a two-anchor system with an anchor on each side of the component center of mass. Extending the above notation with subscripts of "L" and "R" to denote the left and right anchors, respectively, yields Eq. 5-6. Rotation for this solution occurs at the midpoint between the anchors, which may not coincide with the center of mass.

$$k_{s,hanging} = \frac{k_{a,L} \cdot k_{a,R} \cdot \left(\Delta_{a,L} + \Delta_{a,R}\right)^2}{k_{a,L} + k_{a,R}} \qquad \textbf{(5-6)}$$

Because k_s is dependent on anchor stiffness, the stiffness matrix must be updated every time a nonlinear event occurs.

5.2.4 – Damping Solution

Selection of the damping model for NARRAS was a complicated process that evaluated several possible alternatives. For time-history methods that solve the equation of motion through incremental modal analysis, two primary variations of damping formulations are

typically considered: Rayleigh and Wilson-Penzien. The former, shown in Eq. 5-7, has prolific use in modern structural dynamics, and offers a viscosity-based damping solution proportional to a structure's mass and stiffness. The latter, shown in Eq. 5-8, was proposed by Wilson and Penzien (1972), which assumes an orthogonal damping matrix C* between different modes, which may then be used to back-populate a coupled damping matrix consistent with user-defined modal properties. As long as a structure remains linear-elastic, these formulations are similar. The primary advantage of the Wilson-Penzien solution being that the user may customize damping for each mode individually and, in the event of a modal analysis, can prescribe these terms directly.

$$[C] = \delta_1[M] + \delta_2[K]$$

$$\begin{Bmatrix}\delta_1\\ \delta_2\end{Bmatrix} = 2\begin{bmatrix}\frac{1}{\omega_1} & \omega_1\\ \frac{1}{\omega_2} & \omega_2\end{bmatrix}\begin{Bmatrix}\xi_1\\ \xi_2\end{Bmatrix} \quad \textbf{(5-7)}$$

$$[C^*] = 2\begin{bmatrix}\xi_1\omega_1 m_1 & 0\\ 0 & \xi_2\omega_2 m_2\end{bmatrix} \quad \textbf{(5-8)}$$

In either case, the appropriate use of damping methods is an issue of contention, and the popularity of Rayleigh damping stems from its ease of implementation and standard convention (Carr 2015). Carr discusses at great length the inadequacies of current approaches to the damping problem, and states that to date many of the inaccuracies of these methodologies are accepted simply due to a lack of viable alternatives. He argues that these problems become

increasingly apparent as the nonlinear behavior of a structure increases, and having structural stiffness changes as elements yield creates significant complications in determining the proper form of the damping matrix due to its lack of connection to physical properties. Charney (2008) mirrors much of Carr's sentiment, and compiles a list of numerous papers detailing the inaccuracies of "classical" viscous damping approaches and their treatments of nonlinear problems. He notes that conventional damping models have a tendency to create unrealistically high damping forces in nonlinear analyses, and cautions that many proposed solutions to this are only situationally applicable. Notable among his mentions are Shing and Mahin (1987), who discuss that off-diagonal terms may generally be neglected for damping formulations that become non-classical as structures soften. Efforts are underway to try to develop new damping formulations specific to structural behavior, such as Puthanpurayil et al. (2016), but as of yet no definitive models have been proposed.

Using these numerous sources as guidance, NARRAS was originally programmed with a Rayleigh damping solution where the stiffness matrix was taken to be the tangent stiffness at the beginning of a given time step. This allowed for the damping matrix to update and diagonalize properly as the mode shapes of the system changed, and correctly zeroed off-diagonal terms in the damping matrix during the diagonalization process to maintain a classical formulation. A numerical problem resulted from this approach, however, from the fact that as the anchors yielded, only the translational mode's stiffness reduced to zero. The rotational mode retained some level of stiffness, resulting in a high frequency response with an artificially large damping constant. Carr (2015) has observed this effect in several structures, where this large damping force has a tendency to drive the system towards regions of residual plastic displacement and create an artificial ratcheting behavior that is not realistic. An example of this

behavior in NARRAS is shown below in Figure 5-4, where a set of increasing amplitude ground motions run in series shows the analysis continuously drifting in one direction due to damping forces which override the restoring forces. For all upright anchor systems, the solution should always return to zero residual base moment, as the restoring force caused by the overturning moment should drive the system back into the region of response where no anchors are engaged.

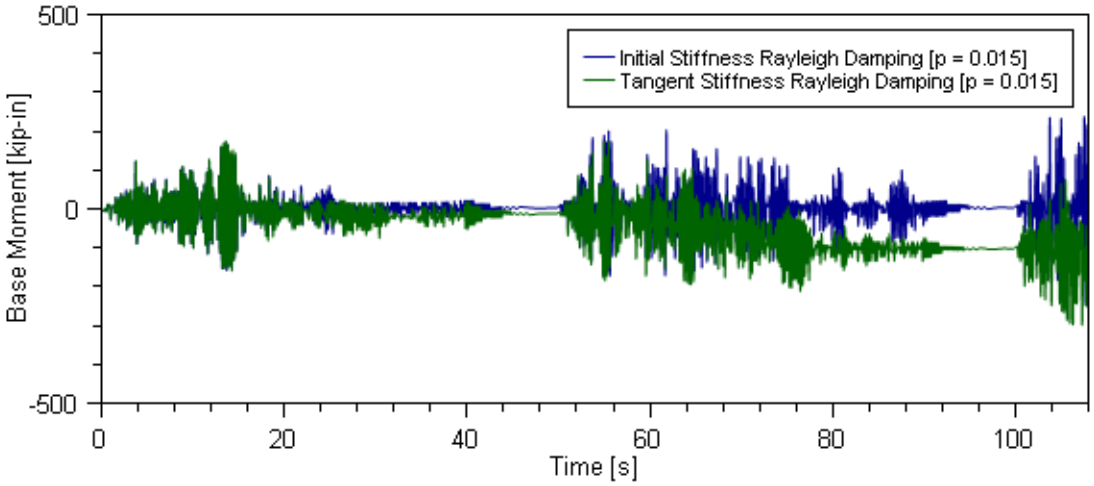

Figure 5-4: Numerical Drifting caused by Tangent Damping Formulation

While not ideal, an alternative was evaluated where the damping matrix remains constant throughout the analysis based strictly on the initial stiffness of the system. This approach results in a non-classical damping matrix once any nonlinear behavior occurs, and causes the off-diagonal terms in the damping matrix to not diagonalize properly during the modal decomposition process. With only two mass degrees-of-freedom in the program, however, problems with runaway damping values due to modes with extremely high frequencies were not a concern. This being the case, Clough and Penzien (1993) advise that the

off-diagonal damping terms may be ignored and still represent a strong approximation of system damping when performing modal superposition.

Ultimately, the direct prescription of damping values per the Wilson and Penzien approach was adopted, and errors due to ignoring off-diagonal terms of the damping matrix were determined to be acceptable. While some small residual offsets can occur due to the damping matrix not properly diagonalizing during plastic response, it can be seen in Figure 5-4 that these influences are small to negligible.

5.2.5 – Tension-Shear Interaction

Tension-shear interaction was added as a feature for anchor scaling by including a user-specified parameter quantifying shear demand on the anchor as a percentage of its ultimate shear force. The interaction surface is a circular function taken from Eligehausen et al. (2006) for post-installed anchors with steel failure modes. This shear force ratio is given as V/V_u in Eq. 5-9, where N_u and V_u are the ultimate tensile and shear forces for pure tensile and shear loads, respectively, and k = 2. The modified ultimate tensile force, N, may then be resolved, and the user-defined anchor force-displacement curve is then scaled via dimensional analysis principles. This was discussed as a potential variable to be used in the parametric studies of Chapter 7, but was decided in meetings with the research program sponsors that it was not of interest to study.

$$\left(\frac{N}{N_u}\right)^k + \left(\frac{V}{V_u}\right)^k = 1.0 \qquad \textbf{(5-9)}$$

5.2.6 – Nonlinear Geometry: P-Delta Influences

For the SDOF solution, P-delta influences were incorporated by performing a rotation of the center-of-mass force-displacement curve. This rotation was associated with a readily-derived reduction in stiffness proportional to the axial force acting on the component divided by the component height. This method is highly advantageous in that it allows for solution of the equation of motion for zero and negative stiffness responses, but is only directly applicable when the component and anchor responses share a one-to-one relationship.

For the two-degree-of-freedom solution, the nonlinear geometry stiffness matrix can be taken from literature (McGuire et al., 2000). The relevant terms can be condensed into the 2x2 stiffness matrix given below in Eq. 5-10.

$$[k_g] = \frac{P}{L}\begin{bmatrix} {}^{6}/_{5} & {}^{-L}/_{10} \\ {}^{-L}/_{10} & {}^{2L^2}/_{15} \end{bmatrix} \quad \textbf{(5-10)}$$

In the event the leading diagonal terms in the stiffness matrix become negative, the mode shapes and natural frequencies can be associated with their positive corollaries. This approach was adapted from work by Schraff (2012), which verifies this assumption provides an exact closed-form solution to the equation of motion for SDOF systems with negative stiffness.

5.3 – Hysteresis Rules

5.3.1 – Upright System: Base Moment-Rotation Hysteresis

While on the surface similar to one another, upright and hanging components have distinct and unique phases. For upright components, three phases exist as follows:

- System is resting on ground. The base moment is not large enough to overcome component weight (overturning moment), therefore no anchor is engaged and response is that of a fixed-base cantilever.
- System has overturned and has engaged an anchor. As the system loads, it follows the user-specified force-displacement curve. If a user-defined point on the force-displacement curve is reached, a nonlinear event is triggered. As it unloads, it follows the anchor initial stiffness until the anchor reaches zero force.
- System has overturned, but the anchors have been plastically deformed such that there is a gap between anchor engagement and the system resting on the ground.

Important to note for upright components is that the force vector of the weight initially holds the component in place, and thus there is a time when no anchors are loaded. Additionally, P-delta influences soften the system, as the base moment required to overturn the system is reduced as the weight moves toward the bearing compression toe. An annotated diagram of hysteretic response of the component base is provided in Figure 5-5.

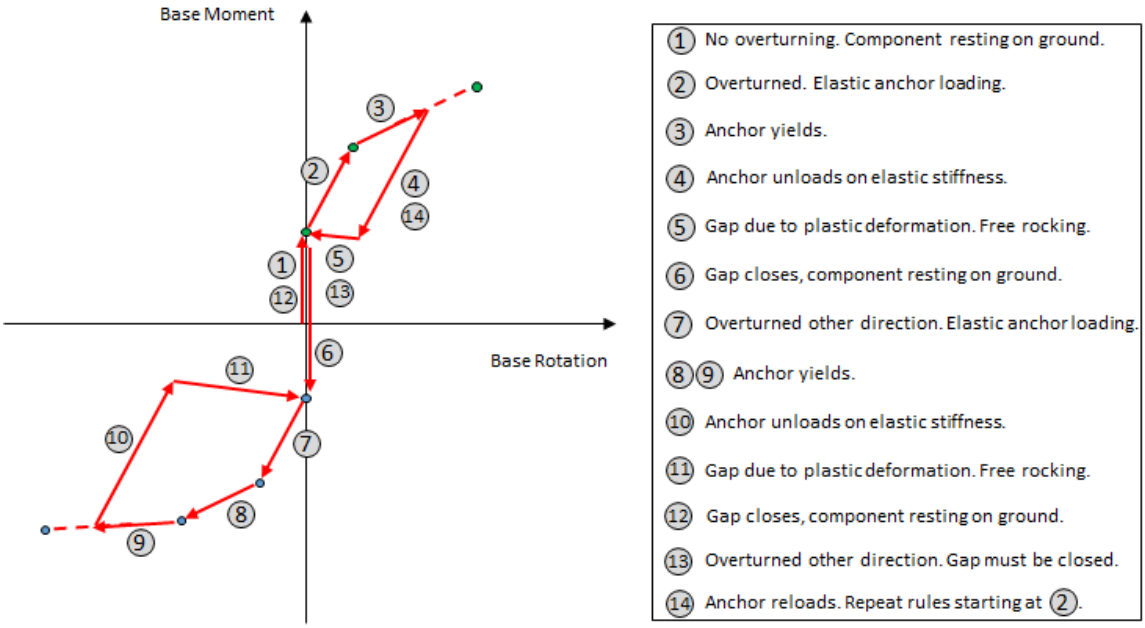

Figure 5-5: Annotated Hysteretic Rules for Base Response of Upright Component

5.3.2 – Hanging System: Base Moment-Rotation Hysteresis

Hanging components have several fundamental differences from the above rules. Firstly, at no point do the anchors ever fully disengage; they must always be resisting a minimum tensile load equal to the component weight. Additionally, rocking occurs as a combination of a one- and two-anchor system, which contrasts with the single-anchor system in the upright component model. This results in a total of four distinct phases:

- System is engaged with two anchors and is hanging without bearing. Rotation occurs about the base of the component at the midpoint between the two anchors.

- System is engaged with a single anchor which maintains a tensile load equal to the component weight, and is hanging without bearing. The system swings freely, with the point of rotation shifting to be on the engaged anchor. This is a zero-stiffness region.
- Component is bearing against the concrete, engaging the anchors, and loading. Depending on the extent of plastic deformation in the anchors, either one or both anchors are engaged. Depending on the geometry at a given time step, a jump between one or two anchor engagement can occur.
- Component is bearing against the concrete, engaging the anchors, and unloading. Depending on the amount of plastic deformation in the anchors, the system will either return to two anchor rocking, or it will unload one anchor. If the latter occurs, the remaining engaged anchor will unload until it reaches equilibrium with the weight of the component, and then become the center of rotation for the second phase.

The rotational behavior of the component base is also significantly more complex than the upright scenario, largely due to a ratcheting effect as the anchors are plastically deformed. Overturning that results in the system bearing on a compression toe must now be determined by a dynamically changing set of base rotation parameters, and the extent of this depends heavily on the geometries and material properties of the different system elements. While the hysteretic behavior is difficult to illustrate with a series of cycles like that shown above for an upright component, it can be described within a set of regions detailed below in Figure 5-6.

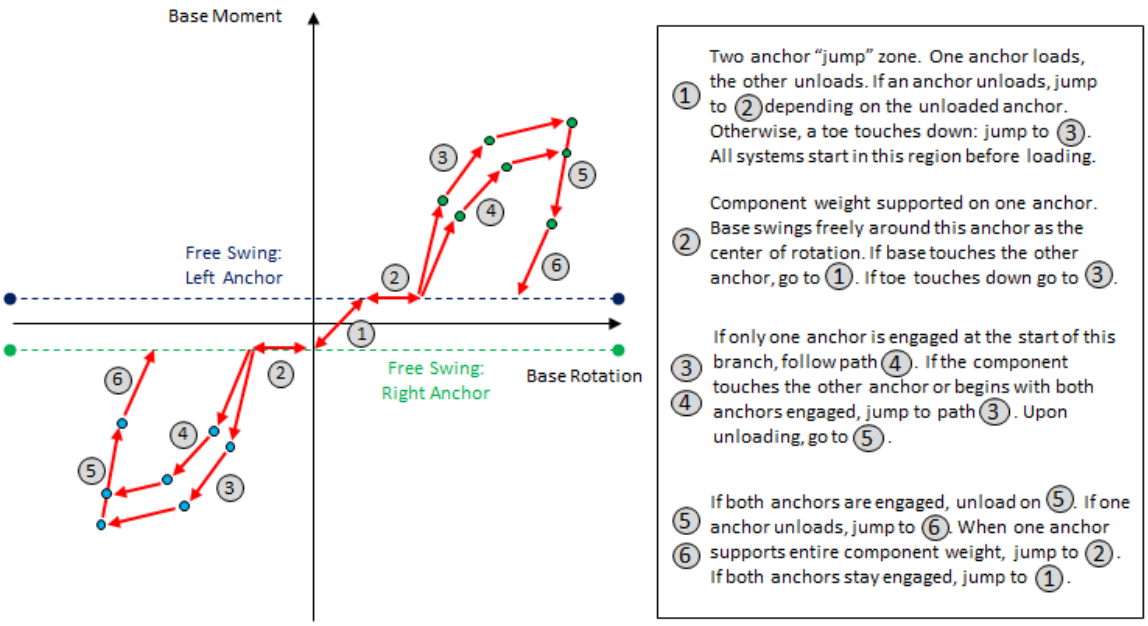

Figure 5-6: Annotated Hysteretic Rules for Base Response of Hanging Component

5.3.3 – Anchor Hysteresis

Anchor hysteretic behavior is consistent between all analysis cases, and the physics of anchor behavior in the components and systems discussed in this dissertation must always carry either no load or a tensile load due to the anchor being secured to the component by a nut-and-washer loading mechanism. As such, the hysteretic behavior of the anchor is well-defined, and – due to the lack of potential compressive forces with tensile strains – can be readily described from the monotonic response as seen in Figure 5-7.

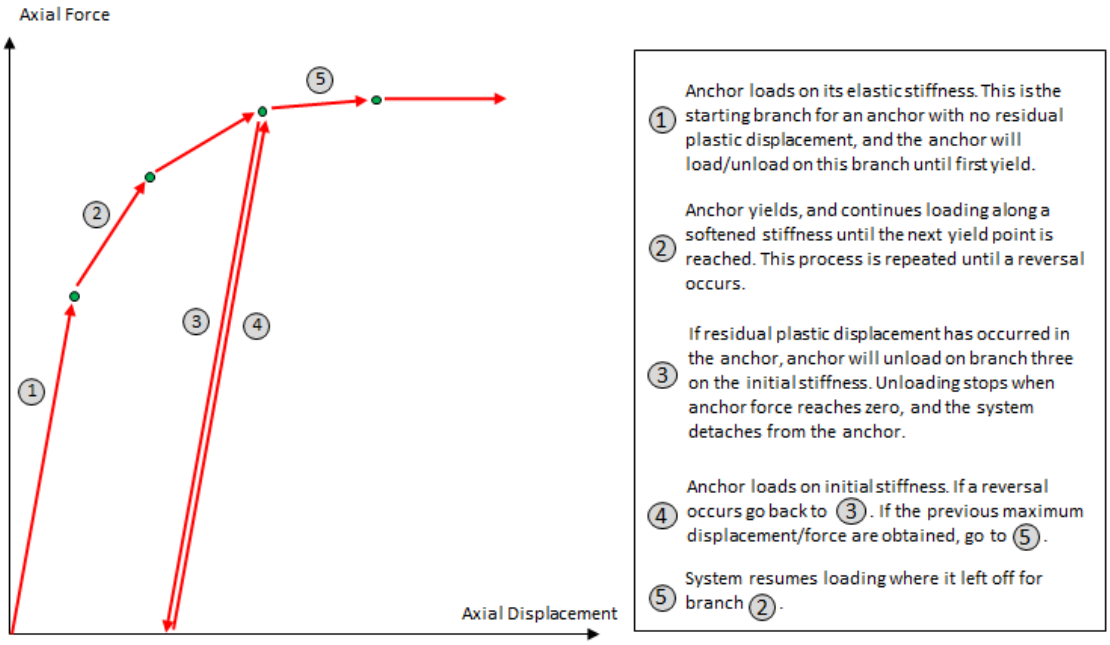

Figure 5-7: Annotated Hysteretic Rules for Anchor Response

5.3.4 – System Reversal

The reversal process consists of two different methodologies: an exact method and an approximate method. Both methods have various advantages and disadvantages, and are approximately convergent to one another as time step size decreases. After considerable effort to get the exact method to work, the approximate method was ultimately adopted as the main reversal approach for the problem.

Both methods have potential convergence issues due to the presence of two modes at points with abrupt changes in stiffness. These errors are consistent in the sense that, for a given large batch of time-history analyses, they are highly likely to occur in some small quantity; they are inconsistent overall, however, in that a single analysis might have several thousand points that reverse with no problem for a given scale factor and parameter set, but a small incremental

decrease or increase in scaled motion amplitude might cause one of these reversal points to become “stuck.” These “stuck” points are when the system continuously flags reversal due to a changing stiffness matrix; one stiffness matrix will point the solution one direction, but changing the stiffness to the unloading stiffness will point the solution back in the direction it came from. The circumstances in which this can occur are relatively rare, and generally occur under two circumstances. First, a nonlinear event has happened “recently” prior to the reversal, causing a change in stiffness a short amount of time prior to the reversal point of contention. Second, the modal behaviors must have the correct distribution of inertial and damping forces such that their influences are negligible in determining the direction of motion of the system. The stiffness terms must be dominant enough in controlling the component response that a change in the stiffness terms can completely overcome the other force components.

The approximate method for reversal determines a change in direction of the base rotation of the component at the start of a time step by comparing the signs of the incremental values of the current and previous time steps. Should a multiplication of the two incremental base rotation deltas result in a negative value, a reversal has occurred. This method treats the point at the start of the time step as the reversal point, changes the stiffness and mode shapes of the model, and re-evaluates the time step with these updated parameters. Should convergence issues occur at a reversal point, starting the analysis from the beginning by further interpolating the ground motion can sometimes solve numerical problems. Increasing rotational mass appears to lead to more cases of this error occurring, though evidence for this is inconsistent and no detailed study was performed.

The exact method of reversal treats a reversal point like a standard nonlinear event, using an iteration scheme to converge on the exact time it occurs. This requires a more detailed

solution scheme, as it is possible for a reversal to occur in-between two base moment increments that occur in the same direction (both values are positive, for example). This is visualized in Figure 5-8, where it is clear that a reversal using the exact solution is not known at a time increment of i+1 after the reversal has occurred if $\theta_{b,i+1} > \theta_{b,i}$. If $\theta_{b,i+1} < \theta_{b,i}$, the reversal is known to have occurred within the time increment between i and i+1. The computational logistics of solving this problem are significantly more complex than the approximate reversal method, which would simply treat $\theta_{b,i+1}$ as the reversal point should this phenomenon occur. As a result, the solution method requires forward-and-backward compatible solutions for moving through the time domain.

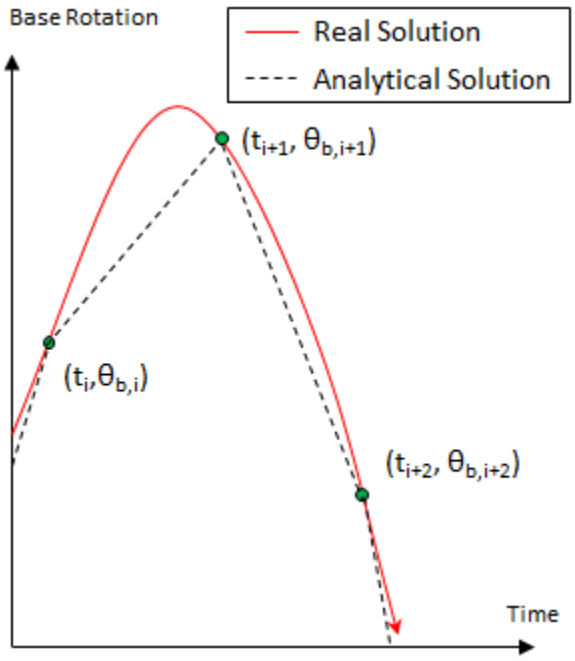

Figure 5-8: Visualization of the Reversal Problem

The exact method offers some future promise for analytical accuracy, for example being able to numerically smooth changes in stiffness by making the stiffness shift over several

individual time steps rather than in a single step. This method shared many of the similar flaws as the approximate method in terms of convergence errors, but the rate of convergence errors was significantly higher due to the use of iteration. Allowing for enlarged time steps following or preceding the reversal point and/or using a smaller base time step size aided with convergence far less reliably than with the approximate method as well. Thus, while a potentially powerful tool to help solve nonlinear time-history analyses, more work needs to be done from a conceptual approach of the reversal phenomenon – such as the aforementioned smoothing methods – before this solution can be reliably implemented.

5.4 – Additional Features

In addition to the core analysis functions mentioned above, the program is built with several architectural features that allow for bulk data processing. The program is entirely self-contained, and is equipped with a post processor that can readily visualize analysis results and was used extensively for both the verification process and development of overall target quantities from bulk analyses. Graphical outputs are generated using the Oxyplot plotting library for C#, and most data presented in Chapter 6 makes use of the post-processing feature set. It has many auxiliary time-history analysis and manipulation features inbuilt that can be run in a batch mode format, such generation of spectral response curves which are required for anchor scaling.

Anchor scaling methods are used to map ground motions and anchor characteristics with appropriate relationships to the ASCE 7-10 design equations. While the real force-displacement responses of the anchors, taken from the structural testing data, were associated with a given set of code parameters, dimensional analysis procedures and associated values used in the ASCE 7-10 equations for anchor design were used to scale anchor forces and

displacements to the minimum values that would be used per code in an anchor design for a given parameter set and ground motion. Anchor forces are scaled linearly, while anchor displacements are scaled by the square root of the force scale factor.

Analysis was programmed to adopt one of two modes: a standard analysis mode which outputs databases of parameters that are used for detailed study of the behavior of the system for a particular motion, and a generalized failure mode that cycles analyses continuously while looking at anchor performance in a strict “pass or fail” criteria. Raw time-history analysis offers a wide array of outputs: displacement, velocity and acceleration of both the ground and component center of mass (translational and rotational); center of mass restoring force and restoring moment; the moment at the component base and associated rotation; and anchor force and displacement responses for each anchor. Each of these quantities can be modally discretized if desired. This module was used to assess performance of individual time-history responses, such as comparison and benchmarking of the program against the structural tests.

Unlike the single time-history run, the failure analysis module starts with a user-specified scale factor for the earthquake, and then runs a batch of earthquakes at this load level. The number of earthquakes that cause anchor failure are noted, and then the scale factor is incremented. This process is continued until no earthquakes fail the anchor, and a table of scale factor versus earthquakes survived is generated using several hundred individual nonlinear time-history analyses. These outputs are called “survival curves” and are detailed in Chapter 7. Outputs from this can be separated based on motion type (real earthquake or broadband) and motion location (ground or floor level).

CHAPTER 6: VALIDATION AND VERIFICATION OF NARRAS

Validation of NARRAS developed in this body of work was benchmarked against four independent sets of data: two external sets and two internal sets. The primary set of comparison data was the structural tests discussed in Chapters 2 and 4, which contained a mixture of anchor types of various displacement capacities and hysteretic behaviors. A two-dimensional SAP2000 model, similar to that developed by Watkins (discussed in Chapter 5), was used as a second source of verification, particularly for elastic rocking behavior. Internal verification took two forms, with the first comparing the single-degree-of-freedom (SDOF) and multiple-degree-of-freedom (MDOF) algorithms with the MDOF routine using a very small value of rotational mass. Finally, an independent analysis program written by the author's advisor was developed without exposure to any of NARRAS' code.

With respect to damping ratios, it should be noted that equivalent viscous damping was not uniform for all anchor types. The component-anchor system had a coupled damping response, which could be readily observed from the dynamic structural tests when WALLE was rocking with and without anchors engaged. NARRAS did not use an adaptive damping ratio based on the anchor engagement state due to the analytical issues associated with changing the damping matrix mid-analysis as discussed in detail in Section 5.2.4. Analytical results from NARRAS were highly sensitive to damping ratio, and damping characterization by Watkins (2011) – summarized and discussed in detail in Section 6.7 – noted equivalent viscous damping ratios as low as 0.04% for some anchor-component combinations. The use of different damping ratios was thus a key part of the verification of NARRAS, and a range of qualitative/quantitative

features – such as matching of failure points, similar maxima, and natural period – were used to determine appropriate levels of equivalent viscous damping for each anchor type.

6.1 – B7 Thread Rod Anchor Verification [N2]

Comparisons with the SAP2000 model were intended to provide verification of nonlinear elastic rocking behavior and show proper emulation of essentially elastic rocking response. Figure 6-1 shows a comparison between structural test results, SAP2000, and NARRAS for the single earthquake motion (SEM) test sequence for the B7 thread rod. All three time histories agree well, with both SAP2000 and NARRAS producing similar values to the peak response of each motion in the sequence as well as predicting anchor failure at 256 seconds. Evaluating appropriate damping values using SAP2000 was difficult given the long run times, so the SAP model shows modal damping of 2% for both modes. Overall damping for NARRAS is discussed in Section 6.7, where the "average" values of 1.75% for first mode and 1.25% for second mode are used in Figure 6-1 for comparison purposes. More accurate capturing of the post-peak behavior as seen between 160 and 180 seconds could be attained by varying the damping ratio of either mode between 1% and 2%. The run time for NARRAS to complete this analysis was roughly 12 seconds, whereas SAP2000 was about 12 hours when analyzed on the same machine.

As NARRAS' analysis routine is primary based on the hysteretic behavior of the component base, validation of base moments was also an important consideration. Base moment computations from the structural tests were taken as a function of both anchor forces for each time interval taken about the base of the mast, while the base moments from NARRAS were computed as a function of the center of mass restoring force and moment quantities. Comparison is provided in Figure 6-2. The close matching of these two quantities supports that

approaching using the customized stiffness matrix discussed in Section 5.2.3 properly develops self-consistent anchor forces associated with rocking behavior. Similar comparisons are shown with the broadband motion, again zoomed in for visual resolution, in Figure 6-3.

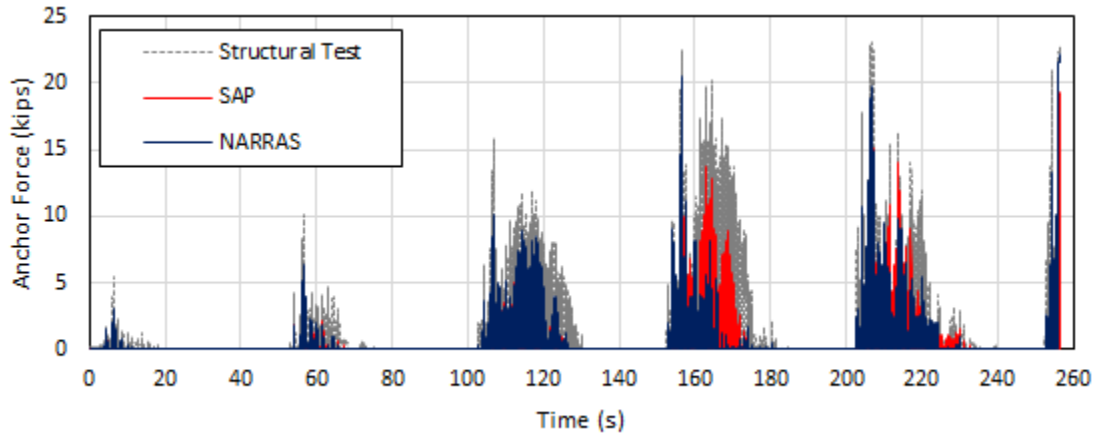

Figure 6-1: Comparison of Structural Test, SAP, and NARRAS for N2 SEM Test

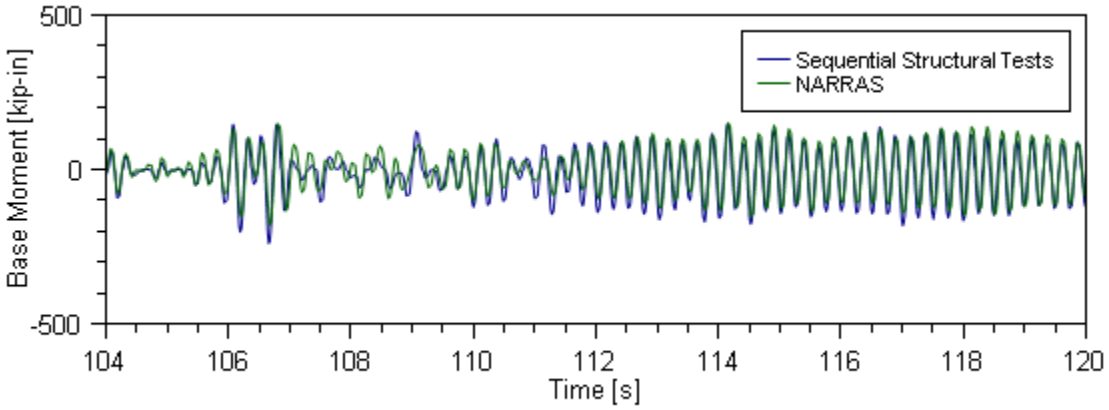

Figure 6-2: Comparison of Base Moments for 3rd Motion in N2 SEM Testing Sequence

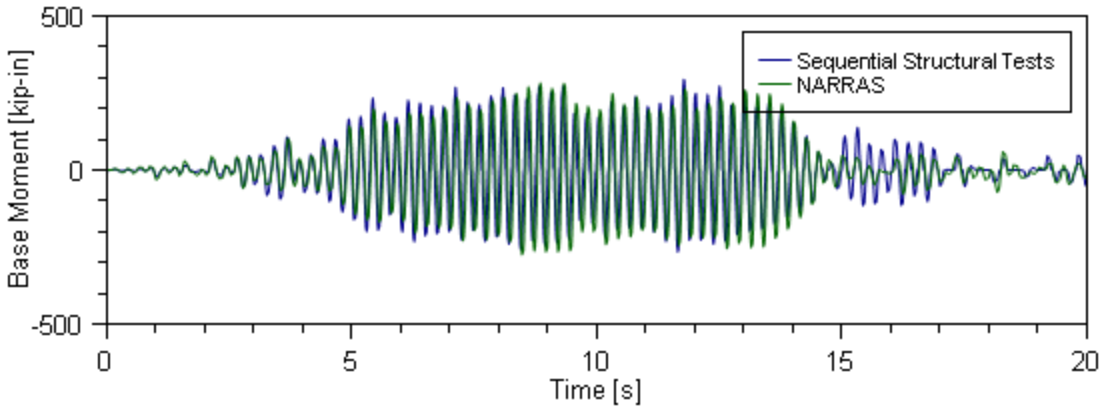

Figure 6-3: Comparison of Base Moments for 1st Motion N2 BBM Testing Sequence

Center of mass responses can also be compared. Filtered acceleration and displacement time-history responses are provided in Figure 6-4 and Figure 6-5, respectively. During peak motion, acceleration values between analysis and structural tests are in agreement, as well as during the majority of off-peak behavior. Displacements match relatively well, but do drift apart at times analytically depending on the damping ratios used. As a general trend with the B7 thread rods, acceleration – and subsequently force – quantities within the analytical model are consistent over a reasonable block of damping ratios. Displacements showed significantly more sensitivity to these parameters, but can be tuned with incremental changes to chosen damping values. As such, damping ratios were selected such that the maxima from the structural tests and analysis matched well, rather than looking at the full breadth of the time-history analysis.

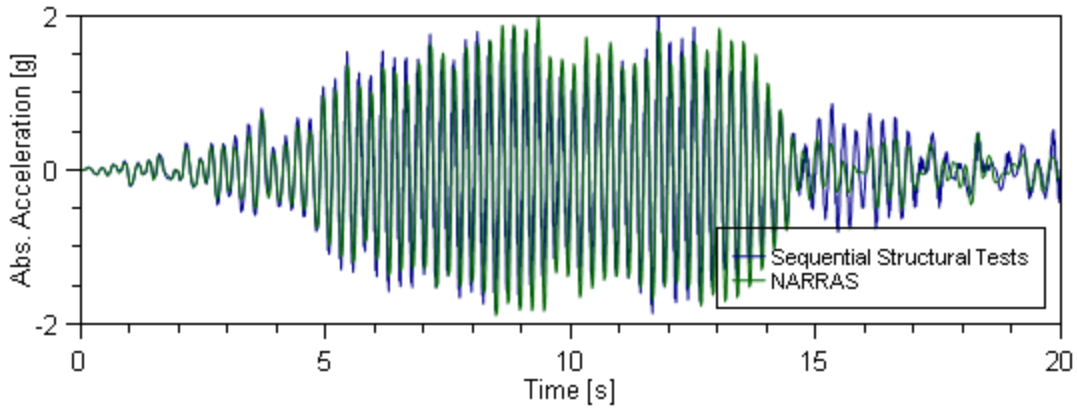

Figure 6-4: Acceleration Time-History Response for Component Center of Mass (1st BBM Test)

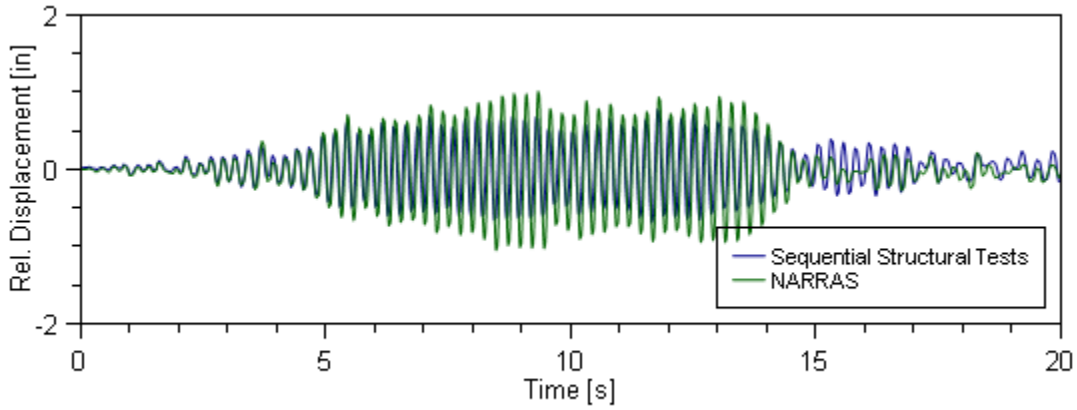

Figure 6-5: Displacement Time-History Response for Component Center of Mass (1st BBM Test)

6.2 – Stainless Steel Anchor Verification [N1]

Stainless steel hysteretic responses for the south and north anchors, benchmarked against the single earthquake tests, are provided in Figure 6-6 and Figure 6-7, respectively. The fourth motion in the test sequence, as seen above in Figure 6-1 with the B7 thread rod, had a notable level of post-peak excitation that NARRAS did not capture well, whereas SAP more accurately reproduced this behavior. This high level of cycling can be observed in plastic displacement levels below 0.2 inches, which NARRAS bounds well and captures in detail. Once the larger ground motions in the test sequence are run, however, NARRAS more accurately captures the accruement of plasticity in the anchors compared with SAP. In Figure 6-7, for example, SAP predicts almost twice the level of plastic displacement measured from the north anchor, with many more additional large cycles than observed in the tests. NARRAS is far more accurate in its predictions for both cyclic behavior and predicted displacement amplitudes.

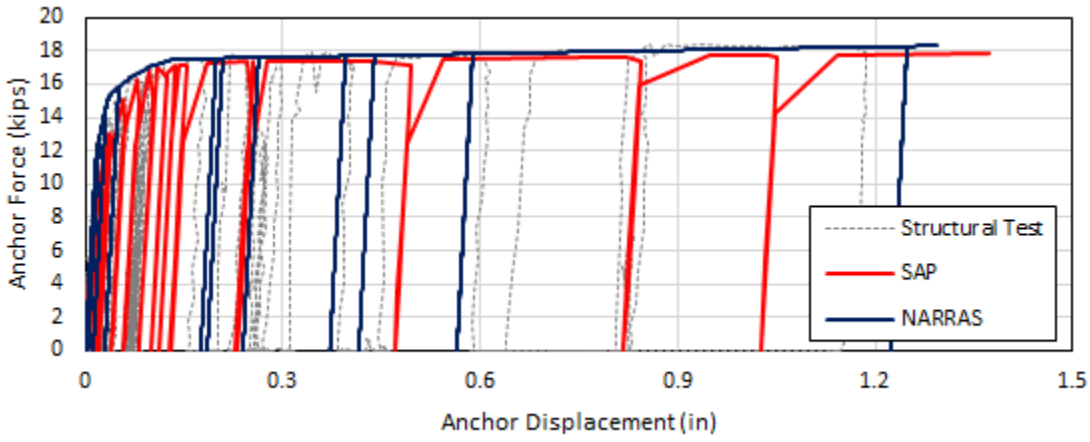

Figure 6-6: South Anchor Force vs. Displacement Response for N1 SEM Test Sequence

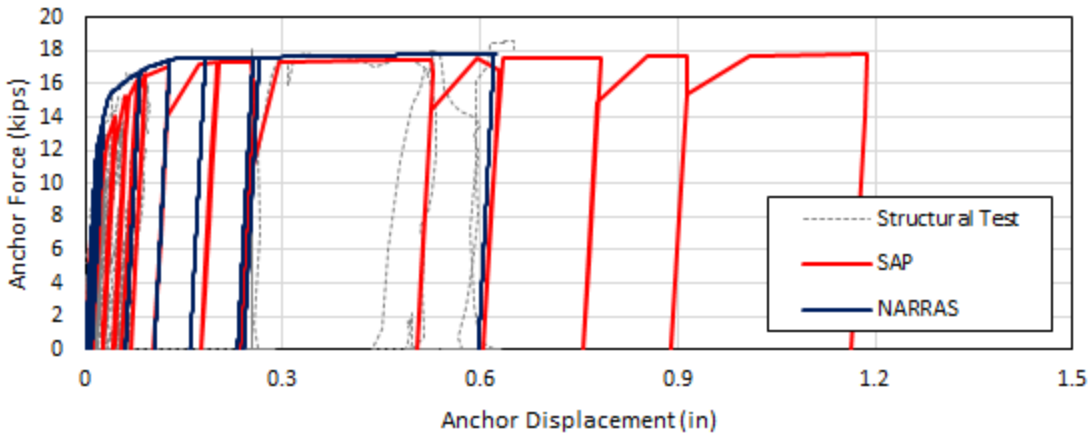

Figure 6-7: North Anchor Force vs. Displacement Response for N1 SEM Test Sequence

While hysteretic comparisons between these three sources appear similar, time-history behavior shows more substantial deviations. Figure 6-8 compares displacement time-history results for the south anchor, with SAP2000 and NARRAS results shown for the same first and second mode damping ratio of 2%. SAP indicates failure within the 5th motion of the sequence, along with over-predicting plastic displacement demand of the anchor for the 4th motion of the sequence. NARRAS follows results from the structural testing sequence much more closely, including predicting near-coincident failure time with the structural tests. The amplitude mismatch between the structural test sequence and NARRAS can be fine-tuned by small numerical adjustments to the independent modal damping ratios, the range of which Watkins noted to be bounded between roughly 0.5% and 3.0% for various anchor types. With SAP2000 run times for this highly nonlinear behavior capable of reaching around 20 hours, however, numerically fine-tuning the SAP2000 model to try to replicate test results was unfeasible.

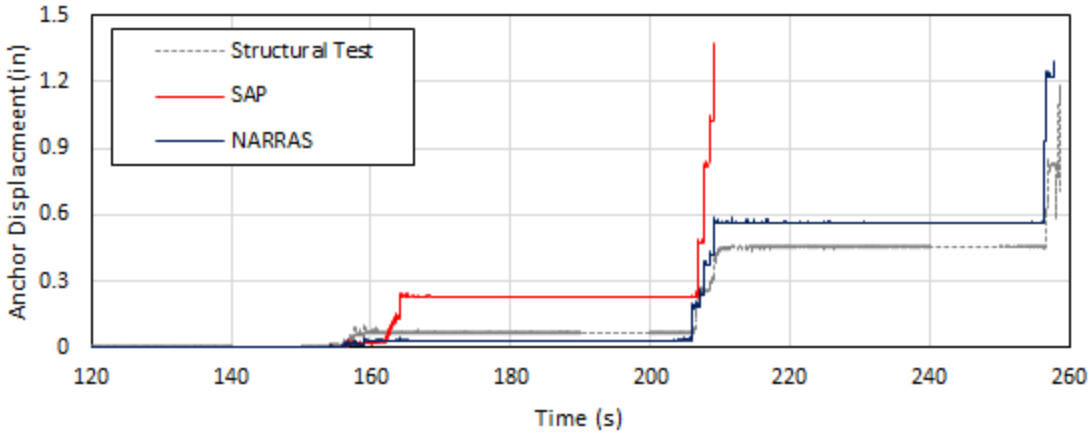

Figure 6-8: South Anchor Displacement Time-History Comparison of N1 SEM Test Sequence

Comparisons of base moment and center of mass responses, zoomed in over a region of the test sequence where NARRAS and the structural tests matched most poorly, are presented in Figure 6-9. Base moments from NARRAS match excitation shown by the structural tests, though NARRAS indicates additional excitation after the strong motion diminishes which the tests do not show. This phenomenon occurs somewhat frequently, with the structural tests indicating excitation of the anchorage system when analytically none is shown, and vice versa. This is surmised to be due to complex dynamical effects of the rocking behavior, as system rocking visually appeared to add a damping effect to component response. Additionally, impact influences of the SAMUs touching down and bouncing off the concrete surface were not captured and were observable during testing. Displacements for this particular portion of the testing sequence matched very closely in one direction, but were analytically over-predicted in the other. Again, this may be due to complex damping of the system rocking, as the disparity between analytical and measured results seem to amplify with each cycle.

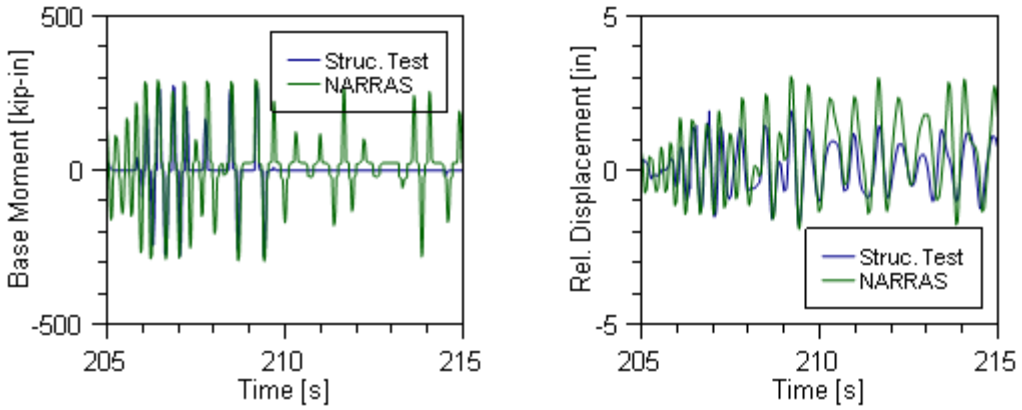

Figure 6-9: Base Moment and Center of Mass Displacement Responses for N1 SEM Test Sequence

6.3 – B7 Spring Anchor Verification [N3]

While the measured hysteretic response of the N3 anchors had nonlinear-elastic features, modeling of these anchors in NARRAS was performed using a linear-elastic representation. NARRAS was only programmed to allow for plastic anchor response, and it was thus desired to verify a linear-elastic approach matched well with nonlinear-elastic anchor modeling in SAP2000 in addition to the structural tests. Capturing of the elastic anchor hysteretic behavior was performed using the transformation method prescribed by Eq. 4-30 of Priestley et al. (1996), which is given below in Eq. 6-1. This equivalent viscous damping ratio is defined for a full tension-compression cycle of hysteretic response, where A_e is the area under the curve of a linear-elastic idealization of a half-cycle, and A_h is the total area encapsulated by a full hysteretic cycle. For tensile-only response which comprises a half-cycle of behavior, this value was accordingly halved.

$$\xi_{eq} = \frac{A_e}{4\pi \cdot A_h} \qquad \textbf{(6-1)}$$

Computation of A_e and A_h from the structural tests is shown below in Figure 6-10, where A_e is represented by the shaded blue triangle with an area of 7.68 k-in. and A_h is represented by the shaded gray parallelogram with an area of 4.8 k-in. Plugging these values in Eq. 6-1 yields an equivalent viscous damping ratio of 5%, which is then halved to account for the half-cycle response of the anchor for a net damping ratio of 2.5%. This was included into the model additively with the NCS damping ratio for the first mode. Structural testing for the N3 anchors exhibited violent response of WALLE, and failure occurred for both the SEM and BBM test sequences with immediate release of the component into the catcher system. It was thus anticipated that, while the anchors added elastic hysteretic damping, minimal contribution was occurring in the component. A damping ratio of 0.5% for both modes – with the added 2.5% on the first mode – yielded reasonably good matching results for both the SEM and BBM tests.

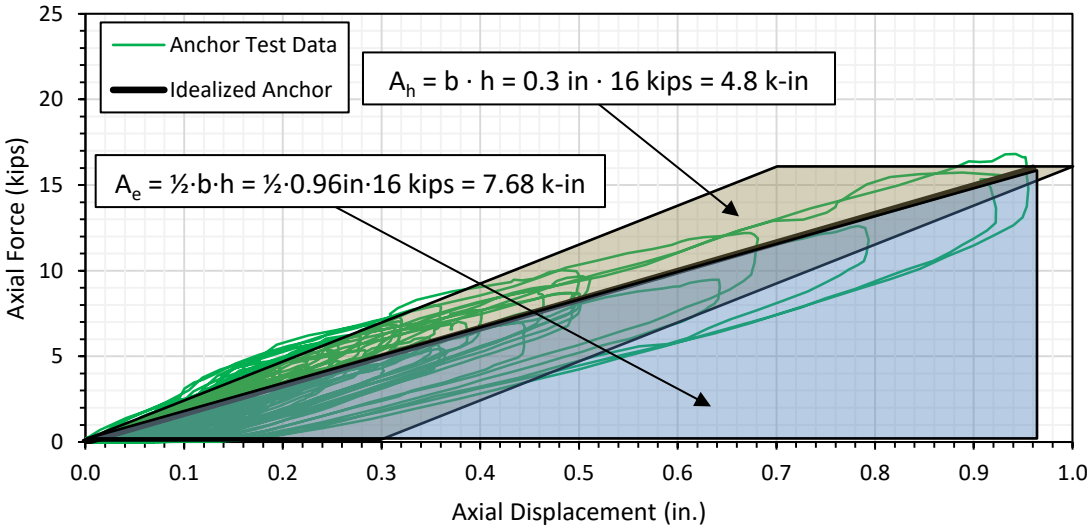

Figure 6-10: Computation of N3 Anchor Equivalent Viscous Damping for Elastic Cycling

Both SAP2000 and NARRAS reproduced the structural testing results reasonably well, and agreed with one another despite several modeling differences. Specifically, anchors in SAP2000 were properly modeled as nonlinear elastic elements, and the program innately considered both anchors as actively resisting single-direction rocking. Comparison of north anchor force time-history results for both computer programs and the SEM structural tests is provided in Figure 6-11, with associated displacement in Figure 6-12. For visual clarity, displayed response is zoomed in to show only the failure motion and the motion prior in Figure 6-11, and only the motion prior to failure for Figure 6-12. NARRAS and the structural tests show failure at the same pulse of earthquake motion, while in SAP2000 failure occurs during the previous pulse.

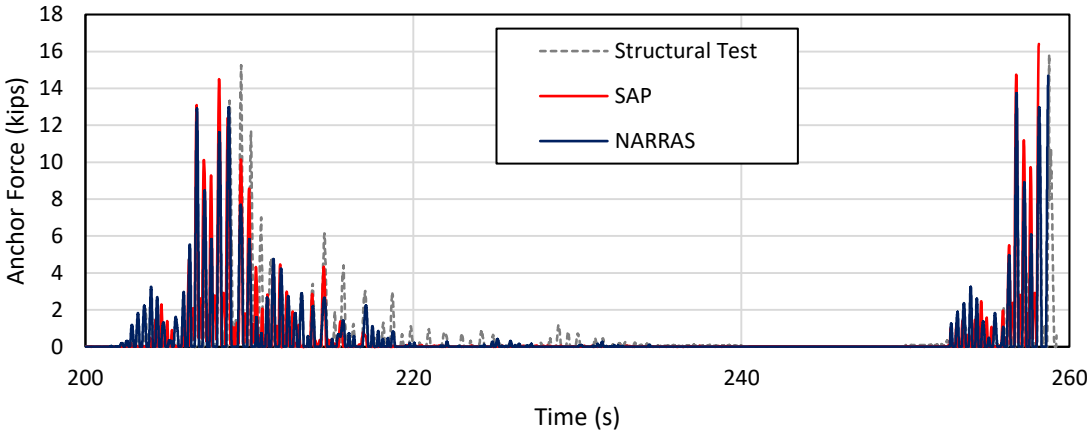

Figure 6-11: Comparison of North Anchor Force Time-History Response for SEM Tests for N3 Anchor

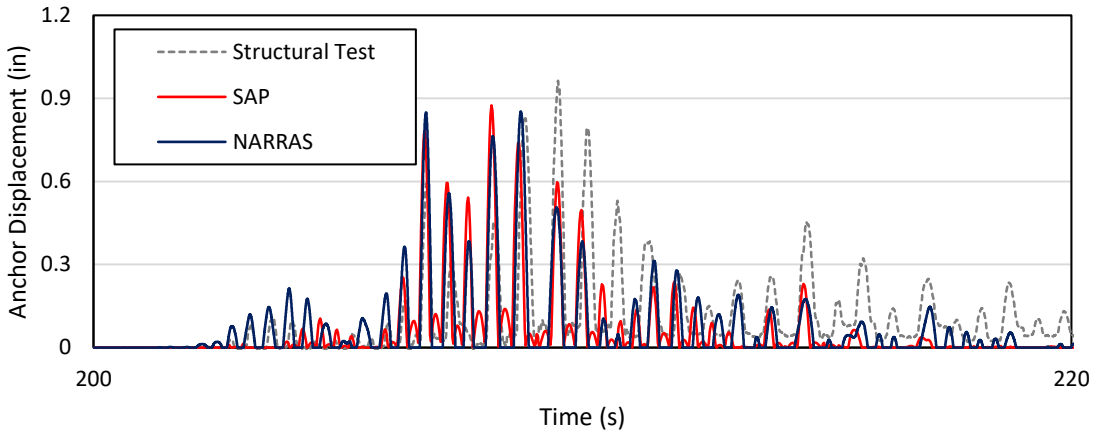

Figure 6-12: Comparison of North Anchor Displacement Time-History Response for SEM Tests for N3 Anchor

Center of mass displacement and acceleration time-history responses over a sample of peak motion from the SEM tests are provided in Figure 6-13 and Figure 6-14, respectively. As with the N2 anchors, accelerations match more closely than displacements. Additional anchor force comparisons for the BBM tests are provided in Figure 6-15, and a base moment comparison is given in Figure 6-16. Each of these figures shows closely matching behavior, though some discrepancy exists in the amplitude of some peaks. Soft elastic anchor response appears to be highly variable analytically, and is more strongly influenced by component parameters than the other anchor types; this is presented in detail in Chapter 7. In general, the first several large amplitude pulses match well between analytical and experimental results, but then experimental results tend to show higher anchor demands for the remainder of the strong motion.

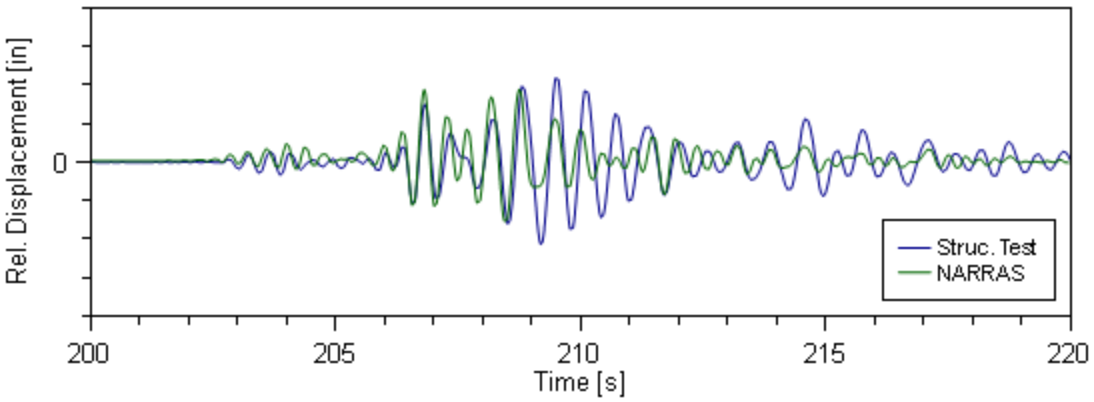

Figure 6-13: Center of Mass Displacement Time-History Response for N3 Anchor [SEM Test]

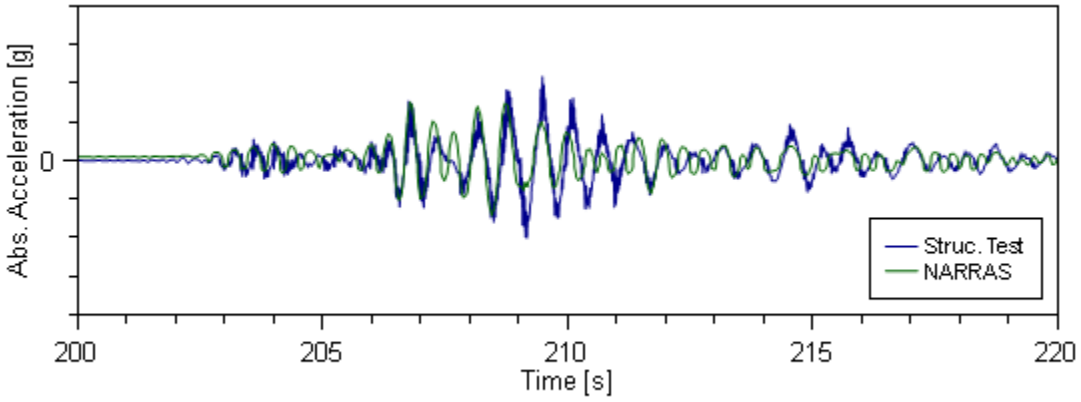

Figure 6-14: Center of Mass Acceleration Time-History Response for N3 Anchor [SEM Test]

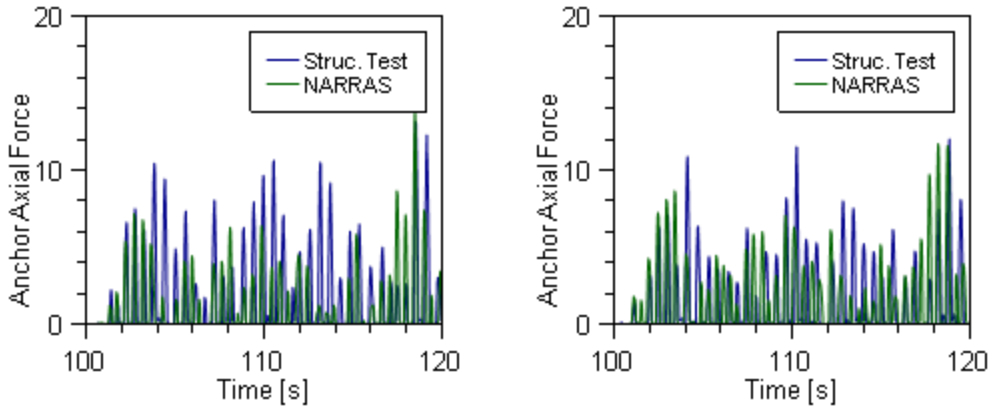

Figure 6-15: BBM South Anchor (Left) and North Anchor (Right) Force Time-History Response for N3 Anchor

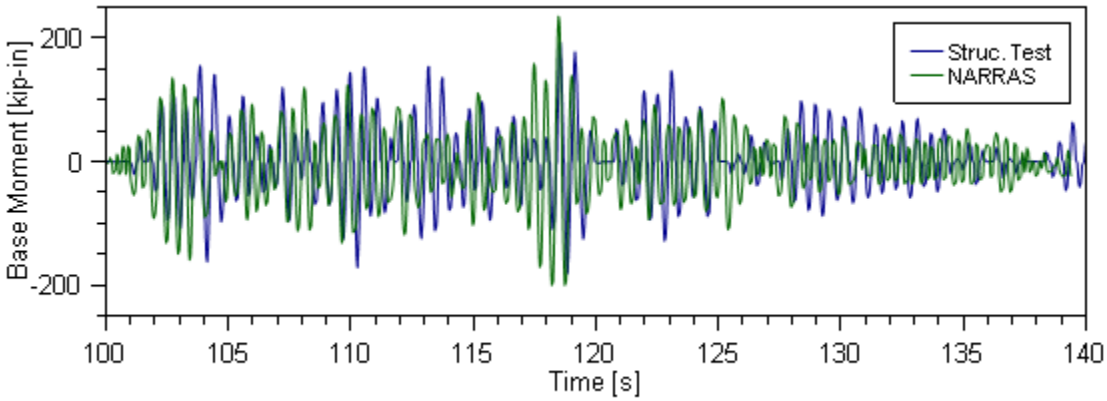

Figure 6-16: Base Moment Time-History Response for 3rd Motion in BBM Testing Sequence for N3 Anchor

6.4 – Expansion Anchor Verification [N5]

Some modeling limitations existed for the N5 anchors, namely the recognition of NARRAS' inability to capture non-trivial levels of preload on the anchors. Anchor displacements were expected to be analytically over-predicted due to this, and anchor preload technically indicates an infinite anchor stiffness until the input motion is strong enough to overcome the combination of the clamping forces from the weight and the anchor. Proper consideration of preload can be done with the physical formulations used to map anchor response to the component stiffness matrix, but the method for doing this was derived late into NARRAS' development cycle and errors from preload modeling were considered acceptable due to the logistics required to implement it into the existing body of code. An example of this displacement over-prediction is provided in Figure 6-17.

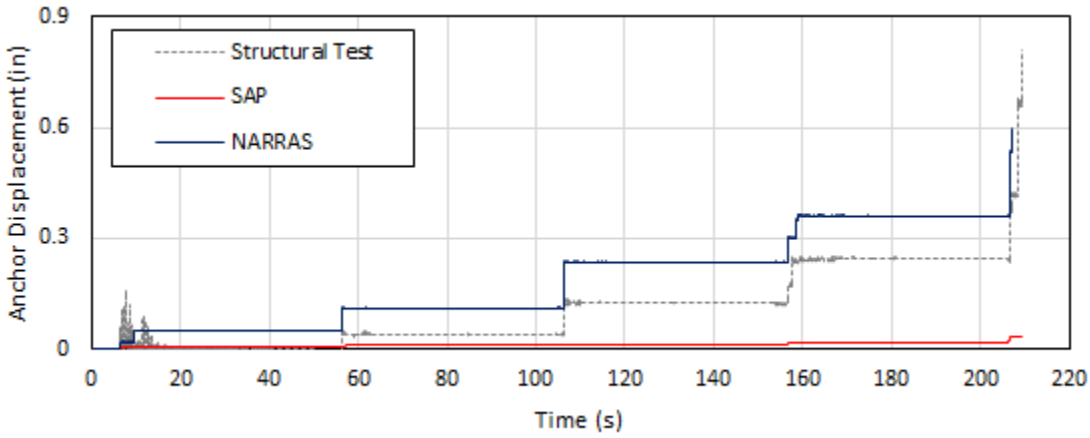

Figure 6-17: North Anchor Displacement Time-History Comparison of N5 SEM Test Sequence

Of all anchor types analyzed, the N5 was the most sensitive to small changes in damping ratio, and the creeping behavior of the damping force toward regions of residual plastic displacement, as mentioned in Section 5.2.4, was present regardless of damping model chosen.

Comparisons between NARRAS and SAP2000 in Figure 6-17 show drastic differences between predicted responses from the two analysis programs despite having the same damping ratios. This can be better visualized in Figure 6-18, which compares the hysteretic response for this same anchor. While both analytical models display sensitivity to relative stiffness values between the initial stiffness and tangential stiffness for regions of large plastic displacement, the SAP2000 model showed much greater fluctuation in behavior due to the larger number of stiffness variables considered: the frame elements comprising the base, gap elements, and hook elements – all which should be theoretically infinitely stiff – being the most pertinent.

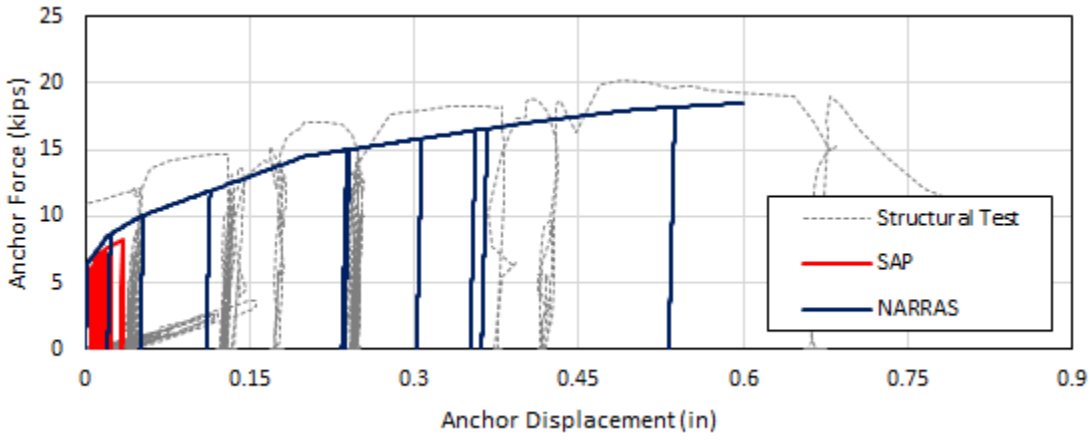

Figure 6-18: North Anchor Hysteretic Response Comparison of N5 SEM Test Sequence

More fine tuning of the damping ratios, such as to the 1.75% and 1.25% values for first and second mode responses as per discussion in Section 6.7, improved the comparison between analytical and structural testing results. More specific refinement of the N5 anchor damping ratios to 1.6% and 1.2% for the first and second modes, respectively, adds further detail as shown in Figure 6-19 and Figure 6-20. Anchor responses from NARRAS match the structural tests quite well, with only the last three pulses of the ground motion showing deviation. Hysteretic

response for both anchors match similarly well, with the only significant deviation being the last large displacement pulse on the north anchor whose demands the analytical model under-predicts. This can be seen in the last unloading cycle in Figure 6-20 at about 0.28 inches, which corresponds to the small increase in plastic displacement in Figure 6-22 at about158 seconds into the sequence.

As a consequence of this difference, the analytical model predicts failure in the south anchor instead of the north anchor, though the structural tests show the north anchor set unloading only just before reaching their ultimate displacement capacity of 0.6 inches. Thus, while the hysteretic behavior of the north anchor appears to be substantially under-predictive of actual demands, the differences between the test results and the analytical model occur only 0.3 seconds apart in real time – the difference in time required for the south anchor to unload and to load and fail the north anchor.

Given the approximations of modeling the pre-tensioning behavior and the sensitivity of these anchors to system stiffness values, behavior of the N5 anchors can overall be captured accurately by NARRAS. Displacement time-histories in Figure 6-21 and Figure 6-22 are consistent with expected errors in displacement predictions by the model.

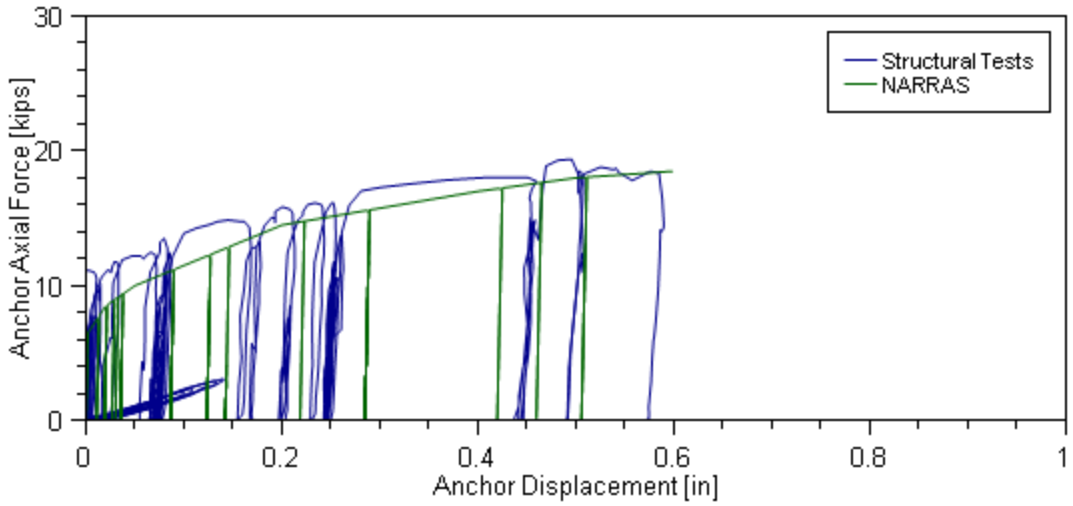

Figure 6-19: Structural Test Comparison of Hysteretic Response of South Expansion Anchor

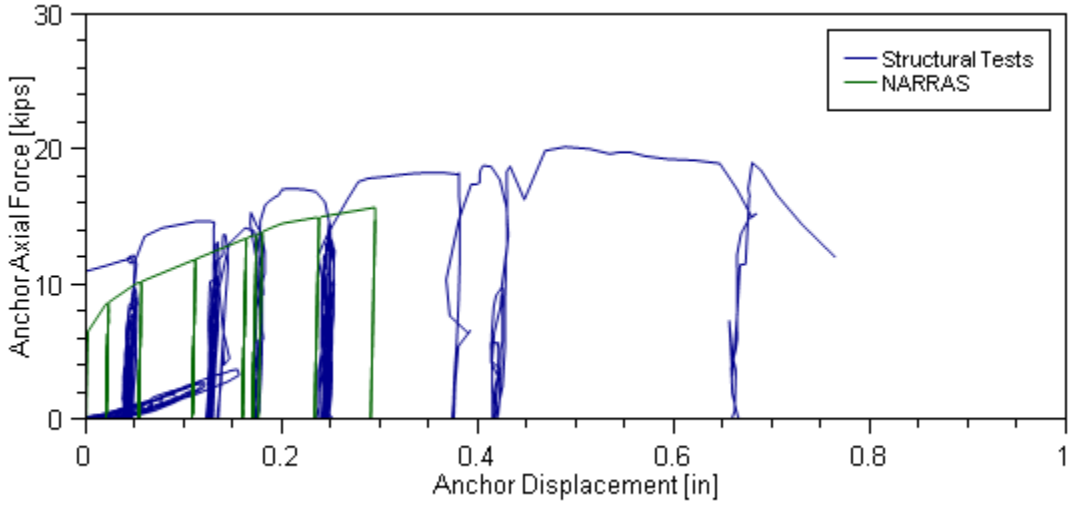

Figure 6-20: Structural Test Comparison of Hysteretic Response of North Expansion Anchor

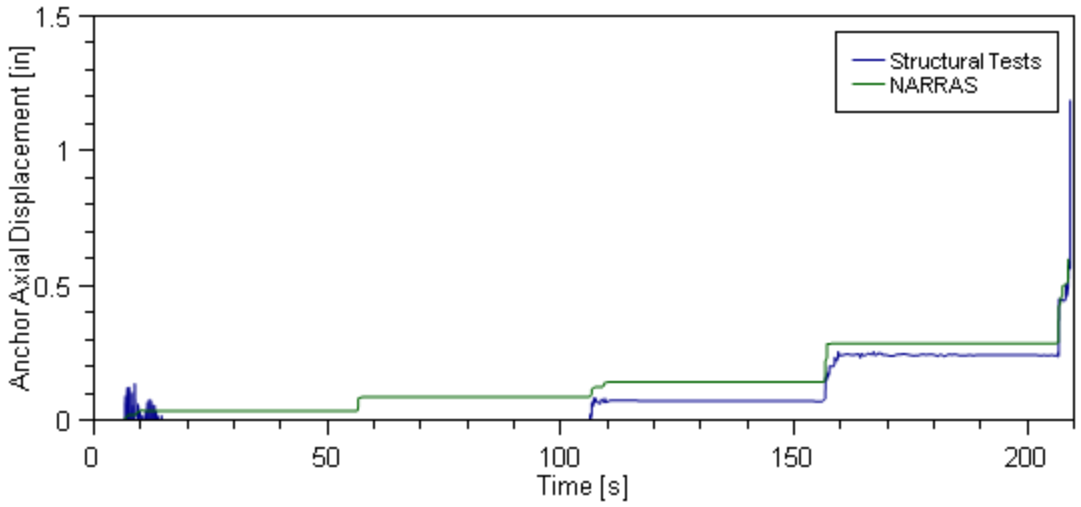

Figure 6-21: Structural Test Comparison of Displacement Time-History of South Expansion Anchor

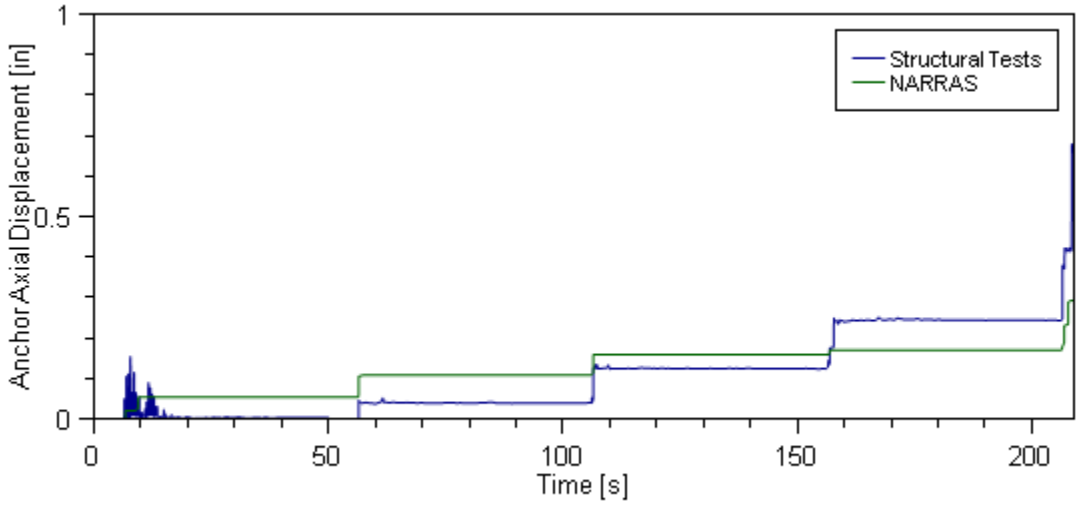

Figure 6-22: Structural Test Comparison of Displacement Time-History of North Expansion Anchor

6.5 – Independent Program Verification

To verify NARRAS' analysis routine was programmed correctly, the author's advisor wrote an independent piece of software with no exposure or access to NARRAS' code. This verification program was written in Fortran using the Microsoft Visual Studio 2003 compiler, while NARRAS was written in C# using the Microsoft Visual Studio 2015 compiler. Two different programming approaches were taken for determination of the base moment versus base rotation hysteresis, which was the fundamental controlling mechanism of component hysteretic response. NARRAS resolved anchor forces directly from statics, and nonlinear event behavior was calculated using anchor forces and displacements. In comparison, the verification program pre-computed the base moment versus base rotation hysteresis from anchor force-displacement response, determined nonlinear events based upon events in this curve, and then solved for anchor forces later as a byproduct of this process. Both programming techniques model and represent the same physical behavior, and when properly written are identical outside of small numerical errors that come from iterating on different values.

Numerical results from both programs were essentially identical, which verifies NARRAS' programming of the analytical module. A sample comparison for base moment and anchor force time-histories for the N2 anchor are provided in Figure 6-23 and Figure 6-24, respectively.

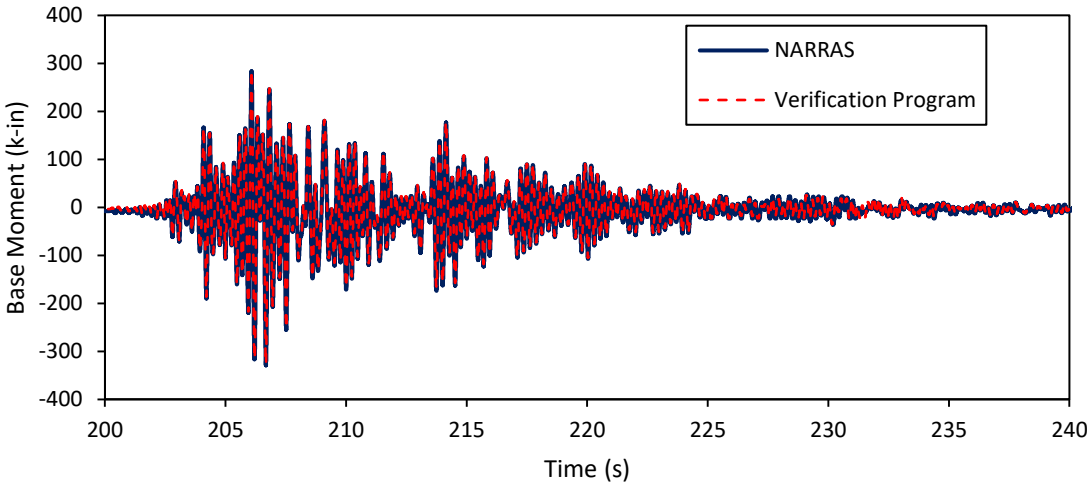

Figure 6-23: Comparison of NARRAS and Verification Program Base Moments

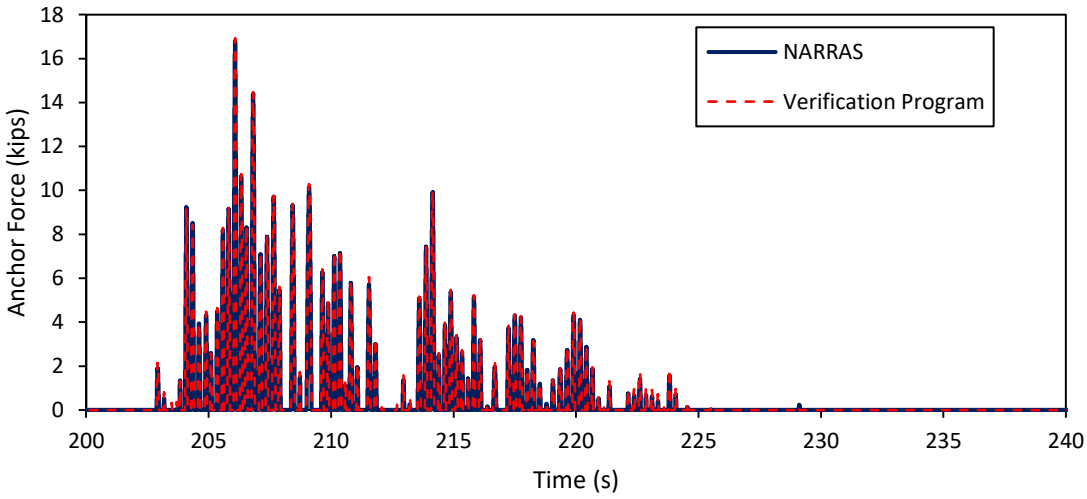

Figure 6-24: Comparison of NARRAS and Verification Program Anchor Forces

6.6 – Quantitative Discussion: N1 and N2 Anchors

In Sections 6.1 through 6.5, presented verification used a mixture of qualitative and quantitative metrics. Coincidence of rise times, failure times, matching of natural period, and other such features were matched visually. Overall statistical analysis was not favored for these comparisons due to the performance of individual peaks showing a great deal of variation. Some peaks had strong agreement between analytical and experimental results, but others showed either analytical or experimental excitation with minimal response from the other. Comparisons in this section were selected based on the following criteria:

- Component displacement, component acceleration, and anchor force compared the analytical response at the five largest peaks of experimental excitation. If the relative error was ≥ 200%, it was determined that this peak was not represented analytically and the next largest peak was selected. This prevented large outliers of individual peak comparison from skewing the statistics, as sometimes adjacent peaks showed comparable behavior whereas an individual peak may not.
- Anchor displacements included both peak displacement comparisons and residual plastic displacement comparisons. Displacement comparisons are presented subtracting the residual plastic displacement after anchor unloading from the peak value to remove errors caused by the differential accumulation of plastic displacement.
- Maxima over the full time of a given motion were compared.

Relative error between analytical and experimental results, derived from peak comparisons, is shown in Figure 6-25 for both the N1 and N2 anchors. The mean, median, and mode for this plot are 23%, 18%, and 10%, respectively, with a standard deviation of 20%. It can

thus be seen that most peaks agree within 40% of one another. Averaging each quantity to help smooth influence of the outliers yields a mean and median of 23% and 25%, respectively, with a standard deviation of 15%.

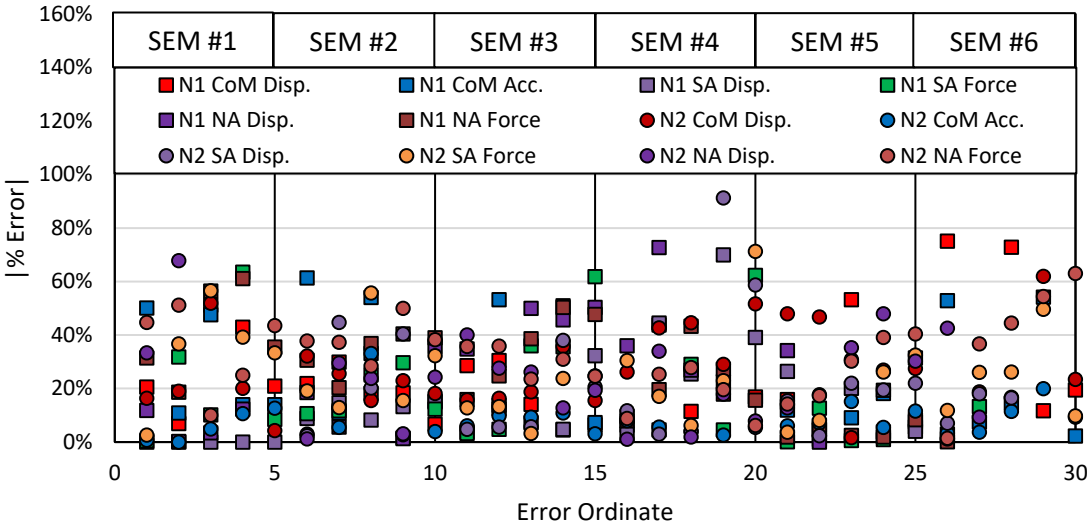

Figure 6-25: Relative Error from Peak Comparisons of Experimental versus Analytical Results of SEM Structural Tests

While peak-to-peak comparisons are interesting, comparing maxima between analytical and experimental results significantly improves relative errors. Re-computing the statistics for each quantity and for each anchor type in Figure 6-25 using only maxima yields a mean, median, and mode of 16%, 10%, and 1%, respectively, with a standard deviation of 2%. Maxima results are presented in Table 6-1 and Table 6-2 for the N1 and N2 anchors, respectively.

Table 6-1: Maxima Comparison of N1 Anchor SEM Tests

SEM Test	CoM Disp. (in)			CoM Acc. (g)			S. An. Disp. (in)			S. An. Force (k)			N. An. Disp. (in)			N. An. Force (k)		
	EXP	ANL	RE	EXP	ANL	RE	EXP	ANL	RE	EXP	ANL	RE	EXP	ANL	RE	EXP	ANL	RE
1	0.22	0.22	2%	0.34	0.51	50%	0.000	0.000	0%	2.95	2.50	15%	0.006	0.006	3%	4.39	4.51	3%
2	0.33	0.39	18%	0.33	0.53	61%	0.007	0.007	3%	5.19	4.98	4%	0.008	0.010	33%	8.31	7.41	11%
3	0.58	0.60	3%	0.64	1.13	77%	0.013	0.014	12%	10.32	8.73	15%	0.021	0.017	18%	12.95	12.79	1%
4	1.01	1.07	6%				0.028	0.021	25%	16.58	15.84	4%	0.045	0.023	49%	16.59	16.72	1%
5	2.03	3.11	53%	2.26	2.07	8%	0.029	0.024	16%	17.91	17.81	1%	0.031	0.024	22%	18.12	17.58	3%
6	3.09	5.48	77%	1.93	2.21	15%				18.06	18.26	1%				17.81	17.83	0%
AVG	27%			42%			11%			7%			25%			3%		

*Note: “CoM” denotes center of mass, “S.” denotes south anchor, “N.” denotes north anchor. “EXP” denotes experimental results, “ANL” denotes analytical results, “RE” denotes relative error.

Table 6-2: Maxima Comparison of N2 Anchor SEM Tests

SEM Test	CoM Disp. (in)			CoM Acc. (g)			S. An. Disp. (in)			S. An. Force (k)			N. An. Disp. (in)			N. An. Force (k)		
	EXP	ANL	RE	EXP	ANL	RE	EXP	ANL	RE	EXP	ANL	RE	EXP	ANL	RE	EXP	ANL	RE
1	0.22	0.26	16%	0.48	0.48	1%	0.00	0.00	0%	2.36	2.30	3%	0.01	0.00	33%	5.48	3.03	45%
2	0.38	0.45	18%	0.86	0.82	4%	0.01	0.01	2%	5.92	5.16	13%	0.01	0.01	13%	10.13	6.36	37%
3	0.58	0.67	16%	1.38	1.23	11%	0.01	0.01	6%	10.04	8.71	13%	0.02	0.01	30%	15.79	10.16	36%
4	0.89	1.27	43%	2.12	2.29	8%	0.02	0.02	2%	17.37	15.98	8%	0.03	0.03	1%	22.45	20.47	9%
5	0.97	1.23	27%	2.30	2.25	2%	0.02	0.03	11%	17.41	16.78	4%	0.03	0.03	18%	23.03	19.77	14%
6	0.86	1.23	43%	2.40	2.48	3%	0.02	0.02	9%	17.89	20.00	12%	0.04	0.04	9%	22.70	22.38	1%
AVG	27%			5%			5%			9%			17%			24%		

*Note: “CoM” denotes center of mass, “S.” denotes south anchor, “N.” denotes north anchor. “EXP” denotes experimental results, “ANL” denotes analytical results, “RE” denotes relative error.

Residual displacements are also compared in Table 6-3. It can be seen that the largest errors occur at relatively small displacements (≤ 0.01 in.), while larger displacements tend to agree within 25%.

Table 6-3: Residual Displacement Comparison of N1/N2 Anchors for SEM Tests

SEM Test	N1 S. An. Residual Disp (in)			N1 N. An. Residual Disp (in)			N2 S. An. Residual Disp (in)			N1 N. An. Residual Disp (in)		
	EXP	ANL	RE	EXP	ANL	RE	EXP	ANL	RE	EXP	ANL	RE
1	0.011	0.011	0%	0.020	0.000	0%	0.001	0.000	0%	0.000	0.000	0%
2	0.027	0.017	0%	0.045	0.000	0%	0.001	0.000	0%	0.002	0.000	0%
3	0.007	0.023	1%	0.007	0.000	1%	0.001	0.000	0%	0.002	0.000	0%
4	0.057	0.061	7%	0.070	0.030	58%	0.003	0.003	0%	0.006	0.007	25%
5	0.250	0.230	8%	0.450	0.560	24%	0.003	0.004	9%	0.012	0.007	40%
AVG	3%			16%			2%			13%		

*Note: “EXP” denotes experimental results, “ANL” denotes analytical results, “RE” denotes relative error.

6.7 – Determination of Appropriate Damping Values for Analytical Study

Determination of appropriate damping values for WALLE was a multi-faceted problem both analytically and experimentally. A core part of Watkins’ (2011) work involved field characterization of NCSs, and damping ratio was one of the field parameters studied. A hammer impact test was used for field testing and applied to WALLE with several anchored systems, which produced damping ratios between 0.4% and 1% critical damping. White noise correlation tests were also used to measure WALLE’s damping ratio, which produced values between 0.04% and 7% critical damping for WALLE’s flexible configuration and 0.04% to 5% for WALLE’s stiff configuration. Damping values had a large amount of scatter, with means of 3.8% and 1.5% for the flexible and stiff configurations, respectively. From a combination of literature review from similar NCSs as WALLE and analytical comparisons of a finite element model to WALLE’s rocking, Watkins concludes a uniform damping ratio of 2% is reasonable.

Using a uniform critical damping of 2% for each mode in both SAP2000 and NARRAS yielded mixed results for the structural tests performed in this body of work, but in general it resulted in under-predictions of anchor forces. Free rocking of WALLE on completion of each structural test was noted to have a long natural period with a small damping ratio, and so values

of critical damping less than 2% were studied via an iterative process. An array was established between 1.0% and 2.0% for each mode, shown in Table 6-4, and a combination of 1.75% for the first mode and 1.25% for the second mode yielded the closest matching results from structural tests.

Table 6-4: Determination Matrix for Equivalent Viscous Damping Ratios

	Mode 1 DR				
Mode 2 DR	**1.00**	**1.25**	**1.50**	**1.75**	**2.00**
1.00	1.00 / 1.00	1.25 / 1.00	1.50 / 1.00	1.75 / 1.00	2.00 / 1.00
1.25	1.00 / 1.25	1.25 / 1.25	1.50 / 1.25	1.75 / 1.25	2.00 / 1.25
1.50	1.00 / 1.50	1.25 / 1.50	1.50 / 1.50	1.75 / 1.50	2.00 / 1.50
1.75	1.00 / 1.75	1.25 / 1.75	1.50 / 1.75	1.75 / 1.75	2.00 / 1.75
2.00	1.00 / 2.00	1.25 / 2.00	1.50 / 2.00	1.75 / 2.00	2.00 / 2.00

Anchor displacement time-history provided the most valuable insight into damping ratio performance of the N1 anchors. Given the essentially elasto-plastic nature of these anchors, matching displacements resulted in matching forces and hysteretic curves. Incremental damping ratios for the first and second modes on either side of the specified value pair in Table 6-4 are shown in Figure 6-26. From this figure, it is seen that the combination of ρ_1 = 1.75% and ρ_2 = 1.25% yields the most closely matching value pair with structural testing results. For the north anchor pair in particular, shown on the right, accumulation of plastic displacements over time and their associated magnitudes are very close to the structural tests.

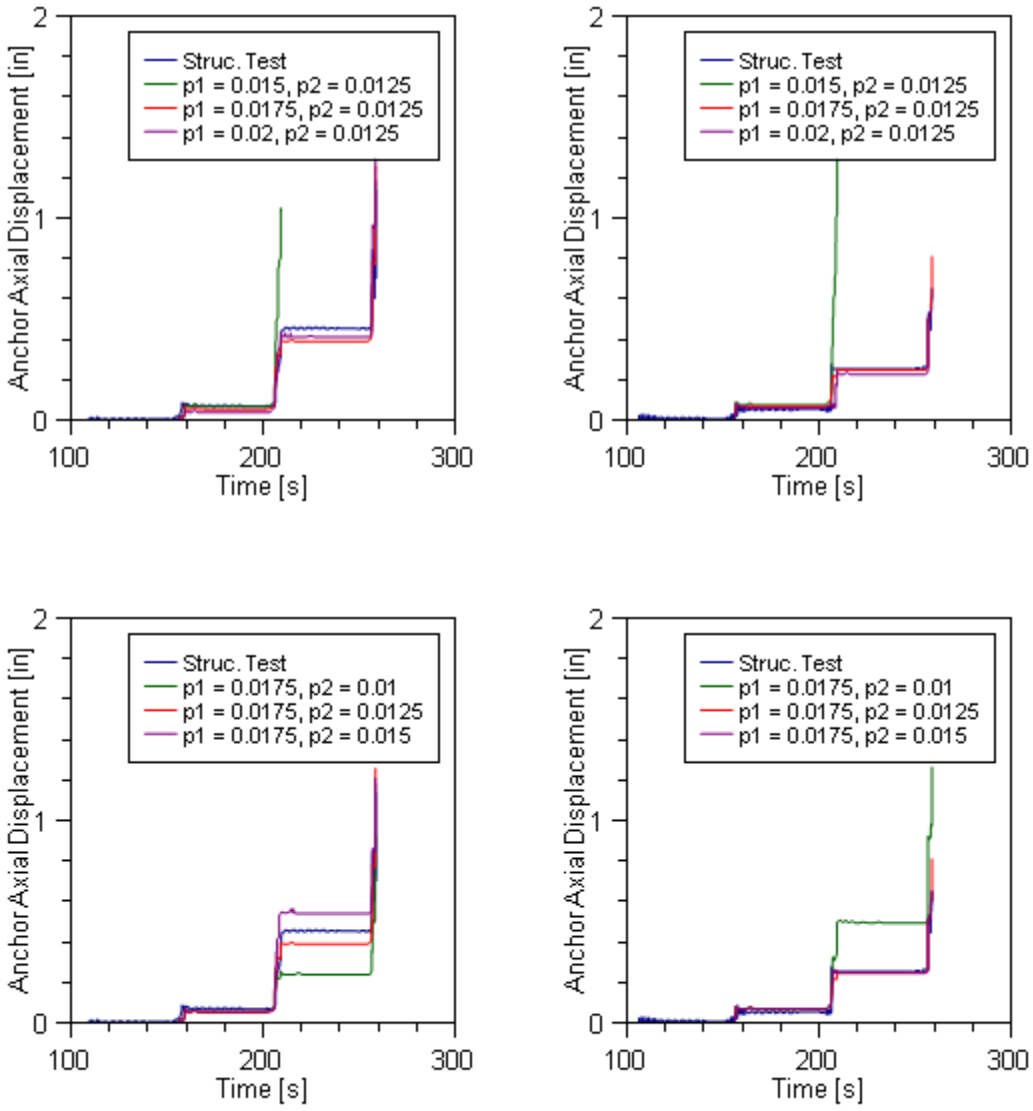

Figure 6-26: N1 Anchor Damping Ratio Comparison for South Anchor (Left) and North Anchor (Right)

Similar damping ratio comparisons as in Figure 6-26 are generated below for the N2 anchors in Figure 6-27. While plastic displacements were a strong metric for accuracy to the structural tests in the N1 anchors, the N2 anchors are force-driven, and thus comparison of forces was more warranted. Comparison was made over the strong motion portion of the earthquake for the motion prior to failure. It can be seen that the N2 anchors are less sensitive

to the selection of damping ratios than the N1 anchors overall, both in first mode and second mode values. Variation of ρ_1 is more significant than ρ_2, and amplitudes match best with structural testing as ρ_1 trends toward 1.25%. While the difference between $\rho_1 = 1.25\%$ and $\rho_1 = 1.75\%$ is notable for peak amplitudes, the differences are not as pronounced as the variations in behavior of the N1 anchors for the same spread of ρ_1 values. This difference in damping behavior is possibly due to the un-anchored rocking behavior of the N1 anchors once a gap has formed between the surface of the concrete and the anchor's nut, as a very slow, long-period oscillatory behavior could be observed when WALLE was not being driven by the ground motion. Regardless, the combination of the $\rho_1 = 1.75\%$ and $\rho_2 = 1.25\%$ value pair offered enough accuracy to be considered reasonable.

No damping study was performed on the N3 anchors, as the inclusion of additional hysteretic damping was required to validate test results. This parameter would not be a quantity readily available to designers based on selection of anchorage, and thus it was omitted from the analytical study. As the values of ρ_1 and ρ_2 were about 0.5% for the N3 anchors, and the included elastic hysteretic damping resulted in $\rho_1 = 3.0\%$, a value pair of $\rho_1 = 1.75\%$ and $\rho_2 = 1.25\%$ was considered reasonable for these anchors as well.

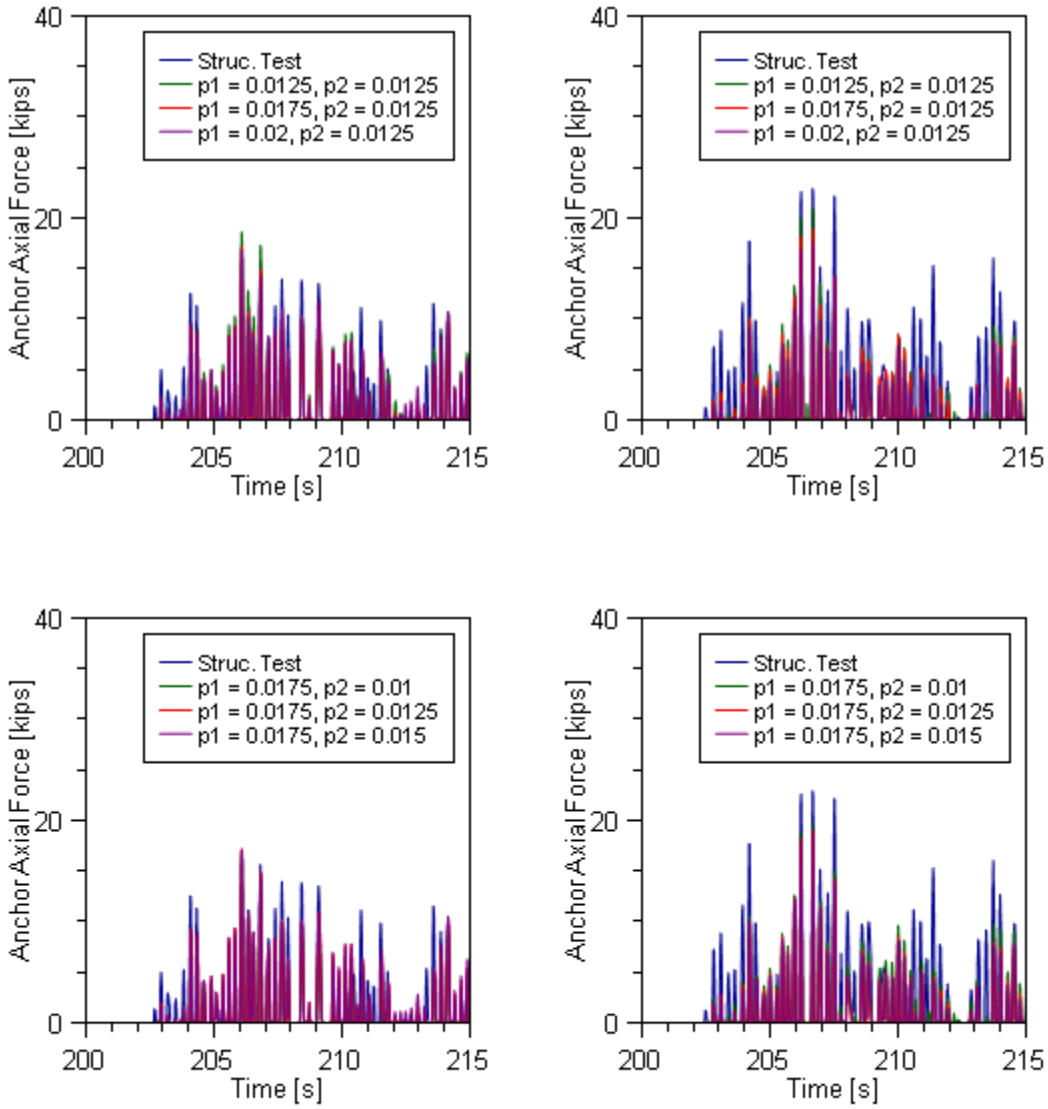

Figure 6-27: N2 Anchor Damping Ratio Comparison for South Anchor (Left) and North Anchor (Right)

Due to having a highly variable plastic force response compared with the N1 anchor, the N5 anchor required a combination of both force and displacement assessment metrics. Variation of ρ_1 including both these metrics is presented in Figure 6-28, with variation of ρ_2 following suit in Figure 6-29. From Figure 6-28, the ρ_1 = 1.50% and ρ_2 = 1.25% damping value pair provides the closest matching of anchor forces for the north anchor, while the ρ_1 = 1.75% and ρ_2

= 1.25% value pair offers the closest matching displacements for the south anchor. Due to the expansion anchors having both pre-load and a high theoretical initial stiffness, forces were naturally lower analytically due to idealization of the anchor force-displacement curve (see Figure 6-19 and Figure 6-20). As such, matching of exact force amplitudes was not as important as matching displacements.

When considered in conjunction with the other anchors, especially the N1 anchor, a damping value pair of ρ_1 = 1.75% and ρ_2 = 1.25% seemed reasonable for the N5 anchor. The combination of well-matching plastic displacements, peak force amplitudes within 10-15%, and matching failure points displayed good reproduction of the structural tests as a whole despite local discrepancies in response. Some loss of accuracy for a particular anchor was expected given the complexity of damping modeling for highly nonlinear problems, and general consistency in accuracy of this pair over all three anchors evaluated was considered acceptable.

As a final comment on damping behavior, selection of a single pair of constant damping values did not adequately capture WALLE's full time-history response regardless of the values chosen. The analytical complexity of modeling damping behavior of nonlinear problems, however, as discussed in Section 5.2.4, made time- and stiffness-dependent variations in the damping matrix unfeasible to implement. More robust damping methodologies, which do not currently exist, are likely required to correctly model damping nonlinearity. Updating the damping matrix proportionally with stiffness and natural period changes showed more pronounced amplification of WALLE's response, consistent with structural tests, but numerical errors associated with this technique strongly outweighed its benefits.

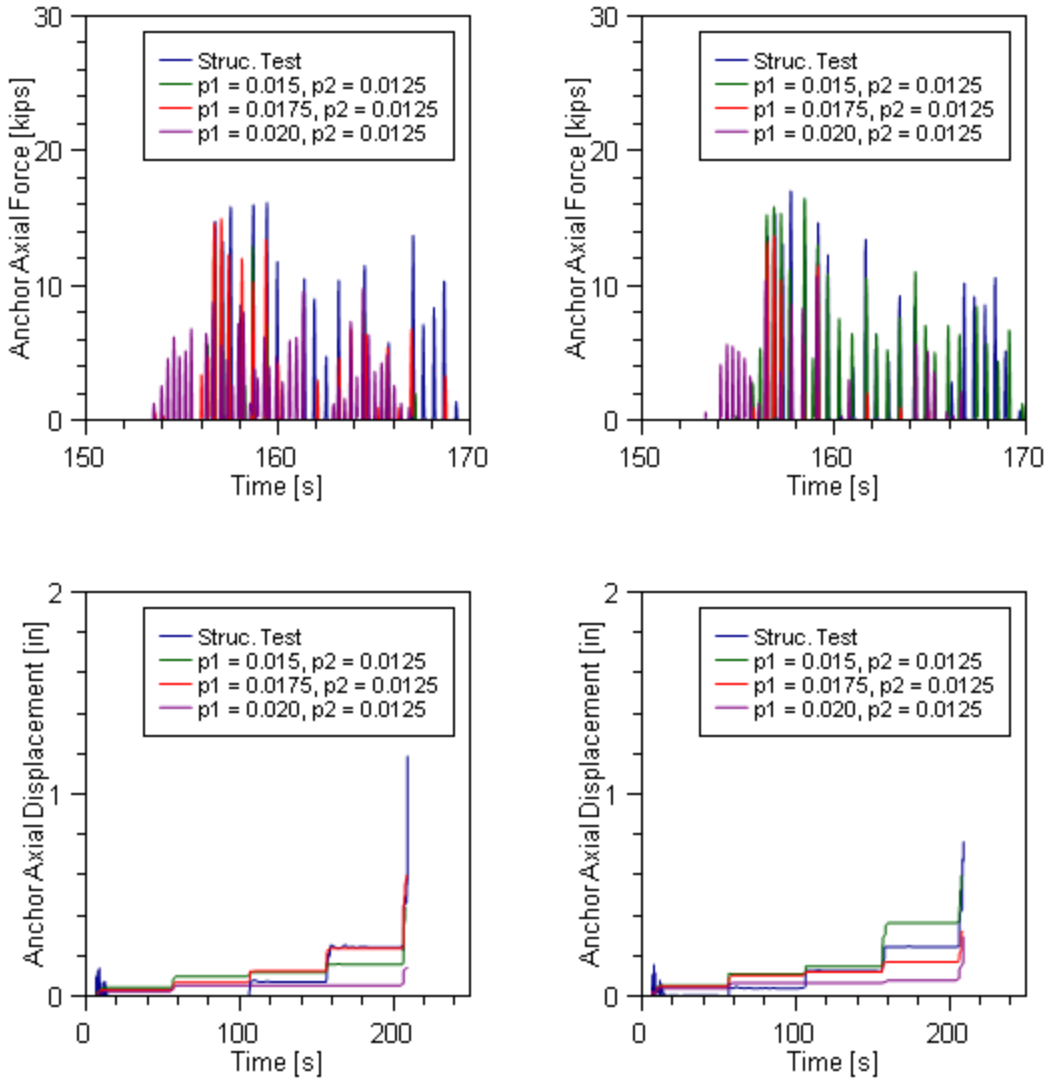

Figure 6-28: N5 Anchor Mode 1 Damping Ratio Comparison for South Anchor (Left) and North Anchor (Right)

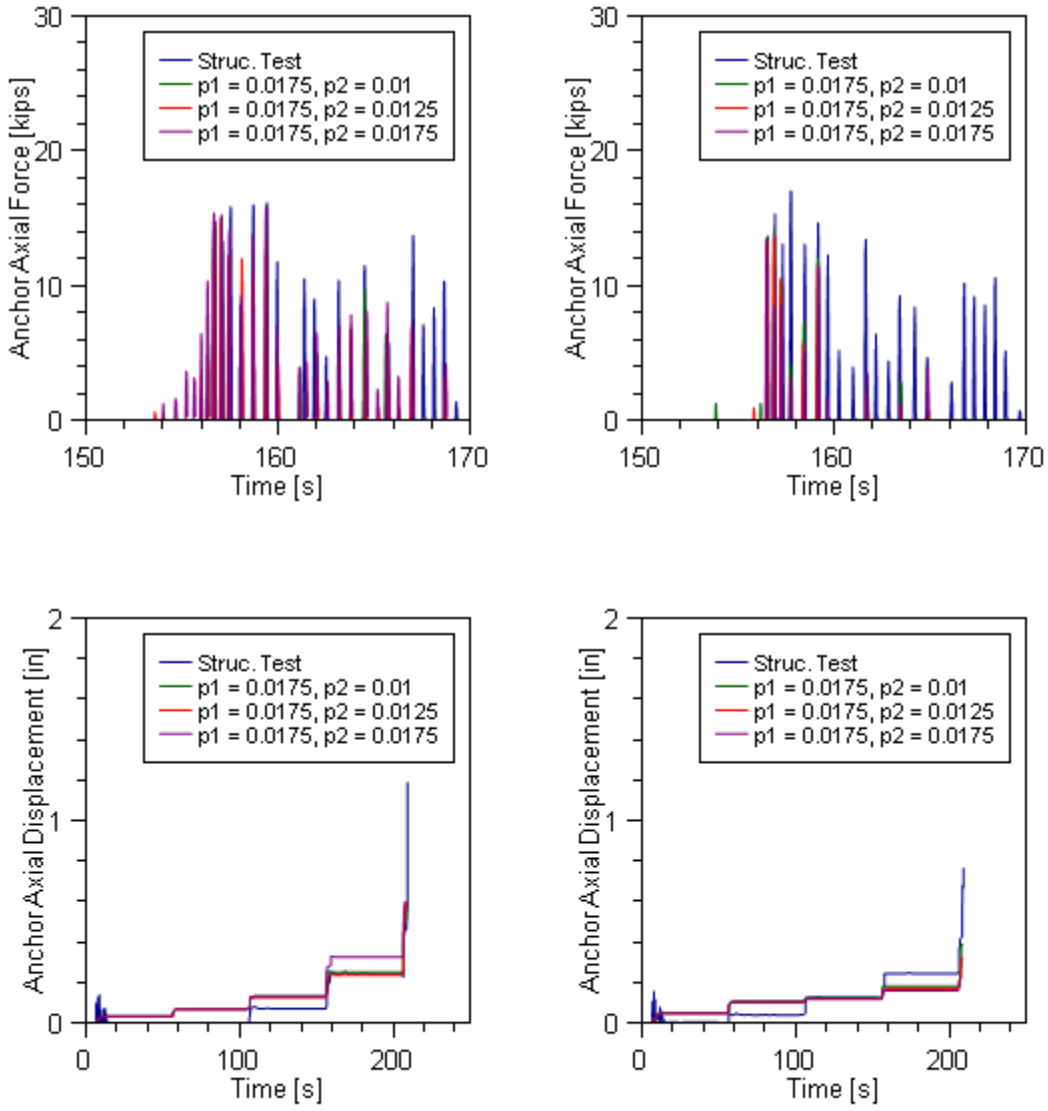

Figure 6-29: N5 Anchor Mode 2 Damping Ratio Comparison for South Anchor (Left) and North Anchor (Right)

CHAPTER 7: ANALYTICAL MATRIX AND RESULTS

To assess values of Ω_0, as it pertains to its implementation in code as a relative performance factor between ductile and non-ductile anchors, three detailed parametric studies were performed: two for upright components and one for hanging components.

For upright components, the first study targeted realistic Ω_0 values derived from code recommendations for a generic, flexible nonstructural component: a variable a_p, based on component natural period, and an R_p value of 1.5. These values are identical to those selected for WALLE, as they represent a NCS with essentially elastic component behavior which will be dynamically amplified by base motion. NARRAS did not include nonstructural component nonlinearity as part of its analysis routine, which implies the correct value of R_p is technically 1.0; however, ASCE 7-10 prescribes a minimum R_p of 1.5 and so this value was maintained to be consistent with code documentation. This resulted in conservative anchor designs, as it lowered the design force used to determine required anchor tensile strength. Conversely, the second study used a fixed, period-independent a_p value of 1.0 and an R_p of 2.5, a common value pair seen in ASCE 7-10 Chapter 13 design tables, to represent a system with unconservative design values which did not properly match actual system behavior.

For hanging components, a single study was performed similar to that of upright components, using a variable a_p based on component natural period and an R_p value of 1.5.

7.1 – Ω_0 Evaluation Process

To evaluate anchor requirements for a specific earthquake motion, a process was followed to associate a given level of Ω_0 with the scale factor of the motion. This had three steps:

- Use the ASCE7 design force equation for F_p, presented earlier in Eq. 1-1 and shown again below, to develop an appropriate lateral design force to apply to the component based on a set of input parameters. From this force, resolve a tensile design force value for the anchor from statics assuming that no overstrength is relevant; that is $\Omega_0 = 1.0$.

$$F_P = \frac{0.4 a_p S_{DS} W_p}{\frac{R_p}{I_p}} \left[1+2\left(\frac{z}{h}\right)\right]$$

- Select an anchor type to be used for analysis. Use dimensional analysis principles to scale the nominal design force of the selected anchor from the structural tests, taken to be 8.2 kips for all anchors, to the above required tensile strength. Anchor forces are then scaled directly by this scale factor, and anchor displacements are scaled by the square root of this factor.
- Scale the input motion to the appropriate level. There are three scaling factors in this process applied multiplied together: the envelope scaling factor to scale the raw motion to the DRS, a floor scale factor to adjust the DRS to a floor level demand taken as the 1+2z/h term from Eq. 1-1, and an overstrength scaling factor of 1 / Ω_0. The overstrength scaling factor is determined from the scaling variables of the F_p equation using the relationship $\Omega_0 F_p = S_{DS} \cdot (1+2z/h)$, where an adjusted S_{DS} is taken as S_{DS} / Ω_0.

This process can be repeated to evaluate the minimum-required Ω_0 value incrementally for a single earthquake motion, and can be further automated to loop through multiple earthquake motions. Each motion will have a critical scale factor of Ω_0 above which the anchor will be safe, and below which the anchor will fail. Anchor failure is defined as the exceedance of the displacement capacity of the anchor, indicating that demand has surpassed capacity. While further detail can be extracted from each time-history analysis if so desired, the primary output of each analysis is a strict pass/fail criterion. Depending on the scale factor increment of Ω_0, an individual earthquake may require anywhere from one to one hundred runs with various scale factors before survival of the anchor is achieved for that particular motion. The number of nonlinear time-history analyses needed to perform these types of evaluations is thus highly unfeasible using the computation times required by conventional finite element packages.

For all performed studies, an estimated 750,000 nonlinear time history analyses were performed. Using an average run time of 3 hours per input motion for finite element modeling such as in SAP2000, not including any post processing, would require about 256 years of continuous run time on the author's computer. Approximate continuous run time for NARRAS to complete these analyses was 4.5 days, which results in roughly 10,000 times faster computational speed.

7.2 – Survival Curves

Using the process discussed in Section 7.1, a curve can be generated by compiling the Ω_0 survival values for numerous earthquake motions run in parallel. Termed a "survival curve" for the sake of these analyses, the curve plots the percentage of ground motions which the anchor survived on the y-axis, and the level of Ω_0 associated with this percentage on x-axis. For an individual parameter set, the curve will start at a user-defined level of Ω_0 which will have a

particular survival percentage. The curve will then be populated using increasing values of Ω_0 at a user-specified increment until the survival rate for that set reaches 100%. While individual curves can be interesting in their own right, the primary advantage of this presentation method is that multiple parameter sets can be plotted alongside one another in various ways to visualize trends in observed behavior. A sample of this process for a single component parameter set, using the four different anchor types intentionally under-designed for visualization purposes, is shown in Figure 7-1. All Ω_0 values presented in the following sections are taken as the point where the survival curve reaches 100%.

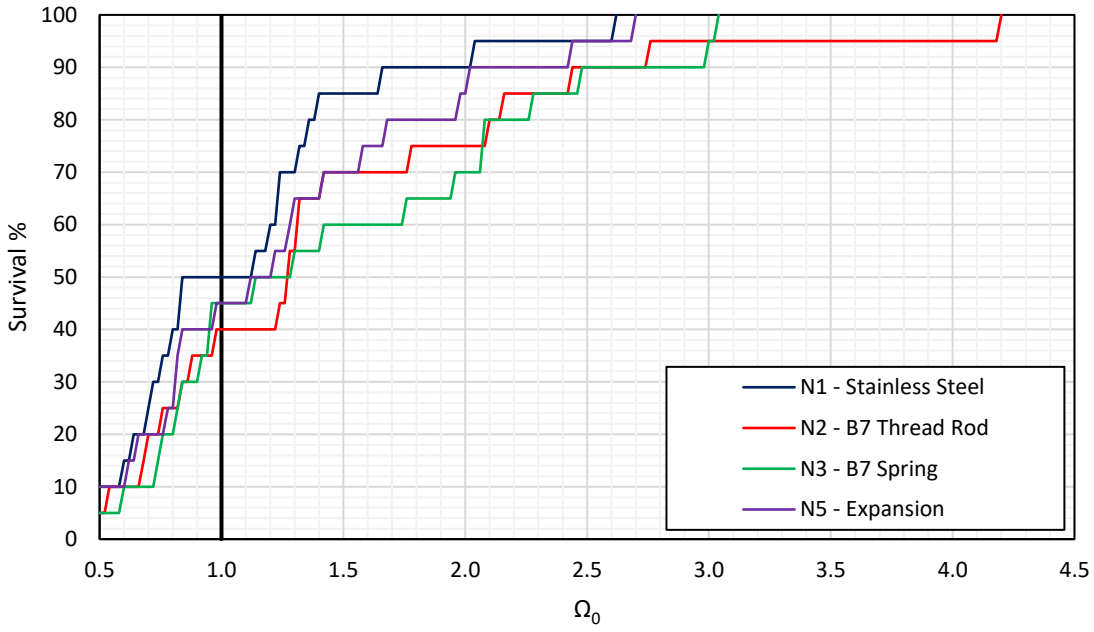

Figure 7-1: Example of Survival Curve for Single Parameter Set with Four Anchors

7.3 – Analytical Matrix

An analytical matrix, presented in Table 7-1, was developed to represent a wide range of potential parameter configurations that might be seen in "cantilever" nonstructural

components. A range of weights was selected for the studies based on a combination of internal meetings within the research team, as well as the NCS component survey performed by Watkins et al. (2009) which placed about 30-40% of components with $W_p \leq 400$ lbf, 60-70% with $W_p \leq 800$ lbf, and 85-95% with $W_p \leq 2400$ lbf. Watkins et al. (2009) classified component weights into different use categories with a total sample size of N = 1093 for a range of hospital, office, and university buildings. Mass was distributed spatially using two block configurations at the center-of-mass: a 1 ft^2 and a 2 ft^2 square.

The natural period, T_n, represented the first mode response of the NCS not including anchorage. Discussion of natural period response in ASCE 7-10 is in Section 13.6.2, and does not consider higher mode influences. A period of $T_n = 0.06$s represented the "rigid component" classification in ASCE 7-10 Chapter 11 definition, which allowed for a_p reductions from 2.5 to 1.0. Smaller natural periods were considered, specifically 0.04s, but these required a very small time step size to accurately capture 2nd mode influences caused potential numerical instabilities (dt = 0.00001s). Natural periods spread between $T_n = 0.10$s and $T_n = 0.50$s represented a range of transitory periods between the equal acceleration, equal energy, and equal displacement regions classified by Newmark and Hall (1982). Newmark and Hall (1982) define $T_n = 0.50$s as the minimum period for which the equal displacement principle is valid.

The four anchor types discussed in previous chapters were used for each parameter set

.

Table 7-1: Analytical Matrix for Ω_0 Comparison

Parameter:	Weight (kips/kN)	Natural Period T_n (s)	Anchor Type	Rotational Mass	Totals
Values:	0.25 / 1.11 0.50 / 2.22 1.00 / 4.44 1.50 / 6.67 2.00 / 8.89 2.50 / 11.12	0.06 0.10 0.20 0.30 0.40 0.50	N1 – Stainless Steel N2 – B7 Thread Rod N3 – B7 Spring N5 – Expansion	12 in^2 block (305 mm^2) 24 in^2 block (610 mm^2)	288 Parameter Sets

7.4 – Upright Components Parameter Study: Results

Two separate studies were performed using the analytical matrix given in Table 7-1 by varying parameters in the design equation (Eq. 1-1). The first study used a variable component amplification factor, a_p, with values ranging from 1.0 to 2.5 corresponding to rigid ($T_n \leq 0.06s$) and flexible nonstructural components per ASCE 7-10. A value of the response modification factor, R_p, of 1.5 was chosen represent realistic design values for the component being analyzed, as this is the smallest value of R_p prescribed by code. NARRAS did not permit nonlinear component behavior beyond rocking, so the actual appropriate value of R_p for analysis would be 1.0; this matched behavior of the component from structural testing as well, which was designed to remain linear-elastic. Use of $R_p = 1.5$ was thus considered conservative, as it assumes some benefit of force reduction due to component nonlinearity which is not present in the analysis model. Specifically for $R_p = 1.5$, the anchor design tensile force was reduced by 33% ($1 / R_p$), which may interpreted as a factor of safety applied to the Ω_0 values presented in this section.

As a result of a R_p selection of 1.5 rather than 1.0, all anchors were under-designed for the imposed forces, but this also introduced an influence of R_p on the resultant values of Ω_0. As

ASCE 7 prescribes a_p and R_p together for different component types, the second study used a fixed a_p of 1.0 and an R_p of 2.5, a typical combination seen in the design tables of ASCE 7-10 Chapter 13, to represent a condition where the selected parameters do not align with the component being analyzed. The selection of these values significantly reduces the design strength of the anchors, as using R_p = 1.5 and a_p = 2.5 – which more correctly represent real system behavioral response – results in a larger design tensile force in the anchors. Such a scenario might occur either by a designer selecting an inappropriate component type for the system being analyzed (from a lack of information about the component at the time of design, for example) or from the values prescribed within the code document not fully agreeing with actual component response. This is representative of a scenario where the anchors have been significantly under-designed for expected seismic forces. As a consequence of this, Ω_0 values will increase to compensate for the significantly decreased design tensile force. The influence of a_p and R_p on these studies will be presented later in this section.

Results from these two studies are presented with two separate interpretations of Ω_0 as it currently influences code provisions. The first manner of assessing Ω_0 considers the factor to be a raw modifier on F_p, which increases design forces on anchors such that all anchors survive imposed demands for a given design value of spectral acceleration, S_{DS}. Important to note about this interpretation is that it directly relates Ω_0 to the performance criteria established in the F_p design force equation. Conversely, the second presentation of Ω_0 assesses its value as a relative performance factor between ductile anchor response and alternative anchor force-displacement responses, which is the intended implementation of Ω_0 within current design code philosophy. This interpretation does not have any direct relation to the component design equation. As such, an important distinction may be drawn between these two methodologies: namely, the

first addresses the impact of Ω_0 on design, and the second addresses of the performance of Ω_0 representing relative performance differentials between ductile and non-ductile anchorage.

The first study presented used a variable a_p from 1.0 to 2.5 (as a functional of natural period) and an R_p value of 1.5 for determining anchor loads. Of the two studies, the first evaluates Ω_0 based on realistically-represented component behavior, while the second study is presented to illustrate the sensitivity of Ω_0 to parameters in the design equation if component behavior significantly deviates from design assumptions. Results for Ω_0, using the first interpretation discussed above, are given in Figure 7-2 in six separate bins based on natural period. Each bin contains twelve points: six weight configurations with two rotational mass inertias for each weight. Within an individual bin, each point represents a given weight and rotational mass inertia, with weights increasing from a minimum of 0.25 kips (1.11 kN) on the left side of the bin to a maximum of 2.5 kips (11.12 kN) on the right side of the bin based on the analytical matrix in Table 7-1. It can be observed from this figure that performance of the stiff elastic [N2] anchors for the T_n = 0.06s, T_n = 0.10s and T_n = 0.20s bins shows many of points require Ω_0 values less than 1, which indicates these anchors are exhibiting 100% pass rates for the required code design loads. From T_n = 0.30s and onward, however, a constant Ω_0 greater than 1 seems appropriate, with some small spillover into the T_n = 0.20s bin. Work from Watkins (2011) notes that 50% of nonstructural components surveyed from a sample size of N = 290 fell between natural periods of T_n = 0.10s to T_n = 0.25s, with 90% of components surveyed having a natural period $T_n \leq 0.25$s. WALLE's reference natural period was T_n = 0.22s. As a general observation, the large elastic displacement anchor [N3] showed an enormous amount of variation in required Ω_0 values both within bins and across all ranges of natural periods studied. Thus, while having potential interest from an analytical point of view, the wide range of

inconsistency implies these anchors are not suitable for practical application and will not be discussed further in the text. Additionally, they were excluded from all proposed envelopes. The envelope shown in Figure 7-2 is mathematically summarized in Eq. 7-1, which presents required Ω_0 values as a simple step function based on fundamental first mode natural period of the nonstructural component (not considering anchorage).

$$\Omega_0(T_n) = \begin{cases} 1.0\,, T_n < 0.2s \\ 1.2\,, T_n \geq 0.2s \end{cases} \quad \textbf{(7-1)}$$

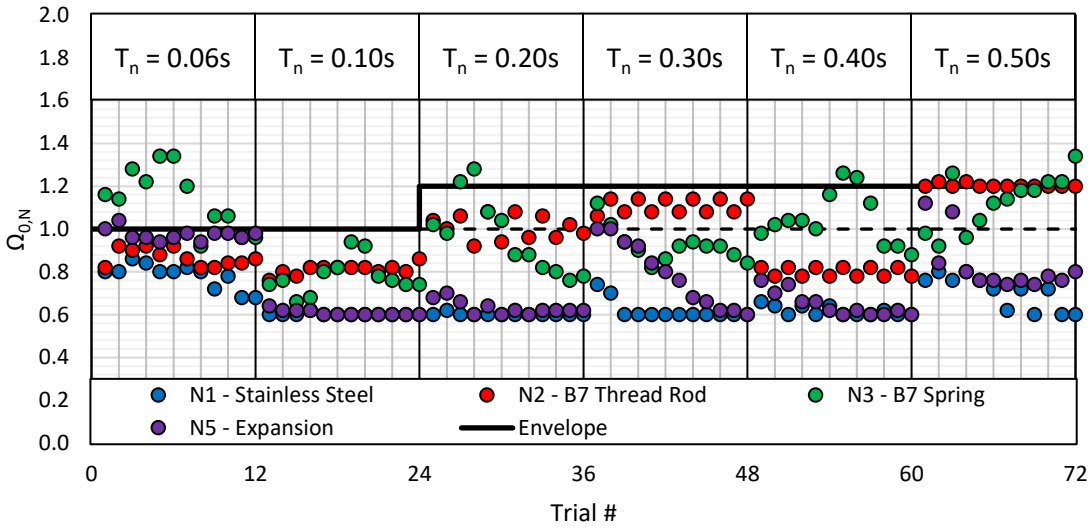

Figure 7-2: Ω_0 Values Discretized by Weight/Rotational Mass for a_p = 1.0-2.5 and R_p = 1.5

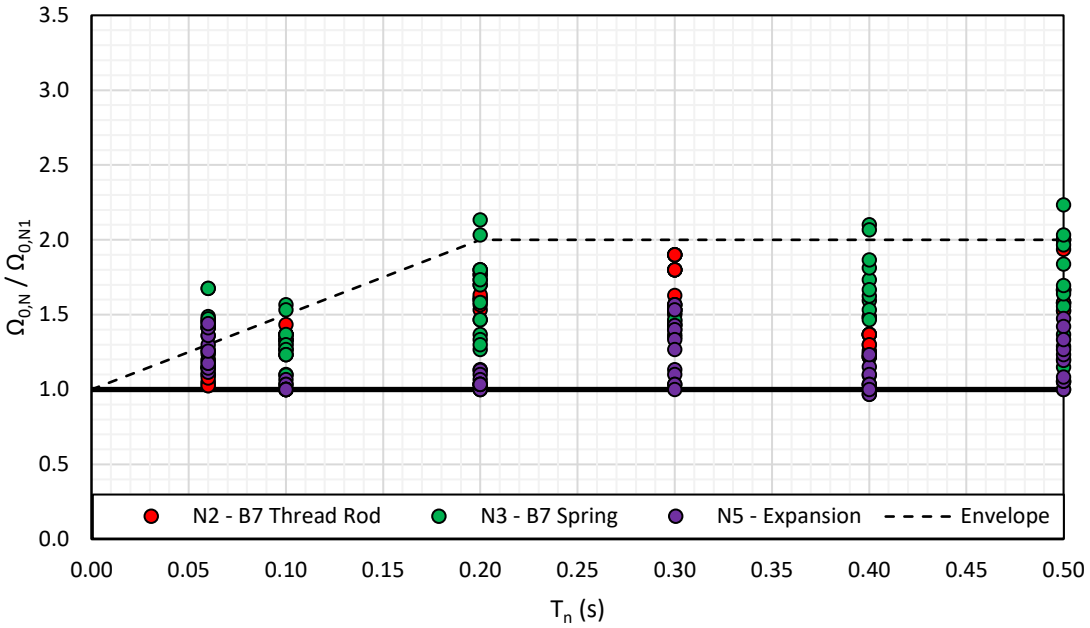

Figure 7-3: Normalized Ω_0 Values for a_p = 1.0-2.5 and R_p = 1.5 [Raw]

Figure 7-3 presents the second interpretation of Ω_0 as a relative performance factor between ductile and non-ductile anchorage. All anchor Ω_0 values were normalized against the stainless steel anchor [N1] Ω_0 values, resulting in the N1 anchor being the "benchmark" anchor associated with ductile response. It should be noted from the structural testing that this anchor's stretch length of 4 in. (101 mm) was 1.25 times that of required minimum in ACI 318 of 3 in. (76.2 mm) (taken as 8 times the anchor diameter). Additionally, it had an ultimate tensile strain capacity of 0.32, which is 2.3 times the required minimum of 0.14, so this anchor possessed ductility characteristics in excess of the minimums prescribed in ACI 318 performance standards. In this figure, a linear variation between T_n = 0s and T_n = 0.20s can be enveloped over the data points, starting at Ω = 1.0 and ending with Ω = 2.0, after which a constant value of Ω = 2.0 can be observed. This value is not significantly different from the ASCE 7-10 value of Ω_0 = 2.5 and agrees closely with the ASCE 7-16 value of Ω_0 = 2.0, indicating that existing code provisions

are reasonably and conservatively predicting the relative performance between extremely ductile and essentially linear-elastic anchor responses for longer natural period response. It should be noted that if a less ductile anchor was used, such as the minimum required by ACI 318, these values of Ω_0 would be expected to drop. These values of Ω_0 may thus be considered conservative. The envelope shown in Figure 7-3 is described by the mathematical relationship in Eq. 7-2.

$$\frac{\Omega_{0,N}}{\Omega_{0,N1}}(T_n) = \begin{cases} 1.0 + T_n/0.2 & , T_n < 0.2s \\ 2.0 & , T_n \geq 0.2s \end{cases} \quad \textbf{(7-2)}$$

An alternative conception of Figure 7-3 is presented in Figure 7-4 to correct for the fact that the relative performance of a non-ductile anchor to the ductile anchor has no inherent attachment to a particular design level. Two adjustments are made to apply this correction. Firstly, any ratio of $\Omega_{0,N}$ / $\Omega_{0,N1}$ which falls below 1 is set to 1: this implies equitable performance between the non-ductile and ductile anchor. Secondly, any Ω_0 value less than 1 is set equal to 1, which indicates strictly that a given anchor is performing as intended at the design level. Upon doing this, the recommendations for $\Omega_{0,N}$ / $\Omega_{0,N1}$ can be seen to converge to the recommendations for the raw Ω_0 values in Eq. 7-1. Modification to the T_n < 0.2s region in Eq. 7-1 is shown in Figure 7-4 as a linear variation between 1.0 to 1.2 for periods of T_n = 0s to T_n = 0.20s.

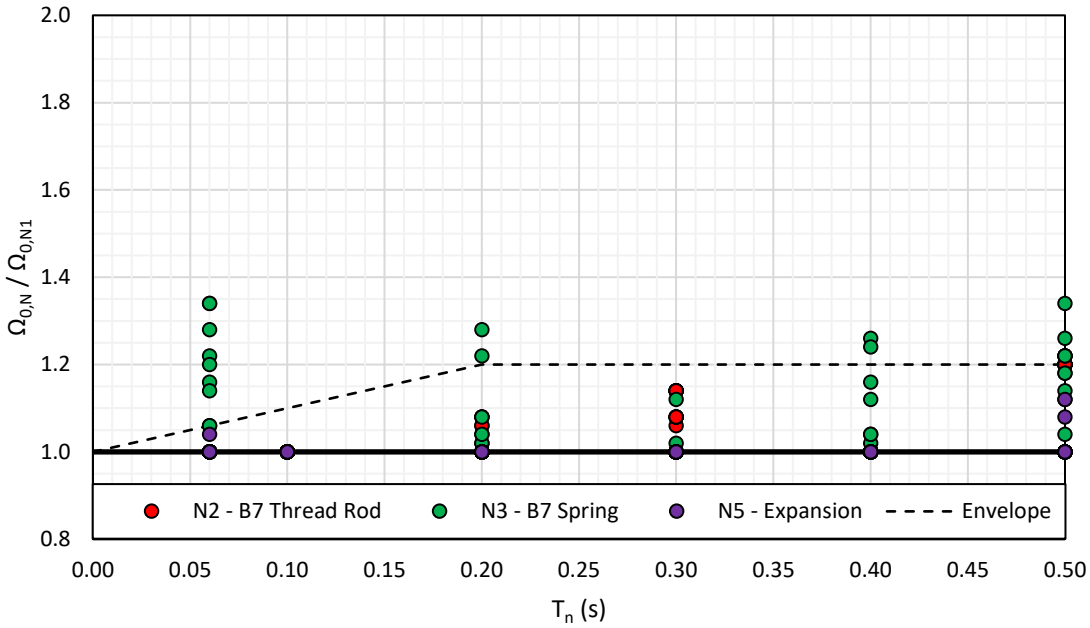

Figure 7-4: Normalized Ω_0 Values for a_p = 1.0-2.5 and R_p = 1.5 [Corrected]

The discussion of the required level of Ω_0 has, until now, been de-coupled from the assignment of R_p and a_p values given in ASCE 7. The selection of these values is dependent on the component descriptions provided in Tables 13.5-1 and 13.6-1. If the actual component response does not correspond to the levels of component amplification and ductility associated with the tabular values, the required level of Ω_0 can vary significantly. To evaluate the influence of incorrect R_p and a_p values on Ω_0, the second study performed as part of this analysis matrix was to run the same parameter set used in the first study, but with design force equation inputs of a_p = 1.0 and R_p = 2.5 – a common value combination given in the design tables of ASCE 7-10 Chapter 13. These values are not representative of the actual system being analyzed as they imply nonlinear behavior in the nonstructural component and no amplification above natural periods of 0.06s; both are untrue.

Figure 7-5 and Figure 7-6 present the same plots as Figure 7-2 and Figure 7-3, respectively, but with differing a_p and R_p values used for the anchor design. As stated previously, the large scatter of the N3 anchors is ignored in this commentary and discussion due to its soft elastic idealization not being representative of anchors used in field installations. All anchors show an increase compared to the first study in required $\Omega_{0,}$ which is to be expected, though the required amount varies with both period and anchor type. Both the highly ductile stainless steel anchors [N1] and the expansion anchors [N5] show smaller required Ω_0 values compared with the stiff elastic anchors [N2], with the N5 anchors having roughly 40% the plastic displacement capacity as the N1 anchors. Based on current code considerations, the N5 anchor is treated as non-ductile with expected performance similar to that of the N2 anchor; this is, however, clearly not the case, suggesting that current code provisions may be too narrow when defining which features of anchor response are contributing to beneficial performance. With the exception of the extremely rigid components in the T_n = 0.06s bin, plastic displacement capacity provides additional survival capacity that increases up through the T_n = 0.30s bin, after which it remains constant.

For all interpretations of Ω_0, an incorrect selection of R_p and a_p results in period-dependent increases in Ω_0 values. Table 7-2 shows a ratio of the average Ω_0 values for the second study divided for the average Ω_0 values for the first study. While a minimum Ω_0 used in the analytical study distorts the accuracy of the exact numbers, a trend can nevertheless be observed that suggests plastic displacement capacity and sensitivity in required Ω_0 are linked.

Table 7-2: Ratio of Ω_0 Increases for Incorrect a_p/R_p Selection

Natural Period, T_n	N1 – Stainless Steel	N2 – B7 Thread Rod	N5 – Expansion
0.06	1.55	1.36	1.52
0.10	2.29	3.48	2.70
0.20	2.37	2.94	3.08
0.30	2.52	3.64	2.96
0.40	2.62	3.50	2.75
0.50	2.98	3.49	3.23

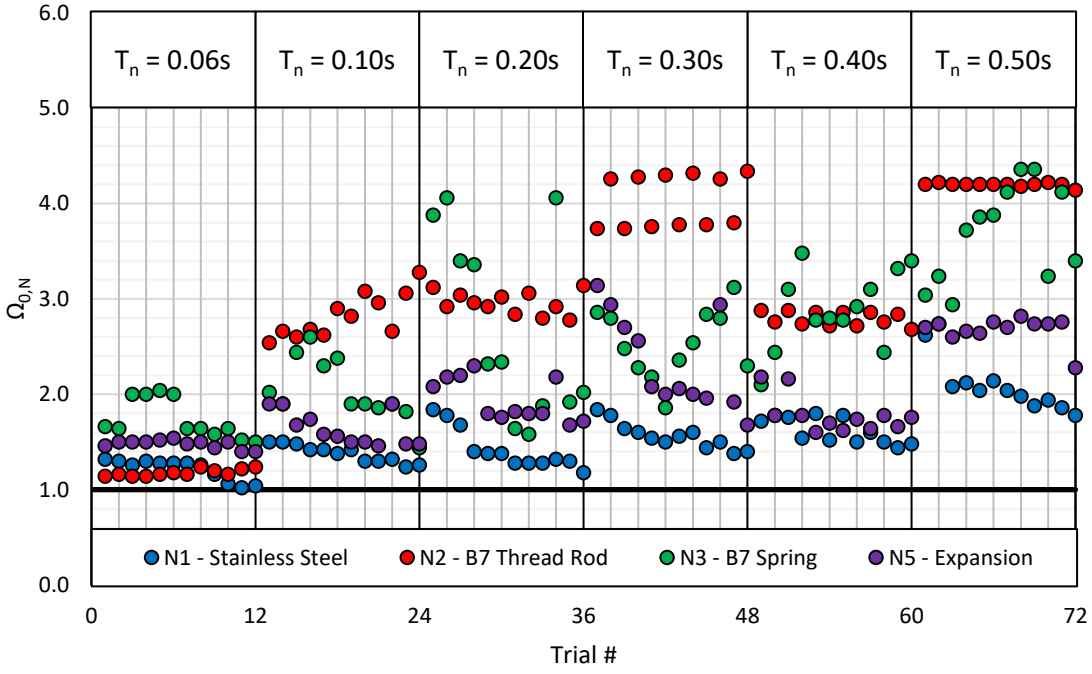

Figure 7-5: Ω_0 Values Discretized by Weight/Rotational Mass for a_p = 1.0 and R_p = 2.5

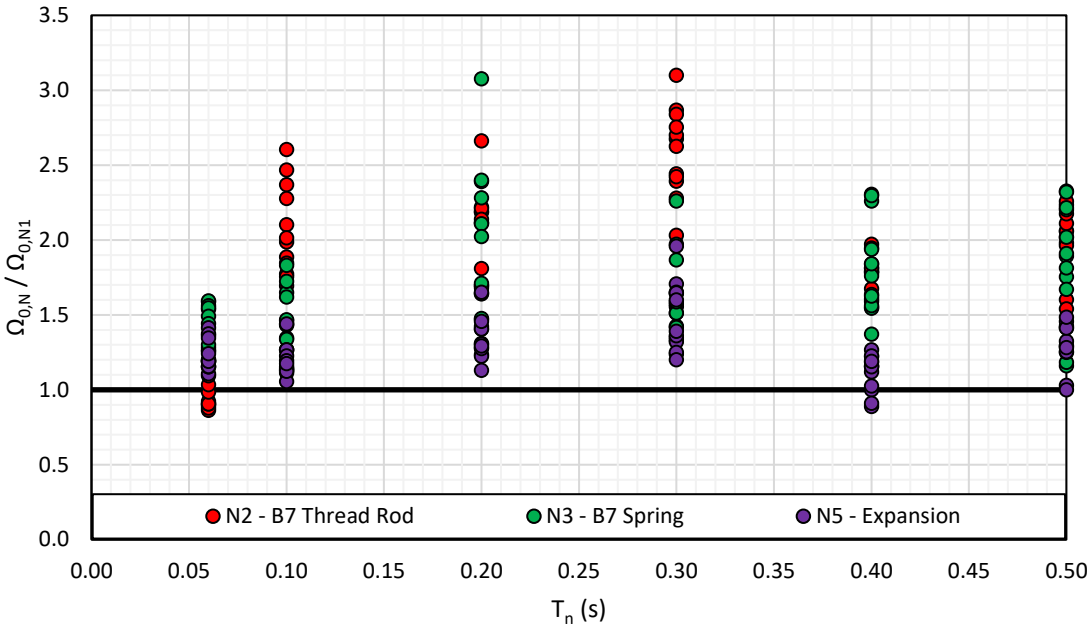

Figure 7-6: Normalized Ω_0 Values for a_p = 1.0 and R_p = 2.5 [Raw]

A demonstration of the influence of R_p and a_p on required Ω_0 values for the N1 and N2 anchors is presented in Figure 7-7. This figure explains the differences between the first and second studies, and it can be noted that the maximum increase in required Ω_0 in these plots of approximately 4 for the N2 anchors is roughly equal to a multiplier of 2.5 in a_p divided by the difference in R_p of 1.5/2.5. As the author of this dissertation is unaware of any body of work studying the relationship of expected component R_p values as they relate to anchor performance, the analytical work presented here suggests this may be a topic of considerable interest to study for anchorage in the future – both in terms of analytical work and physical structural testing.

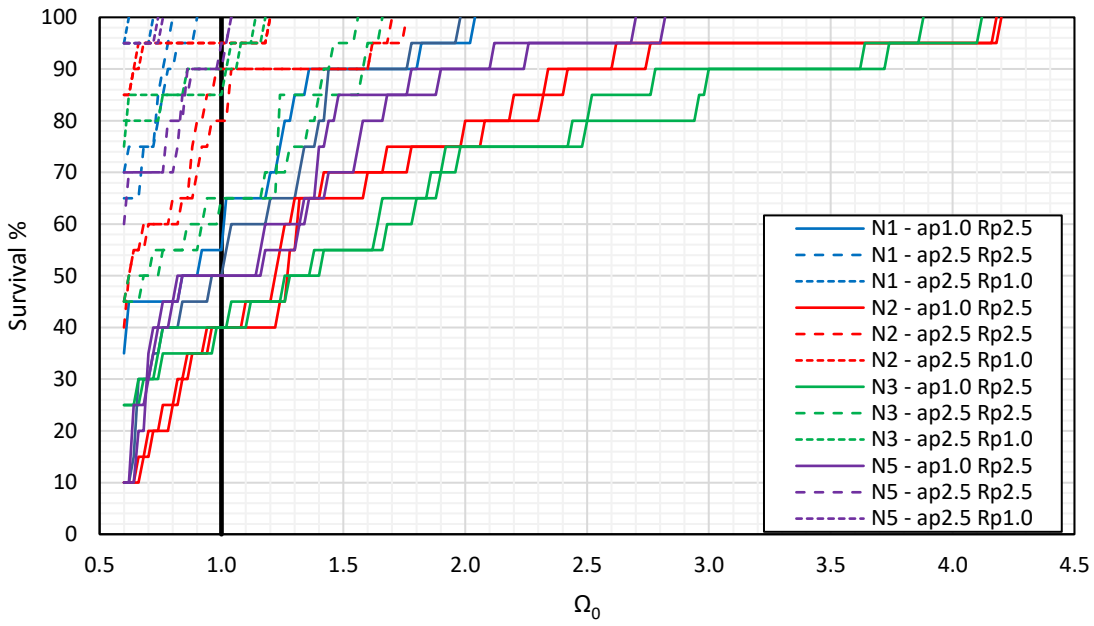

Figure 7-7: R_p and a_p Influence Case Study: W_p = 1.5 kips, T_n = 0.50s.

7.5 – Upright Components Parameter Study: Summary

Two parametric studies were performed to evaluate the overstrength factor, Ω_0, as it is applied to the design of upright nonstructural component anchorage. Four different anchor types (with varying force-displacement characteristics) and a range of nonstructural component natural periods, weights, and rotational masses were assessed using bulk nonlinear time-history analyses and a customized analysis tool specially developed for analyzing tension-dominated nonstructural component anchorage. The key findings were as follows:

a. Recent changes in ASCE 7-16 Ω_0 from 2.5 to 2.0, treating Ω_0 as a relative performance factor between ductile and non-ductile anchorage, are reasonable for upright components. Future research may support reduced values of Ω_0, but the

relationships between the component R_p and a_p values and associated anchor response are not well understood and any further modifications would require a review of the assumptions associated with those terms and the F_p expression in ASCE 7. Contingent on further research to quantify the relationship of R_p to Ω_0, it is not recommended to change Ω_0 at this time. The authors suggest that further research be undertaken to study R_p specifically related to the component-anchor system.

b. Current Ω_0 values as they are applied to the lateral design force equation may not provide a uniform margin of safety. While plastic displacement capacity offers benefit to most anchorage systems, this amount of benefit is highly dependent on the natural period of the nonstructural component and may have no appreciable difference in ensuring that anchors are capable of resisting imposed demands for a given seismic design level.

c. The required Ω_0 can increase significantly if the a_p and/or R_p values used in the component design do not correlate with the actual amplification and ductility of the component. When the system responds in a manner that correlates closely with chosen design values of a_p and R_p, the required Ω_0 may be taken from Eq. 7-1. If the nonstructural component behavior deviates from the response assumed in the design equation, however, the required Ω_0 to protect anchors from failure can increase significantly. In such cases, this study indicates that all anchor types required Ω_0 values larger than 1.0 – including ductile anchors. In general, anchor plastic displacement capacity helped protect the anchor from failure when under-designed for the imposed loads, though the amount of benefit from this property is

dependent on component natural period and the extent of anchor plasticity. For the work in this paper, increases in required Ω_0 for under-designed N1 anchors were 100-200%, while increases in Ω_0 for under-designed N2 anchors were 200-260%.

d. Displacement ductility, defined as the ultimate displacement reached prior to a region of negative stiffness (displacement at peak force) divided by the elastic displacement, was beneficial for all anchors tested. Currently, ACI 318 provisions assume material ductility of the anchorage system to be the sole governing factor of desirable anchor behavior, while the actual benefits appear to be mechanism-independent (i.e. plastic displacement capacity offers the same benefit to anchor performance regardless of the physical mechanisms by which it is obtained). This implies that the force-displacement curve of an anchor governs its overall performance, regardless of the physical mechanisms by which it is generated.

e. Stiff elastic anchor response is highly beneficial to component response because it keeps the component close to the slab and minimizes pounding effects. The large displacement elastic anchors showed potential to perform as well as large plastic displacement anchors, but this was highly unpredictable. At their worst, these anchors performed most poorly by a wide margin – especially for stiff components which can have significant period elongations that are not addressed currently in the code demand equation and formulations of F_p.

7.6 – Hanging Components Parameter Study: Results

The parameter study completed for upright components, presented previously in Table 7-1, was repeated for hanging components. Values of R_p = 1.5 and a variable a_p based on natural period were also repeated. Damping ratios of 1.75% for the first mode and 1.25% for the second mode remained consistent as well.

Raw Ω_0 values as a direct modifier to the F_p equation are presented in Figure 7-8. Of immediate note is the poor performance of all anchors in the T_n = 0.06s bin; the N3 anchors have Ω_0 values from 4.5 to 8.5, and are omitted from view to preserve visual scale in the figure. All anchor types show inadequate performance at the design level associated with F_p. This can be explained by the nature of the hanging component loading, and specifically the a_p term. From the description of hanging component base moment versus rotation hysteresis provided in Section 5.3.2, it can be noted that the hanging system starts in a region where both anchors are loaded with the component weight, W_p. This force generates a pre-load on the anchors, and the system is free to immediately swing; this is contrary to the upright systems, where W_p provides a clamping moment that fixes the system from rotation until the lateral force at the center of mass can overcome it. As a result, hanging systems are much softer innately than upright systems. Single-side swinging of the base (region 2 in Figure 5-6) also significantly softens the system, and no period of stiff response (such as the system touching down after being uplifted for upright components) is guaranteed for a particular cycle within an earthquake motion. Hanging systems are thus significantly more susceptible to period elongations.

As a byproduct of this softening, a reduction in demand associated with stiff response does not happen. A value of a_p = 1.0, which assumes no component amplification occurs, does not accurately represent the swinging nature of the system, which is largely indifferent to the component's state of plasticity when swinging about only one anchor. To demonstrate the inadequacy of the use of a_p = 1.0, the T_n = 0.06s bin of Figure 7-8 was reproduced using a_p = 2.5 in Figure 7-9. Required Ω_0 values decrease significantly, and become agreeable with the general trends in behavior for this bin seen in Figure 7-2 for upright components.

An envelope function that captures relevant Ω_0 values from Figure 7-9 is presented below in Eq. 7-3.

$$\Omega_0(T_n) = \begin{cases} 1.0\,, T_n < 0.2s \\ 1.5\,, T_n \geq 0.2s \end{cases} \quad \textbf{(7-3)}$$

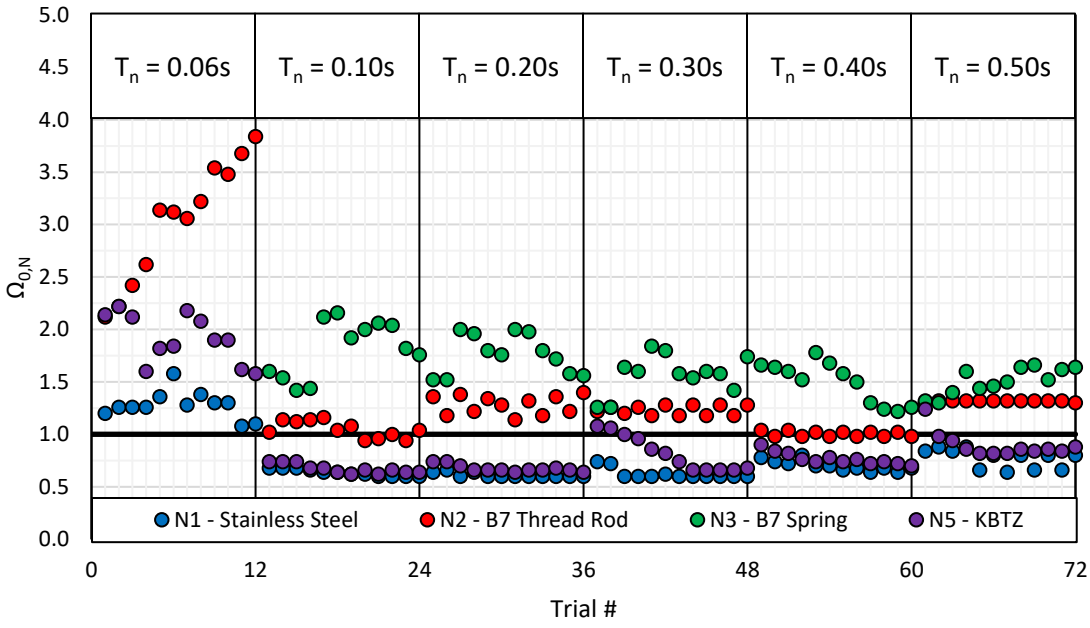

Figure 7-8: Ω_0 Values Discretized by Weight/Rotational Mass for a_p = 1.0-2.5 as f(T_n) and R_p = 1.5

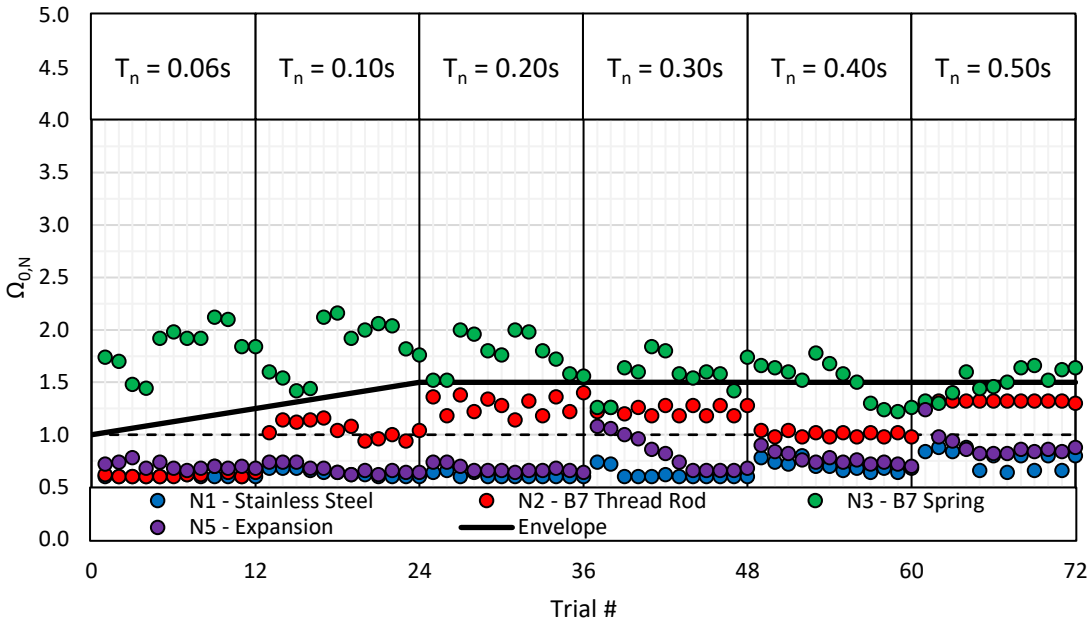

Figure 7-9: Ω_0 Values Discretized by Weight/Rotational Mass for a_p = 2.5 (constant) and R_p = 1.5

Another observation that can be noted in Figure 7-8 is that plastic displacement is generally beneficial to the resistance of larger amplitudes of input motion – even in the bins with small natural periods – and provides a uniform buffer against under-designed anchors. This appears to be due to influences not only of protection against period elongation, but also as a ratio of anchor preload due to the component weight to anchor yield force. While W_p is a fixed parameter in the design process for a given component, anchor ultimate force varies with selection of other parameter inputs into the F_p equation. If preload on the anchors is too close to the design force, the system becomes highly unstable, as the swinging effects occur based upon the need for the anchors to resist a minimum of W_p at all times. Thus, when looking at a comparison between the N1, N2, and N5 anchors in the T_n = 0.06s bin in Figure 7-9, it can be seen that each of these anchors satisfies the design level associated with Ω_0 = 1.0 by a large margin as anchor preload moves away from this instability point.

Relative performance between non-ductile and ductile anchors, $\Omega_{0,N} / \Omega_{0,N1}$, is presented in Figure 7-10 using a variable a_p between 1.0 and 2.5 as a function of T_n. To compensate for the inaccuracy of ap = 1.0 as applied to the T_n = 0.06s bin, as discussed above, a uniform a_p = 2.5 across all T_n values is presented in Figure 7-11. Additionally in Figure 7-11, an envelope is provided which is described below in Eq. 7-4. This envelope is quite similar to that described for upright components in Eq. 7-2.

$$\frac{\Omega_{0,N}}{\Omega_{0,N1}}(T_n) = \begin{cases} 1.0 + 1.5(T_n/0.18) & , T_n < 0.18s \\ 2.5 & , T_n \geq 0.18s \end{cases} \quad \textbf{(7-4)}$$

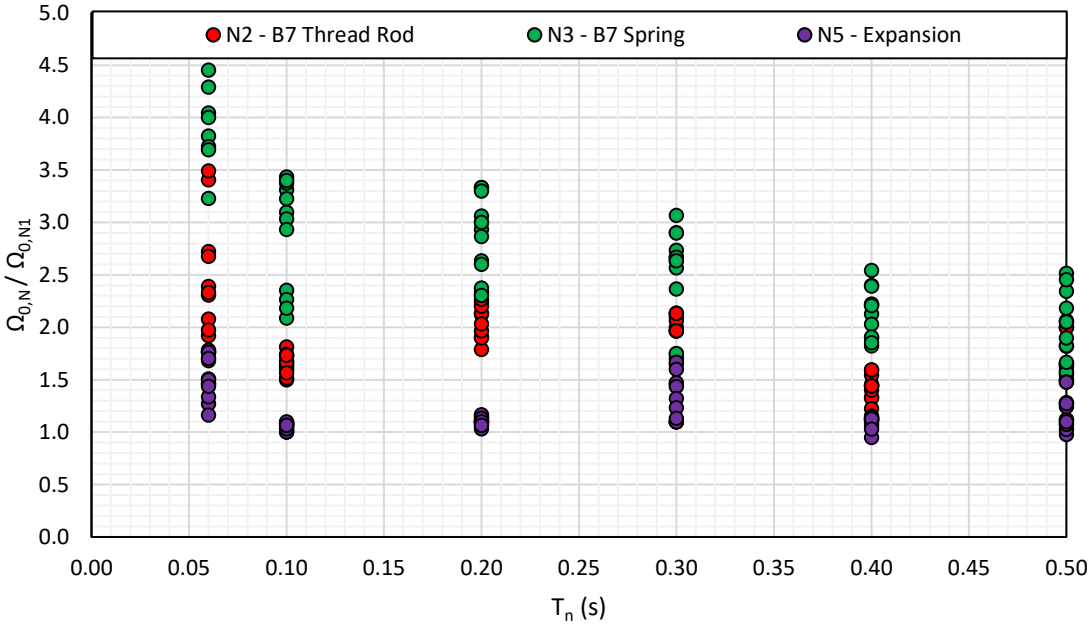

Figure 7-10: Normalized Ω_0 Values for a_p = 1.0-2.5 and R_p = 1.5 [Raw]

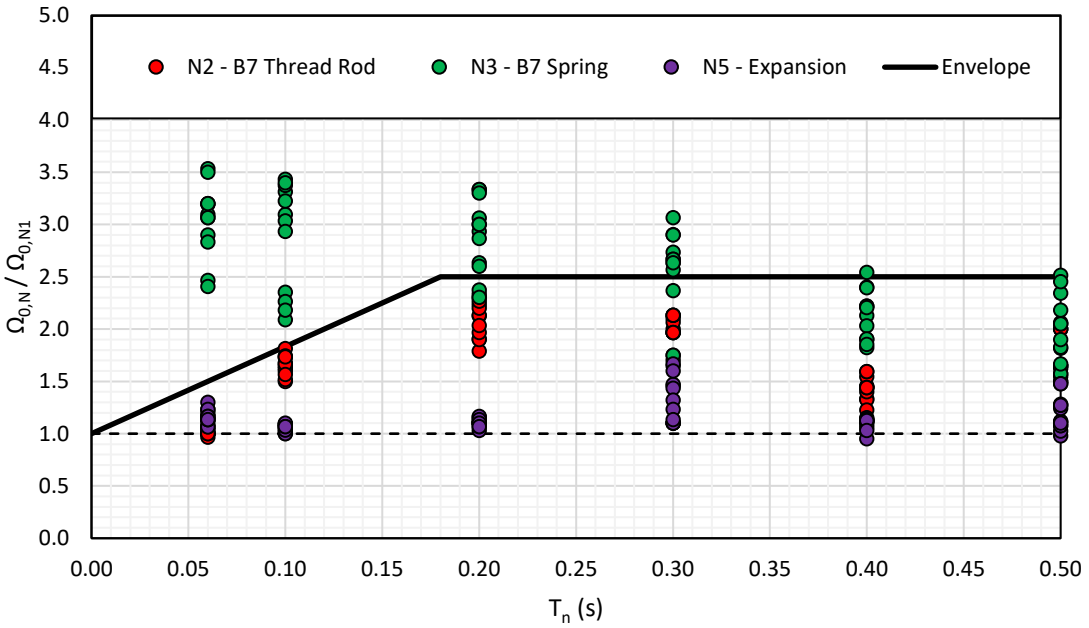

Figure 7-11: Normalized Ω_0 Values for a_p = 2.5 (constant) and R_p = 1.5 [Raw]

Normalization of $\Omega_{0,N} / \Omega_{0,N1}$ from Figure 7-11 is provided in Figure 7-12. The same corrections are applied as for upright components. First, any ratio of $\Omega_{0,N} / \Omega_{0,N1}$ which falls below 1 is set to 1: this implies equitable performance between the non-ductile and ductile anchor. Secondly, any Ω_0 value less than 1 is set equal to 1, which indicates strictly that a given anchor is performing as intended at the design level. Upon doing this, the recommendations for $\Omega_{0,N} / \Omega_{0,N1}$ can be seen to converge to the recommendations for the raw Ω_0 values in 7-3 with the caveat that the transitional period is T_n = 0.18s instead of T_n = 0.20s.

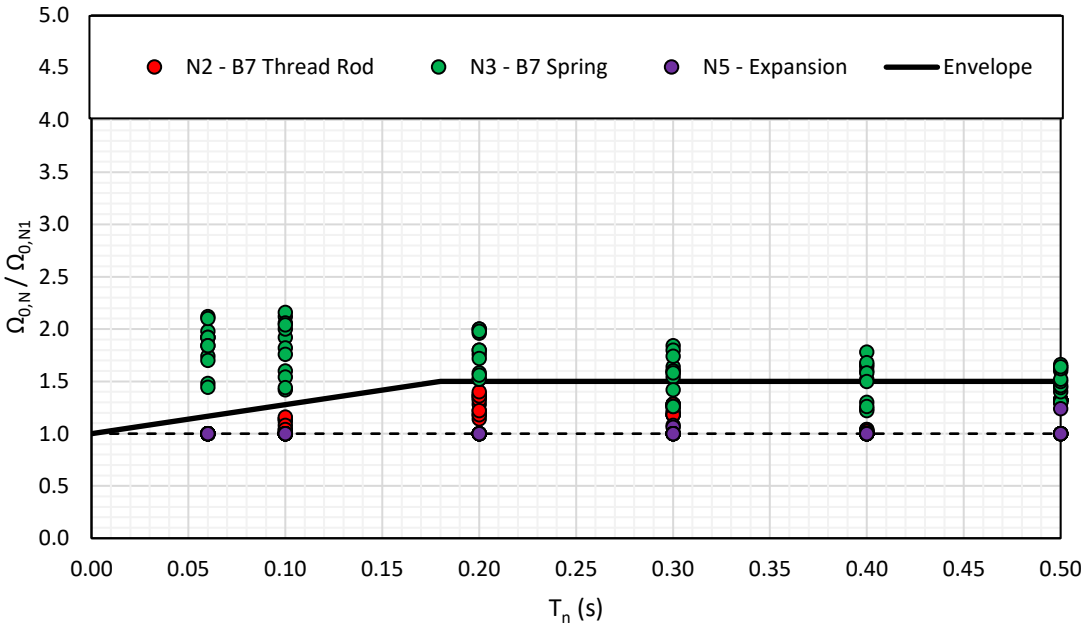

Figure 7-12: Normalized Ω_0 Values for a_p = 2.5 (constant) and R_p = 1.5 [Corrected]

7.7 – Hanging Components Parameter Study: Summary

A parametric study was performed to evaluate the overstrength factor, Ω_0, as it is applied to the design of hanging nonstructural component anchorage. Four different anchor types and a range of nonstructural component natural periods, weights, and rotational masses were assessed using bulk nonlinear time-history analyses. The evaluated parameters were the same as the upright component studies, with the only substantive difference being the base moment versus base rotation hysteresis definition of the component. Relevant key findings are as follows:

a. Both the raw Ω_0 and the relative $\Omega_{0,N} / \Omega_{0,N1}$ interpretations of applicable overstrength increased by approximately 25% for hanging component systems over upright systems. Hanging systems were particularly susceptible to elongations in

component natural period due to soft swinging behavior of the base for stiff systems. Current design practice does not consider anchorage as a part of the NCS design process using the F_p equation, but design for "rigid" or "flexible" response based strictly on the nonstructural component per ASCE 7 is insufficient in capturing hanging system response parameters.

b. Reduced values of $a_p = 1.0$ permitted in ASCE 7 should not be allowed for hanging components. While the nonstructural component may be stiff, the nature of the hanging problem causes significant period elongations such that response of the anchor-component system will experience amplification. For elastic anchors which may restrict the extent of swinging behavior, ACI 318 and ASCE 7 do not account for the percentage of anchor force capacity consumed in supporting the nonstructural component weight, and thus a lower a_p value has potential to significantly under-design anchors for seismic loading if field demands are not in close congruence with the designer's expected load levels.

c. Plastic displacement capacity in the anchorage was a more notably beneficial feature for hanging components compared to upright components, but came with the added drawback of a "snowballing" ratcheting effect as the anchors were plastically deformed. Systems had a tendency to pull toward areas of plastic displacement, as single-side swinging of the base (Region 2 in Figure 5-6) reduced the amount of hysteretic damping provided by the anchors on the side opposite that of the largest plastic displacements. The extent of the ratcheting effect also appears to be related to the ratio of the expended anchor force capacity resisting the nonstructural component's non-seismic dead load relative to the yield force of

the anchors; that is, as the amount of component weight resisted by the anchors relative to the yield force increased, ratcheting behavior appeared to become more pronounced.

7.8 – Summary of Ω_0 Findings

Two major interpretations of Ω_0 were presented in this chapter. A third interpretation, as a modification of one of the base interpretations, was also presented. These are summarized as:

a. Ω_0 as a raw modifier on the F_p equation.
b. Ω_0 as a relative performance factor between ductile and non-ductile anchorage given by the relationship $\Omega_{0,N} / \Omega_{0,N1}$.
c. Ω_0 as a relative performance factor between ductile and non-ductile anchorage given by the relationship $\Omega_{0,N} / \Omega_{0,N1}$, but normalized to the F_p equation by setting all anchors that satisfy the design equation as being equal to 1.

The core findings regarding appropriate values of Ω_0, amalgamated from the previous sections, can be mathematically expressed in Eq. 7-5. This equation describes all three interpretations of Ω_0 based on the presented α factor, whose values are assigned simply based on whether or not the system is upright or hanging. The magnitude of α depends on what interpretation of Ω_0 is chosen.

$$\Omega_0(T_n) = \begin{cases} 1 + \alpha(T_n/0.18) & , T_n < 0.18s \\ 1 + \alpha & , T_n \geq 0.18s \end{cases} \quad \textbf{(7-5)}$$

For interpretations (a) and (c), α converges to the same values. These are:

$\alpha_{upright} = 0.2$

$\alpha_{hanging} = 0.5$

For interpretation (b), these are:

$\alpha_{upright} = 1.0$

$\alpha_{hanging} = 1.5$

Several layers of conservatism are built into these values. These are summarized as follows:

a. An $R_p = 1.5$ was used to determine anchor force capacity, when the actual system analytically was $R_p = 1.0$.
b. Existing code documentation specifies Φ factors that are different between non-ductile and ductile steel failure modes: 0.65 and 0.75, respectively. For these studies, Φ = 0.75 was used uniformly.
c. Anchors were scaled during analysis to exact code design levels. In real systems, it should be expected that additional force capacity would be provided.

It should be noted that these recommended Ω_0 values vary drastically if R_p and a_p as experienced by the NCS in a field installation during a seismic event do not match expected demands from the design process. For the analytical work presented in this dissertation, Ω_0 and R_p were decoupled due to the actual component $R_p = 1.0$. NCSs which have R_p values that exceed 1, however, have potential confluence between Ω_0 and R_p. Additional complication arises for systems with higher-mode response, such as the components studied herein with significant

rotational mass, as expected force reductions from R_p apply only to the first mode of response (translational).

Changes made to existing code documents based on these recommendations should thus be treated with care. Currently, Ω_0 may be acting as a partial compensation factor for values of R_p that are greater than one. To demonstrate this, comparison can be made of the a_p/R_p ratio in the design equation for the non-ductile N2 anchor for upright components. For the real component parameters used to determine the Ω_0 values presented in this section, a_p/R_p = 1.67. From Section 7.4 where incorrect a_p = 1.0 and R_p = 2.5 values were chosen, a_p/R_p = 0.4. Comparing these cases, a difference in design force (ignoring minimums) of 0.4/1.67 = 0.24 is obtained, and 1/0.24 = 4.2. Required raw Ω_0 values for these cases were 1.2 and 4.3, respectively, and 4.3/1.2 = 3.6. These ratios are similar, varying slightly due to minimum F_p values and the presence of rotational mass influences.

Current code values in ACI 318 and ASCE 7 align well with values presented under interpretation (b), though these documents offer no distinction in Ω_0 as a function of natural period, T_n. One significant drawback of interpretation (b) is that it does not properly relate Ω_0 to F_p: though Ω_0 is used as a modifier on F_p, both variables are independent. Should Ω_0, as it currently acts within code, be providing correction for inadequacies in the F_p equation, it is unconservative to lower the values further until a more detailed understanding of the R_p and Ω_0 relationship can be established. Deficiencies for R_p using ductile anchors may also be present, but the anchorage may have enough additional capacity to resist higher demands (required Ω_0 is 0.6 or lower for many of the parameter sets using the N1 and N5 anchors studied, where Ω_0 values < 1 imply the anchors have reserve capacity beyond the design level of F_p).

Considering these influences, it is the author's recommendation that interpretation (b) be adopted until more detailed research programs outlining the R_p and Ω_0 relationship can be performed. Given that many of the components studied herein did not necessarily fall under the equal displacement principle upon which the philosophy of R_p is based, the applicability and efficiency of R_p as a force reduction factor to NCSs within the period ranges studied should also be considered. While R_p is still applicable in the equal energy region of response, it is not conservative to assume it provides the same extent of benefit as in the equal displacement region of response.

7.9 – Acknowledgement of Publications

Sections 7.4 and 7.5 in this chapter are taken, with minor modification, from the following publication, of which the author of this dissertation assumes primary authorship:

> **Johnson, T.P**.; Dowell, R.K.; and Silva, J.F. (2017 – Acceptance Pending Revisions). "Recommendations for Ω_0 for Anchorage into Concrete for Upright Nonstructural Components." *J. Struct. Eng*.

CHAPTER 8: RECOMMENDATIONS AND FUTURE WORK

8.1 – Core Findings and Ω_0 Recommendations

The core findings of this body of work, including the combination of both structural testing and analytical studies, are summarized in the following points:

a. Anchor plastic displacement capacity offers many different performance benefits, but is not as universally-beneficial as current code documentation in ACI 318 suggests. Stiff nonstructural components with stiff elastic, non-ductile anchorage – particularly for upright components – showed similar performance to large-displacement plastic anchors at resisting design-level seismic loads. Significant benefit from anchor plastic displacement capacity only started to appear for periods of $T_n \geq 0.20$s for upright components and $T_n \geq 0.18$s for hanging components. For design-level loads on the anchors, the extent of this benefit was 20% for upright components and 50% for hanging components ($\Omega_0 = 1.2$ and $\Omega_0 = 1.5$, respectively).

b. Benefits of plastic displacement capacity appear to be mechanism-independent. The mechanical pull-through anchors displayed many of the same benefits of the ductile stainless steel anchors, and in regions where plastic displacement capacity added capacity to the system to resist higher earthquake demand levels both anchors provided benefit. Existing code design philosophy only recognizes plastic displacement capacity as obtained by ductile material response to be beneficial, which may be too-narrowly scoped.

c. The relationships between Ω_0, R_p, and a_p are comingled, and perceived benefits of Ω_0 may be addressing deficiencies in understanding of appropriate R_p and a_p values for

anchor design. Systems with intentionally incorrectly-selected R_p and a_p values showed significant increases in required Ω_0 which were generally proportional to the error for elastic response, but less for inelastic response. Of R_p and a_p, R_p shows the most distinct spread of values in ASCE 7, ranging from 1.5 to 12. Work by Fathali and Lizundia (2011) also suggests that existing values of a_p may be too small. As can be rationally expected, anchors under-designed for imposed loads – for example by selecting R_p values that are larger than actually experienced force reductions in the nonstructural component – all required larger Ω_0 values. In general, however, increases in Ω_0 were higher for brittle anchors, and less-so for anchors with plastic displacement capacity, though the extent of the difference is largely period-dependent.

It should thus be considered that observed field benefits of ductile anchorage may be indicative of experienced NCS demands being higher than those predicted by the designer using the F_p equation, and not strictly that ductile anchors are providing better performance at design-level loads. Future efforts should be made to justify R_p values in field conditions are matching the R_p values used in the design of those systems so that R_p and Ω_0 can be better isolated as independent variables and their *in-situ* influences more properly understood.

d. Given the complications of Ω_0, R_p, and a_p discussed in (c), it is not recommended to significantly change Ω_0 at this time. The current implementation of Ω_0 as a relative performance factor between ductile and non-ductile anchorage is conservative, with values of 2.0 and 2.5 being relevant for upright and hanging systems,

respectively.

It should be noted, however, that this implementation is not representative of the intended design level, and a shift in underlying conceptual definition of Ω_0 is warranted. As it is currently used, Ω_0 is partly a performance differential between ductile and nonductile anchorage, but it is also partly an uncertainty factor that accounts for a mismatch between expected seismic loads and experienced seismic loads. For example, if Ω_0 is applied to NCSs with stiff response – say with $T_n = 0.10s$ – benefit of Ω_0 from ductile anchor response is small to negligible. Application of Ω_0 in this system does mitigate uncertainty due to things like period elongations, however, which are not currently captured in the design process.

e. The nonstructural component and the anchorage act as a system, and anchor behavior can significantly impact expected component demands. Nonlinear effects due to rocking for upright components and swinging for hanging components may be nontrivial in NCS performance, and are currently ignored in the design process due to their difficulty to analytically compute or capture.

When evaluating performance of the anchor, plastic displacement capacity was generally beneficial to the anchor – at worst it offered no appreciable benefit, and at best it offered significant increase in the ability to resist large seismic demands. An overlooked drawback of plastic displacement capacity, however, is that it increases the extent of nonlinear response of the NCS, and rocking or swinging behavior may substantially increase component natural period and thus increase

displacement demands. Stiff elastic, non-ductile anchors provided a tradeoff of anchor performance for stability in component performance, as period elongations from these anchors were relatively small for upright components and thus linear-elastic assumptions and analysis procedures about component and anchor interactions are more easily captured. In addition, component displacements can be limited due to rigid body rotations, which may offer better functionality of the component post-seismic event. Stiff elastic, non-ductile anchors should thus not be universally discouraged, and may have tangible benefits if used over ductile anchorage on a case-by-case basis.

8.2 – Future Research: Anchor and NCS Behavior

Both the structural testing and analytical work performed in this dissertation demonstrate several areas of study that would be beneficial for understanding anchor performance.

- The combined influences of nonlinear component behavior and nonlinear anchor behavior have not been well studied. The idealized NCS used in both this research program and several others is strictly elastic. Use of nonlinear components for testing purposes is prohibited largely by fabrication costs, but it may be possible to modify WALLE to capture similar behavior. Rodgers et al. (2006) have developed a detail to capture nonlinear moment-rotation hysteresis that has inbuilt “fuses” to represent nonlinear response. These fuses are cheap and cost-effective to replace, and would provide an efficient means of studying

a wide range of component nonlinear responses in conjunction with nonlinear anchor behavior.

- A more detailed understanding of the relationship of component R_p to anchorage design needs to be understood before significant alterations can be made to appropriate Ω_0 values. The current implementation of Ω_0 appears to be acting partly as a corrective factor for anchors which are under-designed for imposed demands in the field. While existing code values of Ω_0 as a relative performance factor between ductile and non-ductile anchors appear to be mostly accurate, these values are not capturing performance relative to the design level associated with F_p. For systems loaded with demands close to those expected by the anchor design level, large Ω_0 values are not required – a maximum of about 1.2 is observed for upright components, and 1.5 for hanging components. Benefit from Ω_0 beyond these values is accounting for improper force reductions mostly from R_p (and partially from a_p in some cases), and not as added expected benefit of ductile behavior over non-ductile behavior.
- More detailed understanding of the relationships of hanging components and their anchorage should be pursued. The influence of consumed anchor capacity from component dead load prior to seismic loading can have strong influences on hanging system performance, and hanging systems appear to be particularly susceptible to poor performance due to under-designed anchors and large single-sided demands caused by highly nonlinear ratcheting effects of the component on the anchors. Existing code guidelines which treat the component and anchor as two separate systems do not appear to be accurate for hanging

systems, which is quantified by the additional required 20-25% increase in Ω_0 for hanging component design over upright component design.

In addition to anchorage, the nonlinear analysis tool presented in this dissertation has a great deal of potential for performing detailed nonlinear time-history analysis of the complex anchor-component system. Methods of expansion include the following:

- Development of nonlinear component behavior and inclusion of component shear deformations which may be significant for certain NCS geometries.
- Expansion of the component idealization to include multiple translational degrees of freedom that would be representative of NCSs such as telecom racks and other “simple” cantilever-style structures with vertically-spaced translational degrees of freedom.
- Inclusion of flexible base plate behavior and/or flexible foundation behavior, such as a NCS mounted on a rocking mat foundation.
- Expansion of the analysis model to include the full 6x6 modified stiffness matrix in a single analysis package. This could potentially offer an efficient way of modeling fully nonlinear tri-axial shaking table behavior without the need for highly complex finite element formulations.

APPENDIX A: DERIVATIONS AND BUILDING MODEL

Derivation for the stiffness matrix shown in Eq. 5-4 in Section 5.2.3 is presented in this appendix. It is subdivided into three parts: the translational degree of freedom stiffness terms, the rotational degree of freedom stiffness terms, and algebraic simplification of these terms into the final matrix.

Additionally, the steel moment frame building used to determine the broadband floor motions, developed by Dowell (2006), is presented.

MODIFIED STIFFNESS MATRIX INCLUDING ROTATIONAL SOFTENING OF BASE

PART I: TRANSLATIONAL DEGREE OF FREEDOM

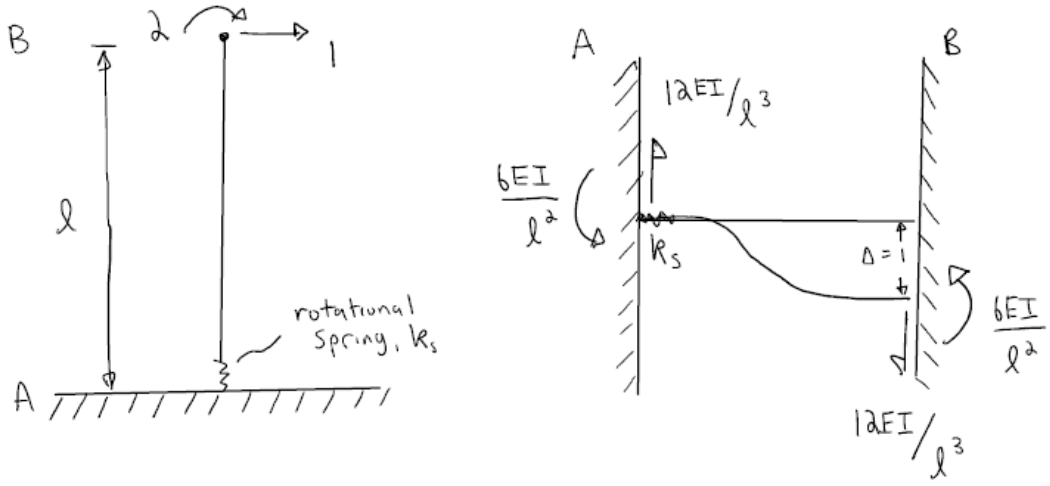

Determine the rotational stiffness of the member and of the spring relative to the total rotational stiffness of the system. Some of the moment developed as a reaction at "A" from the unit displacement at "B" will shed into the rotational spring and allow for rotation. This can be determined via moment distribution.

Member	Rotational Stiffness, k_r	Distribution Ratio
AB	$4EI/l$	$1/(1+\alpha_1)$
Spring	k_s	$\alpha_1/(1+\alpha_1)$
$\sum$	$4EI/l + k_s = (\alpha_1+1)\cdot\frac{4EI}{l}$	

where $\alpha_1 = \dfrac{k_s \cdot l}{4EI}$

$\alpha_1/(1+\alpha_1)$	$1/(1+\alpha_1)$	1
	$-6EI/\ell^2$	$-6EI/\ell^2$
$+6EI\cdot\alpha_1/(1+\alpha_1)\ell^2$	$+6EI/(1+\alpha_1)\ell^2$	$\rightarrow +3EI/(1+\alpha_1)\ell^2$
$+6EI\cdot\alpha_1/(1+\alpha_1)\ell^2$	$-6EI\cdot\alpha_1/(1+\alpha_1)\ell^2$	$-\frac{3EI}{\ell^2}\left[\frac{1+2\alpha_1}{1+\alpha_1}\right]$

where: $-\frac{6EI}{\ell^2} + \frac{3EI}{\ell^2(1+\alpha_1)} = \frac{-3}{\ell^2(1+\alpha_1)}\left[2(1+\alpha)-1\right] = \frac{-3EI}{\ell^2}\left[\frac{1+2\alpha_1}{1+\alpha_1}\right]$

$$\therefore K_{12} = \frac{-3EI}{\ell^2}\left[\frac{1+2\alpha_1}{1+\alpha_1}\right]$$

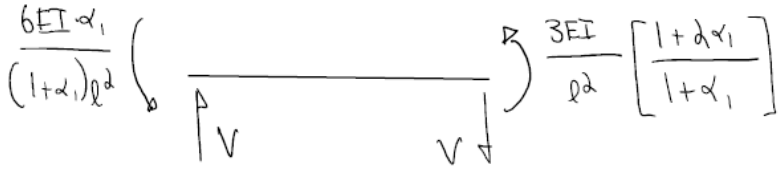

$$V = \frac{1}{\ell}\left[\frac{6EI\cdot\alpha_1}{(1+\alpha_1)\ell^2} + \frac{3EI}{(1+\alpha_1)\ell^2} + \frac{6EI\cdot\alpha_1}{(1+\alpha_1)\ell^2}\right] = \frac{3EI}{\ell^3}\left[\frac{1+4\alpha_1}{1+\alpha_1}\right]$$

$$\therefore K_{11} = \frac{3EI}{\ell^3}\left[\frac{1+4\alpha_1}{1+\alpha_1}\right]$$

for $\alpha = 0$, $K_{11} = 3EI/\ell^3$ ✓

$\alpha = \infty$, $K_{11} = 12EI/\ell^3$ ✓

PART II: ROTATIONAL DEGREE OF FREEDOM

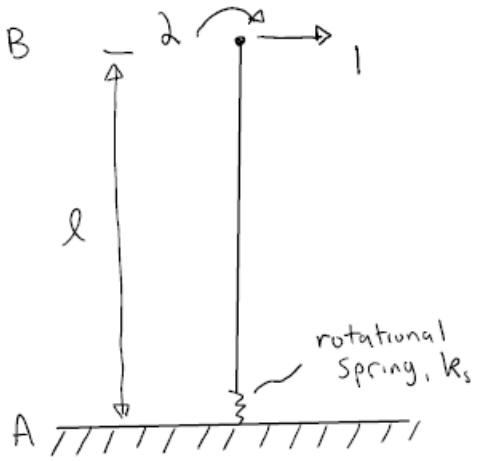

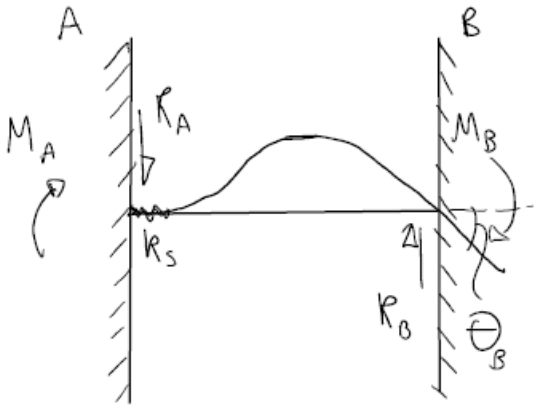

Determine the rotational stiffness of the member and of the spring relative to the total rotational stiffness of the system. An applied moment "M_B" at the free end causes $M_B/2$ to develop at the base. Part of this moment will shed into the rotational spring, causing rotation of the base at A.

Member	Rotational Stiffness, k_r	Distribution Ratio
AB	$3EI/\ell$	$1/(1+\alpha_2)$
Spring	k_s	$\alpha_2/(1+\alpha_2)$

$$\sum \quad 3EI/\ell + k_s = (1+\alpha_2)\cdot\frac{3EI}{\ell}$$

$$\text{where } \alpha_2 = \frac{k_s \cdot \ell}{3EI}$$

$\alpha_2/(1+\alpha_2)$	$1/(1+\alpha_2)$
	$M_B/2$ ← M_B
$-\frac{M_B \alpha_2}{2(1+\alpha_2)}$	$-\frac{M_B}{2(1+\alpha_2)}$
$-\frac{M_B \alpha_2}{2(1+\alpha_2)}$	$+\frac{M_B \alpha_2}{2(1+\alpha_2)}$

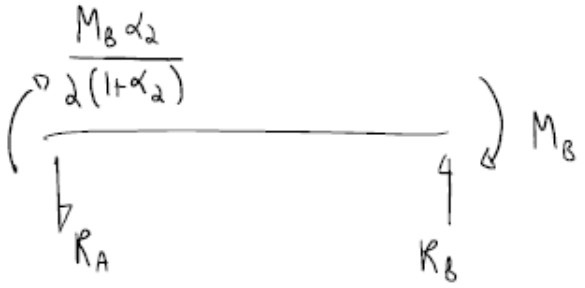

solving for R_A: $\sum M_B = 0 = M_B + \frac{M_B \alpha_2}{2(1+\alpha_2)} - R_A \cdot \ell$

$$R_A = \frac{M_B}{\ell}\left[1 + \frac{\alpha_2}{2(1+\alpha_2)}\right]$$

$$\emptyset \cdot EI = M = \frac{M_B \alpha_2}{2(1+\alpha_2)} - \frac{M_B}{\ell}\left[1 + \frac{\alpha_2}{2(1+\alpha_2)}\right] x$$

$$\theta \cdot EI = \int M = \frac{M_B \alpha_2}{2(1+\alpha_2)} x - \frac{M_B}{2\ell}\left[1 + \frac{\alpha_2}{2(1+\alpha_2)}\right] x^2 + C_1$$

$$\Delta \cdot EI = \iint M = \frac{M_B \alpha_2}{4(1+\alpha_2)} x^2 - \frac{M_B}{6\ell}\left[1 + \frac{\alpha_2}{2(1+\alpha_2)}\right] x^3 + C_1 x + C_2$$

$$@\ x = 0,\ \Delta = 0 \Rightarrow C_2 = 0$$

$$@\ x = 0,\ \theta = \frac{M_A}{k_S} = \frac{M_B \alpha_2}{2(1+\alpha_2)} \cdot \frac{1}{k_S} = \frac{M_B \alpha_2}{2(1+\alpha_2)} \cdot \frac{\ell}{3EI\alpha_2}$$

solve for C_1:

$$\frac{M_B \alpha_2}{2(1+\alpha_2)} \cdot \frac{\ell}{3EI\alpha_2} \cdot EI = 0 - 0 + C_1 \Rightarrow C_1 = \frac{M_B \cdot \ell}{6(1+\alpha_2)}$$

solve for $\theta(x=\ell) = -\theta_B$:

$$-\theta_B \cdot EI = \frac{M_B \alpha_2}{2(1+\alpha_2)} \cdot \ell - \frac{M_B}{2\ell}\left[1 + \frac{\alpha_2}{2(1+\alpha_2)}\right] \ell^2 + \frac{M_B \cdot \ell}{6(1+\alpha_2)}$$

$$= \frac{M_B \cdot \ell}{2(1+\alpha_2)}\left[\alpha_2 - \left(1 + \alpha_2 + \frac{\alpha_2}{2}\right) + \frac{1}{3}\right]$$

$$= \frac{-M_B \cdot \ell}{(1+\alpha_2)}\left[\frac{\alpha_2}{4}+\frac{1}{3}\right] = \frac{-3M_B \cdot \ell}{3(1+\alpha_2)}\left[1+\frac{3\alpha_2}{4}\right]$$

$$\therefore -\theta_B \cdot EI = \frac{-M_B \cdot \ell}{3}\left[\frac{1+3/4\,\alpha_2}{1+\alpha_2}\right]$$

$$\Rightarrow \frac{M_B}{\theta_B} = \frac{3EI}{\ell}\left[\frac{1+\alpha_2}{1+3/4\,\alpha_2}\right]$$

$$\therefore K_{22} = \frac{3EI}{\ell}\left[\frac{1+\alpha_2}{1+3/4\,\alpha_2}\right]$$

for a unit rotation of $\theta_B = 1$:

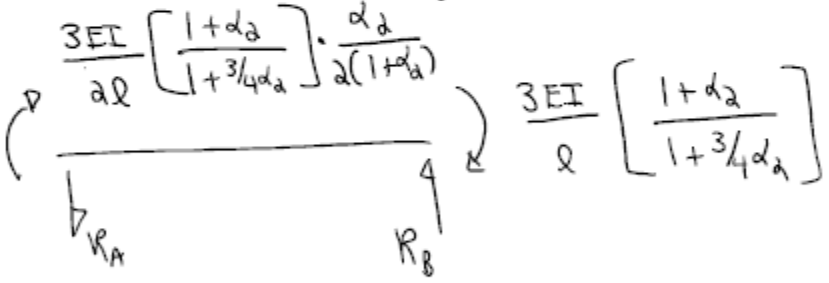

$$\sum M_A = 0 = \frac{3EI}{\ell}\left[\frac{1+\alpha_2}{1+3/4\,\alpha_2}\right]\left[1+\frac{\alpha_2}{2(1+\alpha_2)}\right] - R_B \cdot \ell$$

$$\therefore K_{21} = R_B = \frac{3EI}{\ell^2}\left[\frac{1+\alpha_2}{1+3/4\,\alpha_2}\right]\left[1+\frac{\alpha_2}{2(1+\alpha_2)}\right]$$

PART III: COLLECTION AND SIMPLIFICATION OF STIFFNESS TERMS

$$K_{11} = \frac{3EI}{\ell^3}\left[\frac{1+4\alpha_1}{1+\alpha_1}\right]$$

$$K_{12} = \frac{-3EI}{\ell^2}\left[\frac{1+2\alpha_1}{1+\alpha_1}\right]$$

$$K_{21} = \frac{-3EI}{\ell^2}\left[\frac{1+\alpha_2}{1+3/4\alpha_2}\right]\left[1+\frac{\alpha_2}{2(1+\alpha_2)}\right]$$

$$K_{22} = \frac{3EI}{\ell}\left[\frac{1+\alpha_2}{1+3/4\alpha_2}\right]$$

where $\alpha_1 = \frac{k_s \cdot \ell}{4EI}$ & $\alpha_2 = \frac{k_s \cdot \ell}{3EI} \Rightarrow 4\alpha_1 = 3\alpha_2$

$\therefore \alpha_2 = 4/3\,\alpha_1$

Solving K_{21}:

$$K_{21} = \frac{-3EI}{\ell^2}\left[\frac{1+4/3\alpha_1}{1+\alpha_1}\right]\left[\frac{2+8/3\alpha_1+4/3\alpha_1}{2(1+4/3\alpha_1)}\right]$$

$$= \frac{-3EI}{\ell^2}\left[\frac{1+2\alpha_1}{1+\alpha_1}\right] = K_{12}\ \checkmark$$

$$K_{22} = \frac{3EI}{\ell}\left[\frac{1+4/3\alpha_1}{1+\alpha_1}\right]$$

DUCTILE SAMU DESIGN

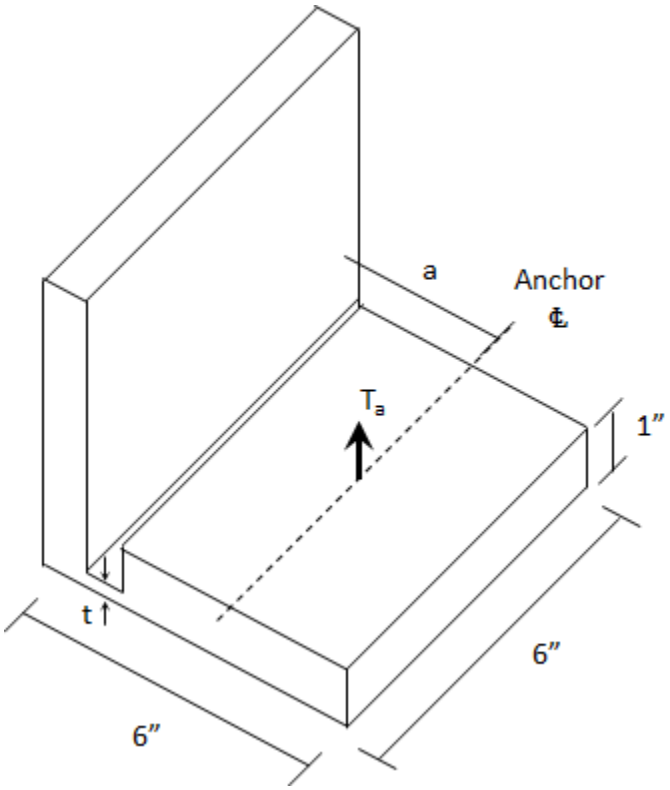

For the notched region, elastic yield:

$$\sigma_y = \frac{M_y c}{I}$$

$$M_y = \frac{\sigma_y I}{c} = \frac{\sigma_y \cdot {}^1\!/_{12} \cdot 6 \cdot t^3}{{}^1\!/_2 t} = \sigma_y \cdot t^2$$

For the notched region, plastic moment:

$$M_p = {}^1\!/_2 t \cdot F_p = {}^1\!/_2 t \cdot \left({}^1\!/_2 t \cdot 6 \cdot \sigma_u\right) = {}^3\!/_2 \cdot \sigma_u \cdot t^2$$

Use A36 steel with σ_y = 36 ksi per AISC 360-11. Per AISC 341-10 Table A3.1, $\sigma_u = R_y\sigma_y$ where R_y = 1.5, so $\sigma_u = 1.5\sigma_y$. Use an expected yield of $\sigma_{ye} = 1.1\sigma_y$.

$$M_p = {}^3\!/_2 \cdot \sigma_u \cdot t^2 = {}^3\!/_2 \cdot {}^3\!/_2 \sigma_y \cdot t^2 = {}^9\!/_4 \cdot \sigma_y \cdot t^2$$

$$\frac{M_p}{M_y} = \frac{{}^9\!/_4 \cdot \sigma_y \cdot t^2}{\sigma_y \cdot t^2} = \frac{9}{4}$$

$$M_p = \frac{9}{4} M_y$$

M_p may be expressed as the distance "a" times the tensile force in the anchor, T_a.

$$M_p = \frac{9}{4} M_y = T_a \cdot a = \frac{9}{4} \sigma_{ye} \cdot t^2 = \frac{9}{4} (1.1\sigma_y) \cdot t^2$$

$$t = \sqrt{\frac{T_a \cdot a}{\frac{9}{4} 1.1\sigma_y}} = \sqrt{\frac{T_a \cdot a}{2.48\sigma_y}} \approx \sqrt{\frac{T_a \cdot a}{2.50\sigma_y}}$$

Design such that $T_a = 0.4T_{a,u} = 0.4 \cdot 8.2$ kips = 3.28 kips. For the SAMU, a = 2.5 in.

$$t_{max} = \sqrt{\frac{T_a \cdot a}{2.50\sigma_y}} = \sqrt{\frac{3.28 \cdot 2.5}{2.5 \cdot 36}} = 0.30\text{in}$$

Use nearest 1/8" thickness rounded down, so:

$$t = 0.25\text{in}$$

STEEL MOMENT FRAME BUILDING FROM DOWELL (2006)

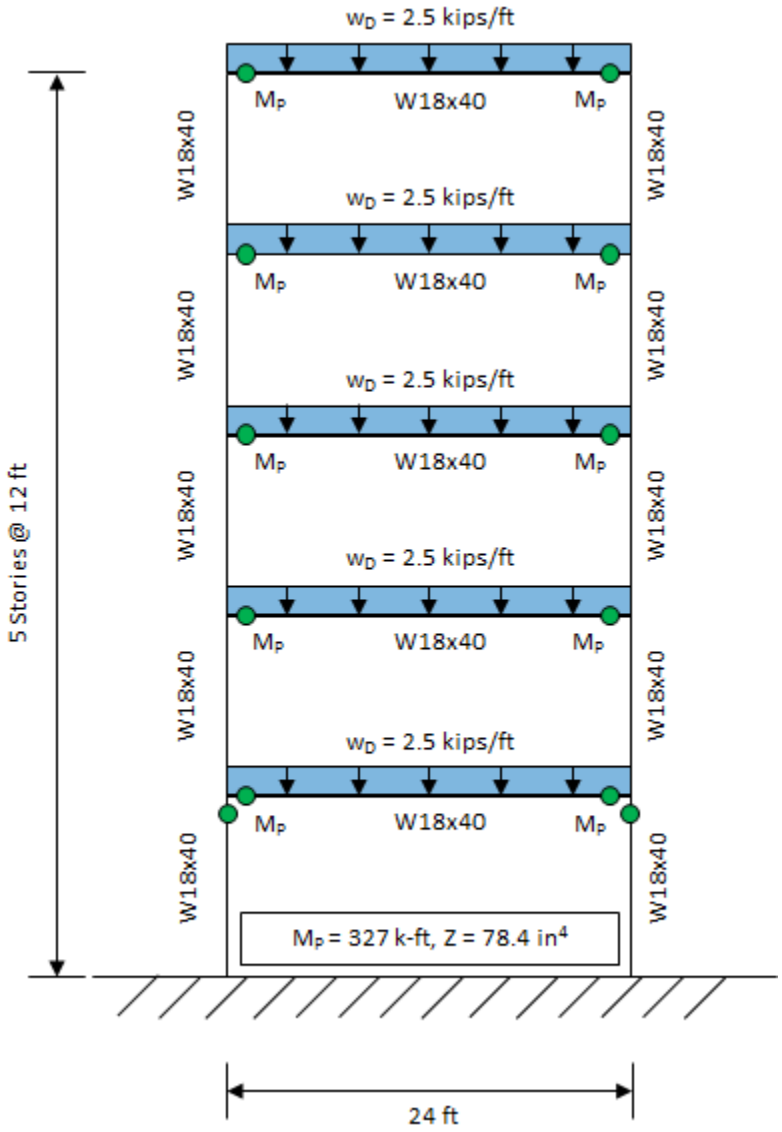

APPENDIX B: DUCTILE SAMU AND SLAB DETAILS

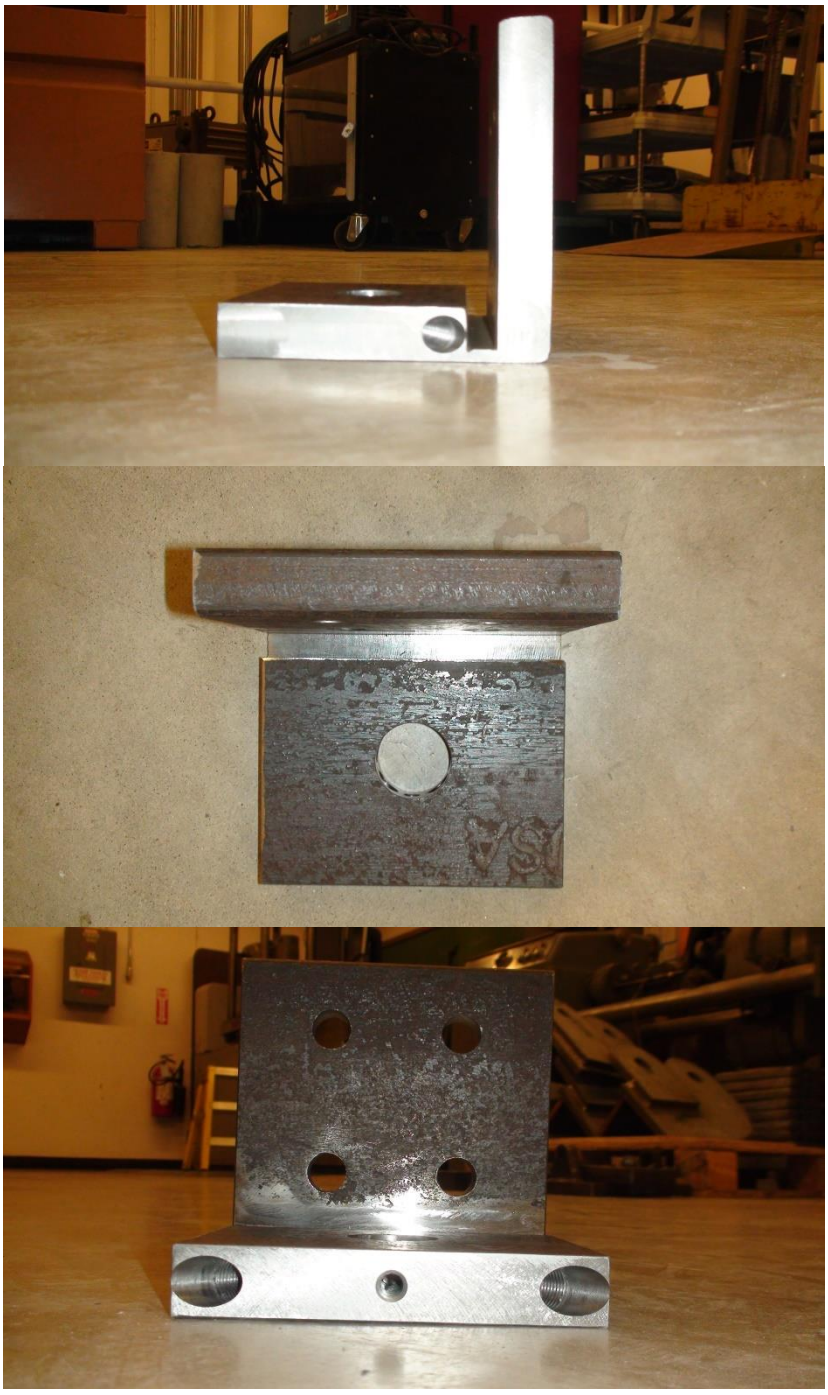

Figure 0-1: Photographs of Ductile SAMU in Elevation (Top), Plan (Middle), and Front (Bottom) Views

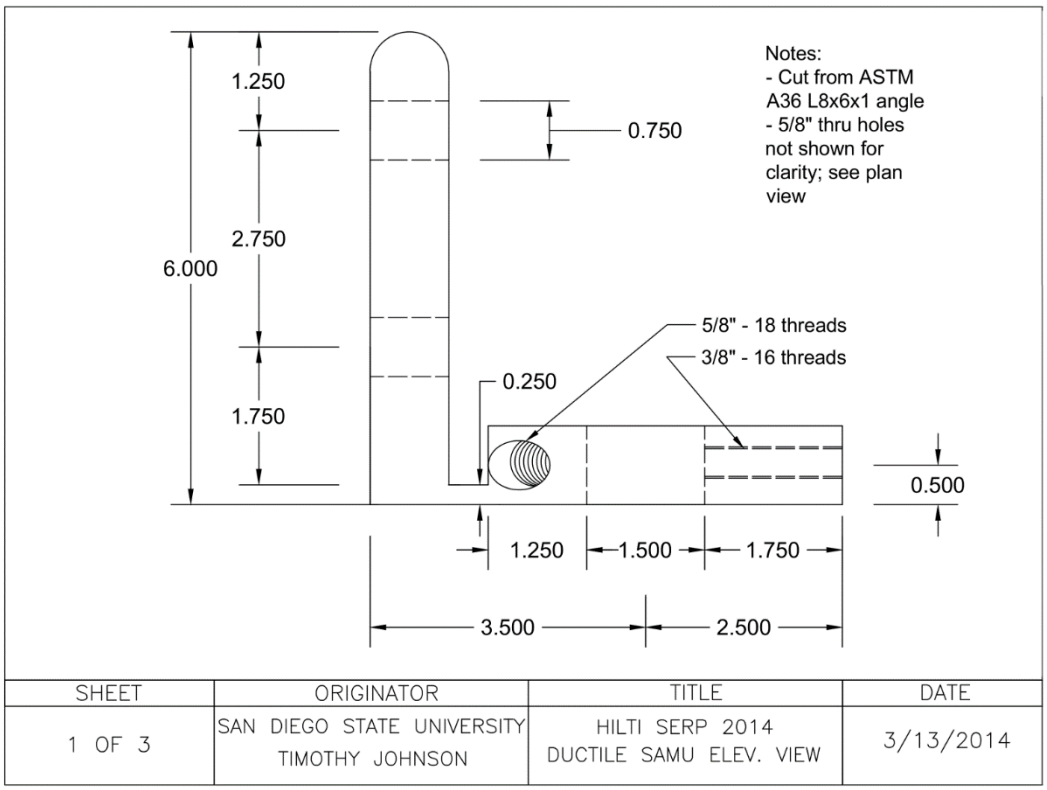

Ductile SAMU Shop Drawing - Elevation View

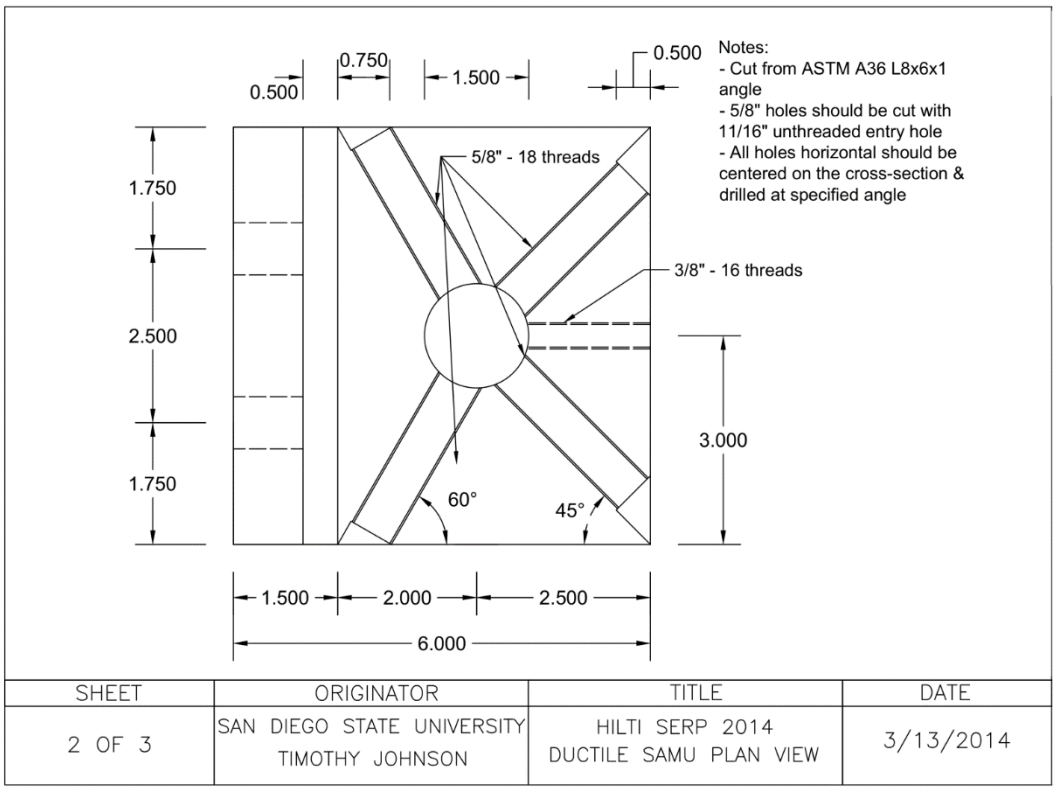

SHEET	ORIGINATOR	TITLE	DATE
2 OF 3	SAN DIEGO STATE UNIVERSITY TIMOTHY JOHNSON	HILTI SERP 2014 DUCTILE SAMU PLAN VIEW	3/13/2014

Ductile SAMU Shop Drawing - Plan View

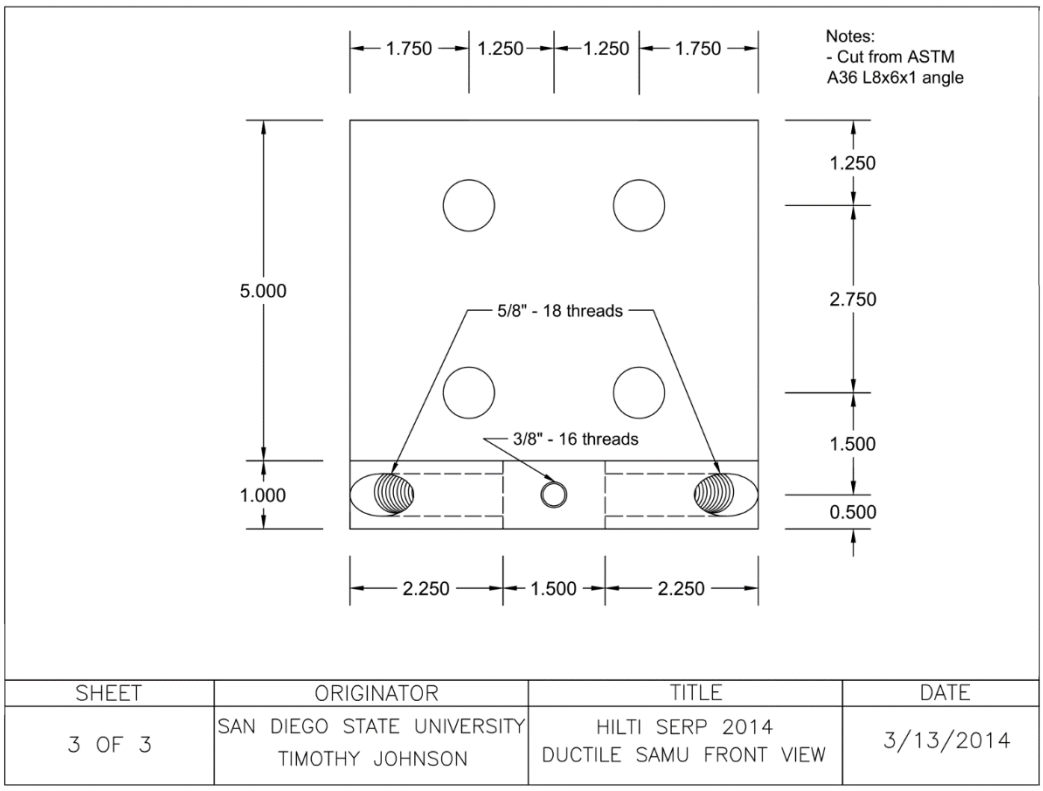

SHEET	ORIGINATOR	TITLE	DATE
3 OF 3	SAN DIEGO STATE UNIVERSITY TIMOTHY JOHNSON	HILTI SERP 2014 DUCTILE SAMU FRONT VIEW	3/13/2014

Ductile SAMU Shop Drawing - Front View

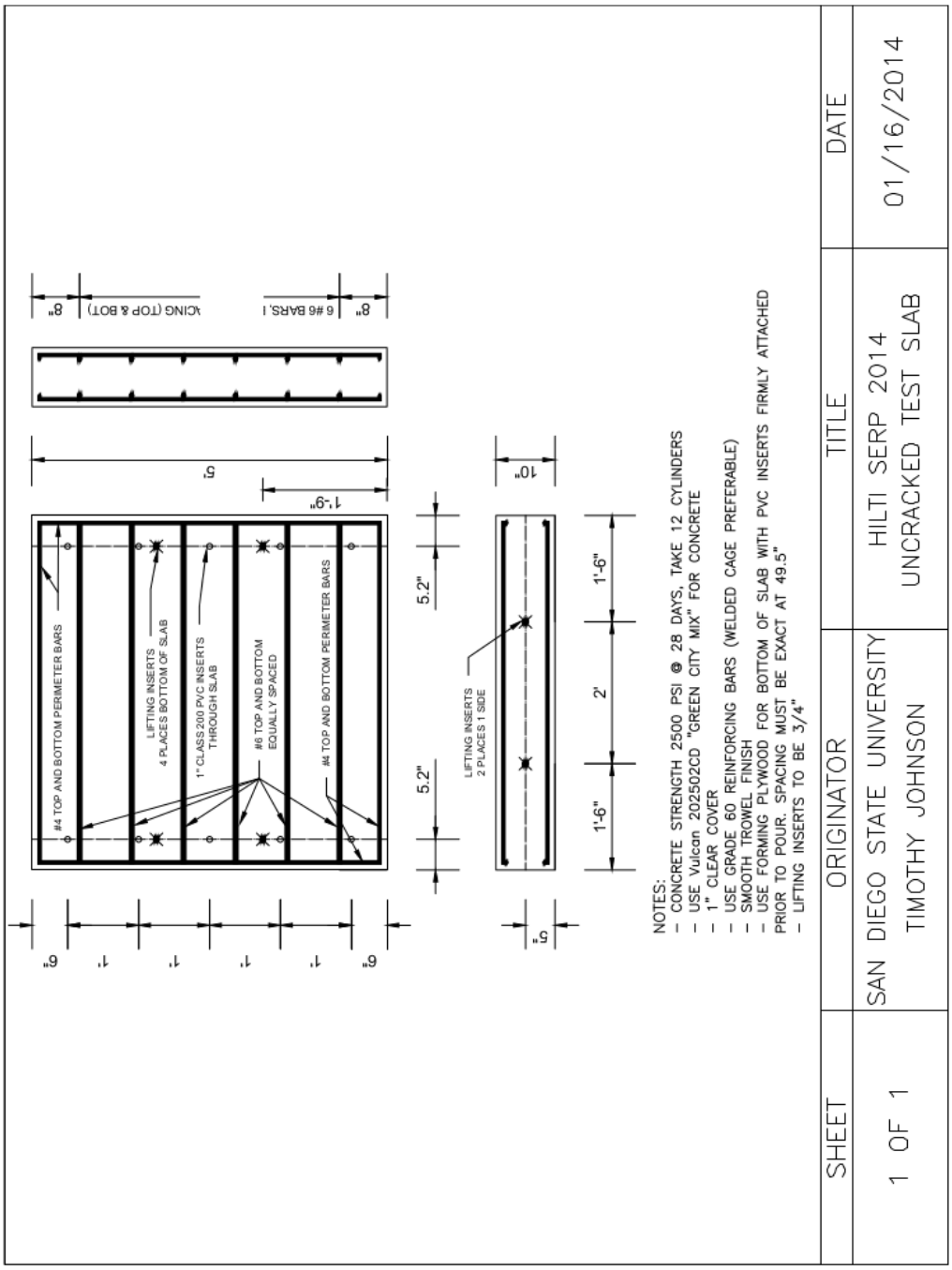

Concrete Slab Detail

APPENDIX C: ADDITIONAL DATA FROM STRUCTURAL TESTING

This appendix contains the full presentation of structural testing data, discussed in 0, for all test sequences. Hysteretic responses show the complete anchor cycling over all ground motions run in succession. When time-history responses are shown, each ground motion for a given anchor test sequence is spaced 10 seconds apart to provide visual clarity of behavior for each individual ground motion.

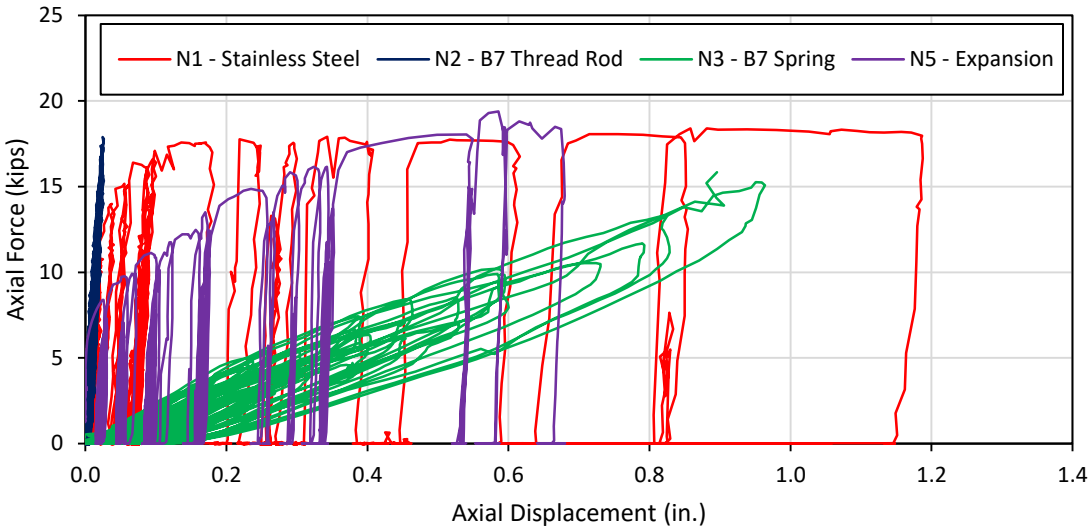

South Anchor Force vs. Displacement Response for SEM Test Sequence

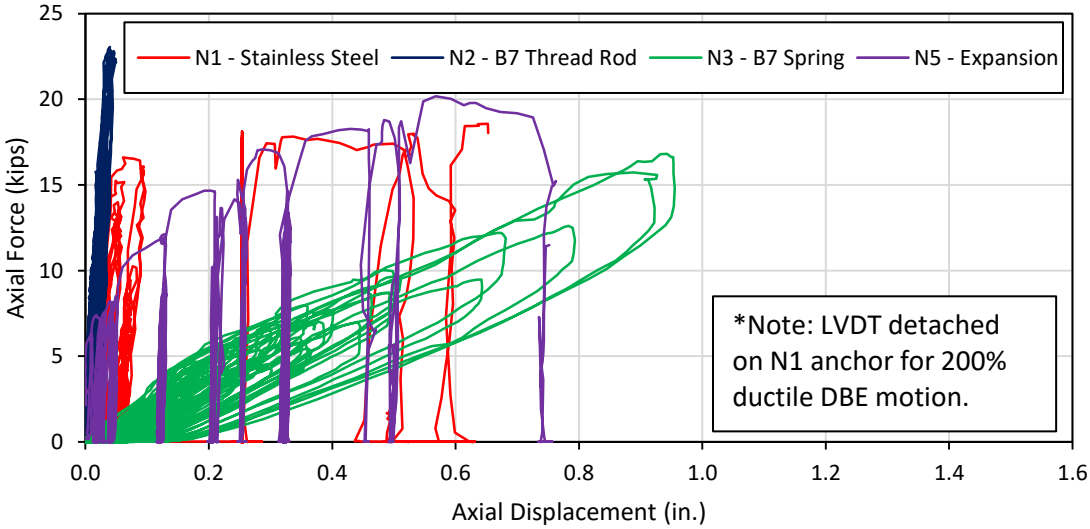

North Anchor Force vs. Displacement Response for SEM Test Sequence

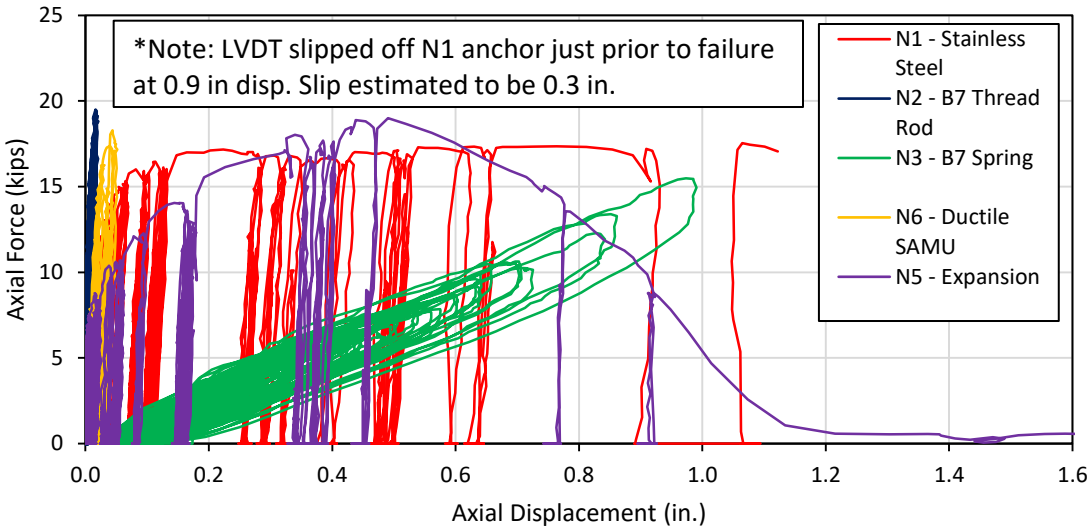

South Anchor Force vs. Displacement Response for BBM Test Sequence

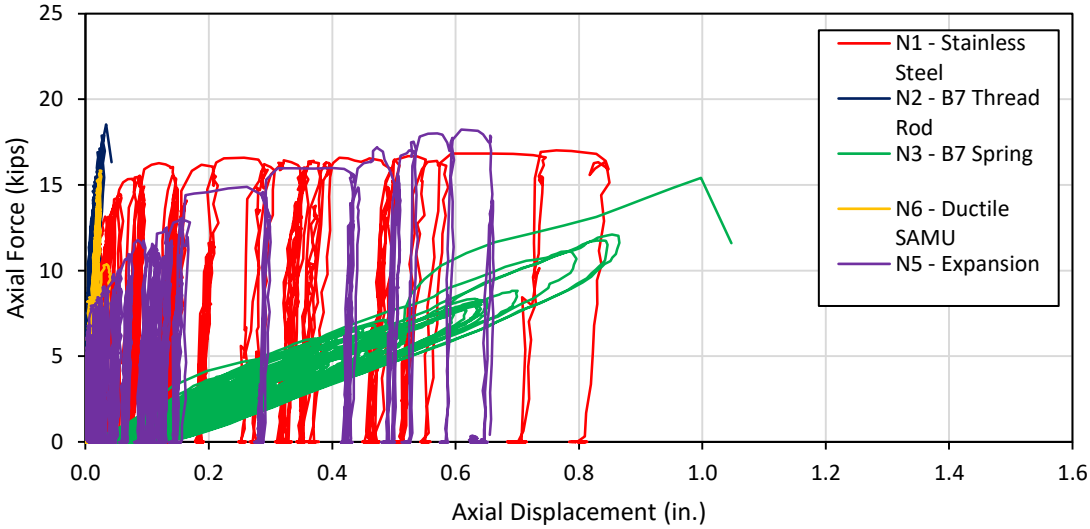

North Anchor Force vs. Displacement Response for BBM Test Sequence

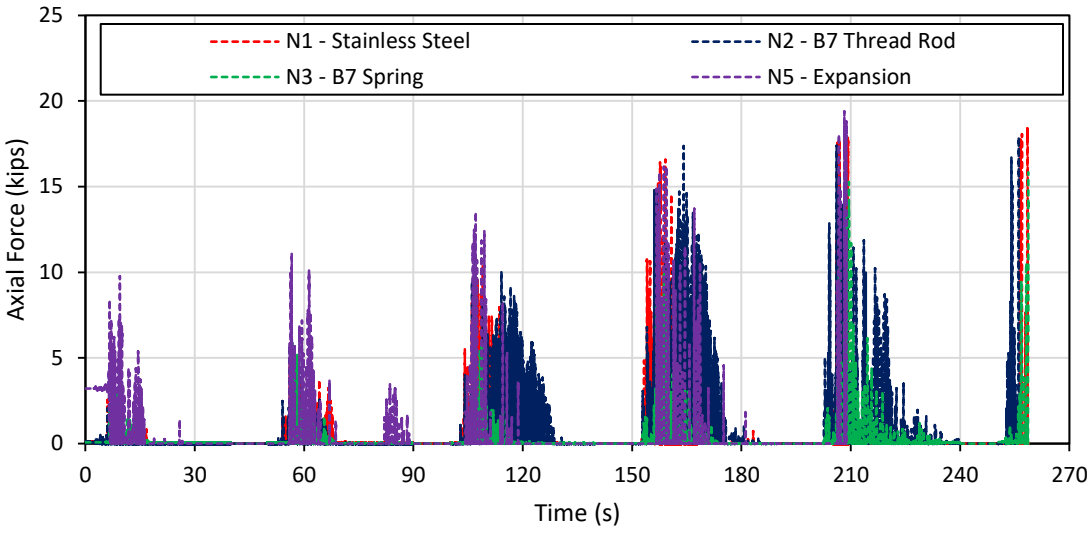

South Anchor Force Time-History Response for SEM Test Sequence

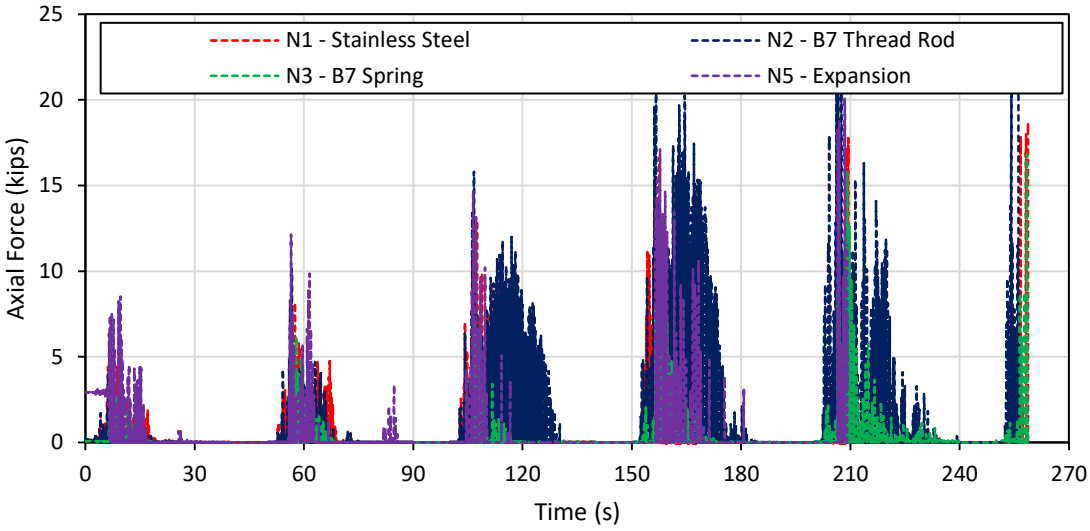

North Anchor Force Time-History Response for SEM Test Sequence

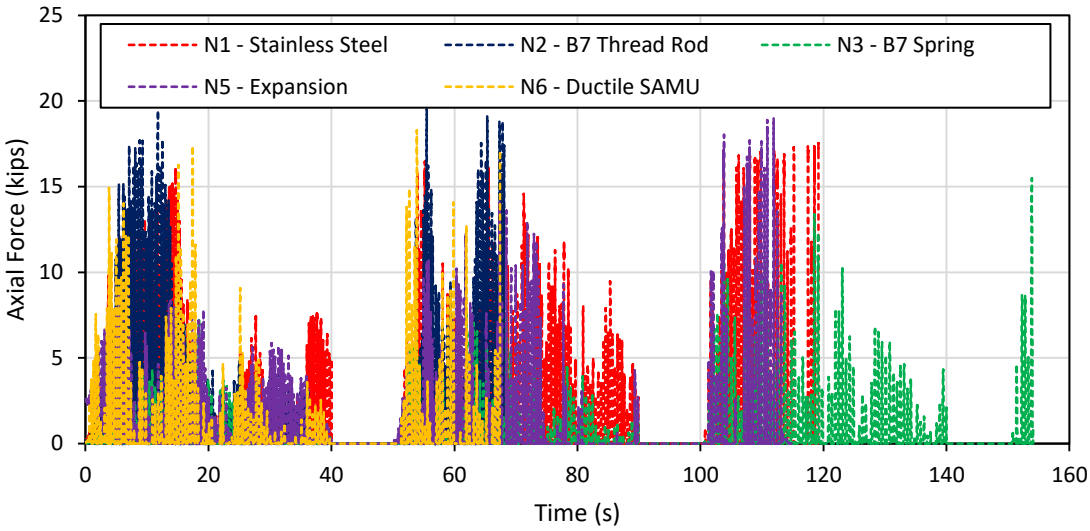

South Anchor Force Time-History Response for BBM Test Sequence

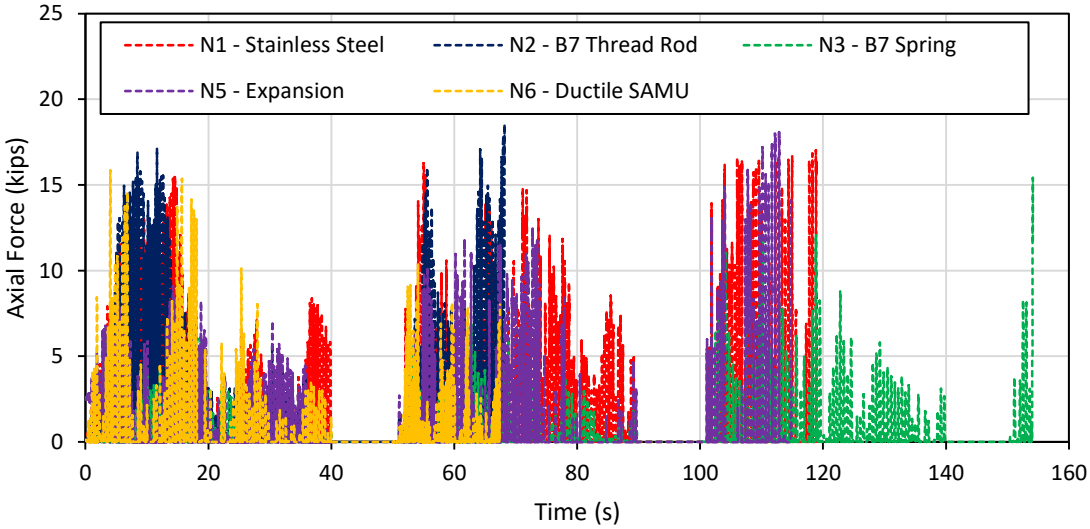

North Anchor Force Time-History Response for BBM Test Sequence

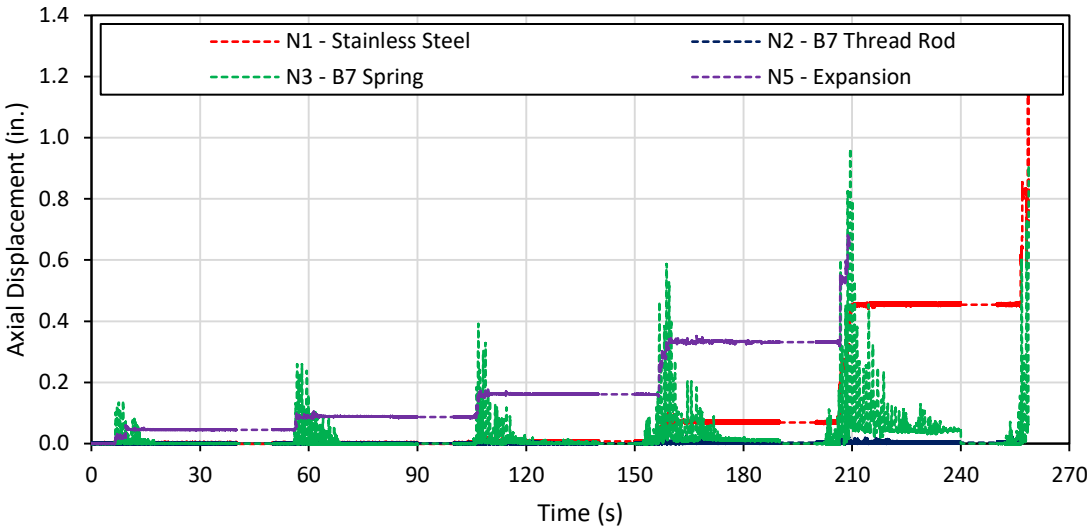

South Displacement Force Time-History Response for SEM Test Sequence

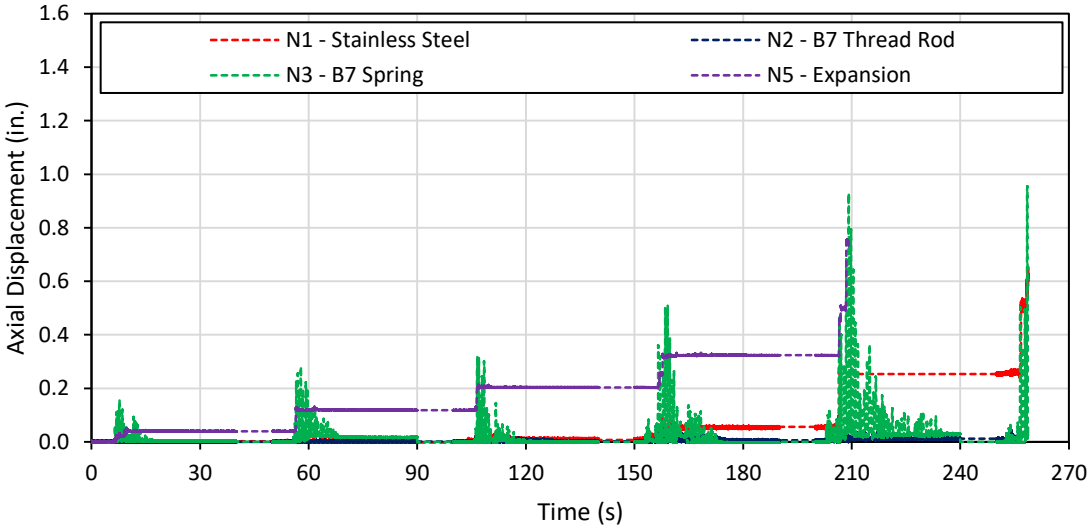

North Displacement Force Time-History Response for SEM Test Sequence

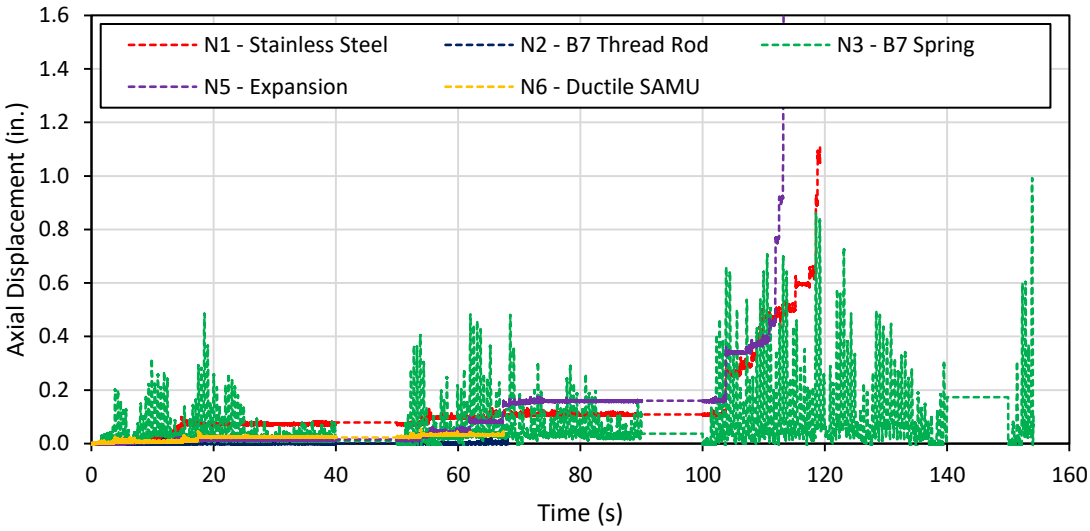

South Displacement Force Time-History Response for BBM Test Sequence

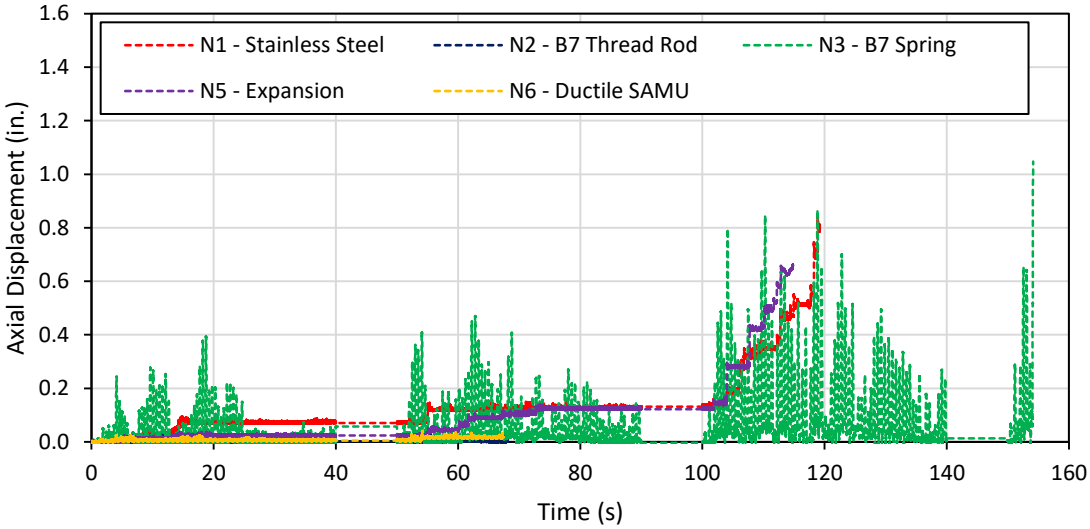

North Displacement Force Time-History Response for BBM Test Sequence

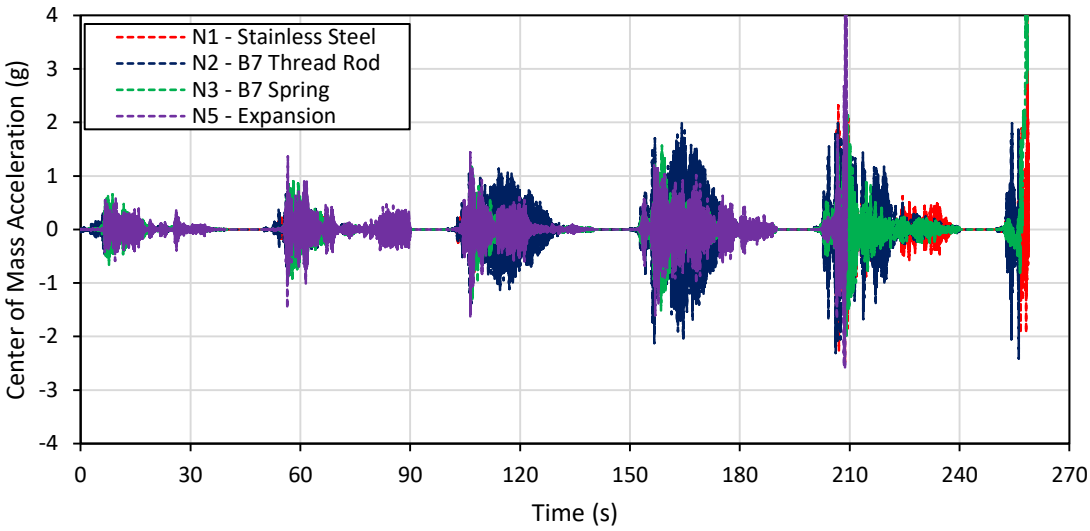

Center of Mass Acceleration Time-History Response for SEM Test Sequence

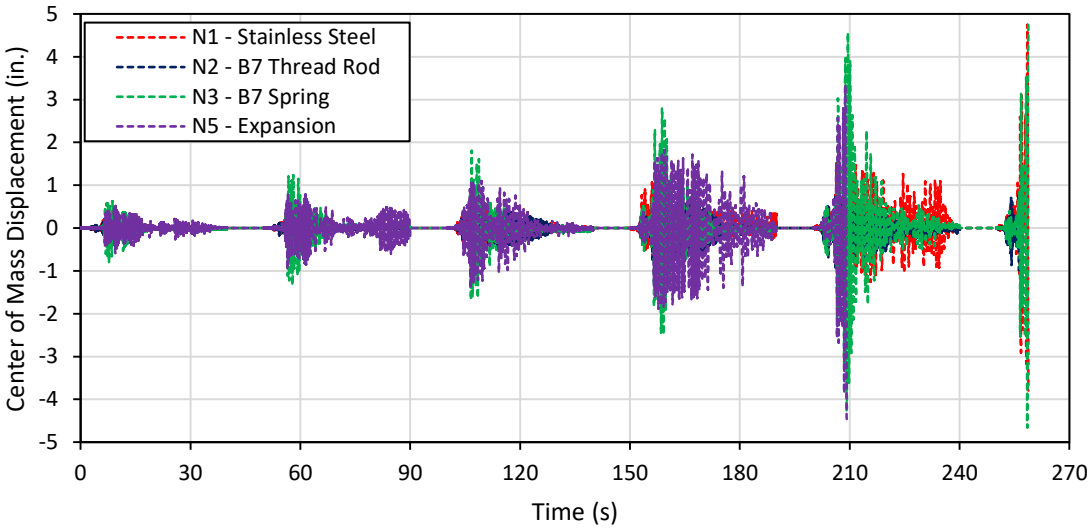

Center of Mass Displacement Time-History Response for SEM Test Sequence

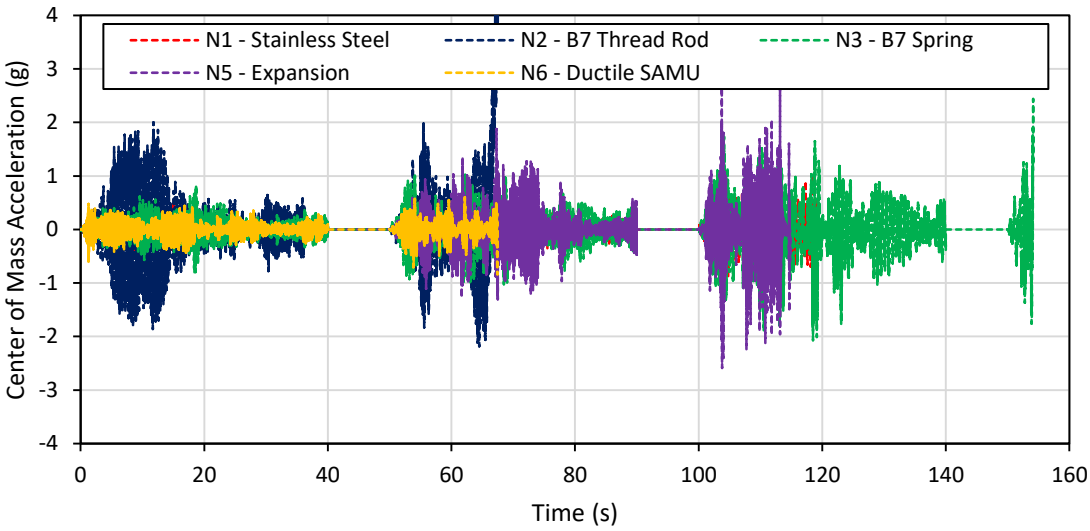

Center of Mass Acceleration Time-History Response for BBM Test Sequence

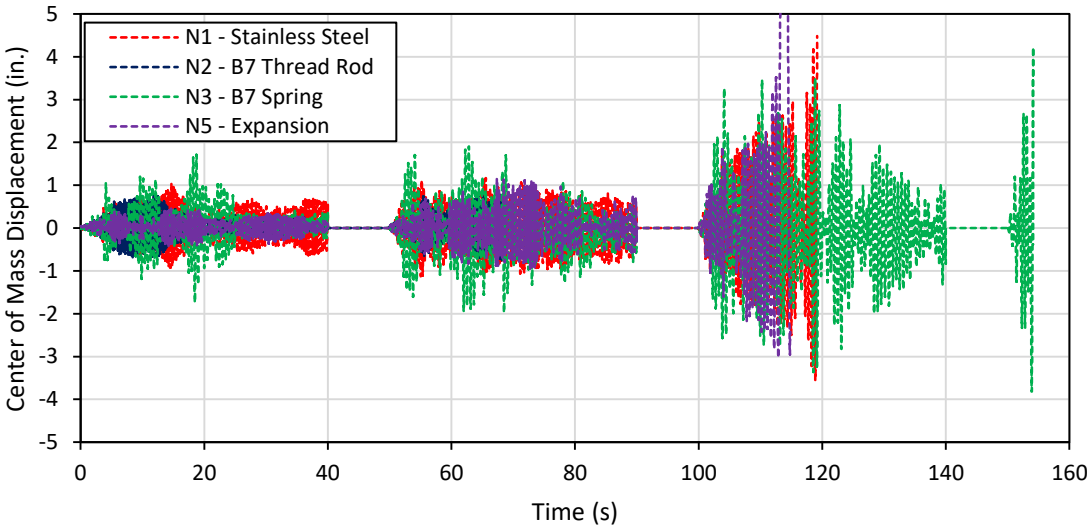

Center of Mass Displacement Time-History Response for BBM Test Sequence

REFERENCES

ACI 318-08 ACI (American Concrete Institute). (2008). "Building Code Requirements for Structural Concrete." *ACI 318-08*. Farmington Hills, MI.

ACI 318-11 ACI (American Concrete Institute). (2011). "Building Code Requirements for Structural Concrete." *ACI 318-11*. Farmington Hills, MI.

ACI 318-14 ACI (American Concrete Institute). (2014). "Building Code Requirements for Structural Concrete." *ACI 318-14*. Farmington Hills, MI.

ASCE 7-05 ASCE (American Society of Civil Engineers). (2005). "Minimum Design Loads for Buildings and Other Structures." *ASCE 7-05*. Reston, VA.

ASCE 7-10 ASCE (American Society of Civil Engineers). (2010). "Minimum Design Loads for Buildings and Other Structures." *ASCE 7-10*. Reston, VA.

Alipour and Zarien (2008) Alipour, A. and Zareian, F. (2008). "Study of Rayleigh Damping in Structures: Uncertainties and Treatments." *14th World Conference on Earthquake Engineering*.

ATC 156-12 ATC (Applied Technology Council). (2012). "Acceptance Criteria for Seismic Certification by Shake-Table Testing of Nonstructural Components." *ATC 156-12*. Redwood City, CA.

Baird et al. (2014) Baird, A.; Tasligedik, A.S.; Palermo, A.; and Pampanin, S. "Seismic Performance of Vertical Nonstructural Components in the 22 February 2011 Christchurch Earthquake." *Earthquake Spectra, Vol. 30, Issue 1.* pp. 401-425.

Bruneau et al. (2011) Bruneau, M.; Uang, C-M.; and Sabelli, R. (2011). "Ductile Design of Steel Structures (2nd Edition)." The McGraw Hill Companies. New York, NY.

Carr (2015) Carr, A.J. (2015). "Ruaumoko Theory Manual." *University of Canterbury*. pp. 4-14.

Celebi (1997) Celebi, M. (1997). "Response of Olive View Hospital to Northridge and Whittier Earthquakes." *J. Struc. Eng., Vol 123, Issue 4.* pp. 389-396.

Charney (2008) Charney, F. (2008). "Unintended Consequences of Modeling Damping in Structures." *J. Struc. Eng.*, *Vol. 134, Issue 4*. pp. 581-592.

Clough and Penzien (1993) Clough, R.W. and Penzien, J. (1993). "Dynamics of Structures *(*2nd Edition)." The McGraw Hill Companies. New York, NY.

CSI (2016) Computer & Structures, Inc. (CSI) "CSi Analysis Reference Manual." *Computers and Structures, Inc*. [SAP2000 Computer Program]

Drake and Bachman (1996) Drake, R. and Bachman, R. (1996). "NEHRP Provisions for 1994 for Nonstructural Components." *Journal of Architectural Engineering*, pp. 26-31.

Dowell (2006) Dowell, R.K. (2006). "Component Accelerations from Nonlinear Time-History Building Analysis." *Internal Report Dowell-2006-01 to Hilti Corporation.*

Dowell et al. (1998) Dowell, R.K.; Seible, F.; and Wilson, E.L. (1998). "Pivot Hysteresis Model for Reinforced Concrete Members." *ACI Structural Journal*, *Vol. 95, Issue 5*. pp. 607-616.

EERIC (1971) Earthquake Engineering Research Institute Committee. (1971). "Damage to the Olive View Hospital Buildings." *United States Geological Survey Professional Paper 733*, pp. 188-190.

Eligehausen et al. (2006) Eligehausen, R.; Mallée, R.; and Silva, J.F. (2006). "Anchorage in Concrete Construction." *Wiley and Sons, Inc.*

Fathali and Lizundia (2011) Fathali, S. and Lizundia, B. (2011). "Evaluation of current seismic design equations for nonstructural components in tall buildings using strong motion records." *Structural Design of Tall and Special Buildings*. pp. S30-46.

Gasparini and Vanmarcke (1976) Gasparini, D.A. and Vanmarcke, E.H. (1976). "SIMQKE: Simulated Earthquake Motions Compatible with Prescribed Response Spectra." *Department of Civil Engineering, Massaschusetts Institute of Technology. Research Report R76-4.*

Gatscher et al. (2004) Gatscher, J.A.; Caldwell, P.J.; Bachman, R.E.; and Littler, S.R. "Seismic Qualification Testing of Nonstructural Components and Equipment." *Structures Congress 2004.*

Gilton and Uang (2002) Gilton, C.S. and Uang, C-M. "Cyclic Response and Design Recommendations of Weak-Axis Reduced Beam Section Moment Connections." *J. Struc. Eng., Vol. 128, Issue 4.* pp. 452-463.

Gould and Marshall (2012) Gould, N.C. and Marshall, J.D. (2012). "Structural and Nonstructural Damage to Industrial Facilities during the 2011 Christchurch, New Zealand Earthquake." *Structures Congress 2012*. pp. 1069-1079.

Goodno et al. (2011) Goodno, B.J.; Gould, N.C.; Caldwell, P.; and Gould, P.L. "Effects of the January 2010 Haitian Earthquake on Selected Electrical Equipment." *Earthquake Spectra, Vol. 27, Issue S1.* pp. S251-S276.

Heo et al. (2011) Heo, Y.A.; Kunnath, S.K.; and Abrahamson, N. "Amplitude-Scaled versus Spectrum-Matched Ground Motions for Seismic Performance Assessment." *J. Struc. Eng, Vol. 137, Issue 3.* pp. 278-288

Hoehler (2006) Hoehler, M.S. (2006). "Behavior and Testing of Fastenings into Concrete for Use in Seismic Applications." *PhD Dissertation, University of Stuttgart, Germany*. p. 32.

Hoehler and Dowell (2009) Hoehler, M.S. and Dowell, R.K. (2009). "Reference Tension and Shear Tests on Single Anchors to be Used in Shake Table Tests in Uncracked Concrete." *San Diego State University, HSP-2009-05*.

Hoehler and Dowell (2010) Hoehler, M.S. and Dowell, R.K. (2010). "Pushover Tests of Weighted Anchor-Loading Laboratory Equipment (WALLE) in Uncracked Concrete." *San Diego State University, HSP-2010-04*.

Hoehler et al. (2011) Hoehler, M.S.; Dowell, R.K.; and Watkins, D.A. (2011). "Shear and Axial Load Measurement Device for Anchors in Concrete." *ASTM Journal of Testing and Evaluation.* p. 39.

Huang et al. (2011) Huang, Y-N.; Whittaker, A.S.; Luco, N.; and Hamburger, R.O. "Scaling Earthquake Ground Motions for Performance-Based Assessment of Buildings." *J. Struc. Eng., Vol 137, Issue 3.* pp. 311-321.

Johnson et al. (2016) Johnson, T.P.; Dowell, R.K.; and Silva, J.F. (2016). "A Review of Code Seismic Demands for Anchorage of Nonstructural Components." *Journal of Building Engineering*, Vol 5. pp. 249-253.

Johnson and Dowell (2017a) Johnson, T.P. and Dowell, R.K. (2017 - Acceptance Pending Revisions). "Evaluation of the Overstrength Factor for Nonstructural Component Anchorage into Concrete via Dynamic Shaking Table Tests." *Journal of Building Engineering*.

Johnson and Dowell (2017b) Johnson, T.P. and Dowell, R.K. (2017 - Acceptance Pending). “Single Node Stiffness Formulation for Rocking Cantilever Structures with Inelastic Anchorage.” *Computers & Structures*.

Johnson et al. (2017) Johnson, T.P, Dowell, R.K., and Silva, J.F. (2017 - Acceptance Pending Revisions). “Recommendations for Ω_0 for Anchorage into Concrete for Upright Nonstructural Components.” *J. Struc. Eng.*

Klingner et al. (1998) Klingner, R.E.; Hallowell, J.M.; Lotze, D.; Park, H.-G.; Rodriguez, M.; and Zhang, Y.-G. (1998). “Anchor Bolt Behavior and Strength during Earthquakes.” *U.S. Nuclear Regulatory Commission NUREG/CR-5434*, p. 147.

Lepage et al. (2012) Lepage, A.; Shoemaker, J.M.; and Memari, A.M. (2012). “Demands on Nonstructural Components During Nonlinear Seismic Response of Multistory Structures.” *J. Archit. Eng, Vol. 18, Issue 4.* pp. 285-297.

Mahrenholtz et al. (2014) Mahrenholtz, P.; Hutchinson, T.C.; and Eligehausen, R. (2014). “Shake Table Tests on Suspended Nonstructural Components Anchored in Cyclically Cracked Concrete”. *J. Struc. Eng, Vol 140, Issue 11.*

Miranda and Taghavi (2009) Miranda, E. and Taghavi, S. “A Comprehensive Study of Floor Acceleration Demands in Multi-Story Buildings.” *Improving the Seismic Performance of Existing Buildings and Other Structures.* ASCE. pp. 616-626.

Miranda et al. (2012) Miranda, E.; Mosqueda, G.; Retamales, R.; and Pekcan, G. “Performance of Nonstructural Components during the 27 February 2010 Chile Earthquake.” *Earthquake Spectra, Vol 28, Issue S1*. pp. S453-S471.

Mosqueda et al. (2009) Mosqueda, G.; Retamales, R.; Filiatrault, A.; and Reinhorn, A. (2009). “Testing Facility for Experimental Evaluation of Nonstructural Components under Full Scale Floor Motions.” *Struc. Design Tall Spec. Build.*, pp. 387-404.

Mukherjee and Gupta (2002) Mukherjee, S., and Gupta, V.K. (2002). “Wavelet-based Generation of Spectrum-Compatible Time-Histories.” *Journal of Soil Dynamics and Earthquake Engineering*, 799-804.

Newmark and Hall (1982) Newmark, N.M and Hall, W.J. (1982). “Earthquake Spectra and Design.” *Earthquake Engineering Research Institute (EEERI).* Berkeley, CA.

Pantoli et al. (2013) Pantoli, E.; Wang, X.; Chen, M.; Hutchinson, T.; Meacham, B.; and Park, H.J. (2013). "Shake Table Testing of a Full-Scale Five-Story Building: Performance of the Major Nonstructural Components – Egress and Facades." *ASCE Structures Congress 2013*.

Perry et al. (2009) Perry, C.; Phipps, M.A.; and Hortacsu, A. (2009). "Reducing the Risks of Nonstructural Earthquake Damage." *ATC & SEI 2009 Conference on Improving the Seismic Performance of Existing Buildings and Other Structures*, pp. 674-685.

Priestley et al. (1996) Priestley, M.J.N.; Seible, F.; and Calvi, G.M. (1996) "Seismic Design and Retrofit of Bridges." *John Wiley and Sons, Inc.*

Puthanpurayil et al. (2014) Puthanpurayil, A.M, Carr, A.J., & Dhakal, R.P. (2014). "A generic time domain implementation scheme for non-classical convolution damping models." *Engineering Structures*.

Puthanpurayil et al. (2016) Puthanpurayil, A.; Lavan, O.; Carr, A.; and Dhakal, R. (2016). "Elemental damping formulation: an alternative modeling of inherent damping in nonlinear dynamic analysis." *Bulletin of Earthquake Engineering*.

Reyes and Kalkan (2012) Reyes, J.C. and Kalkan, E. (2012). "How Many Records Should Be Used in an ASCE/SEI-7 Ground Motion Scaling Procedure?" *Earthquake Spectra, Vol. 28, Issue 3.* pp. 1223-1242.

Rodgers et al. (2006) Rodgers, J.E.; Mahin, S.A.; and van Dam, M. (2006). "Versatile mechanical connections for use in research and education related to the inelastic seismic behavior of steel frames." *Proc., 4th Int. Symp. on Steel Struc.*, pp. 1214-1224.

Rustogi and Gupta (2004) Rustogi, S. and Gupta, A. (2004). "Modeling the Dynamic Behavior of Electrical Cabinets and Control Panels: Experimental and Analytical Results." *J. Struc. Eng, Vol. 130, Issue 3*. pp. 511-519

Sankar. and Medina (2007) Sankaranarayanan, R. and Medina, R.A. "Acceleration response modification factors for nonstructural components attached to inelastic moment-resisting frame structures." *Earthquake Eng. Struct. Dyn., Vol 36.* pp. 2189-2210.

Saragoni and Hart (1974) Saragoni, G.R. and Hart, G.C. (1974). "Simulation of Artificial Earthquakes." *Earthquake Eng. Struct. Dyn.*, *Vol.2.* pp. 219-267.

Sarva et al. (2007) Sarva, S.S.; Deschanel, S.; Boyce, M.C.; and Chen, W. (2007). "Stress-strain behavior of a polyurea and a polyurethane from low to high strain rates." *Polymer*, pp. 2208-2213.

Scheidel (2010) Scheidel, J.T. (2010). "Shear Behavior of Anchors for Squat Attached Building Components under Severe Earthquake Loading." *Master's Thesis. San Diego State University*.

Schraff (2012) Schraff, A.C. (2012). "Closed Form Solutions for Nonlinear Single Degree of Freedom Systems." *Master's Thesis. San Diego State University.*

SeismoArtif Seismosoft Ltd. (2013). "SeismoArtif." Pavia, Italy: [Computer Program].

Shing and Mahin (1987) Shing, P.B. and Mahin, S.A. (1987). "Elimination of spurious higher-mode response in pseudodynamic tests." *Earthquake Engineering and Structural Dynamics*, *Vol 15*. pp. 425-445.

Silva (2010) Silva, J.F. (2010). "Seismic Design Requirements for Nonstructural Components." *Structures Congress 2010*, pp. 2247-2257.

Silva and Hoehler (2008) Silva, J.F. and Hoehler, M.S. (2008). "Ductility Requirements for the Anchorage of Nonstructural Components." *Structures Congress 2008*.

Singh et al. (2006a) Singh, M.P.; Moreschi, L.M.; Suarez, L.E.; and Matheu, E.E. (2006). "Seismic Design Forces I: Rigid Nonstructural Components." *J. Struc. Eng., Vol. 132, Issue 10.* pp. 1524-1532.

Singh et al. (2006b) Singh, M.P.; Moreschi, L.M.; Suarez, L.E.; and Matheu, E.E. (2006). "Seismic Design Forces II: Flexible Nonstructural Components." *J. Struc. Eng., Vol. 132, Issue 10.* pp. 1533-1542.

Smith and Dowell (2010) Smith, J.W. and Dowell, R.K. (2010). "Nonstructural Component Amplification." *Technical Report HSP-2010-03, University of California San Diego*.

Soong et al. (1993) Soong, T.T.; Chen, G.; Wu, Z.; Zhang, R-H.; and Grigoriu, M. (1993). "Assessment of the 1991 NEHRP Provisions for Nonstructural Components and Recommended Revisions." *Technical Report NCEER-93-0003. National Center for Earthquake Engineering Research.*

Soules et al. (2016) Soules, J.G.; Bachman, R.E.; and Silva, J.F. (2016). "Chile Earthquake of 2010: Assessment of Industrial Facilities Around Concepción." *ASCE*. Reston, VA.

Tokas (2011) Tokas, C.V. (2011). "Nonstructural Components and Systems - Designing Hospitals for Post-Earthquake Functionality." *Architectural Engineering Conference (AEI) 2011*. pp. 378-389.

Watkins (2011) Watkins, D. (2011). "Seismic Behavior and Modeling of Nonstructural Components Considering the Influence of Cyclic Cracks." *PhD Dissertation, University of California San Diego*.

Watkins et al. (2009) Watkins, D.A.; Hutchinson, T.C.; and Hoehler, M.S. (2009). "Survey and Characterization of Floor and Wall Mounted Mechanical and Electrical Equipment in Buildings." *University of California San Diego*.

Wey et al. (2010) Wey, E.; Hays, T.; and Silva, J.F. (2010). "Earthquake Design Considerations for Anchorages in Industrial Facilities." *Structures Congress 2010*. pp. 2461-2472.

Wilson and Penzien (1972) Wilson, E. and Penzien, J. (1972). "Evaluation of Orthogonal Damping Matrices." *International Journal for Numerical Methods in Engineering*, *Vol 4*. Pp. 5-10.